UNIVERSITY OF OKLAHOMA

GRADUATE COLLEGE

PERFORMANCE OF MULTI-HAZARD-RESISTANT HOLLOW-CORE FRP-CONCRETE-STEEL COLUMNS WITH HIGH-STRENGTH SCC OR UHPC

A THESIS

SUBMITTED TO THE GRADUATE FACULTY

in partial fulfillment of the requirements for the

Degree of

MASTER OF SCIENCE

By

JACKSON C. MILNER
Norman, Oklahoma
2023

PERFORMANCE OF MULTI-HAZARD-RESISTANT HOLLOW-CORE FRP-CONCRETE-STEEL COLUMNS WITH HIGH-STRENGTH SCC OR UHPC

A THESIS APPROVED FOR THE
SCHOOL OF CIVIL ENGINEERING AND ENVIRONMENTAL SCIENCE

BY THE COMMITTEE CONSISTING OF

Dr. Jeffery S. Volz, Chair

Dr. Royce W. Floyd

Dr. Shreya Vemuganti

Acknowledgments

The culmination of this research project was not solely due to my efforts and commitment. I owe thanks to the many friends, family, co-workers, and professional colleagues who supported and assisted me throughout this project.

First, I would like to thank my family for their constant support: My dad, Clay Milner, for fostering and supporting my interest in engineering at a young age; My mom, Tracy Folsom, for ensuring that no matter how many hours I worked or how late I got home, I always had a roof over my head and a full stomach; My brothers, Reece and Owen Milner, for always injecting some fun, laughs, and good times into an unrelenting, stressful and busy time of my life: And my other family members including my grandparents, Marsha and Gary (Pop) Barger. I also want to thank my girlfriend, Rhema Harris, for her unwavering support and encouragement to continue moving forward. She kept me put together, even when I would do everything in my power to dismantle myself. She sat with me at the lows, sailed with me on the highs, and made me smile and laugh even on my toughest and longest days. I could not have accomplished what I did, to the degree that I did it, in the time that I did it without you in my corner, Rhema.

I would like to acknowledge my friends and co-workers who I spent many hours with throughout my tenure at Fear's Lab. The collective insight, ideas, solutions, and assistance were invaluable in aiding me in delivering the highest quality of work that exemplified the spirit of research and innovation. The camaraderie and companionship were an essential part of completing my research. I would like to specifically thank my advisor, Dr. Jeffery Volz, for his guidance, leadership, and support throughout my research process, and my committee members: Dr. Royce Floyd and Dr. Shreya Vemuganti. I would also like to recognize Dr. Stephen Roswurm, Zachary Tiry, Omar Yadak, Jacob Choate, Jacob Starks, Courtney Dawson, and other fellow graduate research students for their assistance on this research project. Additionally, I would like to acknowledge Dr. Chris Ramseyer and his contributions to this research project, including material and equipment donations. These donations facilitated the completion of this research project and Dr. Ramseyer's guidance and support was invaluable.

Finally, I would like to give an extra special thank you to my Lab Manager, John Bullock. I could not have fabricated the testing frame from scratch without John and his exceptional

fabricating and welding capabilities. John supported me throughout nearly every step of the process and weathered long hours, grueling heat, very early mornings, and my near-constant pessimism and OCD tendencies. We managed to do so much while being given very little and made everlasting memories along the way, and for that, I will be forever grateful.

Lastly, I want to thank the University of Oklahoma faculty, staff, and facilities that helped make this project possible, the Oklahoma Department of Transportation for the funding and the opportunity to work on this research project, and Dolese Bros. Co. for the material donations that made this project, and many others at Fear's Lab, possible. The contributions and commitment of these institutions and companies support the continuation of research and development of new structural technologies and the education and development of students and educators along the way.

Abstract

The Federal Highway Administration (FHWA) and state departments of transportation (DOTs) are actively promoting accelerated bridge construction (ABC) to minimize construction costs by reducing construction time, which in turn enhances work-zone safety and reduces the impact on facility users. While ABC has proven highly effective with bridge superstructures, the construction timeline is still hindered by the time required to construct the supporting bridge substructures. Applying ABC techniques to pier columns to reduce or eliminate form construction and removal, reinforcement assembly, and concrete curing time would reduce construction time and costs while enhancing work-zone safety.

Several ABC bridge columns have been researched and developed to eliminate or reduce formwork and column reinforcement while using standard concrete. However, some of these methods also produced undesirable tradeoffs such as complex column reinforcement, large increases in material cost, and increased column weight. The most promising and least researched of these column alternatives are hollow-core fiber-reinforced polymer tube-concrete-steel tube (HC-FCS) columns. HC-FCS columns have the potential to combine the benefits of other alternatives including significant concrete confinement, improved axial and flexural strength, and enhanced ductility and energy absorption. HC-FCS columns consist of a concrete core sandwiched between an outer fiber-reinforced polymer (FRP) tube and an inner steel tube. The FRP and steel tubes function as stay-in-place forms, with the FRP providing corrosion resistance and the steel tube providing column reinforcement and reducing congested connections. Furthermore, the concrete core provides local buckling resistance to the FRP and steel tubes.

The benefits of using high-strength self-consolidating concrete (HS-SCC) and ultra-high-performance concrete (UHPC) instead of standard concrete in most applications are well known, including ABC. The benefits of HC-FCS columns with HS-SCC or UHPC, when compared to traditional reinforced concrete (RC) columns, are unknown but will likely further reduce construction time, increase strength and ductility, and allow for thinner, lighter columns. These qualities would further promote HC-FCS columns for ABC. Design procedures and recommendations would need to be developed, or amended, for HC-FCS columns that utilize the benefits of HS-SCC and UHPC.

The main goal of this research project was to implement HC-FCS columns for accelerated bridge construction (ABC) in the State of Oklahoma by demonstrating enhanced performance compared to traditional spiral reinforced concrete (RC) columns and the additional cost/benefit of using HS-SCC or UHPC for the concrete core. The main objective of this research project is to determine the improved column axial and flexural strength, ductility, and overall performance provided by HC-FCS columns when compared to traditional RC columns and to determine the benefits, or potential tradeoffs, of using HS-SCC and UHPC for the concrete core.

Five half-scale column specimens were designed and constructed following AASHTO and ACI guidelines and recommendations from previous research studies. The column specimens consisted of one RC column, two HC-FCS columns with HS-SCC used for the concrete core, and two HC-FCS columns with UHPC used for the concrete core. The specimens were subject to displacement-controlled, cyclic lateral loading under a constant axial compressive load. The testing results of the column specimens, including the lateral load versus displacement at the column head, the peak flexural capacities, and the strain gauge data were analyzed and compared between HC-FCS column types and against the RC control column. HC-FCS columns demonstrated increased peak flexural capacity, ductility, and durability, with the UHPC cores demonstrating superior properties and performance compared to the HS-SCC cores.

Table of Contents

List of Tables

List of Figures

Chapter 1: Introduction

1.1 Background

The Federal Highway Administration (FHWA) and state departments of transportation (DOTs) are actively promoting accelerated bridge construction (ABC) to minimize construction costs by reducing construction time, which in turn enhances work-zone safety and reduces the impact on facility users. Past research and implementation have predominantly focused on using ABC techniques to accelerate the construction of bridge superstructures such as beams, girders, and decks. However, limited techniques have been developed and implemented to accelerate the construction of bridge substructures such as piers, columns, abutments, and foundations. While ABC has proven highly effective with bridge superstructures, the construction timeline is still hindered by the time required to construct the bridge substructures that support these superstructures.

Bridge substructures predominantly consist of two major components: abutments and piers, both with respective foundations. ABC techniques can optimize both components, with the greatest impact and improvement to the bridge piers due to many subcomponents, complexity, and proximity to active roadway compared to bridge abutments. These subcomponents consist of the pier foundation, column, and pier cap or girder. The pier foundation is typically a drilled shaft, spread footing, or pile and pile cap system. Drilled shafts are preferred in the state of Oklahoma due to the proximity of the rock line and are efficient to construct with limited formwork required. Drilled shafts are only hindered by concrete curing time and the need for more intensive inspection to ensure that no voids occur during construction. The pier column is generally either rectangular or cylindrical with both methods requiring large amounts of formwork and experiencing congestion from heavy reinforcement at the foundation and cap interfaces. Column construction time is hindered by form construction and removal, reinforcement assembly, and concrete curing time. The pier cap or girder encounters the same challenges as the columns with the addition of variable geometry, slope, and pedestal or bearing layout, therefore ABC techniques are more difficult to apply to pier caps. Applying ABC techniques to pier columns to reduce or eliminate form construction and removal, reinforcement assembly, and concrete curing time would have the largest impact on reducing construction time and costs while enhancing work-zone safety.

Several ABC bridge columns have been researched and developed to eliminate or reduce formwork and column reinforcement while using standard concrete. However, some of these methods also produced undesirable tradeoffs such as complicated column reinforcement assembly, large increases in material cost, and increased column weight. Previously researched column alternatives include, but are not limited to, concrete-filled steel tubes (CFSTs), concrete-filled fiber-reinforced polymer tubes (CFFTs), hollow-core concrete (HCC) columns, and hollow-core fiber-reinforced polymer tube-concrete-steel tube (HC-FCS) columns. The most promising, and least researched and developed, of these column alternatives are HC-FCS columns due to combining the benefits of other alternatives including significant concrete confinement, improved axial and flexural strength, and enhanced ductility and energy adsorption. HC-FCS columns consist of a concrete core sandwiched between an outer fiber-reinforced polymer tube and an inner steel tube. The fiber-reinforced polymer (FRP) and steel tubes function as stay-in-place forms, with the FRP also providing improved corrosion resistance compared to other column alternatives. The steel tube can be extended into the foundation and pier cap to create a moment connection and eliminate the need for column reinforcement and congested connections. In turn, the concrete core provides local buckling resistance to the FRP and steel tubes.

The benefits of using high-strength self-consolidating concrete (HS-SCC) and ultra-high-performance concrete (UHPC) instead of standard concrete in most applications are well known, including accelerated bridge construction (ABC). The benefits of HC-FCS columns with HS-SCC or UHPC, when compared to traditional reinforced concrete (RC) columns, are unknown but are understood to further reduce construction time, increase strength and ductility, and allow for thinner, lighter columns. These improved qualities would further elevate the benefit of using HC-FCS columns for ABC of bridge substructures. Design procedures and recommendations would need to be developed, or amended, for HC-FCS columns that utilize the proposed benefits of HS-SCC and UHPC.

1.2 Goals, Objectives, and Scope of Work

The main goal of this research project is to implement HC-FCS columns for accelerated bridge construction (ABC) in the State of Oklahoma by demonstrating enhanced performance compared to traditional spiral reinforced concrete (RC) columns and the additional cost/benefit

of using HS-SCC or UHPC for the concrete core. Additionally, another goal of this research project is to further the body of knowledge concerning the effectiveness and enhanced performance of HC-FCS columns and the benefits and applications associated with using HS-SCC and UHPC in place of normal concrete for the concrete core.

The main objective of this research project is to determine the improved column axial and flexural strength, ductility, and overall performance provided by HC-FCS columns when compared to traditional RC columns. Furthermore, the benefits of using HS-SCC and UHPC for the concrete core will be evaluated. Five half-scale column specimens will be constructed and consist of one RC column, two HC-FCS columns with HS-SCC used for the concrete core, and two HC-FCS columns with UHPC used for the concrete core. The testing results of the column specimens, including the lateral load versus displacement at the column head, the peak flexural capacities, and the strain gauge data will be analyzed and compared between HC-FCS column types and against the RC control column. The anticipated outcome of this research project is to evaluate the enhanced performance and properties of HC-FCS columns compared to traditional RC columns and the benefits of using HS-SCC and UHPC for the concrete core of HC-FCS columns.

To achieve the main objectives of this research project, the following scope of work was implemented:

- Research and review applicable literature.
- Develop a research strategy.
- Conceptualize column specimens and testing apparatus.
- Design, fabricate, and construct column testing frame.
- Design and layout each component of each column specimen type.
- Assemble each column component for each column specimen type.
- Construct and cast each column specimen’s reinforced concrete base and applicable column section.
- Rotate, place, and anchor each column specimen to the testing frame.
- Construct and cast each column specimen’s column cap.
- Assemble and attach lateral loading system and instrumentation and apply constant axial compressive load.

- Test each column specimen to maximum displacement and record data.
- Deconstruct and document damage to each column specimen after testing.
- Analyze results and perform a comparative analysis between the column types.
- Develop conclusions and recommendations.
- Document information obtained from this research study into a thesis.

1.3 Outline

This thesis is comprised of nine chapters and appendices. Chapter 1 introduces the background information relating to the benefits of using ABC techniques compared to traditional methods for bridge substructures, previously researched ABC column configurations, the need for additional research to implement HC-FCS columns with HS-SCC or UHPC used for the concrete core, and this research study's main goals, objectives, and scope of work. Chapter 2 is a review of the literature describing previous research studies conducted on the topic of different ABC column alternatives and configurations and the non-proprietary UHPC mix design that was developed at the University of Oklahoma. Chapter 3 details the development and design of the column specimen testing apparatus and the design and layout of each component of the column specimens. Chapter 4 presents the construction procedure and methods of each column type and the process of preparing a completed column specimen for testing. Chapter 5 describes the column testing procedure, the modifications to the testing frame and procedure following the initial column test and presents the results of each column test. Chapter 6 provides an analysis of the results obtained from the RC and HS-SCC HC-FCS column tests and a comparison of the behavior of the two HS-SCC column specimens. Chapter 7 provides an analysis of the results obtained from the UHPC HC-FCS column tests and a comparison of the behavior of the two UHPC column specimens. Chapter 8 provides a comparative analysis of the performance and behavior of the different column types that consisted of a comparison of the RC and HS-SCC HC-FCS columns and the HS-SCC and UHPC HC-FCS columns. Chapter 9 presents the findings, conclusions, and recommendations for future work. Finally, the appendix includes complete strain gauge plots at each location on each column specimen.

Chapter 2: Literature Review

This chapter presents a review of the literature describing previous research studies conducted on the topic of different ABC column alternatives and configurations and the non-proprietary UHPC mix design that was developed at the University of Oklahoma.

2.1 Column Alternatives

Concrete-filled steel tubes (CFSTs) are commonly used as bridge columns in Europe, Japan, and China. CFSTs have exceptional strength-to-weight ratios, less strength degradation than reinforced concrete sections, and more damping of the structural response than structural steel sections, which leads to superior seismic performance compared to traditional reinforced concrete or structural steel columns (Perea et al., 2014; He et al., 2019). This improved performance is due to the confining effect of the steel tube on the concrete core while the concrete core enhances the local and global buckling resistance of the steel tube. CFSTs also reduce construction time because the steel tube provides a stay-in-place form for the cast-in-place concrete and eliminates the need for supplemental reinforcement of the concrete core. CFSTs are also more resistant to fire than structural steel sections alone due to the insulation and thermal coefficient provided by the concrete core.

Fiber-reinforced polymer (FRP) tubes have been investigated as an alternative to the steel tubes used in CFSTs. Concrete-filled FRP tubes (CFFTs) offer many of the same benefits as CFSTs, at a significantly lower weight and with enhanced corrosion resistance. However, research has shown that without the addition of supplemental reinforcement of the concrete core, CFFTs have significantly lower strength and ductility compared to CFSTs (Zhu et at., 2006; Ozbakkaloglu, 2013; Zohrevand and Mirmiran, 2013; Ozbakkaloglu and Vincent, 2014).

Compared to solid concrete columns, hollow-core concrete columns provide a significant reduction in material usage, and therefore substructure weight and material costs, while still maintaining excellent strength and ductility for tall bridge piers. Mander et al. (1983) investigated square, hollow-core concrete columns with two layers of longitudinal and transverse reinforcement, including cross ties between the two layers, as shown in Figure 2-1. The applicable design code required cross ties in potential plastic hinge regions. The full-scale tests demonstrated excellent energy dissipation characteristics with negligible strength degradation

under cyclic loading, as shown in Figure 2-2. The columns also exceeded the predicted ultimate strength capacity, with failure instigated by spalling the outer and inner concrete cover, followed by fracturing of the transverse reinforcing steel hoops, and, finally, crushing the concrete. However, this performance must be weighed against the increased labor and material costs of the elaborate reinforcing cage construction.

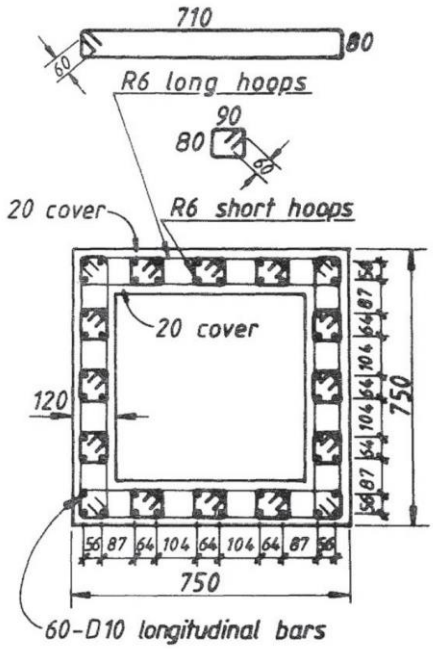

Figure 2-1: Hollow-Core Concrete Column with Two-Layers of Reinforcement and Cross Ties (Mander et al., 1983) (Dimensions in mm)

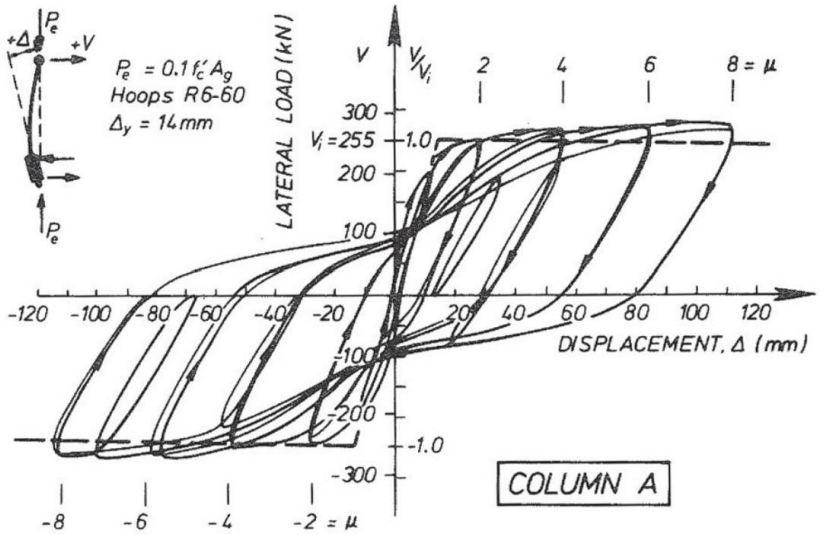

Figure 2-2: Load-Displacement Response of Hollow-Core Concrete Column with Two Layers of Reinforcement and Cross Ties (Mander et al., 1983)

Several researchers have investigated hollow-core concrete columns with a single layer of longitudinal and transverse reinforcement placed near the outer wall to reduce the costs and complexity of the double-layer reinforcing cage system (Zahn et al., 1990; Hoshikuma and Priestley, 2000; Ranzo and Priestley, 2001). One of the specimens tested by Hoshikuma and Priestley (2000) is shown in Figure 2-3. As discussed by the researchers and shown in Figure 2-4, these specimens can exhibit limited ductility for a restricted range of axial load, wall thickness-to-section diameter ratio, and longitudinal reinforcement ratio. However, for most applications, the single-layer system provides less than 50% of the strength and ductility of the double-layer system, with premature failure caused by spalling of the concrete on the inner surface due to lack of confinement.

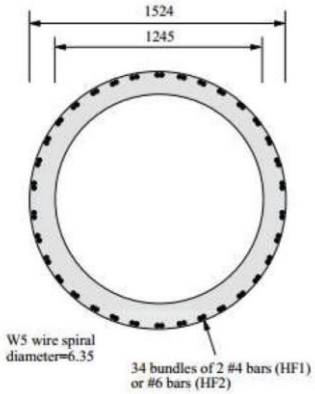

Figure 2-3: Hollow-Core Concrete Column with One Layer of Reinforcement (Hoshikuma and Priestley, 2000) (Dimensions in mm)

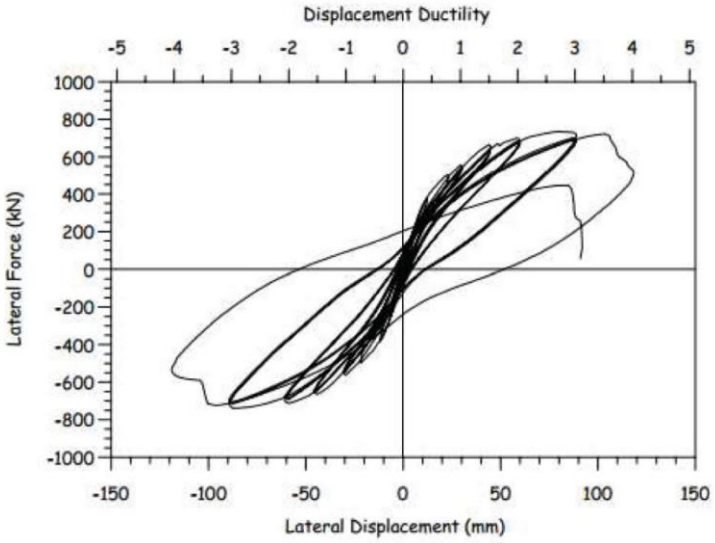

Figure 2-4: Load-Displacement Response of Hollow-Core Concrete Column with One Layer of Reinforcement (Hoshikuma and Priestley, 2000)

Montague (1978) developed the concept of a double-skinned, composite cylindrical shell using an inner and outer layer of sheet metal bonded together with an epoxy resin and glass filler. Building on that concept, designers and researchers developed bridge columns constructed with two concentric steel tubes infilled with concrete (Shakir-Khali and Illouli, 1987; Yagishita, 2000). This system combined the benefits of CFSTs with the benefits of hollow-core concrete columns; it also eliminated the need for a reinforcing cage for the concrete infill. The inner and outer steel tubes provide the necessary confinement of the concrete core without the cost and complexity of an elaborate double-layer reinforcing cage. The steel tubes also provide stay-in-place forms for the concrete, further reducing costs. Teng et al. (2004) refined this concept by replacing the outer steel tube with an FRP tube to develop the concept of hollow-core FRP-concrete-steel columns (HC-FCS). The outer FRP tube still provides the necessary confinement of the concrete core, while also significantly improving the corrosion resistance and durability of the system.

Several researchers have investigated HC-FCS columns under a variety of loading conditions, including axial compression, bending, combined axial compression and bending, and combined axial compression and lateral cyclic loading (Yu et al., 2006; Teng et al., 2007; Han et al., 2010; Lu et al., 2010; Zhang et al., 2012; Abdelkarim and ElGawady, 2014; Li et al., 2014; Ozbakkaloglu and Idris, 2014; Albitar et al., 2015). In general, the results showed significant concrete confinement, improved axial and flexural strength, and enhanced ductility and energy absorption compared to solid reinforced concrete, hollow-core reinforced concrete, and CFST columns. This improved response is shown in Figure 2-5, which illustrates the improved confinement, and in Figure 2-6, which shows the improved ductility and lateral cyclic load performance.

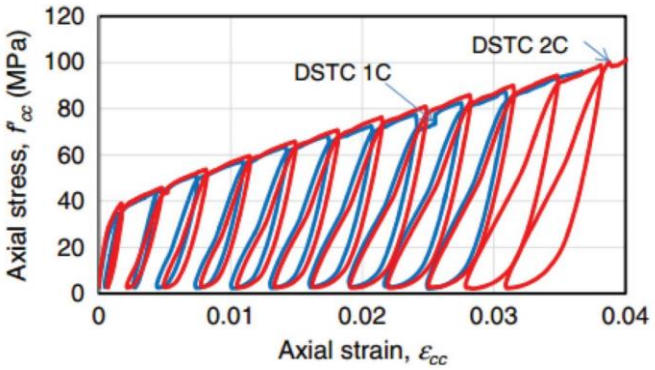

Figure 2-5: Axial Strain-Axial Stress Relationship of HC-FCS Column (Albitar et al., 2013)

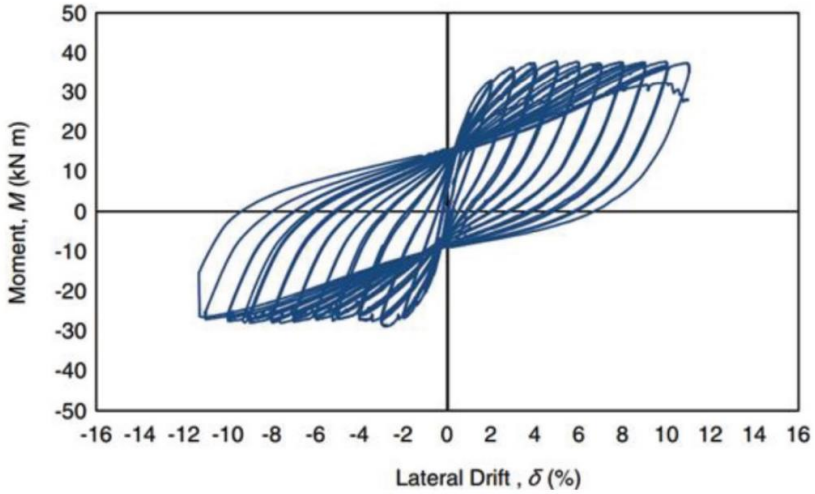

Figure 2-6: Moment-Lateral Drift Relationship of HC-FCS Column (Ozbakkaloglu and Idris, 2014)

The next logical step in the evolution of this column system is to investigate both high-strength self-consolidating concrete (HS-SCC) and ultra-high-performance concrete (UHPC) for the concrete core due to a range of enhanced properties offered by each respective concrete.

2.2 Concrete Alternatives

HS-SCC and UHPC offer a wide range of improvements over standard concrete. Both HS-SCC and UHPC flow and consolidate under their own weight, without the need for external vibration. This reduces labor costs, improves placement speed, minimizes void potential, improves consolidation in congested and hard-to-reach areas, improves pumpability, and reduces construction noise. Additionally, the enhanced material properties of high-strength SCC and UHPC will further improve the strength, ductility, corrosion resistance, and durability of this

column system or allow a reduction in the concrete core thickness to further reduce material costs and overall column weight.

McDaniel (2017) and Looney et al. (2019) investigated multiple series of mix designs examining particle packing, cementitious material reactivity, and mix designs developed in previous research to identify an optimal UHPC mix design using materials locally available in Oklahoma. This research resulted in three primary mix designs, shown in Table 2-1, that focused on slag cement, fly ash, or Type III cement, respectively, along with Type I Portland cement. These three mix designs were then subjected to testing with steel fibers and different heat curing regimens. The mix design with the best performance in the material properties study, shown as UHPC 2 in Table 2-1 and J3 in Figure 2-7, utilized slag cement and silica fume as the primary supplementary cementitious materials, with 2% steel fibers by volume.

Table 2-1: Final UHPC Mix Designs Evaluated by Looney et al. (2019)

Material	UHPC 1	UHPC 2	UHPC 3
Type I Cement, lb	1179.6	1179.6	786.4
Type III Cement, lb	0	0	196.6
Fly Ash, lb	294.9	0	0
GGBFS, lb	0	589.8	786.4
Silica Fume, lb	196.6	196.6	196.6
VCAS™, lb	294.9	0	0
w/cm	0.2	0.2	0.2
Masonry Sand, lb	1966	1966	1966
Steel Fibers, lb	255.2	255.2	255.2
HRWR, oz/cwt	15.77	15.77	14.88

This mix design was then subjected to extensive material evaluation by Dyachkova (2020) and Campos (2020) with varying fiber content. Adequate flowability was achieved for mixes with up to 4% steel fibers by volume, after which a significant loss of flowability was observed. The variation of compressive strength without the aid of heat curing is shown in Figure 2-7, which indicates that the addition of steel fibers has a minor influence on compressive strength, with a range of 17,000 psi to 18,000 psi at 56 days of age. All mixes achieved approximately 12,000 psi at 3 days of age and higher compressive strengths when heat cured. Figure 2-8 shows the results of flexural tensile strength and splitting tensile strength testing conducted by Dyachkova (2020) and direct tensile testing conducted by Campos (2020).

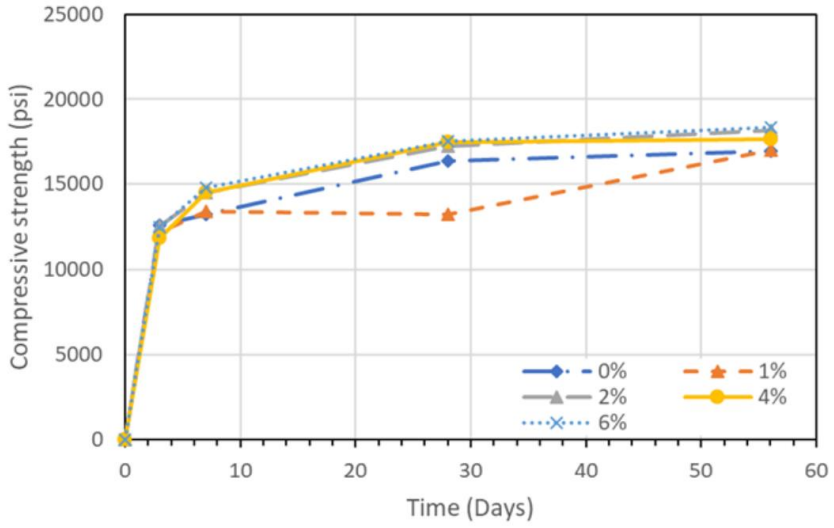

Figure 2-7: Compressive Strength Results for J3 with Different Steel Fiber Contents and No Heat Curing (Dyachkova, 2020; Campos, 2020)

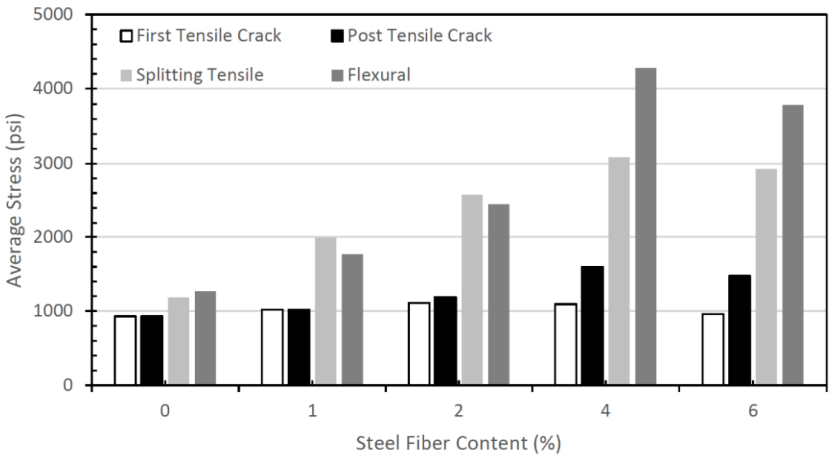

Figure 2-8: Comparison of Direct and Indirect Tension Test Results for OU J3 UHPC (Dyachkova, 2020; Campos, 2020)

As expected, the indirect tensile strengths exceeded the direct tensile strength, but, with any addition of steel fibers, the UHPC was able to provide post-cracking strength, with values exceeding 1,100 psi for specimens with 2% or more steel fibers by volume. Campos (2020) also developed regression models to predict the direct tensile strength of UHPC using compressive strength and results from indirect tensile tests. The conclusion of these research projects shows that UHPC is superior to traditional concrete, ODOT Class AA in this case, but due to the associated high material cost and more intensive formwork requirements, UHPC should be used selectively to render the best cost/benefit ratio.

Chapter 3: Testing Apparatus and Specimen Design

The column testing frame was designed, fabricated, and assembled to meet the needs and limitations presented by the strong floor at the Donald G. Fears Structural Laboratory at the University of Oklahoma. Additionally, five column specimens were designed including one conventional reinforced concrete (RC) column control specimen and four hollow-core fiber-reinforced polymer tube-concrete core-steel tube (HC-FCS) columns. Each component of the column specimens was designed using design codes, standards, recommendations from previous research, and engineering judgment.

3.1 Column Testing Frame Design

3.1.1 Testing Frame Conceptual Layout

The strong floor consisted of large steel I-shaped girders that were embedded within a concrete mat. The top flanges were left exposed with a predetermined and drilled bolt-hole pattern. Each flange was approximately one foot wide with girders spaced at approximately eight feet from center to center. Due to the strong floor arrangement and previous testing by Missouri University of Science and Technology (Missouri S&T), it was determined that column test specimens would consist of a large concrete base with an embedded column protruding and a concrete column cap on top that would be tested laying horizontally as opposed to vertically. Testing column specimens horizontally presented a significant challenge given the need for a fixed-moment connection, expected large loads, column complexity, and limited space and arrangement on the lab's strong floor.

A design was developed that would span three of the four available strong floor beams using steel I-shaped girders held in place by triangular braces. The column testing frame layout allowed for a fixed-moment connection that redistributed the imposed moment and shear produced by the column being loaded at the column cap, with the column itself acting as a lever arm, along the span of the testing frame and out to the triangular anchoring braces. This effectively reduced the bending forces applied to the braces and the shear forces imposed on the bolted connections to the strong floor. The resulting layout is shown in Figure 3-1 and Figure 3-2 Additionally, the loading apparatus consisted of a steel I-shaped girder running perpendicular to the strong floor girders with a smaller triangular brace bolted on top. The floor beam distributed

the applied load between the three strong floor beams and supported large, solid steel rollers that would support the column cap and limit vertical deflections that would lead to torsion in the column and potential damage to the loading mechanism. The smaller triangular brace served to mount the hydraulic actuator and load cell that would be used to displace the column and measure the corresponding load.

3.1.2 Testing Frame Design Overview

The column testing frame was designed using RISA-2D structural analysis software and in general accordance with the AISC 15th edition Steel Construction Manual using the Load Factor and Resistance Design (LRFD) method. Structural members were sized sequentially by following the load transfer path from the column specimen to the strong floor connection by first modeling the member and applicable determined loads in RISA-2D and then selecting the member size from the Steel Construction Manual. All structural members were assumed to be ASTM 572 Gr. 50 steel with a 50 ksi yield stress. Connection layouts, welds, and bolt sizes were conservatively decided according to efficiency, limitations, and engineering judgment. All welds were assumed to be 1/4-inch minimum fillet welds.

3.1.3 Main Structural Member Design

Due to simple and controlled loading, the applied load at the column cap was conservatively chosen to be 150,000 pounds or 150 kips with no load factors from load combinations. This estimate was based on previous research by Abdelkarim and ElGawady (2014) at Missouri S&T and engineering judgment. The loading point and resulting moment arm were taken as 132” or 11 feet from the bottom of the column base at the connection with the testing frame. The assumed load and location resulted in a design moment of 1650 foot-kips. A minimum of two members in strong axis bending were chosen to function as the main part of the frame. After analysis and checks for lateral torsional buckling, W24x68 beams were selected using Section 3-19 and Table 3-10. Stiffeners were placed in each beam at critical load or connection points and designed with guidance from the AISC manual. The stiffeners were chosen to be ½-inch thick, full-depth stiffeners extending to the flanges' edges. The W24x68 beams were braced and connected by three W18x35 beams at quarter points with L3x3x¼ angles. The angles were welded to the web of the W24x68 sections and bolted with ASTM A325 ¾” diameter bolts.

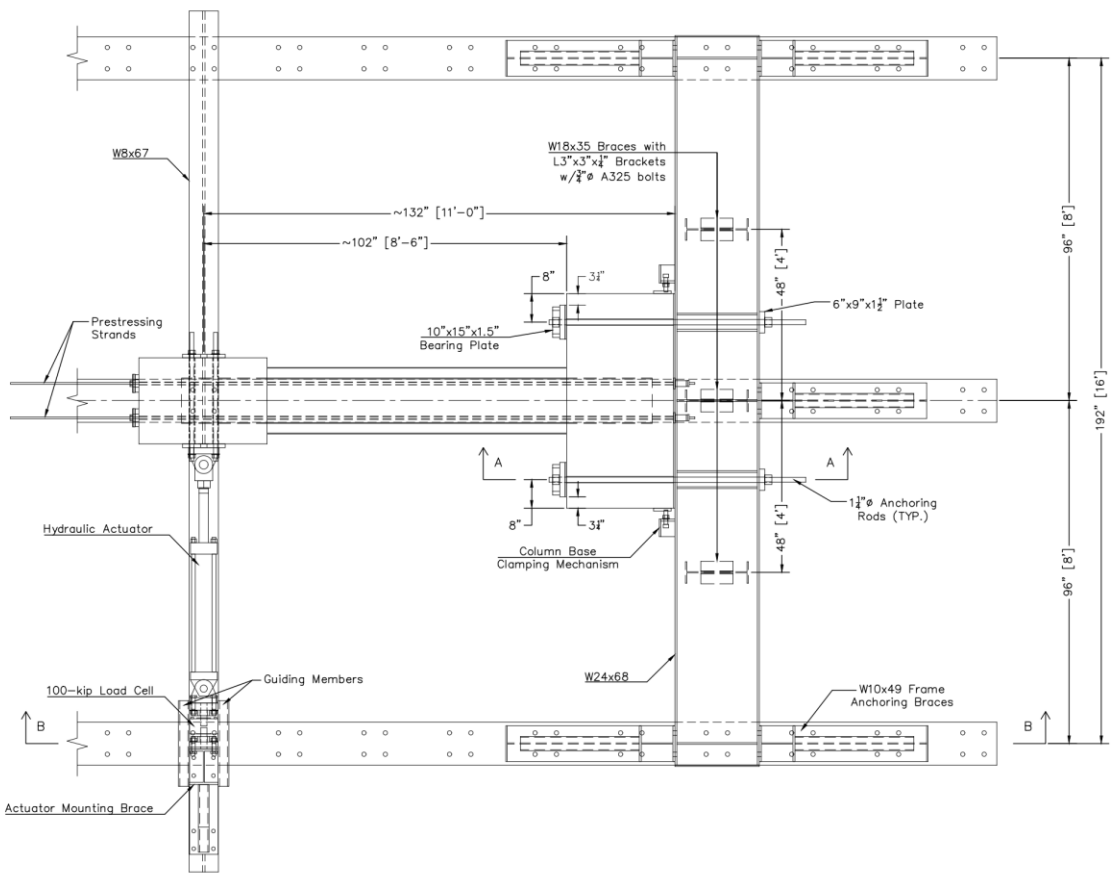

Figure 3-1: Column Testing Frame Layout

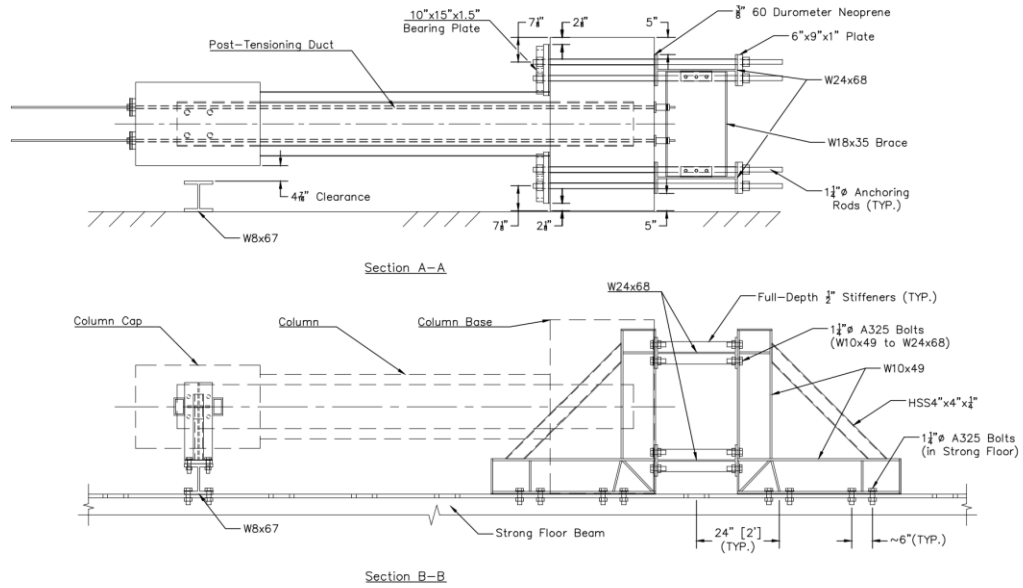

Figure 3-2: Column Testing Frame Sections A and B

3.1.4 Fixed-Moment Connection & Steel Anchor Rod Design

The column specimen was designed to be connected to the testing frame by creating a fixed-moment connection with large threaded steel rods that passed through the column base and W24x68 beam with bearing plates and nuts on either end of each rod. The bearing plates were designed to evenly distribute the load across the concrete base to not crush the concrete. Sixty durometer neoprene pads were also placed between the bearing plates and concrete base, as well as between the concrete base and the steel testing frame, to account for surface irregularities in the concrete finish. Two anchor rods at each corner were chosen to reduce torsional effects on the W24x68 beams and to distribute the applied tension and shear loads. The steel rods were placed 8 inches from the extreme face in the direction of loading. This was done to reduce the applied prying force and to provide sufficient cover and confinement against tear-out. The applied tension force was determined to be 450 kips distributed across four steel anchor rods opposite the direction of the applied load. This resulted in 150 ksi high-strength steel 1.25-inch diameter threaded steel rods designed to resist 112.5 kips each.

The column base was braced against lateral movement by steel clamping mechanisms that mitigated the applied shear force to the steel anchoring rods. The steel clamping mechanism consisted of a WT-shaped section cut from a W10x43 with a stiffener cap plate. Additionally, 1-inch machine bolts, nuts, and steel plates were used to bear against the side of the concrete base and restrict lateral movement. The WT-shaped sections were designed to resist the applied bending moment caused by the shear load at the interface connection from the applied load at the column cap. The machine bolts were checked for the tension capacity of the threads due to the applied axial load. Two clamping mechanisms, each containing two bolts and nuts, were welded to the top flange of the W24x68 beams.

3.1.5 Strong Floor Anchoring Braces Design

The triangular anchor braces were designed to resist applied axial loads from the W24x68 beams and transmit the load to the strong floor. Pairs of braces were placed at each end of the frame with an additional fifth brace placed in the middle behind the location of the column base connection. The middle brace provided additional stiffness and further limited frame deflection. Each anchor brace consisted of a vertical, horizontal, and diagonal structural member. The vertical and horizontal members were chosen to be I-shaped steel sections due to ease of

connection and utilization of strong axis bending. The diagonal member was selected to be a square hollow steel section (HSS) for ease of welding and equal strength for both axes of bending.

After modeling each brace in RISA-2D, assuming that only one brace on each side of the frame was in use during loading, Section 3-19, and Table 3-10 from the AISC manual were used to size each structural member. The vertical and horizontal members were chosen to be W10x49 beams. The wide flanges allowed for easy connection to the W24x68 beams and to the strong floor with four bolt-hole patterns. The diagonal brace was selected to be an HSS4x4x¼ section that provided sufficient bending capacity and perimeter for welding. Stiffeners were placed in each W10x49 beam at critical load or connection points and designed with guidance from the AISC manual. The stiffeners were chosen to be ½-inch thick, full-depth stiffeners extending to the flanges' edges. End caps were also added for additional stiffness and safety. Due to limitations presented by the existing bolting pattern in the strong floor beam flanges, the bolts' location, size, and spacing between the anchoring brace and the strong floor were predetermined. Each anchoring brace was held in place by two bolt groups of four ASTM A325 1¼-inch bolts. The bolts were checked for applied shear force, tension force from prying action, and bearing and tear-out according to Table J3.2 and found to be more than sufficient.

3.1.6 Column Cap Support Member & Loading System Design

The actuator member underneath the column cap that supported the column cap and hydraulic actuator during testing was designed to resist the bending moment transferred to it by the hydraulic jack at some distance above the beam. A reduced profile was required to maintain clearance underneath the column cap while also providing enough flange width to mount to the floor and support the actuator mounting brace. The lever arm was taken to be 20.5 inches and the assumed moment was found to be 256.25 foot-kips. A W8x67 was selected to resist the applied moment and checked for lateral torsional buckling using Section 3-19 and Table 3-10.

A 75-kip linear hydraulic actuator with a stroke of 28 inches was supported and mounted with a brace of similar design and construction to the frame anchoring braces. A W10x43 was chosen for the vertical member and an HSS 3x3x⅜ was selected for the diagonal member. Both were checked for axial and bending capacity by using a RISA-2D model. Each member was securely welded to a 1-inch-thick, 8-inch-wide steel plate. Due to poor weld penetration that

resulted in a failed weld during testing, the initial HSS was replaced with an HSS5x3x⅜ to provide additional weld perimeter.

The 100-kip Interface load cell was attached by a steel adapter plate consisting of a thick steel plate with a threaded hole through the center, a four-hole bolt pattern aligned with the corners, and a system of vertical stiffeners in a tic-tac-toe formation. The plate thickness was sized to resist tear-out from the threaded steel rod coming from the load cell and the stiffeners were added to reduce the bending moment experienced by the plate when the plate was subject to tension. After yielding the one-through steel rod design, the loading system and load cell mounting were updated to consist of two steel adapter plates with HSS members used as guides. This was done to move the load cell to the opposite end of the hydraulic jack and the guides prevented rotation of the assembly.

3.2 Column Specimen Design

Hollow-core fiber-reinforced polymer tube-concrete-steel tube (HC-FCS) columns consist of a concrete core sandwiched between an outer fiber-reinforced polymer (FRP) tube and an inner steel tube. The steel tube would generally be embedded in the foundation and supported substructure while the FRP tube is not. The concrete core can be either monolithic with the foundation or cast separately. Similarly, conventional spiral-reinforced concrete (RC) columns consist of longitudinal reinforcement with lap splices to reinforcement cast within and extending from the foundation. The longitudinal reinforcement also extends into the bridge pier cap for continuity. The surrounding concrete can also be monolithic with the foundation or cast separately. To accurately represent an in-service bridge column, a column testing specimen would require a fixed-moment connection at its base to represent fixity and continuity with the foundation and a free-end at the top representing the supported bridge pier cap. Additionally, to better emulate real-world conditions and behavior, the test specimen would need to be under an axial compressive load to simulate the dead load presented by the weight of the bridge that the column would be supporting. Each in-service condition must be considered and accounted for to design, construct, and test a representative column specimen. The design, construction, and testing setup are outlined in this section.

3.2.1 Column Conceptual Design & Layout

The column test specimens were preliminarily conceptualized based on previous research by Abdelkarim and ElGawady (2014) at Missouri S&T. The concrete column base dimensions were initially chosen to be 60 inches long, 48 inches wide, and 36 inches tall, with the long dimension in the direction of loading, while the column itself would nominally be 24 inches in diameter with a 30-inch long, 30-inch wide, and 36-inch-tall concrete column cap. These dimensions were chosen to reflect previously tested column configurations and match commercially available prebuilt formwork dimensions. During the design of the column testing frame, the width of the column base was increased to 50 inches due to the frame layout and to increase the concrete cover around the anchoring rods. Additionally, the column base height was reduced to 30 inches, the nominal column diameter was reduced to 18 inches, and the column cap was reduced to decrease the overall height and weight of the column specimens such that they could be moved by the overhead bridge crane at Fears Lab. The column length was chosen to be 84 inches or 7 feet, to facilitate easier sourcing of the FRP tube and to align well with the limitations presented by the loading system. Thus, the applied cyclic lateral displacement-controlled load was applied at 102 inches or 8.5 feet from the top of the column base. The final column specimen dimensions and layout are shown in Figure 3-3. Each specimen was constructed by first preparing, assembling, and casting the concrete column base with an embedded steel tube or spiral-reinforced rebar cage. Next, the column was assembled and cast, and the specimen was moved into the testing frame. Lastly, the concrete column cap was assembled and cast with the specimen in place for testing due to the limited load capacity and lifting capabilities of the facility's crane.

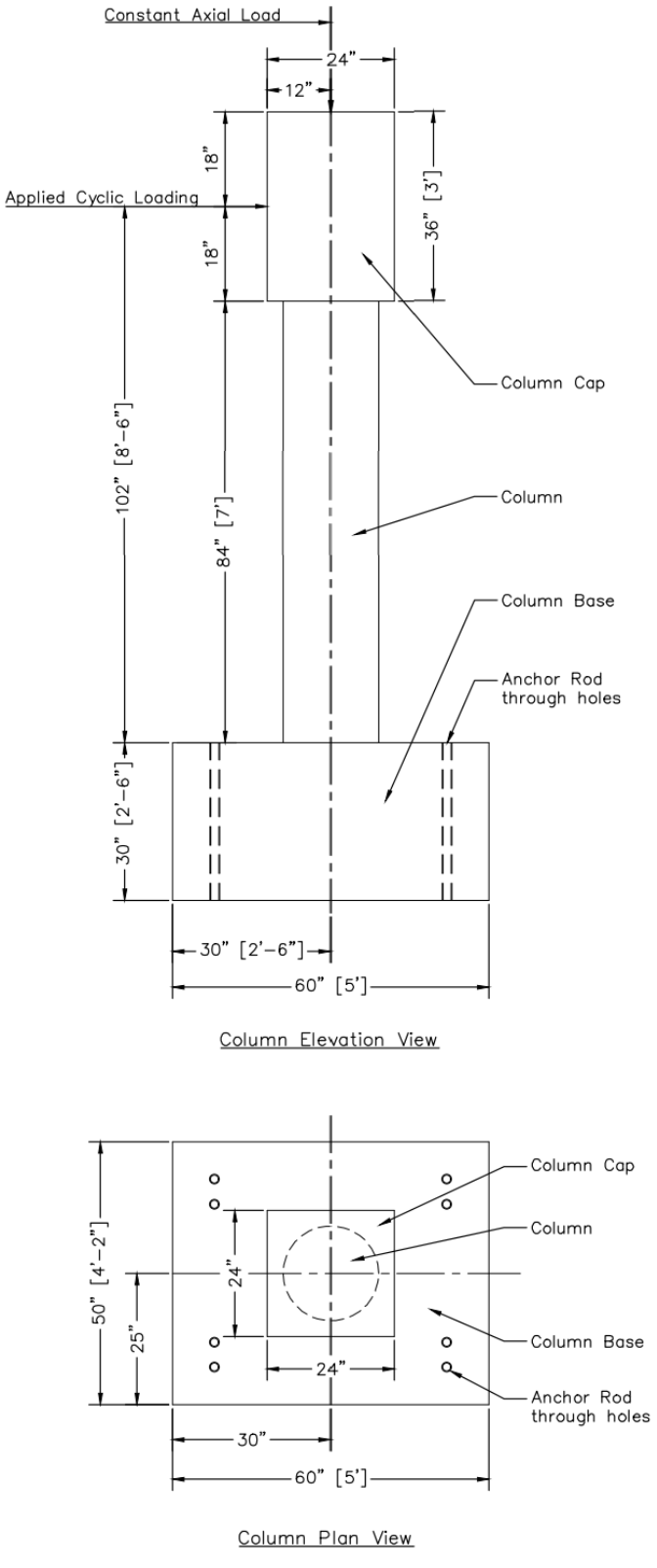

Figure 3-3: Column Specimen General Layout

3.2.2 Column Base Design & Layout

The concrete column base was designed to function as a fixed-moment connection for the column specimens, transferring the required overturning and shear forces from the columns to the supporting steel frame. The design of the reinforced concrete base of the column specimens followed both a traditional Euler-Bernoulli beam analysis and a strut and tie modeling approach. Initially, a traditional beam analysis was used to determine the flexural and shear reinforcement to resist the overturning moment at the base of the columns. This approach ensured strain compatibility between the subsequent strut and tie model and the elastic strains.

For the strut and tie analysis, the overturning moment was converted to a force couple centered at the locations of the high-strength steel anchoring rods that connect the base to the steel frame. A simple truss consisting of a horizontal tension member and a diagonal compression strut, shown in Figure 3-4, formed the basis of the analysis. The strut and tie analysis confirmed that the flexural reinforcement from the traditional analysis was sufficient. However, due to the span-to-depth ratio of the base, additional horizontal tie reinforcement was needed for shear friction. The strut and tie analysis also indicated a minimum size for the bearing plates at the location of the high-strength rods to satisfy the compression stresses at the primary CCT node.

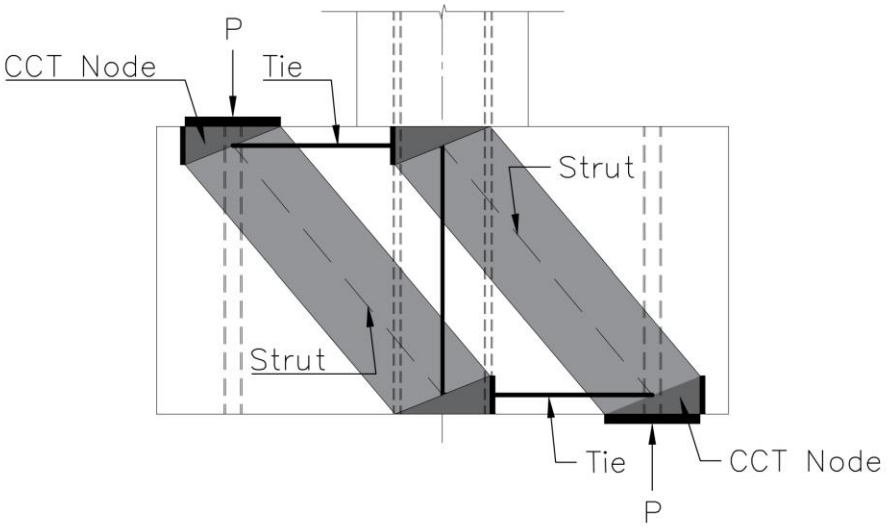

Figure 3-4: Column Base Strut and Tie Model

The required concrete strength was taken as 6000 psi and the reinforcement was taken as Gr. 60 steel rebar with an assumed minimum yield stress of 60 ksi. The concrete mix design was provided by Dolese Bros. Co. and is outlined in Section 4.1.2. The resulting reinforcement consisted of 20, ACI 17 bar bend, No. 8 longitudinal bars, 10 on top and 10 on bottom at equal spacing, 24, ACI S3 bar bend, No. 4 vertical stirrups in pairs along the base width, 12 pairs on each side of the column at equal spacing, and 16, ACI T9 bar bend, No. 4 horizontal stirrups along the base length, 8 on each side at equal spacing. Each bent bar corresponds to a standardized shape, bend radius, hook type, and length in ACI 315 Details and Detailing of Concrete Reinforcement (2018). The layout of the reinforcement was adjusted to accommodate the concrete base containing eight through holes for the steel anchoring rods and the embedded steel tube or spiral-reinforced cage. The resulting layout is shown in below Figure 3-5.

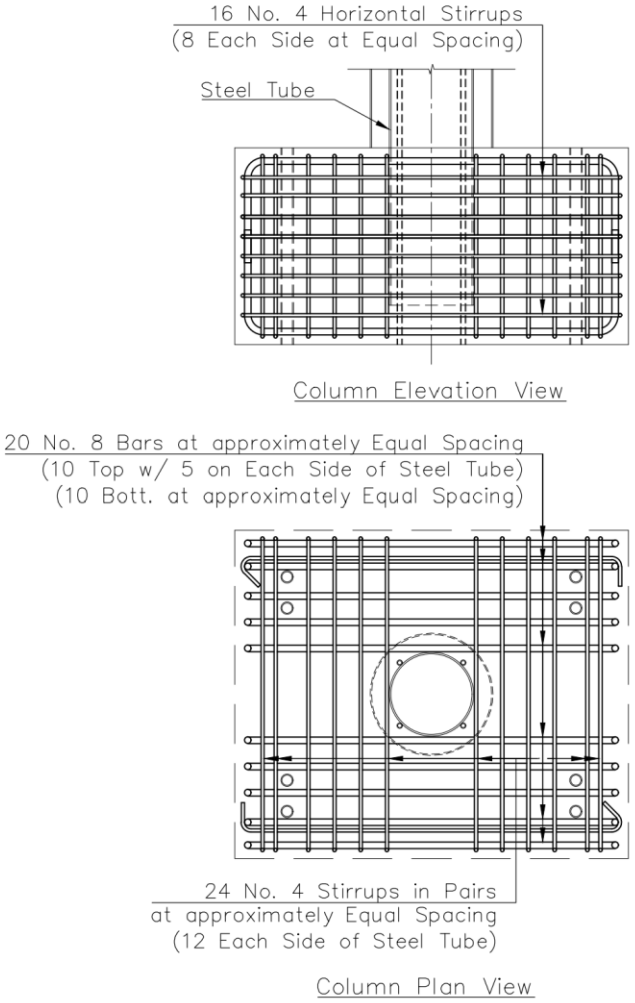

Figure 3-5: Column Base Reinforcement and Layout

3.2.3 Conventional RC Column Design & Layout

The conventional spiral-reinforced concrete (RC) column was designed per ACI 318 Building Code Requirements for Structural Concrete specifications, AASHTO LRFD Bridge Design Standards (2020), and the ODOT Bridge Directives (2017). The column diameter was 18 inches and was formed using an 18-inch diameter Sonotube. Column reinforcement was provided by a continuous, embedded spiral-tied rebar cage. Longitudinal reinforcement was determined from the AASHTO minimum required area of reinforcement of 1% of the gross column area. A gross column area of 254.5 square inches yielded a minimum required area of reinforcement of 2.54 square inches. To better emulate the performance of the steel tube, and evenly distribute the reinforcement across the cross-section, 8 bars were used with a bar at each primary axis and halfway in between each primary axis. Eight, ACI 18 bar bend, No. 6, Gr. 60 bars were used and provided a total longitudinal reinforcement area of 3.52 square inches (1.38%).

The transverse spiral tie was a No. 4 at a 3-inch pitch as opposed to the ACI 318 code recommendation of a No. 3 tie and a conventional pitch of 6 inches. The concrete cover to the outside of the longitudinal bar and transverse spiral tie was 1.25 inches and 0.75 inches, respectively. Half of the code required concrete cover to the ties was used due to the column being half-scale. The spiral tie had one and a half flat turns at the top and bottom per AASHTO specifications. The transverse spiral tie and longitudinal reinforcing extended to the same depth of embedment as the steel tube to provide a closer comparison of the behavior of the two different column types. Additionally, the reinforcing cage was placed and cast into the concrete column base in the same manner as the steel tube, therefore no lap splices were used. This configuration and cross-sectional layout are shown in Figure 3-6.

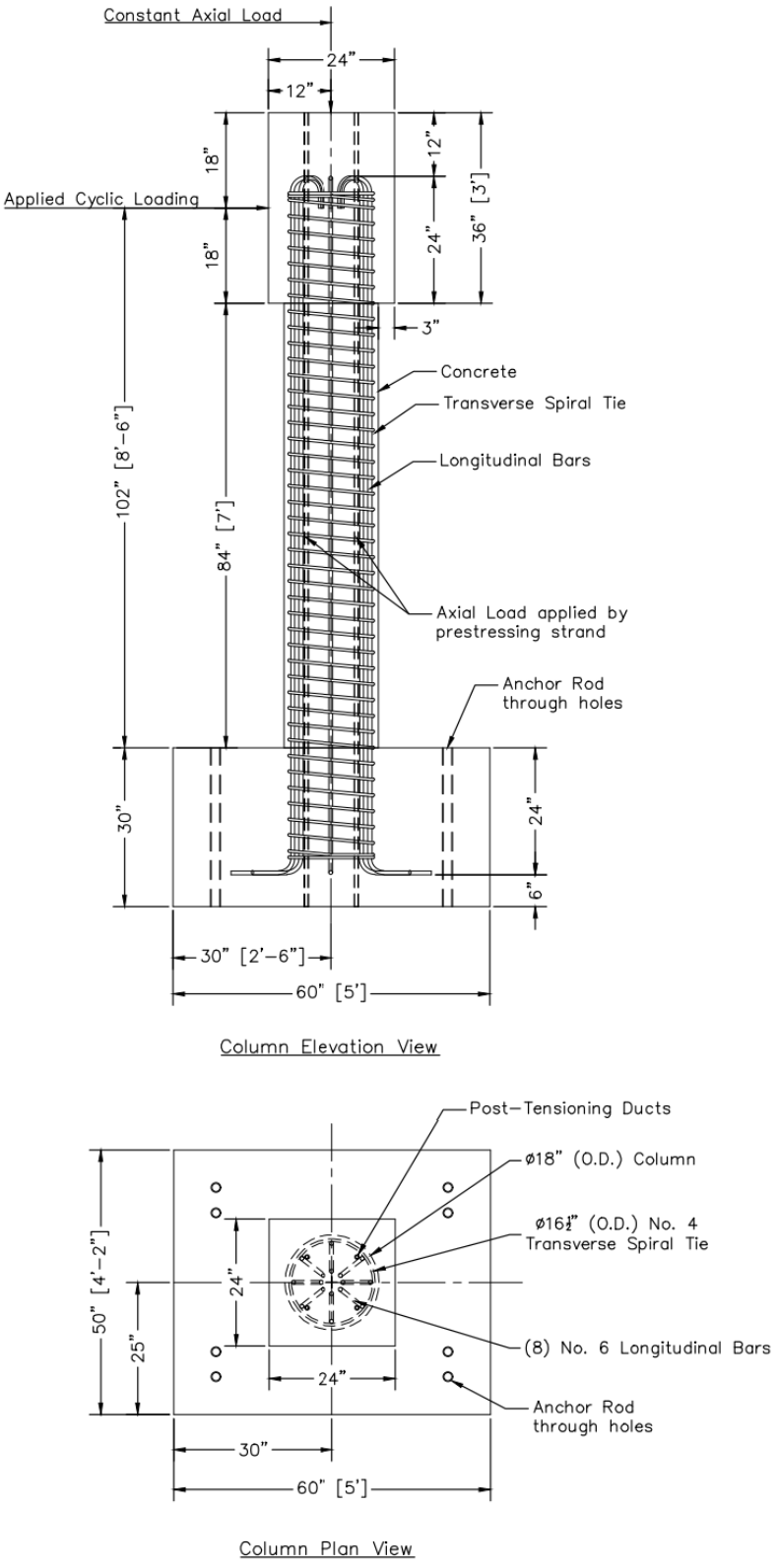

Figure 3-6: Conventional RC Column Layout

Each column was subjected to an axial compressive load of approximately 5% to 10% of the RC control column's nominal capacity based on AASHTO. The applied axial load was determined to be approximately 79 kips, assuming a concrete strength of 6000 psi. This load was applied through a series of post-tensioned, unbonded, prestressing strands running through PVC pipes along the length of the column specimens. The post-tensioning was anchored outside of the column base and cap. Four, 0.5-inch special, 7-wire, Gr. 270 prestressing strands with a specified ultimate tensile strength of 270 ksi were used to distribute the applied axial compressive load. Each strand would be post-tensioned to 21 kips, or approximately 127 ksi, to account for short-term prestress losses and to ensure an applied load of at least 5%. The post-tensioning ducts were placed alongside the longitudinal reinforcement and were rotated 45 degrees from the primary axes to prevent effects on the performance of the concrete core caused by the PVC pipe reducing the concrete cross-section.

A concrete mix design for the conventional RC column was developed following guidance for Class A concrete detailed in the Oklahoma Department of Transportation (ODOT) 2019 Standard Specifications for Highway Construction. In Section 701.01 Mix Design and Proportioning, Table 701:1 Concrete Classes, ODOT specifies material proportions and properties for Class A concrete that is used for pavement and substructure construction. Table 3-1 summarizes ODOT Class A concrete requirements.

Table 3-1: ODOT Class A Mix Design Requirements

Minimum Cement Content	517 lb/yd^3
Air Content	6 ±1.5%
Water/Cement Ratio	0.25 - 0.48
Slump	2 ±1 in.
Min. 28-day Compressive Strength	3000 psi

ODOT specifies in Table 701:1 to “ensure the slump reflects a workability appropriate for the application”, therefore the target slump was increased with a high-range water-reducing (HRWR) admixture to 8 inches to promote workability. Additional workability can also be achieved by substituting some of the Portland cement with fly ash, at the cost of slower strength gain. According to Table 701:2, the maximum percent by weight that fly ash can be substituted for Portland cement is 20%. This substitution helped increase the slump of the concrete without

adding additional water or HRWR. Furthermore, typical ODOT Class A mix designs utilize #57 stone, or 1-inch nominal, aggregate. Due to the limitations presented by the limited concrete cover to the reinforcement cage and concerns of potential voiding and decreased flowability, a 5/8-inch nominal aggregate was used instead. This aggregate size is representative of approximately half the typical nominal aggregate size used, which aligns with the half-scaled specimen. The reduced aggregate size increased flowability and thus reduced voiding and honeycombing potential while ensuring adequate concrete cover. The developed mix design is shown in Table 3-2 and Table 3-3.

Table 3-2: ODOT Class A Mix Design Properties

Water/Cementitious Material Ratio	0.48
Fly Ash Replacement (by Mass)	20.0%
Volume of Fine Aggregate	50.0%
Design Air Content	7.0%
Design Slump	8 in.
Target Strength Minimum	3000 psi

Table 3-3: ODOT Class A Mix Design Proportions

Type I/II Cement	414.0 lb/yd^3
Class C Fly Ash	103.0 lb/yd^3
Fine Aggregate	1536.0 lb/yd^3
Coarse Aggregate	1536.0 lb/yd^3
Water	248.0 lb/yd^3
Air-Entrainer, MB-AE 90	0.2 fl. oz/cwt
HRWR, Glenium 7920	4.0 fl. oz/cwt

3.2.4 HC-FCS Column Design & Layout

HC-FCS columns consist of three distinct layers that act together to form a composite system. The outer FRP tube confines the concrete core while also functioning as stay-in-place formwork. The concrete core supports the applied axial load while also confining the steel tube and increasing its buckling capacity. The steel tube provides bending resistance and some axial capacity, continuity with the foundation through embedment, and also functions as stay-in-place

formwork. All HC-FCS columns did not contain any shear or flexure reinforcement other than the steel tube, which remained hollow on the inside other than embedment at each end.

The FRP tubes were selected to be high-performance glass fiber-reinforced polymer (GFRP) commercial water line pipes with a nominal 40 ksi hoop stress strength. The steel tubes were API 5L PSL 2 grade X52M commercial water line pipe with a theoretical minimum yield stress of 52.2 ksi and mill test certified average yield stress of 65.3 ksi. All properties for the FRP and steel tubes were based on the manufacturers' provided data sheets. The concrete core consisted of either high-strength self-consolidating concrete (HS-SCC) with a 28-day compressive strength of 10 ksi or ultra-high-performance concrete (UHPC) with a 28-day compressive strength of 18-20 ksi. Dimensions of each component including diameters and thicknesses were determined from procedures derived from recommendations of previous research studies (Teng et al., 2007; Lu et al., 2010; Zhang et al., 2012; Abdelkarim and ElGawady, 2014; Ozbakkaloglu and Idris, 2014; Albitar et al., 2015):

a. Initial outer diameter (D_o) of the column
b. Minimum concrete wall thickness (t_c) based on the following relationship:

$$t_c = 0.15D_o$$

c. Steel tube outer diameter (D_i) based on the following relationship:

$$D_i = D_o - 2t_c$$

d. Steel tube thickness (t_s) based on the following relationship (higher end of the range prevents local buckling of steel tube alone subjected to compressive stresses):

$$t_s = D_i/64 \text{ to } D_i/32$$

e. FRP tube thickness (t_f) based on the following relationship (where f'_c is the unconfined concrete compressive strength of the core and f_t is the ultimate hoop tensile strength of the FRP tube):

$$t_f = 0.035D_o f'_c/f_t \text{ (for low seismic regions)}$$
$$t_f = 0.105D_o f'_c/f_t \text{ (for high seismic regions)}$$

The initial outer diameter (D_o) of the column was taken as 18 inches to represent half-scale specimens. This resulted in a minimum concrete wall thickness (t_c) of 2.7 inches, or approximately 3 inches. Next, the steel tube's outer diameter (D_i) was determined to be 12 inches. The steel tube's recommended thickness (t_s) was within the range of 3/16 and 3/8 inches,

with a mean recommended thickness of approximately 1/4 inch. Lastly, the FRP tube's thickness (t_f) was determined to be between 0.105 and 0.315 inches when using the unconfined concrete compressive strength of the HS-SCC at 10 ksi. Oklahoma is considered a low seismic region, therefore the FRP tube's thickness should be greater than 0.105 inches.

FRP and steel tube diameter and thickness combinations presented some limitations, therefore recommended diameters and thicknesses were adjusted to match commercially available products. The FRP tubes were selected with an inner diameter of 18.25 inches, an outer diameter of 18.625 inches, and a 3/16-inch wall thickness. The inner liner was removed, and additional exterior wraps were added to increase the design hoop stress strength to a nominal 40 ksi, subsequently increasing the tube's thickness. The steel tubes were chosen to have an outer diameter of 12.75 inches, an inner diameter of 12.25 inches, and a 1/4-inch wall thickness. This configuration resulted in a concrete core thickness of 2.75 inches, very close to the recommended 2.7 inches. The resulting configuration and cross-sectional layout are shown in Figure 3-7.

Based on previous studies, an embedment depth of 1.6 D_i, or 20.4 inches for the steel tubes used, is recommended to prevent the steel tube from pulling out of the column base. The steel tubes were embedded 24 inches, or approximately 1.9 D_i, at each end of the column, in the cap and base. This was done to ensure the column specimen would not fail due to pulling out. Furthermore, the steel tube would not be capped such that concrete could freely flow into the inside of the tube therefore completely encasing the connection in concrete. Additionally, four half-inch PVC pipes were placed outside of the steel tube within the concrete core. These pipes served as post-tensioning ducts for the 0.5-inch special prestressing strands. The ducts were placed in an X-pattern rotated 45 degrees from the primary axes to prevent effects on the performance of the concrete core caused by the PVC pipe reducing the concrete core thickness.

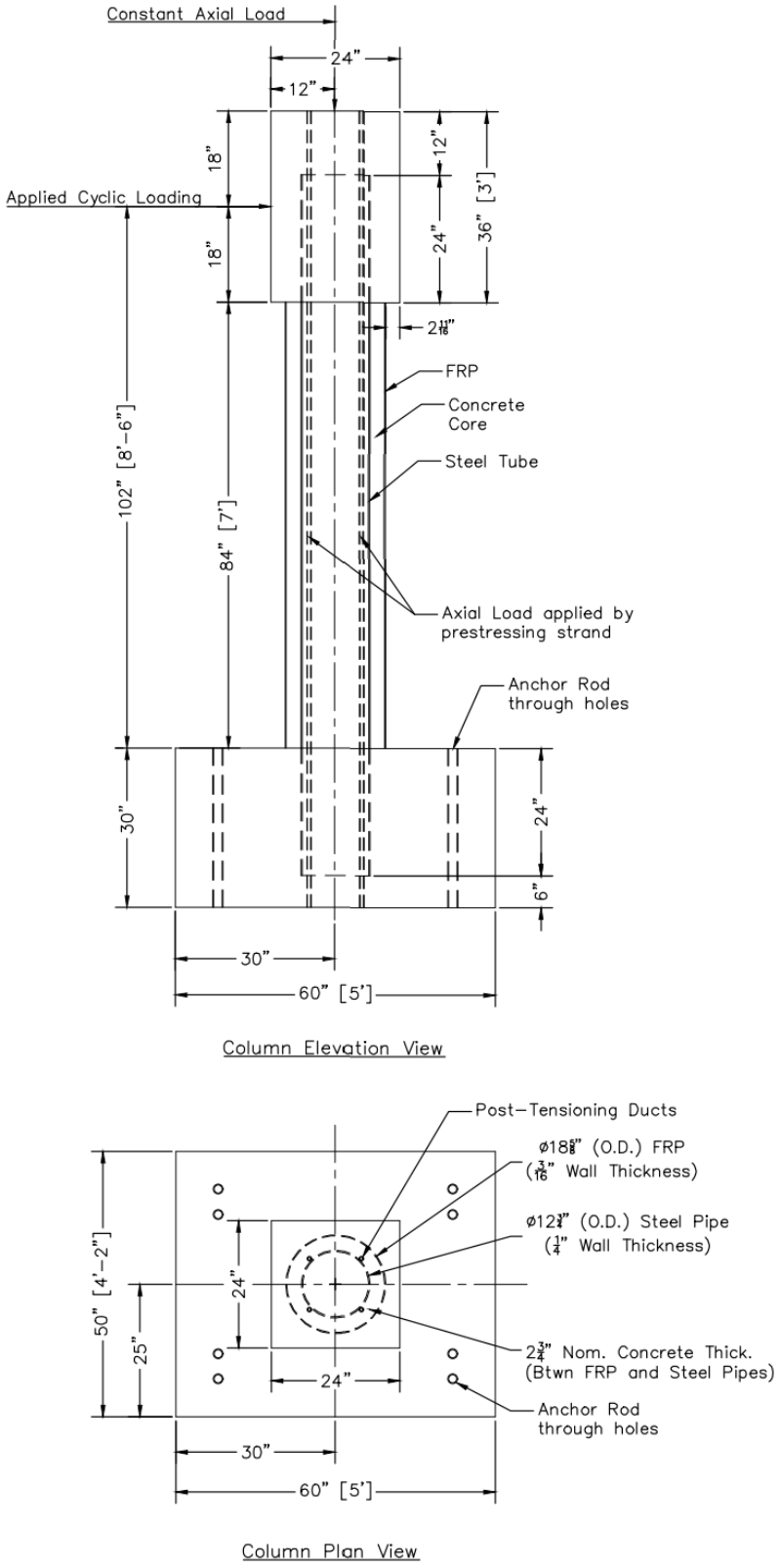

Figure 3-7: HC-FCS Column Layout

HC-FCS column specimens contained a concrete core of either HS-SCC or UHPC. Both concrete mix designs were previously developed at the University of Oklahoma. The goal of each mix design used was to provide sufficient flowability to consolidate well within the stay-in-place formwork and minimize voids without any external or internal vibration. Furthermore, a stratification of concrete strength and properties was prioritized to develop and analyze HC-FCS column configurations. Tiry (2023) developed a high-strength self-consolidating concrete to be used for prestressed girders with congested reinforcement that was capable of quickly reaching sufficient strength for de-tensioning. The mix design is outlined in Table 3-4 and Table 3-5. The HS-SCC mix was ideal for the concrete core because of its high flowability, material availability and cost, and compressive strength. A compressive strength target of 10 ksi was approximately twice that of the ODOT Class A mix for the RC column and about half of the target compressive strength of the UHPC used.

Table 3-4: HC-SCC Mix Design Properties

Water/Cementitious Material Ratio	0.35
Volume of Fine Aggregate	50.0%
Design Slump Flow	26 in.
Target Strength	10000 psi

Table 3-5: HC-SCC Mix Design Proportions

Type I/II Cement	825.0 lb/yd^3
Fine Aggregate	1445.0 lb/yd^3
Coarse Aggregate	1476.0 lb/yd^3
Water	289.0 lb/yd^3
HRWR, Adva 575	8.0 fl. oz/cwt

McDaniel (2017) and Looney et al. (2019) investigated multiple series of mix designs examining particle packing, cementitious material reactivity, and mix designs developed in previous research to identify an optimal UHPC mix design using materials locally available in Oklahoma. The final nonproprietary mix design is known as J3, and the mix design properties and proportions used for this research are shown below in Table 3-6 and Table 3-7. J3 offered

excellent flowability, workability, consolidation, and high compressive strength and tension capacity from the added steel fibers.

Table 3-6: UHPC J3 Mix Design Properties

Water/Cementitious Material Ratio	0.20
Type I/II Cement (by Volume)	60.0%
Silica Fume (by Volume)	10.0%
GGBFS (by Volume)	30.0%
Volume of Aggregate	50.0%
Volume of Steel Fibers	2.0%
Design Flow	10 in.
Target Strength	20000 psi

Table 3-7: UHPC J3 Mix Design Proportions

Type I/II Cement	1179.6 lb/yd^3
Silica Fume	196.6 lb/yd^3
GGBFS	589.8 lb/yd^3
Masonry Sand	1966.0 lb/yd^3
Steel Fibers	264.5 lb/yd^3
Water	393.2 lb/yd^3
HRWR, Glenium 7920	20.0 fl. oz/cwt

3.2.5 Column Cap Design & Layout

The final component of each column specimen was the concrete column cap that served to anchor the post-tensioning and apply the axial compressive load to the column, as well as provide a mounting location for the hydraulic actuator for cyclic lateral loading. To adequately apply the axial load, the cross-section of the column cap had to be greater than the diameter of the column and longer than the embedded steel pipe or reinforcement cage. Prefabricated formwork panels were used to reduce cap assembly time and increase testing turnaround efficiency. Prefabricated formwork was available in one-foot increments and needed to be greater than 18 inches in width and height and greater than 24 inches long with sufficient concrete cover

for post-tensioning anchorage bearing. The cap was determined to be 24 inches wide by 24 inches tall and 36 inches long.

Due to the column cap being cast while the column specimen is mounted to the testing frame, only one column cap could be prepared and cast at a time. Therefore, to reduce the time between column tests, the HS-SCC mix was used to provide high-early strength such that the columns could be tested three days after their respective column cap was poured. Minimal reinforcement was designed to reduce concrete cap shrinkage cracking and other stresses imposed by lateral loading. The column cap reinforcement cage consisted of 6, ACI T1 bar bend, No. 4 stirrups at 5 inches center to center with a No. 4 bar at each corner of the stirrups, for a total of 4 No. 4 bars. All reinforcement was Gr. 60. The stirrups were spaced out to distribute the reinforcing and to avoid the PVC holes through the column cap for the loading fixture anchorage. Initially, a one-through-hole design was implemented to affix the loading fixture to the column cap. However, after testing the first column specimen, the single, threaded steel rod buckled due to the unbraced length of the rod. A new layout was designed and implemented that utilized four smaller threaded steel rods that better distributed the applied load and eliminated the previous unbraced length of the rod. The final column cap design and layout are shown in Figure 3-8.

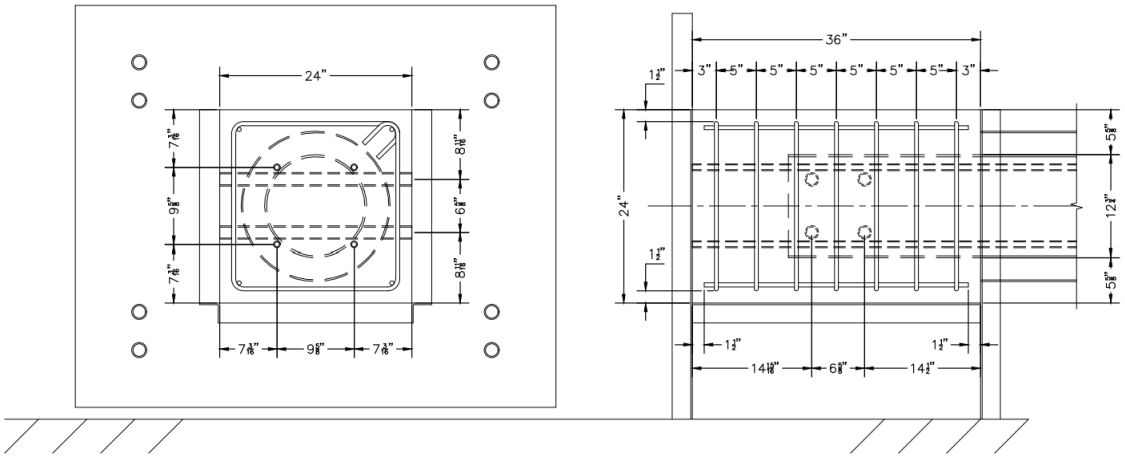

Figure 3-8: Column Cap Reinforcement and Layout, Cross-sectional View (l), Side View (r)

3.2.6 Column Specimen Instrumentation

In addition to column dimensions and material properties, instrumentation was also laid out before column specimen construction. Internal instrumentation was placed before concrete casting and additional external instrumentation, including strain gauges on the FRP and wire pots, was added after construction and before testing. Strain gauges were used to measure the longitudinal strain along the steel tube and the circumferential or hoop strain on the FRP during testing. The gauges were placed along the primary axes at heights of 3 inches and 9 inches above the column base. This layout was selected to capture the strains at the critical locations and neutral axis from the nature of the loading. Placing two strain gauges at each location with a variation in height sought to capture the strain profile along the critical section of the steel tube or reinforcement cage. Additionally, multiple gauges provided redundancy if they did not survive the casting process or failed early during testing. Due to the layout of the spiral tie on the RC column reinforcement cage, one set of strain gauges was placed at 2 inches and 8 inches above the column base to avoid the spiral tie. Strain gauges placed on the steel tubes and rebar cage were oriented perpendicular to the column base while gauges placed on the FRP were parallel to the base due to the direction of the desired strain to be measured. A summary of each strain gauge layout is shown below in Figure 3-9. Note that “H” and “V” denote the orientations of the strain gauges as either horizontal or vertical to the column base, respectively.

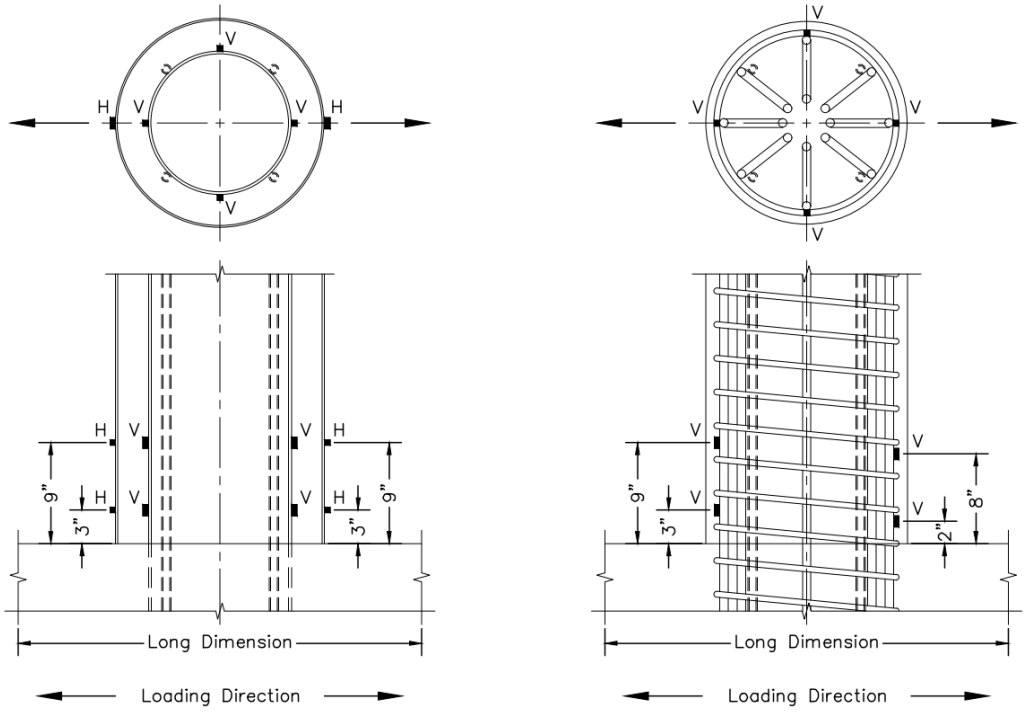

Figure 3-9: Column Strain Gauge Layout: HC-FCS Column (l), RC Column (r)

Chapter 4: Column Specimen Construction and Testing Setup

The RC and HC-FCS column specimens were constructed starting with the base and protruding steel reinforcement, then the column, and finally the column cap. The specimens were constructed vertically following a sequence that emulated practices and procedures in the field. Each specimen was tested horizontally after tilting the column and base over, placing it within, and anchoring it to the testing frame. Once in the frame, the column cap was added, the loading system was attached, and the constant axial load was applied through post-tensioning. Finally, the remaining instrumentation was added, and the column specimen was fully prepared for testing.

4.1 Column Specimen Construction

Each column specimen consisted of a reinforced concrete base, hollow-core or conventional column, and a concrete cap. These components were designed and detailed in Chapter 3. The reinforced concrete base was constructed by tying the reinforcement cage, assembling the formwork and base layout, placing the steel tube or conventional spiral-tied reinforcement cage, and pouring the concrete. Next, the column's internal instrumentation was added, and the column was prepared and cast. Lastly, the column specimen was moved into the testing frame, and the column cap was assembled and poured. This section outlines the construction sequence and the methods used to construct and prepare the column specimens for testing.

4.1.1 Column Component Assembly

Each column specimen's components were assembled before constructing the full specimen. This was done due to the logistics of constructing the specimen and in part to replicate the construction sequence in the field. The base formwork and reinforcement cage were assembled first, followed by the conventional spiral-tied reinforcement cage, steel tubes, and lifting loops. Lastly, the column cap formwork and reinforcement cage were assembled. The construction of each component is detailed in this section.

The reinforced concrete column bases were 50 inches wide by 60 inches long by 30 inches deep. Prefabricated concrete formwork was used due to the available dimensions, ease of

assembly, strength, and ease of cleaning. The bottom of the formwork was a mat of plywood topped with a special type of plywood with outer smooth, nonstick plies known commercially as Ellis board. The anchoring rod holes were achieved by casting 1½-inch PVC pipes into the concrete that were held in place by wooden dowels and a jig to ensure the same hole positioning for each column base. The dowels were anchored into the bottom floor of the formwork while the H-shaped jig was mounted to the top of the formwork. The formwork, dowel layout, and PVC pipes are shown below in Figure 4-1. Furthermore, the ½-inch PVC pipes for the post-tensioning were also held in place by aluminum dowels that were affixed to the formwork floor. These pipes extended out of the base and up the steel tube or spiral-tied reinforcement cage.

Figure 4-1: Column Base Formwork, Formwork Floor Dowels (l) and Base PVC Pipes (r)

The base reinforcement cage was assembled by first supporting the top No. 8 bars and tying on the vertical No. 4 paired stirrups closest to the center. Each set of vertical No. 4 stirrups was paired together before assembling the cage. The first set of bars was placed such that a 13-inch by 13-inch opening was created for the steel tube with some tolerance. Next, the rest of the top No. 8 bars and vertical No. 4 stirrups, besides the outer bars of each, were tied. The cage was then lifted with the crane and the bottom and remaining top No. 8 bars were added with the hooks staggered alongside one another. Lastly, the final vertical No. 4 stirrups and all of the horizontal No. 4 stirrups were added. The horizontal No. 4 stirrups were placed on the second interior No. 8 on each side for constructability. Four 1-inch steel high chairs were affixed to the bottom of the cage underneath the vertical No. 4 stirrups to facilitate the appropriate concrete cover. Each cage was test-fitted within the base formwork to ensure each PVC pipe could be placed and leveled before applying the release agent to the formwork. This was done to reduce

the chances of form-release contacting the reinforcement cage. This process is shown in Figure 4-2.

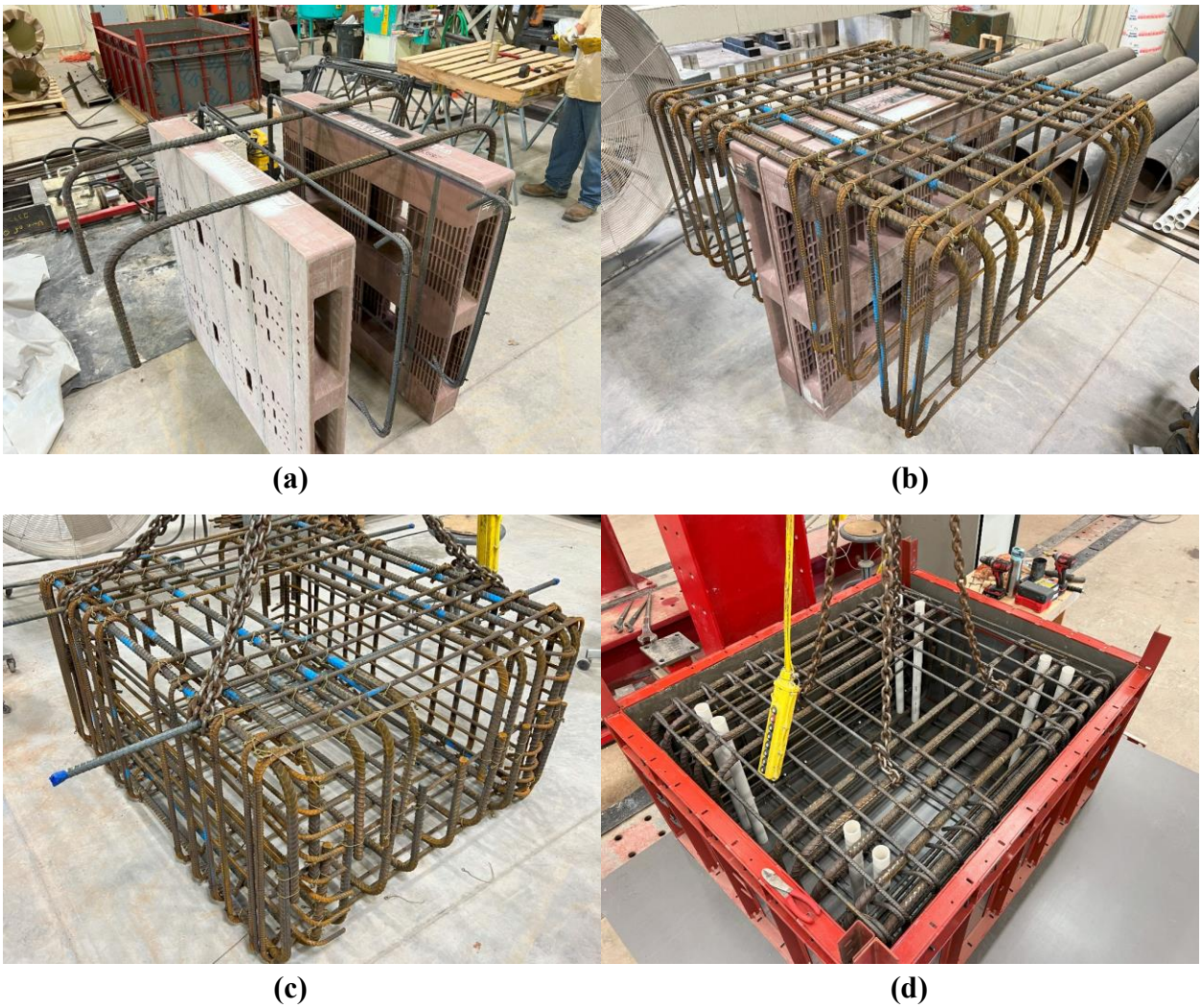

(a) **(b)**

(c) **(d)**

Figure 4-2: Base Reinforcement Cage Assembly, (a) Initial Bar Placement, (b) Completed Top Reinforcement, (c) Completed Reinforcement Cage, (d) Test-fitting Completed Cage

The conventional spiral-tied reinforcement cage was constructed similarly to the base reinforcement cage. First, a wooden jig was created by drilling holes at 3 inches center-to-center along the centerline of a 2x6 board and then splitting it down the centerline. The jig and spiral were supported, and the spiral was stretched and held in place by the jig. This ensured the No. 4 spiral tie would be at a 3-inch pitch. Additionally, the one-and-a-half flat turns were created at each end of the cage. Each longitudinal No. 6 bar was then added, and the reinforcement cage was tilted upright, as shown in Figure 4-3.

Figure 4-3: Assembled Spiral-Tied Reinforcement Cage, Horizontal Construction (l) and Titled Upright (r)

Due to the bottom hooks of the No. 6 bars protruding outward beyond the diameter of the column, and the spiral-tied cage having a larger diameter than the steel tubes, the column cage was placed within the base cage before the base cage was placed within the formwork. This was achieved by cutting the top No. 8 bars and vertical No. 4 stirrups loose and shifting them sideways. Next, the column cage was inserted at a vertical angle to the base cage and then tilted upright. Once in place, 6-inch tall, steel HSS sections were used to support the spiral-tied cage at the appropriate height. The bars that were moved were then shifted back against the vertical cage and tied in place. Additional temporary support bars were added for transportation and insertion of the combined cage. The final assembly is shown in Figure 4-4 and Figure 4-5.

Figure 4-4: Combined RC Column and Base Cages

Figure 4-5: Closer Look at the Combined RC Cages

Compared to the complicated process of preparing the conventional spiral-tied reinforcement cage, the preparation of the steel tubes was fairly minimal. Each tube was washed with a power washer, dish soap, and a rag to eliminate any surface oils that might inhibit bonding with the concrete. The steel tubes used possessed a black, corrosion-preventing coating that was ground off before any external welding. Two 1-inch-long sections of C4x7.25 were added as picking points to the top of the steel tube on opposite sides. Additionally, four legs made from L1½x1½x⅛ steel angle, with ¼-inch thick steel plates as feet, were welded to the inside of the tube. The feet were added to suspend the tube 6 inches above the bottom of the formwork to achieve the designed 24 inches of embedment. Furthermore, four 1-inch-long sections of C4x7.25 were welded to the inside of the steel at approximately 6 inches from the bottom to serve as supplemental anchorage. This was done to prevent the steel tube from pulling out of the base during testing. These additions are shown in Figure 4-6, and the completed component is shown in Figure 4-7. The bottom of all steel tubes was left open to allow concrete to freely enter and fill the bottom embedment of the steel tube.

Figure 4-6: Steel Tube Preparation, Lifting Points (l), Supporting Legs and Anchorage (r)

Figure 4-7: Completed Steel Tube Ready to be Tilted and Placed

Prestressing strand loops were implemented to lift and move the column specimens due to commonly being used at precast facilities. The prestressing strand offers high strength and ductility and is also an available waste material around Fears Lab. The strand lifting loops were based on recommendations from the PCI Design Handbook and a PCI Journal: *Industry survey results on the use of prestressing strand lifting loops* (2020). The capacity of each lifting loop was taken as 8 kips based on the recommended capacities for a 0.5-inch diameter strand. However, a 0.5-inch special strand with a larger cross-sectional area was used and therefore had a higher capacity than estimated. The strand lifting loops required a minimum embedment of 24 inches and were extended approximately 6 inches beyond the top of the concrete. The bending radius was approximately 6 inches in an inverted V shape and the ends of the loops were at least 3 inches from the bottom of the formwork. The typical lifting loop and location are shown in Figure 4-8. Four prestressing strand lifting loops were used with one loop in each corner of the concrete base for balance. This resulted in a lifting capacity of 32 kips.

Figure 4-8: Prestressing Strand Lifting Loop, Standard Shape (l) and Typical Location (r)

The column cap formwork was also prefabricated formwork panels due to readily available sizes and ease of assembly and cleaning. A custom piece of formwork was created to surround the protruding column during casting that was capable of splitting into two halves to be removed. The formwork was supported by four legs, each with a welded nut and bolt for formwork leveling and adjustment. Similar to the base formwork and configuration, metal dowels were used on multiple faces of the formwork to hold either the 1¼-inch or ½-inch PVC pipes in place during casting. The column cap reinforcement cage was prepared by suspending the two top No. 4 bars in each corner of the No. 4 stirrups and then tying the stirrups in place at the appropriate spacing. Next, the two lower No. 4 bars were tied into each corner and two diagonal bars, one on top and the other on the side of the cage, were added to provide stability during casting. Four 1.5-inch plastic chairs were placed at each corner on the No. 4 stirrups to support the cage and achieve the appropriate concrete cover. The completed reinforcement cage and column cap formwork are shown in Figure 4-9.

Figure 4-9: Column Cap Components, Rebar Cage (l) and Prefabricated Formwork (r)

4.1.2 Column Base Construction

The reinforced concrete base was the first part of each column specimen to be built. Due to the manner and nature of the testing, the base was one of the most complex parts of the specimen. Each base consisted of an extensive reinforcement cage, eight PVC pipes for the anchoring through-holes, four prestressing strand lifting loops, and either a vertical spiral-tied reinforcement cage or steel tube protruding from the base. The complexity of the base layout coupled with limitations presented by available equipment made the sequence of the construction crucial. The same steps were used to assemble each column base with minor modifications made to account for the added complexity of the RC column cage.

Upon verifying that the base reinforcement cage adequately fit around each of the PVC pipes in the base, the formwork was prepped. All internal seams were sealed with silicone and the horizontal formwork seam and any other formwork holes were covered by aluminum foil duct tape before casting concrete. The inside faces and tops of the formwork panels were also coated with a form-release agent before casting, as shown in Figure 4-10. Care was taken to limit form-release around the wooden and metal dowels that held the PVC pipes in place due to form-release inhibiting silicone setting. The base reinforcement cage was then carefully lowered into the formwork using the overhead bridge crane to limit contact with the walls to avoid the rebar contacting the form-release agent.

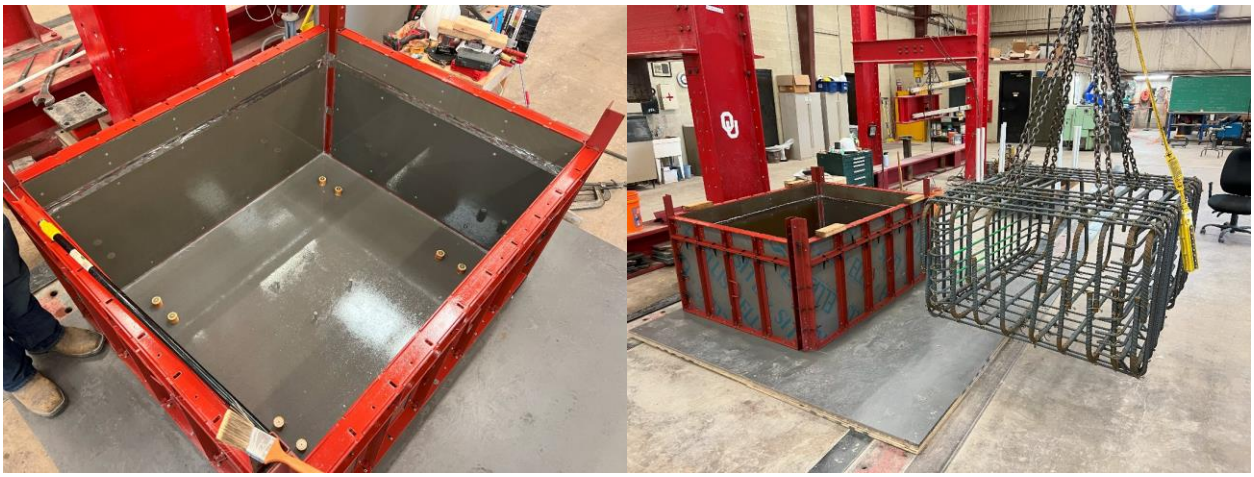

Figure 4-10: Column Base Preparation, Formwork Preparation (l) and Completed Cage (r)

The cage was set such that each 1½-inch PVC pipe could be vertically leveled, and nearly equal cover was present on each side of the cage. Additional 1-inch steel chairs were used to maintain the standoff distance to the formwork and prevent the cage from moving during casting and consolidation. Next, the 1½-inch PVC pipes were coated with a form-release agent and placed through the cage and onto the dowels. The pipes were wiped down to make them easier to remove from the concrete base for additional tolerance if all eight through holes did not align with the testing frame. Additionally, each end of the PVC pipes was sealed with silicone to account for irregularities in cutting and prevent the concrete paste from infiltrating. Then the H-shaped jig was placed onto the base, each PVC pipe was lined up, the jig was secured to the formwork, and each PVC pipe was sealed with silicone at the top. The four prestressing strand lifting loops were placed in the rebar cage alongside the jig and were suspended by rods resting on top of the jig. The lifting loops were placed such that they did not interrupt the future placement of the bearing plates. This process is shown in Figure 4-11.

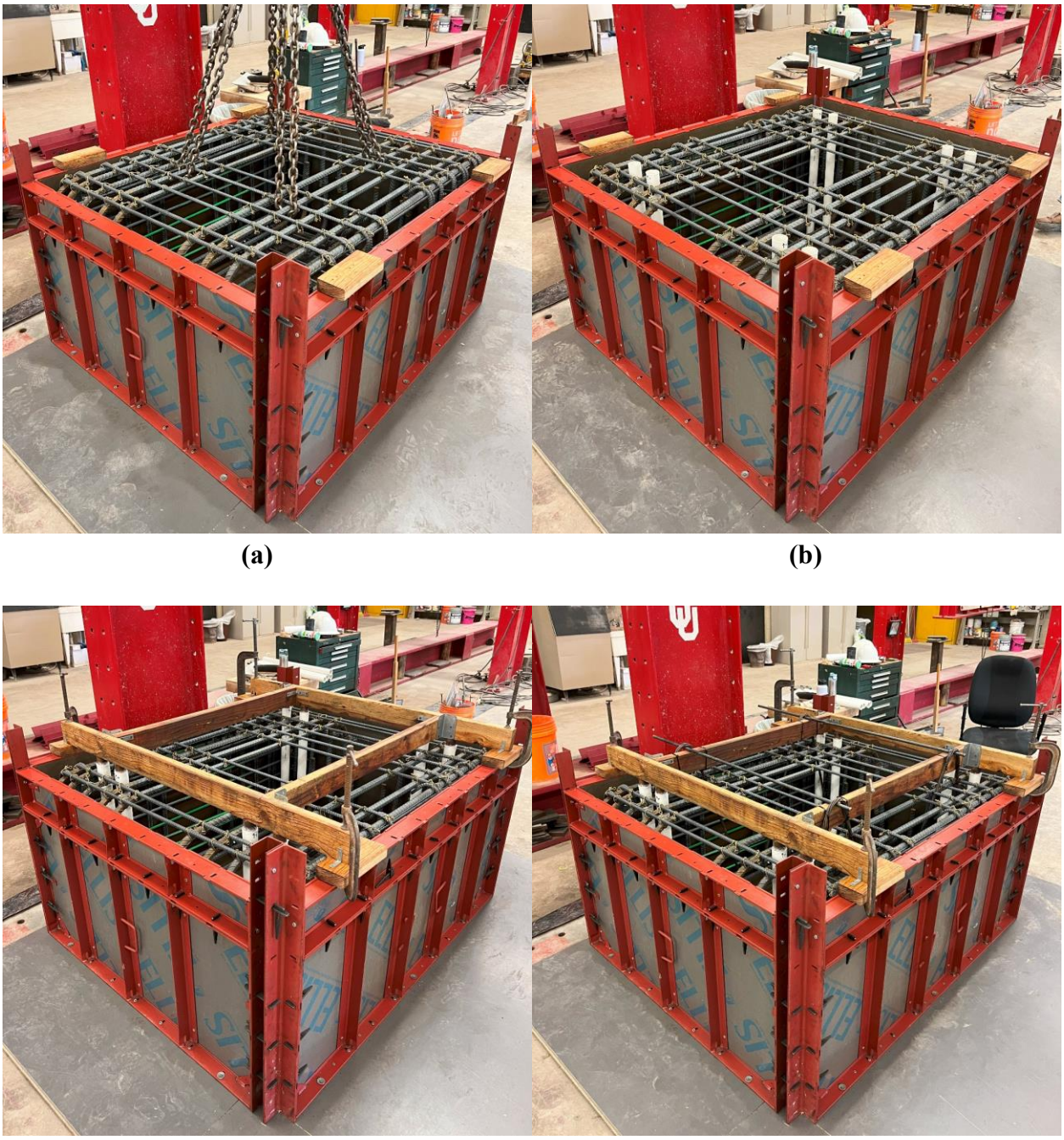

(a) **(b)**

(c) **(d)**

Figure 4-11: Column Base Assembling, (a) Placing Rebar Cage, (b) Inserting and Checking PVC Pipes, (c) Attaching H-shaped Jig, (d) Positioning Prestressing Strand Lifting Loops

After the base was prepared, the column was prepped. For the RC column, the spiral-tied column cage and base cage were placed as one unit into the formwork due to the complexity of the bottom hooks of the column cage. Due to limited lifting height, the combined cages were

placed using the forklift instead of the overhead bridge crane used for the lone base cages. Once placed, the column cage was supported via steel HSS blocks to the correct embedment length and centered in the formwork. Next, the column cage was leveled and held in place by a steel clamping apparatus that extended from a steel testing frame next to the specimen. This allowed for the column cage to be leveled in both directions and firmly held in place during casting. Finally, the ½-inch PVC pipes for the post-tensioning were dropped into place from the top of the column cage and onto the dowels in the formwork. These PVC pipes ran alongside and were affixed to the longitudinal bars of the spiral-tied reinforcement cage and were sealed with silicone at the bottom and covered with tape on the couplings at the top.

Figure 4-12: RC Column Base Assembly, Combined Cage Transportation and Placement (l) and Finalized Specimen Ready for Casting (r)

The steel tube insertion into the base reinforcement cage exemplified the decreased complexity and construction time of HC-FCS columns. The steel tubes were tilted up using the overhead bridge crane, as shown in Figure 4-13. Due to the limited height of the crane, a forklift was used to place the steel tubes by lifting them underneath the welded C-channel sections at the

top. The tubes were inserted through the opening of the reinforcement cage, shown in Figure 4-14, quickly centered, leveled, and clamped in place. The slim profile of the steel tube with no hooks or anchorages extending beyond the diameter was ideal for placing it within the already constructed base cage. Furthermore, the increased rigidity of the steel tube as opposed to the inherent flexibility of the conventional column cage aided in an easier centering, leveling, and clamping process.

Figure 4-13: Preparing Steel Tubes for Insertion by Tilting Upright with the Crane

Figure 4-14: Steel Tube Placement, Lifting with the Forklift (l) and Insertion into the Reinforcement Cage (r)

The ½-inch PVC pipes for the post-tensioning were placed alongside the steel tube and secured by the dowels in the floor. The PVC pipes were roughly leveled and taped to the side of the steel tube. Lastly, the PVC pipes were sealed with silicone at the bottom and covered with tape on the couplings at the top. Due to the hollow nature of the steel tubes, a line was drawn at the embedment depth inside each tube, and a camera was suspended inside the tubes during casting to ensure concrete filled the embedded portion. The camera assembly and finalized column specimen are shown in Figure 4-15.

Figure 4-15: HC-FCS Base Assembly, Camera for Monitoring Internal Concrete Level (l) and Finalized Specimen Ready for Casting (r)

Once the column base and column reinforcement were assembled, the base was poured. In addition to casting the column base, twelve 4x8 concrete cylinders were made for 3-day, 7-day, 28-day, and test-day compressive strength testing in general accordance with ASTM C39. The concrete mix design for the specimen bases was requested from, and the concrete was supplied, by Dolese Bros. Inc. due to the volume of concrete required. A concrete mix with a target 28-day strength of 6000 psi and an 8-inch slump was requested and is outlined in Table 4-1 and Table 4-2. The 8-inch requested slump would provide adequate flowability for the concrete to consolidate within the rebar cage and fill the embedded region of the steel tube. A concrete vibrator was used to further promote consolidation and filling of the steel tube. A suspended camera was used to verify the concrete level within the steel tube.

Table 4-1: Dolese Mix Design Properties

Water/Cementitious Material Ratio	0.40
Design Slump	8 in.
Target Strength Minimum	6000 psi

Table 4-2: Dolese Mix Design Proportions

Type I/II Cement	682.0 lb/yd^3
Fine Aggregate	1356.0 lb/yd^3
Coarse Aggregate	1725.0 lb/yd^3
Water	275.0 lb/yd^3
HRWR	4.0 fl. oz/cwt

After pouring the concrete into the base and ensuring the appropriate level within the steel tube and formwork, the top surface of the base was struck off and a smooth finish was delicately applied. Figure 4-16 and Figure 4-17 illustrate the casting process from the internal camera view, while Figure 4-18 and Figure 4-19 depict the completed base specimens immediately after casting and formwork stripping. Once the concrete had sufficiently set, the base and concrete cylinders were covered with wet burlap and plastic. The burlap was routinely wet down for seven days during the curing process, even after the formwork was stripped and the specimen was moved from the casting area. After curing for three days, the formwork was stripped by removing only two adjacent sides, the specimen was lifted with the crane and moved out of the casting area, and the formwork was cleaned and reassembled for the next column base. This procedure was repeated for all column bases.

Figure 4-16: RC Column Base Casting at Various Heights,
Column Base View (l) and Camera View (r)

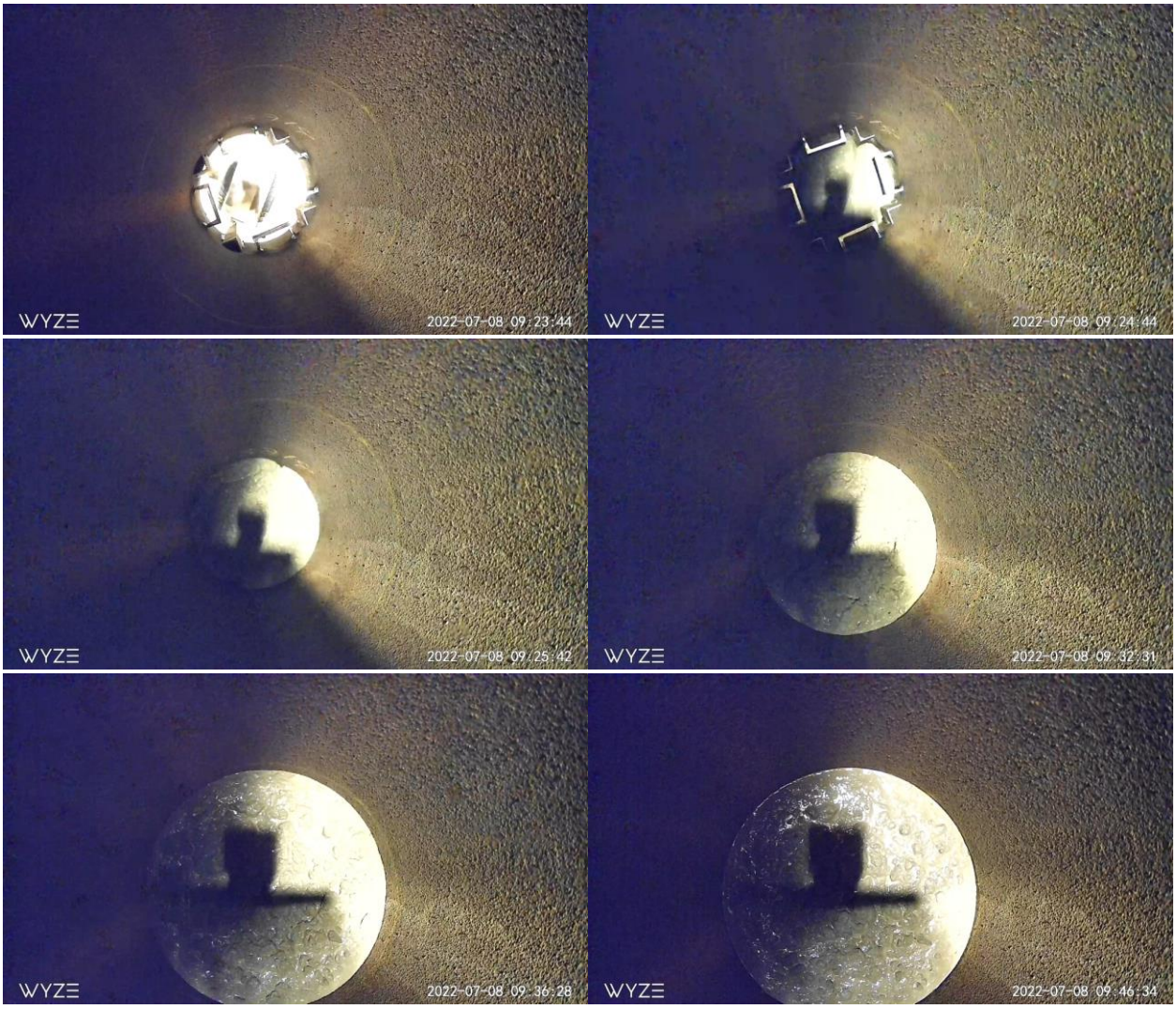

Figure 4-17: Camera View Inside Steel Tube During Casting of HC-FCS Column Base

Figure 4-18: RC Column Base Construction, Immediately After Casting and Finishing (l) and After Stripping the Formwork (r)

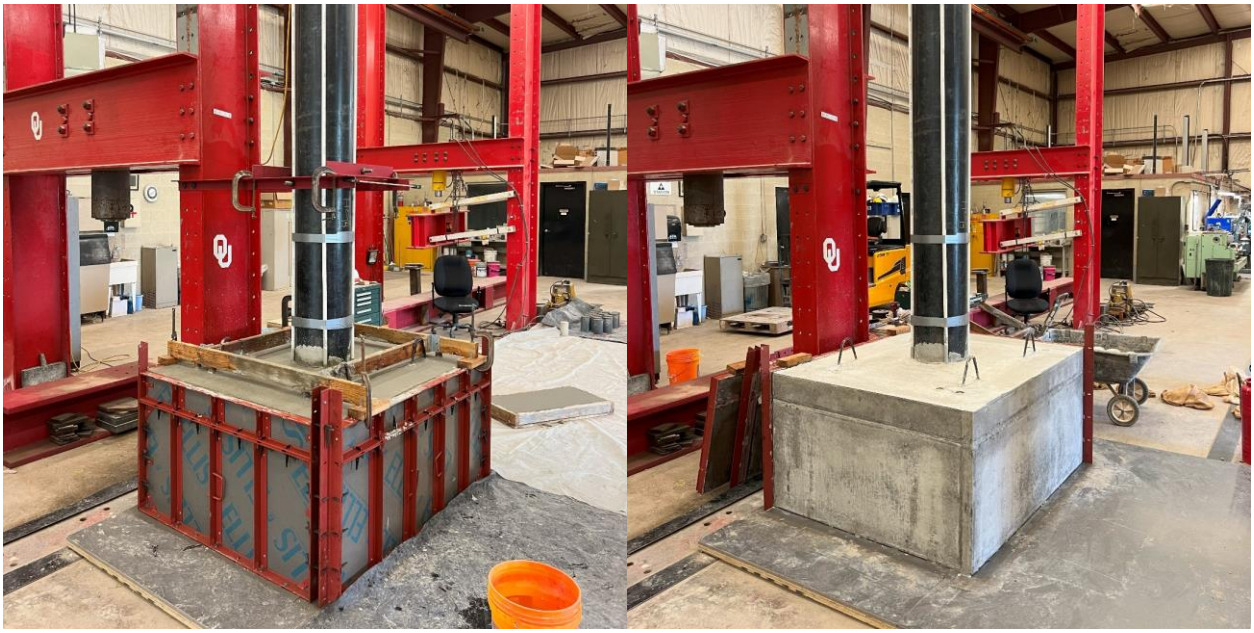

Figure 4-19: HC-FCS Column Base Construction, Immediately After Casting and Finishing (l) and After Stripping the Formwork (r)

Figure 4-20: Completed Column Bases

4.1.3 Column Internal Instrumentation

After the conclusion of the seven-day covered wet curing process, work began to prepare the column bases for the addition of internal instrumentation. First, each column base was labeled with cardinal directions that represented the direction that each face of the base, or side of the column, would face once the specimen was mounted in the testing frame. East and west aligned with each physical direction while north and south corresponded to up and down respectively. The gauge's placement corresponded to the direction of loading and the neutral axis was perpendicular to the direction of loading, referred to as the primary axes. The strain gauges were spaced vertically along the reinforcement cage or steel tube as shown in Figure 3-9 in Section 3.2.6. All gauges placed internally on steel reinforcement were oriented perpendicular to the column base, or vertically along the steel reinforcement. A framing square, level, and tape measure were used to carefully lay out the location of each strain gauge along the circumference and height of the reinforcement. Strain gauges were placed on the extreme longitudinal bars of the RC column cage along the primary axes. The gauges were placed vertically by measuring upward from the column base. The west strain gauges were placed an inch lower than the other gauges to avoid the spiral tie. For the HC-FCS columns, strain gauges were placed on the outside

of the steel tube in the same locations. Due to variable heights in the finish of the concrete bases, and the ease of consistently measuring off of the top of the steel tube, the strain gauges were placed vertically by measuring downward from the top of the steel tube. The final strain gauge layout for each specimen type is shown in Figure 4-21.

Each strain gauge was applied to the steel reinforcement in the same manner following a multiple-step process. First, a flat spot was created by a 200-grit electric handheld grinder. Next, the spot was further ground by hand with 240-grit sandpaper, followed by 320-grit sandpaper. The area was then wiped clean with acetone, followed by an acid and then a base. Each cleaner was applied with a cotton swab after the previous cleaner had thoroughly dried. All strain gauges were checked with a multimeter before application to verify each gauge was in working order. Electrical tape was used to separate the unshielded lead wires from the steel reinforcement. The gauges were held in place with Scotch tape, peeled back to reveal the underside of the gauge, and then a drop of super glue adhesive was applied. After pressing firmly on the gauge for approximately 30 seconds, the Scotch tape was carefully removed to assess if the gauge had adhered to the steel. The strain gauges were allowed to dry overnight before a small amount of silicone was applied to cover and protect the gauge. Once the silicone had sufficiently dried, the gauges were covered by aluminum foil sealant tape and checked again with a multimeter.

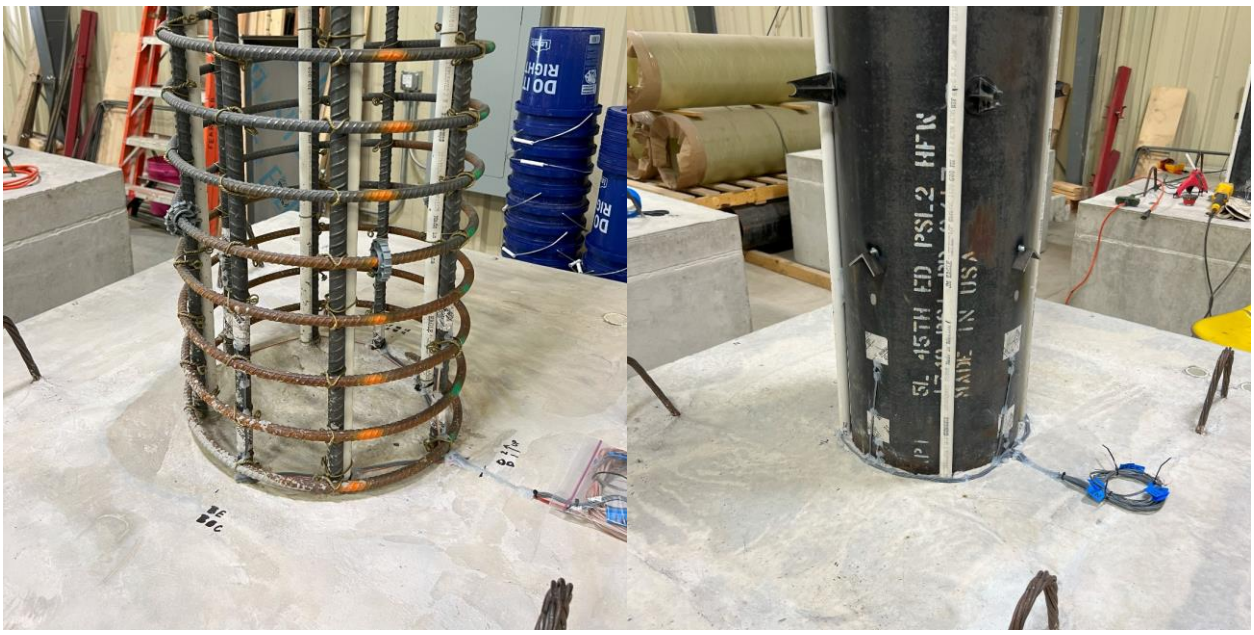

Figure 4-21: Internal Strain Gauge Application, RC Column (l) and HC-FCS Column (r)

Hot glue was used to create a strain relief loop underneath each gauge to further protect it from being damaged during the casting of the column and testing process. The wire extensions from all of the gauges on a given column were routed down the column and along the base to a central point in the south direction. A small channel was cut into the column base for the wires to pass underneath the concrete core and exit the column as opposed to cutting a notch in the GFRP and creating a weak point. Additionally, a ¾-inch wide section of L1½x1½x⅛ steel angle was tack welded to the steel tube at 6 inches above each top strain gauge or 15 inches above the column base. The tack weld ensured that the piece of angle lacked sufficient connectivity to act as a shear connection to the concrete core. The angle was added as a rooftop to protect the gauges from the impact of falling concrete during the casting of the column. The RC column strain gauges were assumed to be shielded from falling concrete by the spiral tie above each gauge.

4.1.4 RC Column Construction

Following the application of the internal instrumentation, the remaining preparations were made for the column section addition. The PVC post-tensioning ducts were approximately leveled and held in place by tying them to the longitudinal reinforcement. The couplings at the top were covered with tape to prevent concrete from entering during the casting process. Additionally, plastic stand-off rollers were trimmed and added to the spiral-tied cage in three layers at 12, 42, and 72 inches vertically from the column base, with four rollers in each layer. The bottom layer was rotated 45 degrees from the primary axes and placed next to the post-tensioning to shift the rollers away from critical locations. The top and middle layers were placed along the primary axes. Next, an 18-inch diameter Sonotube was carefully lowered over the reinforcement cage and around the plastic stand-offs. Due to the required lifting height, this was done using a forklift with a makeshift crane attachment as shown in Figure 4-22. Once in place, the interface between the bottom of the Sonotube and the top of the column base was sealed with silicone. The bottom of the Sonotube was also wrapped with duct tape for additional hoop strength to safeguard from any potential blowout or failure of the Sonotube. Lastly, the tube was leveled and clamped in place by four ratchet straps connected to an H-shaped assembly. A completed assembly ready for casting is shown in Figure 4-22.

**Figure 4-22: RC Column Form Placement and Preparation,
Lowering the Form into Place (l) and Column Ready for Casting (r)**

The ODOT Class A concrete mix design was prepared and mixed on-site and yielded a slump of 6.5 inches, slightly lower than the target of 8 inches, and an air content of 4%. The inside of the form and the steel reinforcement were misted with water before the concrete was placed. The concrete was poured from a concrete bucket with a chute that was lifted by the forklift such that the concrete entered the form from above the middle of the reinforcement cage. A concrete vibrator was inserted from the top of the column to the bottom and was slowly raised as the concrete height rose within the column. Furthermore, the outside of the Sonotube was struck with mallets as the concrete rose to promote better consolidation. Figure 4-23 shows the column before and after casting. In addition to casting the column, nine 4x8 concrete cylinders were made for 7-day, 28-day, and test-day compressive strength testing in general accordance with ASTM C39.

After the casting was complete and the concrete had adequately set up, wet burlap was applied to the concrete surface and concrete cylinders, and the top of the column was covered in plastic. After seven days, the burlap and plastic were removed and the Sonotube was stripped off the column in layers, as shown in Figure 4-24. Despite the consolidation efforts, and due to the

limited clear cover and lower slump, the column had minor surface honeycombing along the bottom, from a few inches up to a foot above the column base. The surface of the column was sufficiently wet, and a cosmetic mortar patch was applied that consisted of cement, masonry sand, and water. Figure 4-25 illustrates the honeycombing and cosmetic patching process. Finally, the column was painted white to provide increased contrast for spotting cracking during testing. The final RC column test specimen after painting is shown in Figure 4-26.

Figure 4-23: RC Column Construction Before Casting and After Casting

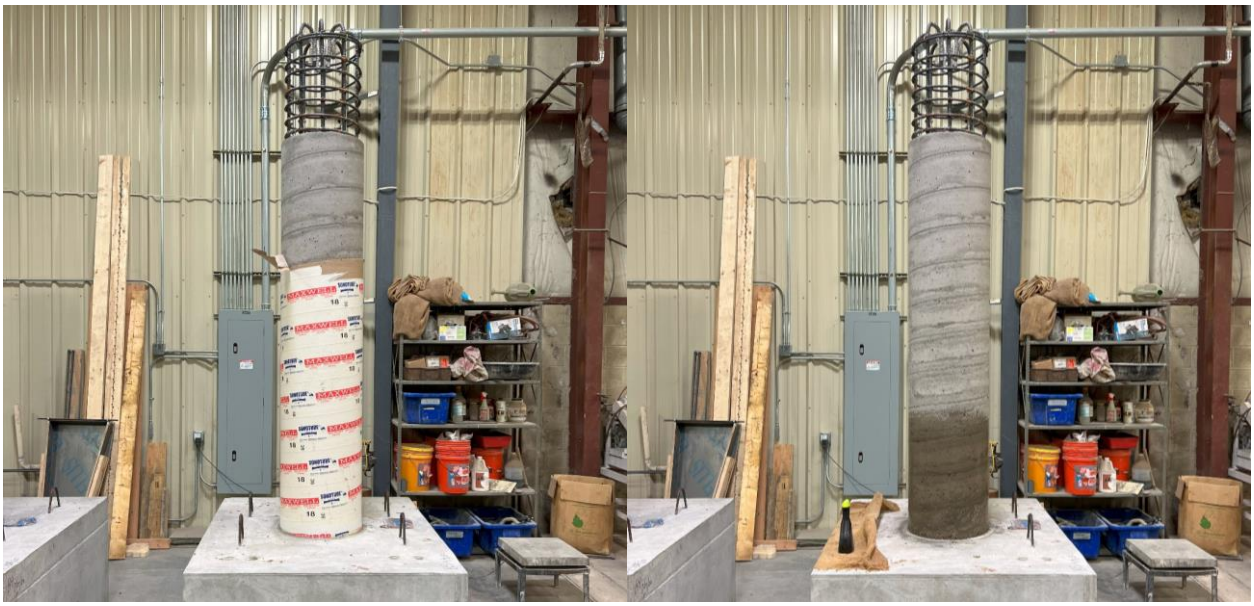

Figure 4-24: RC Column After Casting, Stripping the Form (l), Saturating Patch Area (r)

Figure 4-25: RC Column Honeycombing and Cosmetic Patching

Figure 4-26: RC Column Specimen Before and After Painting

4.1.5 HC-FCS Column Construction

For the HC-FCS columns, similar to the RC column, the PVC post-tensioning ducts were approximately leveled and affixed to the steel tubes by hot glue. The couplings at the top were covered with tape to prevent concrete from entering during the casting process. Excess concrete from the base casting process was cleaned off of the steel tube and post-tensioning ducts. Additionally, plastic chairs were trimmed down and hot-glued to the sides of the steel tube. This was done in two layers, 12 inches from the top and 24 inches from the bottom of the column, with four chairs in each layer. The bottom layer was rotated 45 degrees from the primary axes and placed next to the post-tensioning to move the chairs away from critical locations. The top layer was placed along the primary axes. Next, the 18-inch diameter GFRP tube was carefully lowered over the steel tube and around the plastic stand-offs as shown in Figure 4-27. Once in place, the interface between the bottom of the GFRP tube and the top of the column base was sealed with silicone. The GFRP tube was leveled and clamped in place by four ratchet straps connected to a steel H-shaped assembly shown in Figure 4-28. All HC-FCS columns were prepared the same way.

Figure 4-27: HC-FCS Column GFRP Placement and Specimen Ready for Casting

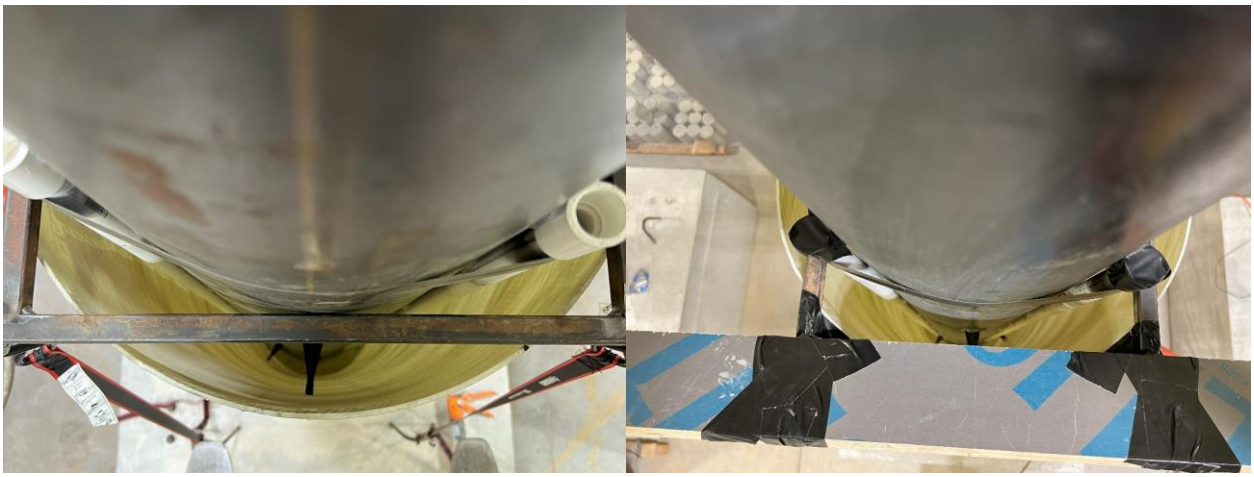

Figure 4-28: HC-FCS Column Clamp Orientation and Interior View, HS-SCC Casting (l) and UHPC Casting (r)

HC-FCS columns were poured following a similar procedure to the RC column. The HS-SCC and UHPC mix designs were both prepared and mixed on-site. The HS-SCC concrete cores were poured first, followed by the UHPC cores. Each column is numbered by the type of concrete used and the chronological order in which created. HS-SCC 1 and HS-SCC 2 had slump spread flows of 27.5 and 26.5 inches, respectively. UHPC 1 and UHPC 2 had flows of 10 and 13 inches respectively, with a 4% air content. It should be noted that the flow characteristics and testing methods for each concrete type differ, therefore a direct comparison of the measured flows should not be conducted. The concrete was poured from a concrete bucket with a chute that was lifted by the forklift. The concrete entered the form from the side of the steel tube above the GFRP tube and was directed down the steel tube as shown in Figure 4-29. The concrete was added in two subsequent, but unequal, lifts due to the capacity of the concrete bucket. Figure 4-30 displays the concrete level between lifts and the final level after casting. A concrete vibrator was not used due to limited space and the self-consolidating properties of both concretes. However, the outside of the GFRP tube was struck with mallets similar to the RC column.

Figure 4-29: HC-FCS Column Casting, HS-SCC Core (l) and UHPC Core (r)

Figure 4-30: HC-FCS UHPC Core During and After Casting

In addition to casting the column, nine concrete cylinders were made for 7-day, 28-day, and test-day compressive strength testing in general accordance with ASTM C39. The HS-SCC mix used 4x8 concrete cylinders for compressive strength testing while the UHPC mix required 3x6 cylinders due to its high compressive strength. After the casting was complete and the concrete had adequately set up, wet burlap was applied to the concrete surface and concrete cylinders, and the top of the column was covered in plastic. After seven days, the burlap and plastic were removed. Due to the GFRP tube functioning as stay-in-place formwork, there was no formwork to strip after the column was cast. However, the silicone seal at the base of the GFRP tube was later removed, as shown in Figure 4-31, to monitor damage propagation and separation from the base during testing. The same casting and test preparation process was repeated for all HC-FCS columns.

Strain gauges were applied to the outside of the GFRP tubes in similar locations to the internal strain gauges on the steel reinforcement. The gauges were placed in the east and west directions at the same heights as the internal gauges. Figure 3-9 in Section 3.2.6 outlines the strain gauge layout. All gauges placed externally on the GFRP tube were oriented parallel to the column base, or circumferential on the tube. A framing square, level, and tape measure were used to carefully lay out the location of each strain gauge along the circumference and height of the tube. Due to variable heights in the finish of the concrete bases, the strain gauges were placed vertically by measuring downward from the top of the GFRP tube. Each strain gauge was applied to the outside of the GFRP tubes in the same manner following a multiple-step process similar to that of the gauges applied to the steel reinforcement. A flat spot was created, sanded, and cleaned. The gauge was checked, glued, protected, and checked once more. Strain relief loops were created underneath each gauge and the wire extensions were directed along the column circumference to the south where the internal wire extensions exited the column core. The final layout is shown in Figure 4-31 below.

Figure 4-31: HC-FCS Column Application of External GFRP Instrumentation

4.2 Column Specimen Testing Setup

Column specimens were constructed vertically, using techniques and procedures that replicated standard practices in the field. However, given the limitations presented, the column cap was unable to be constructed vertically and was constructed after the column specimen had been placed and anchored within the column testing frame. Once the column cap was added, the testing procedure could begin. First, the testing apparatus was mounted to the column cap and then the constant axial compressive load was applied. Next, the remaining instrumentation was

installed, all of the instrumentation was checked, and the data acquisition system and program were set up. This section outlines the final construction steps, testing setup, and procedures for testing and obtaining data from the column specimens.

4.2.1 Column Specimen Placement & Fixation to Testing Frame

The column specimens were constructed and moved vertically; however, the testing frame was designed such that the specimens were tested horizontally. Consequently, the specimens had to be tilted over to be placed within the testing apparatus. This was done by utilizing both the overhead bridge crane and the forklift as shown in Figure 4-32. First, a large neoprene block was placed underneath the long side of the column specimen's base, causing the specimen to lean. Next, the bridge crane was attached to the two prestressing strand lifting loops on the side above the neoprene block. The crane was slowly raised such that the specimen continued to tilt further until it began to roll over on its own. The forklift was used to catch the protruding steel tube and balance the column to better control the descent.

Figure 4-32: Column Specimen Tilting Process

Once the column specimen was laid horizontally, the lifting loops were cut off from most column bases due to impeding the placement of the bearing plates. The area around the PVC through-holes in the base was ground to remove large surface irregularities at the location of the bearing plates. These preparations are shown in Figure 4-33. The overhead crane was then used to transport and place the column specimen into the testing frame by using two No. 10 steel rebars running through the PVC pipes in the base.

Figure 4-33: Prestressing Strand Lifting Loop Removal and Base Grinding Process

Once in the testing frame, the column specimen was partially anchored, then leveled, squared, and fully anchored onto the frame. The column specimen was placed near the frame onto four ¼-inch solid steel rollers. The rollers helped account for large variations in the concrete floor and allowed the specimen to more easily be drawn into the frame by the threaded steel rods. Both the bridge crane and forklift were used to move, slide, and tilt the base such that each of the threaded steel anchoring rods was able to be pushed through the frame and column base. After the eight steel rods were in place, the bearing plates were lowered into place, and nuts and washers were installed on both sides of each rod. The nuts were set on the front side of the bearing plates at 1 inch from the end of the steel rods. The nuts on the rear of the frame were then sequentially tightened to draw the column specimen in the remaining distance.

This process and result are shown in Figure 4-34. Before being fully tightened down, the column specimen was checked for level and approximate alignment with the center of the frame. This was done by placing a level on the column portion of the specimen and a laser level aligned along the centerline of the middle strong floor beam, as shown in Figure 4-35. Once the specimen was sufficiently aligned, each threaded rod was sequentially tightened down, and column cap preparation began.

Figure 4-34: Column Specimen Placement and Fixation to the Testing Frame

Figure 4-35: Specimen Alignment Checks, Checking for Level (l), Checking for Square (r)

4.2.2 Column Cap Construction

The reinforced concrete column cap was the last part of each column specimen to be constructed. The column cap was one of the most complex parts of the specimen, similar to the column base, but with components in multiple directions in a confined space. Each column cap consisted of a simple reinforcement cage, four PVC pipes for the loading apparatus connection, a continuation of the four PVC pipes for the post-tensioning, and either an embedded spiral-tied reinforcement cage or steel tube. The complexity of the cap layout made the sequence of the

construction crucial. The same steps were used to assemble each column cap with minor modifications to account for the added complexity of the RC column cage.

The RC column cap construction required no plug but did require some manipulation of the embedded reinforcement cage. A few longitudinal rebar hooks and a small section of the spiral tie were removed to accommodate the 1¼-inch PVC pipes. For the HC-FCS columns, a circular plywood plug with four small pieces of angle was tack welded and sealed with silicone inside the steel tube to the depth of the top of the column. The plug prevented concrete from entering the hollow portion of the column while maintaining the steel tube embedment in the column cap. Then, eight holes, four on each side of the protruding steel tube, were torch-cut to allow the 1¼-inch PVC pipes to pass through. A jig with a laser level was used to determine the center of each hole and a magnet was used as a template for each hole. The plug and through-holes are shown in Figure 4-36. Additionally, four small holes were torched into the top of the steel tube to allow air to escape as the embedded region filled with concrete.

Figure 4-36: HC-FCS Column Cap Preparation, Plug Installment (l) and Laser and Jig Used to Determine Through-Hole Locations (r)

All column specimens required the ½-inch PVC pipes to be extended 12 inches beyond the end of the reinforcement cage or steel tube. Next, the custom formwork surrounding the protruding column was placed, and the column cap cage was added and suspended. The inside faces of the column cap formwork were coated with a form-release agent while the edges were

left bare for silicone application. Each formwork seam or gap was sealed with silicone to prevent concrete from leaking and to improve the clean-up and turnaround process. The bottom and east sides of the formwork were assembled first and set in place. Then, the 1¼-inch PVC pipes were inserted through gaps in the reinforcement cage or the holes in the side of the steel tube. The 1¼-inch PVC pipes were also coated with a form-release agent to aid in their removal should the actuator mounting assembly require additional tolerances. The west side of the formwork was added and each of the PVC pipes was lined up with the corresponding dowels. Next, the north formwork end was added, and each ½-inch PVC pipe was inserted over its supporting dowel. All PVC pipe ends were sealed with silicone to limit concrete paste infiltration. Finally, the custom formwork piece on the south end was moved into place, secured, and sealed with silicone. Figure 4-37 and Figure 4-38 show the column specimens before and after being prepared for the column cap addition.

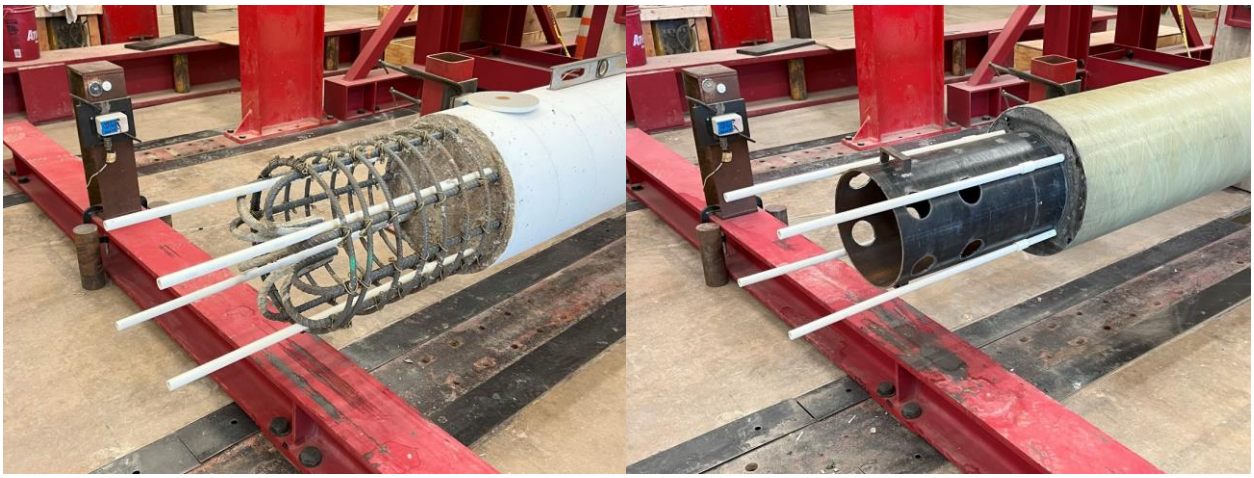

Figure 4-37: Column Specimens Before Column Cap Addition, RC (l) and HC-FCS (r)

Figure 4-38: Final Column Cap Assembly Before Casting, RC (l) and HC-FCS (r)

The HS-SCC mix design was used for the column caps. This concrete mix design offered high early strengths that facilitated testing the column specimens within three days of casting the column cap. Furthermore, the HS-SCC offered high flowability and consolidation properties that were ideal for the congested cap. The HS-SCC concrete mix design was prepared and mixed on-site and yielded an average slump spread flow of 25 inches. The concrete was dispensed into the formwork via a concrete bucket, and a concrete vibrator was used to ensure sufficient consolidation within the embedded region of the steel tube. The outside of the formwork was struck with mallets for additional consolidation. In addition to casting the cap, 4x8 concrete cylinders were made for 3-day, 28-day, and test-day compressive strength testing in general accordance with ASTM C39. The column cap and concrete cylinders were covered with wet burlap and plastic for three days. After three days of curing, the formwork was stripped from the column cap. First, the bottom was freed, then the east and west sides were removed, followed by the north and south ends. The south end formwork was capable of splitting into two halves to be removed from the specimen. A completed column cap ready for testing is shown in Figure 4-39. The formwork was cleaned and reassembled as necessary, and the process was repeated for each column cap.

Figure 4-39: Column Cap During Casting and Completed and Ready for Testing

4.2.3 Loading System Assembly

Following the completion of the column cap, the cyclic lateral loading and measurement system was assembled and attached to the cap. The loading assembly was mounted by first inserting four 1⅛-inch diameter high-strength threaded steel rods through the PVC pipes through the side of the column cap. Next, 1-inch thick, 12-inch-wide square spreader plates were installed over the steel rods on either side of the cap. The hydraulic actuator was then lifted into place with the crane and attached to the load cell adapter plate at the rear of the actuator. The forklift was used to hold the actuator level while it was extended to approximately half of its available stroke length and over the protruding steel rods from the column cap. Once contact was initiated with the cap and spreader plate, the spreader plate was positioned and leveled, and nuts and washers were added to both ends of the steel rods. A half inch of thread was left extended beyond the nut on the actuator side. Finally, the rear spreader plate was leveled, and each rod was firmly tightened down. The finalized loading system attachment is shown in Figure 4-40. Lastly, two 3-inch diameter solid steel rollers were placed underneath the column cap to prevent vertical deflection during testing. Vertical deflections would not only cause undesirable torsion on the column but also potentially damage the hydraulic actuator and load cell system. The rollers were placed parallel to the column cap on ½-inch diameter solid steel rods that ran parallel to the direction of loading and perpendicular to the column cap.

Figure 4-40: Attachment of Loading System Assembly

4.2.4 Constant Axial Compressive Load Application

Four 7-wire Gr. 270 prestressing strands running along the length of the columns were used to apply the constant axial compressive load to the column specimens by post-tensioning. The axial load represented the dead weight that the column would be subject to in service. Each prestressing strand was inserted through the cast-in-place PVC pipes that served as post-tensioning ducts. Sufficient length was left extended beyond the column base and cap such that the appropriate anchoring hardware could be installed. At the column base, 3-inch-wide, ½-inch thick steel plates were used as spreader plates underneath each pre-tensioning chuck. For the first two column specimens tested, a through-hole load cell was placed underneath one of the chucks during the post-tensioning process to calibrate the hydraulic post-tensioning jack and to ensure the correct load was applied to the prestressing strands. The jacking pressure that corresponded to the desired load after anchorage seating losses was noted. After post-tensioning, the load cell was left in place and occasionally monitored during testing of the second column specimen.

At the column cap, post-tensioning anchors were used so that each strand was post-tensioned at the column cap. Spacer plates were used underneath the anchors such that each anchor bore flat on the column cap. After the first column specimen was tested, an additional notched 1-inch spacer plate was added for easier removal of the post-tensioning after testing. The strands were sequentially tensioned in an X-shaped pattern starting with the top left strand, followed by the bottom right, top right, and then bottom left. This loading procedure was done to mitigate bending moments applied to the column from unbalanced post-tensioning forces. The

post-tensioning was removed in the same order after testing. Large concrete blocks were placed at either end of the column specimen to protect against potential strand failure and deflect any fractured strands. Both anchorage systems are shown below in Figure 4-41.

Figure 4-41: Constant Axial Load Application Utilizing Post-Tensioning

4.2.5 Final Column Instrumentation & Layout

Column specimen instrumentation consisted of a load cell, four wire pots, and either 8 or 12 strain gauges depending on the specimen. The load cell was placed behind the linear hydraulic actuator to measure the load required to displace the column cap. Additionally, wire pot 1 (WP1) was used to measure the lateral displacement of the column cap at the centerline of the applied load. A second wire pot, wire port 2 (WP2) was positioned at the midspan of the lever arm from the applied load to the bottom of the column, approximately 51 inches above the top of the column base. Wire pots 3 (WP3) and 4 (WP4) were placed behind the column base and testing frame and were used to measure the rotation of the base during testing at the middle of the rear vertical edges on either side of the base. All of the strain gauges were applied to each specimen before its introduction into the testing frame. The RC column specimen had only 8 internal gauges on the steel reinforcement while the HC-FCS columns possessed 4 external gauges on the GFRP tube in addition to 8 internal gauges on the steel tube. Before each column test was initiated, each sensor was checked and attached to the data acquisition system to ensure data was being collected. The load cell was checked by manually pushing on the column cap and

each wire pot was checked by extending and retracting the wire a known distance. Each strain gauge was checked with a multimeter for a valid signal before being connected to the data acquisition equipment. All 56 strain gauges between the five column specimens tested registered a valid signal before testing. The column specimen instrumentation is shown in Figure 4-42, and a final, completed column specimen testing arrangement is shown in Figure 4-43.

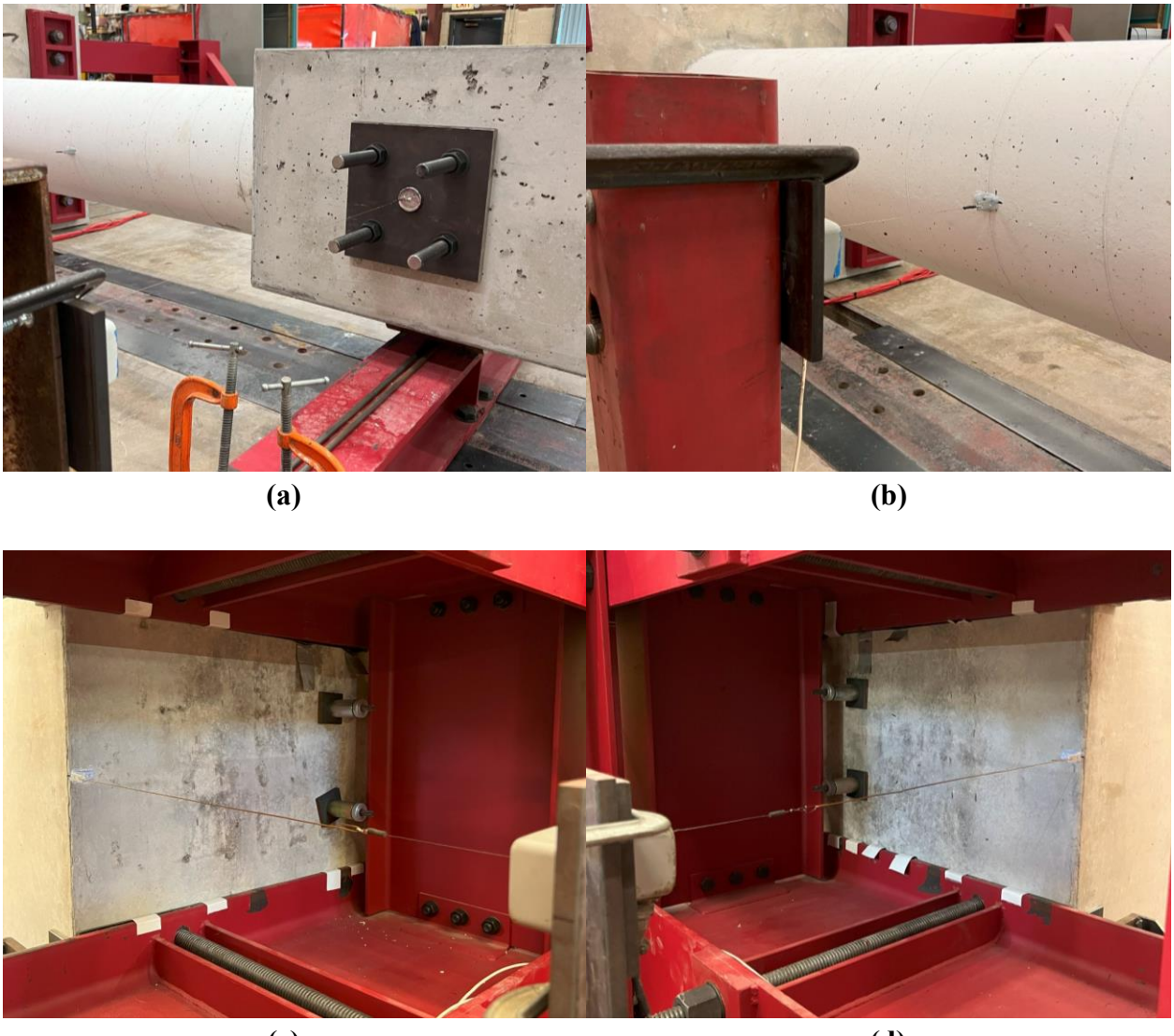

(a) **(b)**

(c) **(d)**

Figure 4-42: Column Specimen Instrumentation, (a) WP1 at the Column Head, (b) WP2 at the Column Midspan, (c), WP3 at the SW Base Edge, (d) WP4 at the SE Base Edge

Figure 4-43: Completed Column Specimen Testing Arrangement

Chapter 5: Column Specimen Testing and Results

Each column specimen was tested under a constant axial compressive load and subjected to a displacement-controlled, cyclic lateral loading. Several modifications were made during and following the testing of the first column specimen due to unforeseen issues caused by the novelty of the column testing frame and procedure. The results of each column test, including concrete compressive strengths, forensic photographs, and load-deflection and representative strain gauge plots, are presented in this chapter.

5.1 Column Specimen Testing Procedure

The RC and HC-FCS column specimens were tested under a constant axial compressive load that was approximately 5% of the axial capacity of the RC control column. The displacement-controlled, cyclic lateral loading followed FEMA P-2082-1 (2020) guidelines. The novelty of the newly developed and constructed column testing frame led to modifications of the testing frame and testing procedure. These modifications were made to the initial testing procedure during and after testing the first column specimen, HS-SCC 1. The first specimen was tested in three distinct stages with modifications made as issues arose. The modifications and resulting testing procedures are outlined in this section.

5.1.1 Column Specimen Loading Protocol

The column specimens were subjected to cyclic lateral loading that was displacement-controlled and followed FEMA P-2082-1 (2020) guidelines, which outline increasing each subsequent displacement amplitude by 40% with two cycles for each displacement increment. The initial displacement increment was selected to be 0.05 inches and was controlled by the conventional RC column due to the stiffness, lower ductility, and assumed lower flexural capacity. The loading protocol was determined by multiplying the previous displacement step by 1.4 to determine the displacement for the subsequent step, which is shown in Figure 5-1.

The loading protocol was administered manually at a steady pace via an electric pump and a calibrated thumb. The lateral loading was instigated by extending the actuator outward in the west direction and each specimen test was initiated in the same manner. Extending outward, or pushing the column, registered a positive compression load on the load cell and a negative

deflection on WP1 and WP2 as the wire was drawn inward. Retracting the actuator inward, or pulling the column, registered a negative tension load on the load cell and a positive deflection on WP1 and WP2 as the wire was extended outward. The contradiction of normal sign convention caused by the orientation of the wire pot was later fixed during the post-processing of the data.

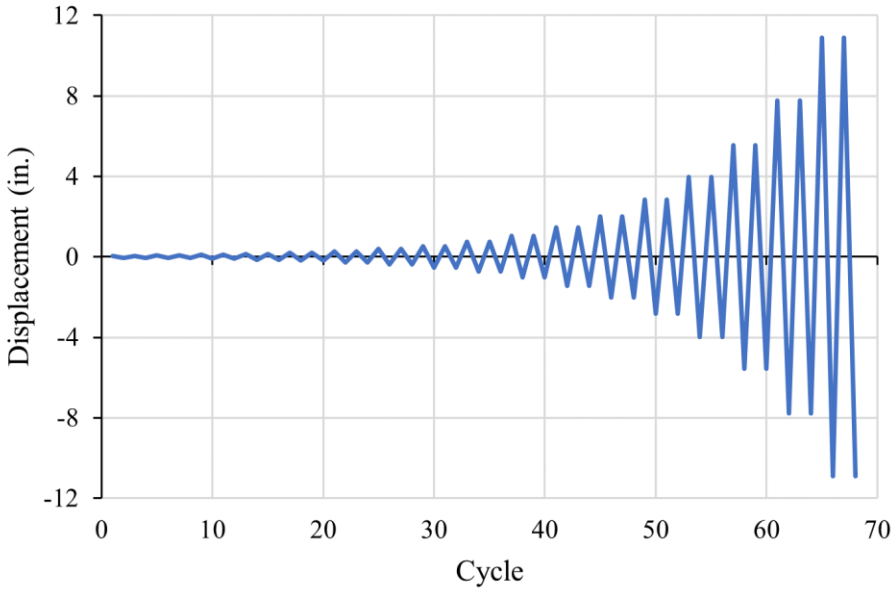

Figure 5-1: Lateral Displacement Loading Protocol

5.1.2 Initial Testing Procedure Modifications from Trial & Error

Column testing began by testing the HS-SCC HS-FCS columns instead of the RC control column. This was done due to the novelty and uncertainty of the newly developed testing frame, given that two HS-SCC columns were created compared to the lone RC column. The testing of the first column specimen, HS-SCC 1, or SCC 1 for short, was done in three parts due to unforeseen complications caused by the strain gauge data acquisition and the loading assembly. Due to initial difficulties with the strain gauges and data acquisition system, strain gauge data was not obtained during the first part of the column test. However, testing was permitted to continue and at a lateral loading of approximately 38 kips applied in tension, the weld restraining the bottom of the diagonal HSS support on the actuator mounting brace fractured. No other damage to the loading system or frame was noted, however, the specimen was returned to zero deflection and the test was stopped. After closer analysis and examination of the fractured weld,

it was determined that the weld had poor penetration. The actuator mounting brace was rebuilt with a wider HSS section that allowed for an increased welding perimeter. Additionally, better surface preparation and welding procedures were implemented and previous welding on the brace was reinforced. The fractured weld and reconstruction of the loading system mounting brace are shown in Figure 5-2. Testing was resumed by reattaching the loading assembly to the column and restarting at the beginning of the previously incomplete cycle.

Figure 5-2: Loading System Fractured Weld and Reconstruction

After completing four additional cycles, the column was pushed outward to begin cycle five when the original single-through threaded steel rod design buckled nearing 41 kips. It was determined that the steel rod buckled due to an unbraced length of the rod creating a hinge point due to the hinge in the actuator's knuckle nearby. This is shown in Figure 5-3. Testing was immediately halted due to the compromised rod, and the column was attempted to be brought back to zero deflection. However, the column was unable to be brought back to zero deflection and safely detached from the loading assembly due to residual plastic deformations, therefore the specimen was brought back to minimum load. This failure prompted a redesign of the loading assembly that led to the load cell being moved behind the actuator, guide rails installed along the load cell assembly, and a new layout of four smaller threaded rods through the loading stub. The redesigned and reconstructed loading system is shown in Figure 5-4. Hilti epoxy and threaded rod anchors were used to adapt the specimen to the new loading setup. This was done by drilling into the loading stub until the steel tube was contacted and gluing in new threaded rods. Testing was resumed by pulling the loading stub back to a manually measured zero deflection starting point, noting the applied load, and resulting deflection, and then applying a tare to the data

acquisition program. The measured load was later adjusted to account for the initial load required to pull the column back to zero.

Figure 5-3: Buckling Failure of Original Loading System

Figure 5-4: Original Loading System Failure (l) and the Redesigned Loading System (r)

Upon completion of the first column specimen, the second specimen HS-SCC 2, or SCC 2 for short, was tested. Dissimilar to the testing of SCC 1, the through load cell on the post-tensioning strand was monitored during testing. The maximum deflection of the loading system

was initially controlled by the stroke length of the hydraulic actuator used and was taken as 14 inches. However, while testing the second column specimen and monitoring the load cell on the post-tensioning strand, it was determined that the maximum allowed displacement based on the loading protocol would be 10.89 inches. This was due to geometric constraints that caused the strands on one side of the column to increase in load while the opposite side decreased in load during displacements. A displacement of 10.89 inches resulted in the post-tensioning strands approximately exceeding 80% of the specified ultimate tensile strength of 270 ksi. While SCC 1 was unknowingly pushed beyond this limit, pushing any future columns beyond the 10.89-inch displacement cycle was deemed unsafe.

5.2 Column Specimen Testing Results

Column specimen testing began with the HS-SCC HC-FCS column specimens, followed by the RC column specimen, and then the UHPC HC-FCS column specimens. However, the RC column results will be presented first, followed by the HS-SCC and UHPC HC-FCS specimen results. This section presents the results of each column test, including the 28-day and test-day concrete compressive strengths, forensic photographs of the resulting damage and deconstruction, and each specimen's load-deflection and representative strain gauge plots.

5.2.1 Concrete Compressive Strength Results & Discussion

Concrete compressive strengths at 28 days after casting and on the day the specimen was tested were determined in general accordance with ASTM C39. The resulting compressive strengths for each component of each column specimen are summarized in Table 5-1. The concrete compressive strength for the reinforced concrete base of the RC specimen was determined at 56 days instead of 28 days. Furthermore, due to the issues encountered with the initial column test, the test day compressive strengths of the HS-SCC 1 specimen were determined after the third and final part of testing concluded, approximately 56 days after casting the column cap. This resulted in the test-day compressive strength of the column cap to resemble the 28-day compressive strength more closely. The other column specimens were tested within a week of casting the column cap.

Table 5-1: 28-Day and Test-Day Concrete Compressive Strengths for Each Component

Specimen		Base		Column		Cap	
Type	Label	f_c' at 28 Days (psi)	f_c at Test Day (psi)	f_c' at 28 Days (psi)	f_c at Test Day (psi)	f_c' at 28 Days (psi)	f_c at Test Day (psi)
RC		5,120*	4,230	7,630	7,410	10,210	8,680
HC-FCS	HS-SCC 1	4,450	4,040	10,220	9,650	9,600	9,560**
	HS-SCC 2	4,500	4,180	9,800	9,330	9,820	8,730
	UHPC 1	4,290	3,850	19,390	19,740	10,650	9,180
	UHPC 2	4,870	4,020	19,510	20,810	10,420	9,150

*56-day compressive strength

**HS-SCC 1 test-day cylinders were tested after part three of testing the column

5.2.2 RC Column Specimen Testing Results & Discussion

The RC column specimen tested represented a traditional, spiral-tied reinforced concrete column and served as a control specimen and baseline comparison for column ductility, durability, and flexural capacity. The specimen ready for testing is shown in Figure 5-5. Due to the nature of the column, significant spalling was observed during testing that eventually revealed the transverse spiral tie and longitudinal reinforcement. The specimen during and after testing is shown in Figure 5-6. Furthermore, the longitudinal bars were observed to buckle while in compression, and some eventually fractured while in tension. A total of three longitudinal bars were fractured during testing, including each bar at the extreme fiber on both sides of the column, and a bar next to one of the extreme fibers. Figure 5-7 and Figure 5-8 illustrate the column damage on the west and east sides, respectively, before and after loose concrete removal.

During testing, the instrumentation captured the load and displacement at the column head, which is plotted in Figure 5-9. The maximum load sustained by the column was 29.3 kips at a measured displacement of 7.77 inches in the eastward, or extension, direction. Additionally, strain gauges on the steel reinforcement captured the strain in the longitudinal bars at each extreme fiber and along the neutral axis of the column. There were no external strain gauges on the RC column specimen. Due to the nature of the testing, the strain gauges were eventually damaged, leading to incoherent or constant readings. These errant readings were removed from the strain gauge plots by trimming the data back to the last comprehensible reading. A

representative strain gauge plot from the steel reinforcement at the extreme fiber is shown in Figure 5-10, while a gauge at the neutral axis is shown in Figure 5-11. Supplemental strain gauge plots from the other gauges not presented can be found in the Appendix.

Figure 5-5: RC Column Specimen Before Testing

Figure 5-6: RC Column Specimen During (l) and After Testing (r)

Figure 5-7: RC Column West Side After Testing (l) and Removal of Loose Concrete (r)

Figure 5-8: RC Column East Side After Testing (l) and Removal of Loose Concrete (r)

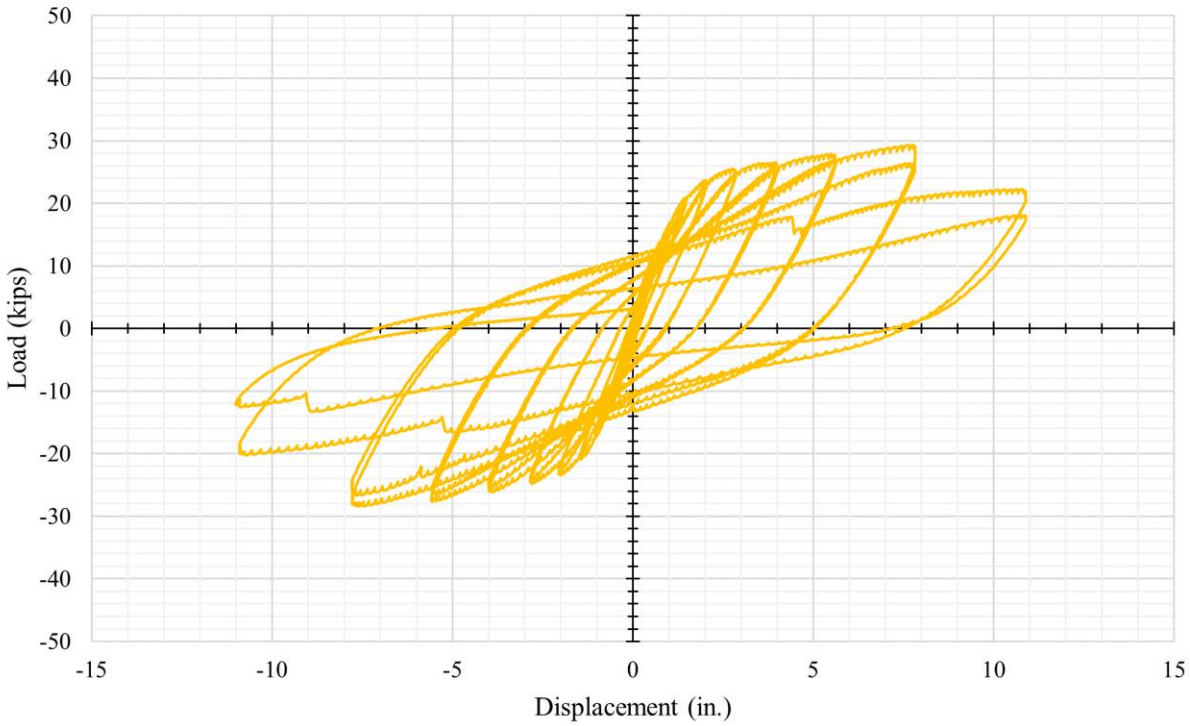

Figure 5-9: RC Column Lateral Load vs. Displacement at Column Head

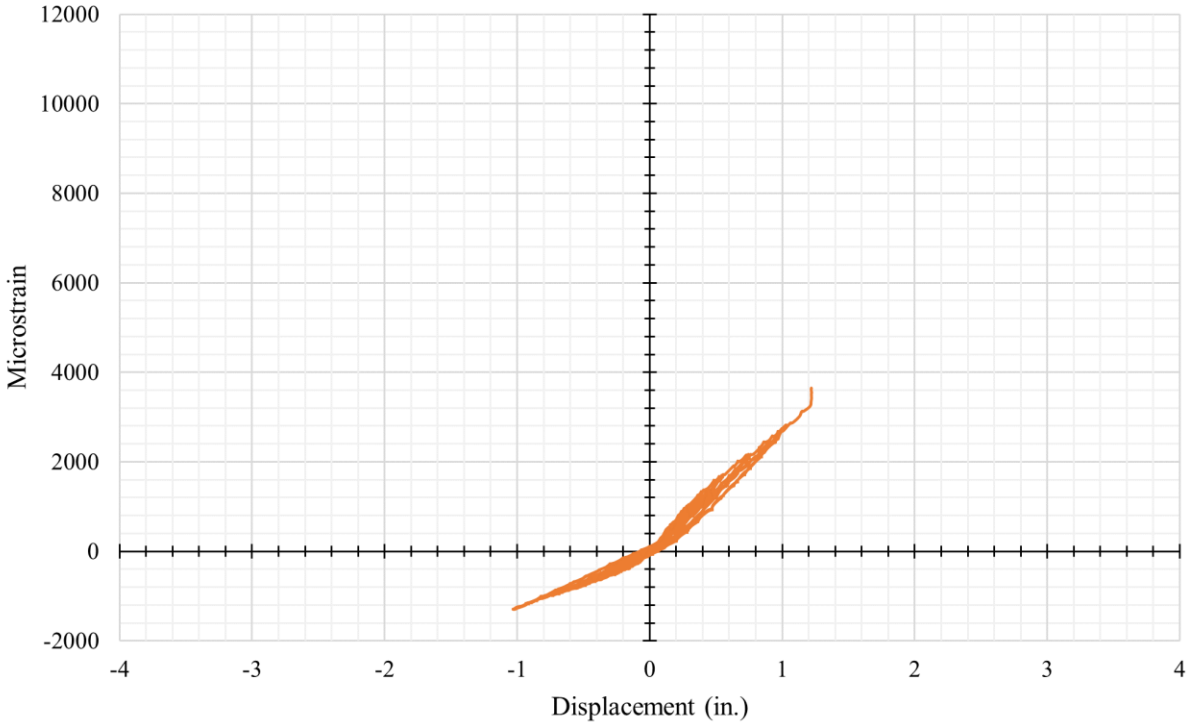

Figure 5-10: RC SW1 Steel Strain Gauge vs. Displacement at Column Head

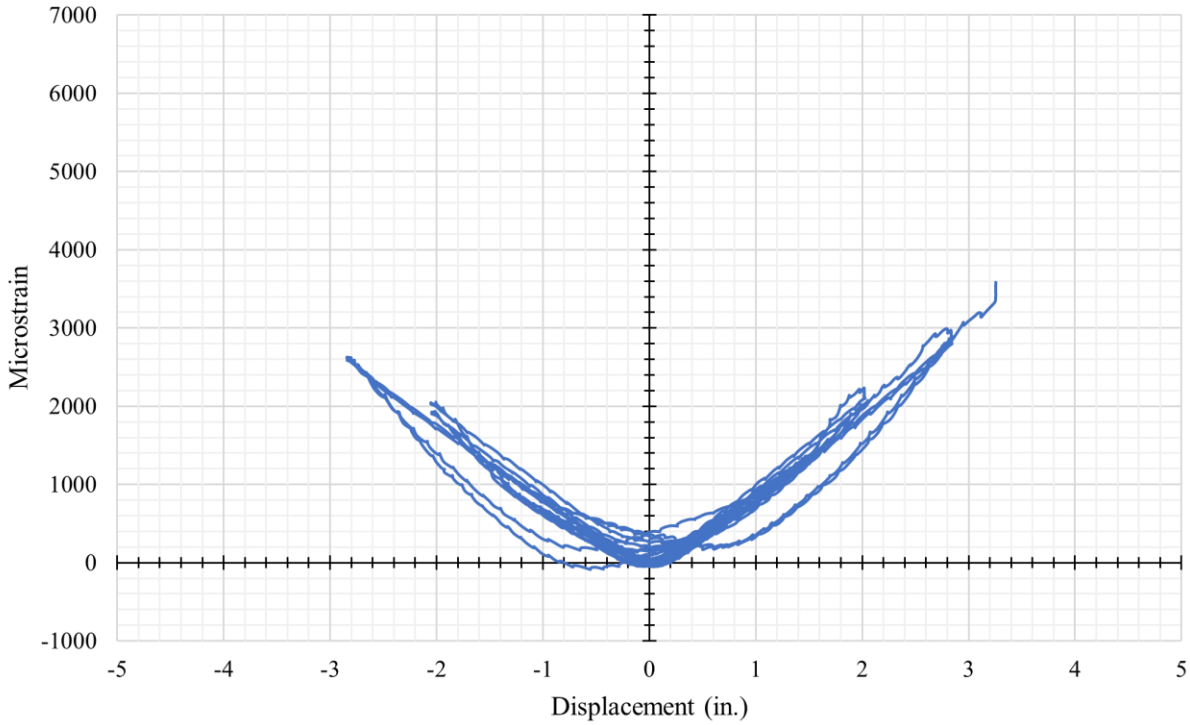

Figure 5-11: RC SN1 Steel Strain Gauge vs. Displacement at Column Head

5.2.3 HS-SCC 1 HC-FCS Column Specimen Testing Results & Discussion

HS-SCC 1 was the first HC-FCS column specimen tested. The testing consisted of three distinct segments with each corresponding to an issue encountered with the newly constructed and developed testing frame and procedure. A more detailed breakdown of each segment is presented in Section. The specimen ready for testing is shown in Figure 5-12. Due to the nature of HC-FCS columns, the outer GFRP layer prevented the observation of cracking in the concrete core during testing. However, a gap formed between the column and base during testing, and eventually the GFRP shell began to show more significant signs of distress at larger displacements. Figure 5-13 shows the specimen during and after testing. Figure 5-14 shows the gap between the GFRP tube and the concrete base during testing. Figure 5-15 shows the GFRP tube's condition after testing was completed.

Figure 5-12: HS-SCC 1 Column Specimen Before Testing

Figure 5-13: HS-SCC 1 Column Specimen During (l) and After Testing (r)

After testing, the lower 15 inches of the GFRP tube was sectioned off, split in half, and removed from the column to reveal the concrete core underneath, as shown in Figure 5-16. The GFRP tube was cut along the top neutral axis to limit disturbance to the concrete core that might obscure accurate crack observation along the extreme fibers. Next, loose portions of the concrete core were removed so that the damage to the steel tube could be observed. The steel tube was found to have buckled along the extreme fibers of both sides of the column and fractured on one side. Figure 5-17 illustrates the steel tube damage after concrete removal.

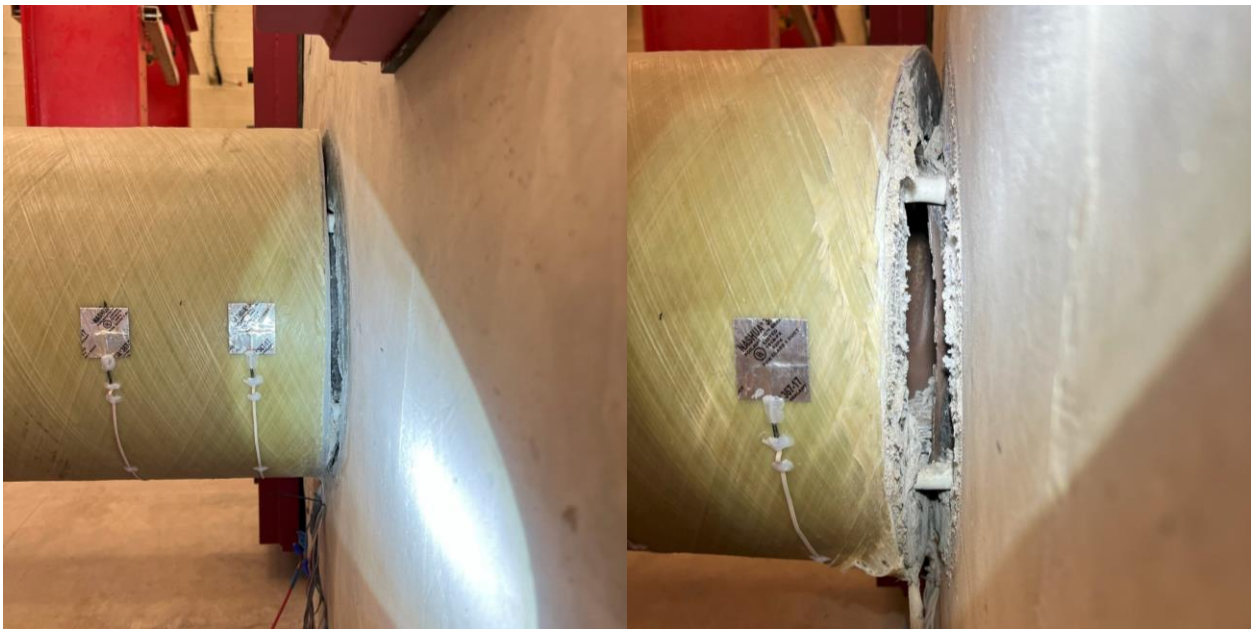

Figure 5-14: HS-SCC 1 Column Separation and Fractured Steel Tube During Testing

Figure 5-15: HS-SCC 1 GFRP Tube West (l), Top (m), and East Side (r) Damage After Testing

During testing, the instrumentation captured the load and displacement at the column head, which is plotted in Figure 5-18. The maximum load sustained by the column was 45.2 kips at a measured displacement of 5.56 inches in the westward, or retraction, direction. Additionally, strain gauges on the steel reinforcement captured the strain in the steel tube at each extreme fiber and along the neutral axis of the column. A representative strain gauge plot from the steel tube at the extreme fiber is shown in Figure 5-19, while a gauge at the neutral axis is shown in Figure

5-20. Furthermore, external strain gauges on the GFRP tube captured the hoop strain at each extreme fiber, and a representative plot is shown in Figure 5-21. Due to the testing procedure of HS-SCC 1, initial strain gauge measurements were not obtained and therefore not shown in the strain gauge plots. HS-SCC 1 strain gauge plots are presented as graphical comparisons and should not be used to directly compare measured strains due to the missing initial data.

Figure 5-16: HS-SCC 1 Concrete Core After Testing and Light Removal of Concrete

Figure 5-17: HS-SCC 1 Steel Tube West (l), Top (m), and East Side (r) Damage After Testing

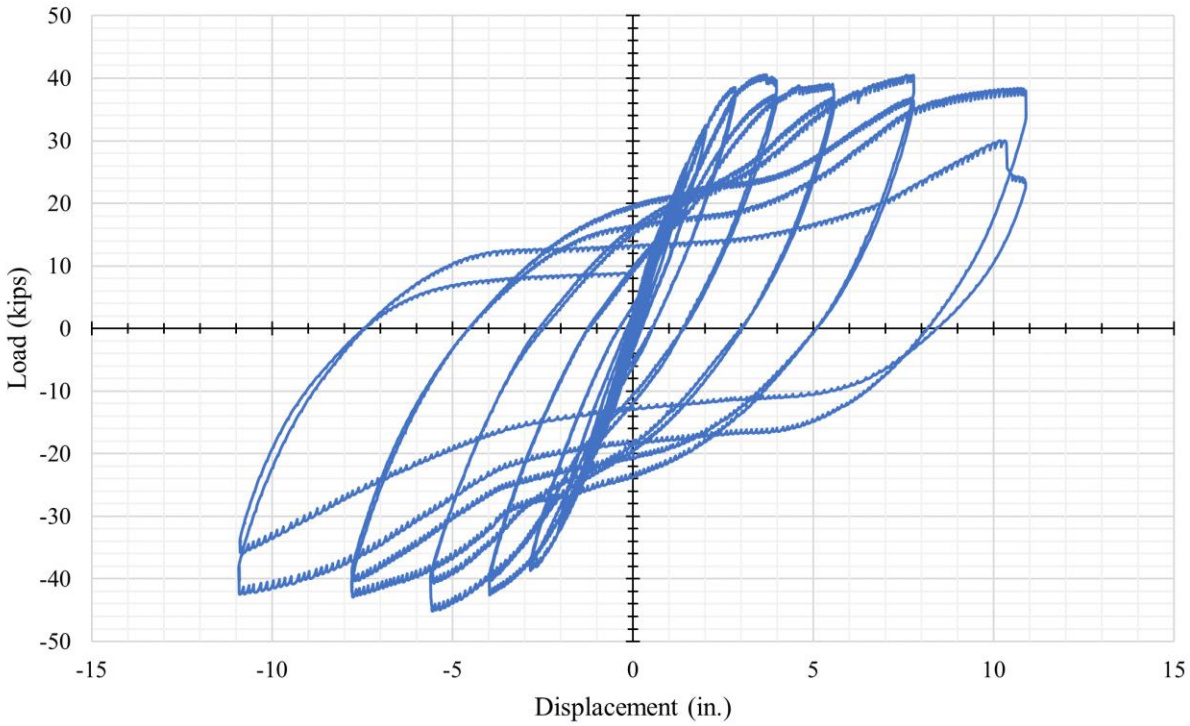

Figure 5-18: HS-SCC 1 Column Lateral Load vs. Displacement at Column Head

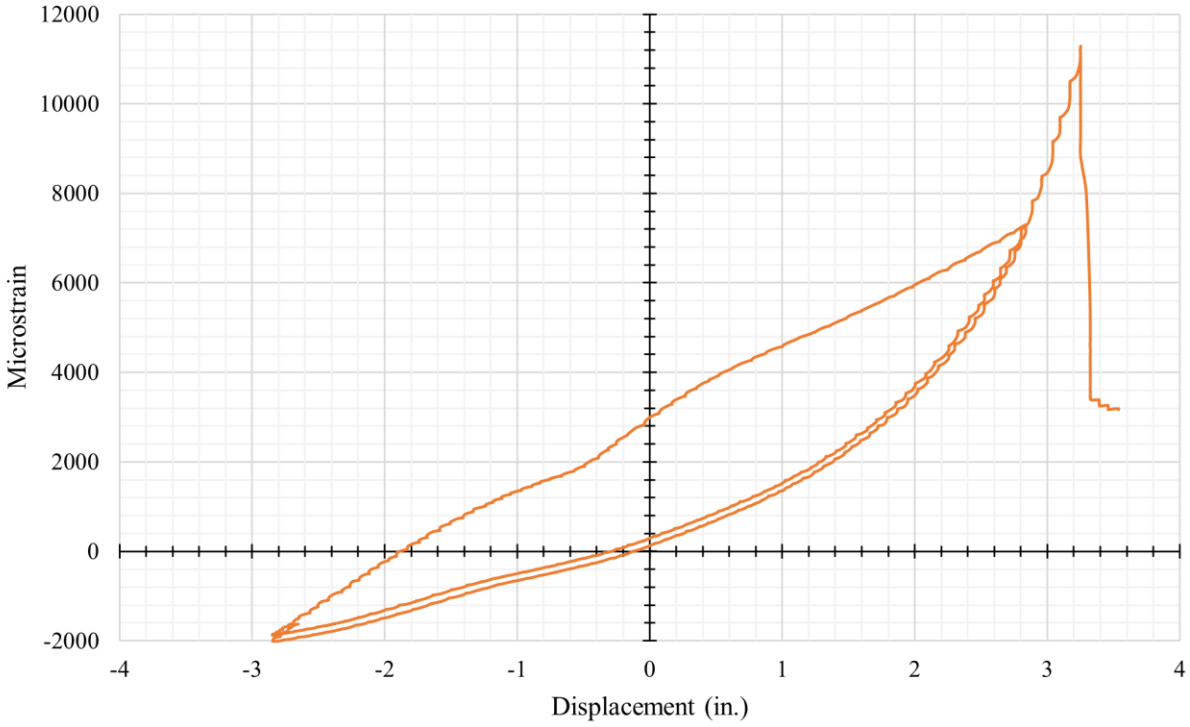

Figure 5-19: HS-SCC 1 SW1 Steel Strain Gauge vs. Displacement at Column Head

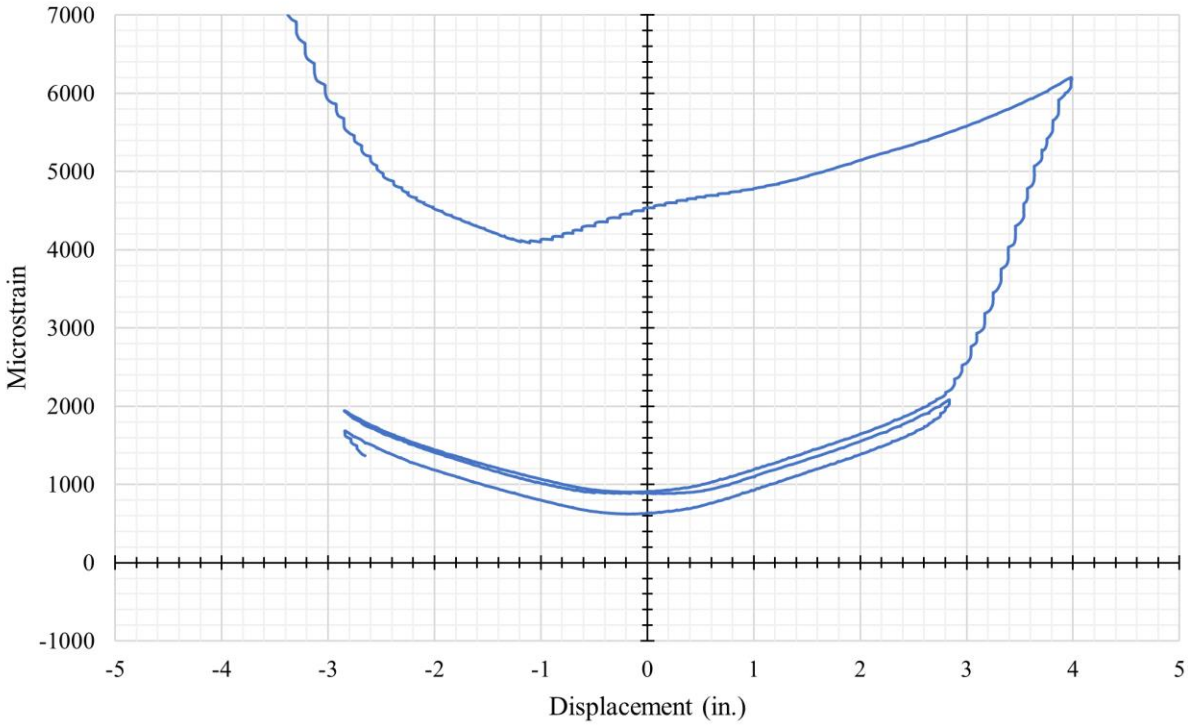

Figure 5-20: HS-SCC 1 SN1 Steel Strain Gauge vs. Displacement at Column Head

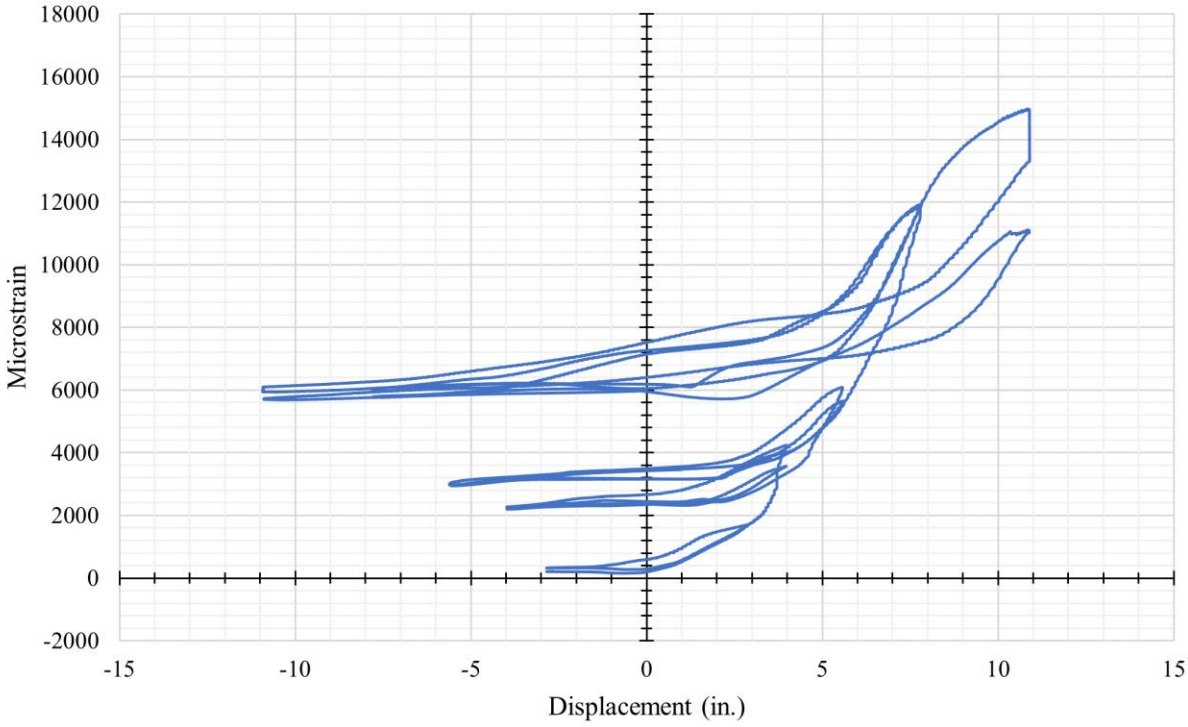

Figure 5-21: HS-SCC 1 GE1 GFRP Strain Gauge vs. Displacement at Column Head

5.2.4 HS-SCC 2 HC-FCS Column Specimen Testing Results & Discussion

HS-SCC 2 was the second HC-FCS column specimen tested. The specimen ready for testing is shown in Figure 5-22. HS-SCC 2 displayed similar behavior and damage characteristics to that of HS-SCC 1. Similar to the first HS-SCC HC-FCS specimen tested, a gap formed between the column and base during testing, and eventually the GFRP shell began to show more significant signs of distress at larger displacements. Figure 5-23 shows the GFRP tube's condition after testing was completed.

Figure 5-22: HS-SCC 2 Column Specimen Before Testing

After testing, the lower 15 inches of the GFRP tube was sectioned off, split in half, and removed from the column to reveal the concrete core underneath as shown in Figure 5-24. Next, loose portions of the concrete core were removed so that the damage to the steel tube could be observed. The steel tube was found to have buckled along the extreme fibers of both sides of the column and minor fracturing on both sides. Figure 5-25 illustrates the steel tube damage after concrete removal.

Figure 5-23: HS-SCC 2 GFRP Tube West Side (l) and East Side (r) Damage After Testing

Figure 5-24: HS-SCC 2 Concrete Core After Testing and Light Removal of Concrete

Figure 5-25: HS-SCC 2 Steel Tube West (l), Top (m), and East Side (r) Damage After Testing

During testing, the instrumentation captured the load and displacement at the column head, which is plotted in Figure 5-26. The maximum load sustained by the column was 43.6 kips at a measured displacement of 5.23 inches in the westward, or retraction, direction. Additionally, strain gauges on the steel reinforcement captured the strain in the steel tube at each extreme fiber and along the neutral axis of the column. A representative strain gauge plot from the steel tube at the extreme fiber is shown in Figure 5-27, while a gauge at the neutral axis is shown in Figure 5-28. Furthermore, external strain gauges on the GFRP tube captured the hoop strain at each extreme fiber, and a representative plot is shown in Figure 5-29.

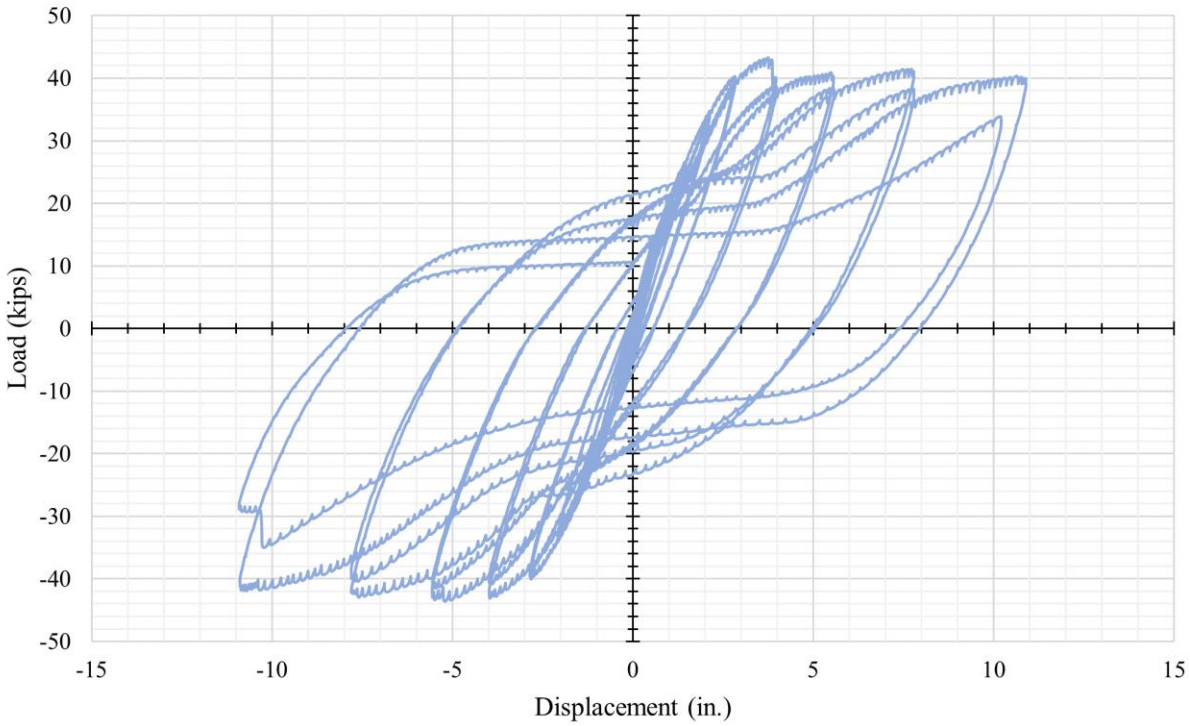

Figure 5-26: HS-SCC 2 Column Lateral Load vs. Displacement at Column Head

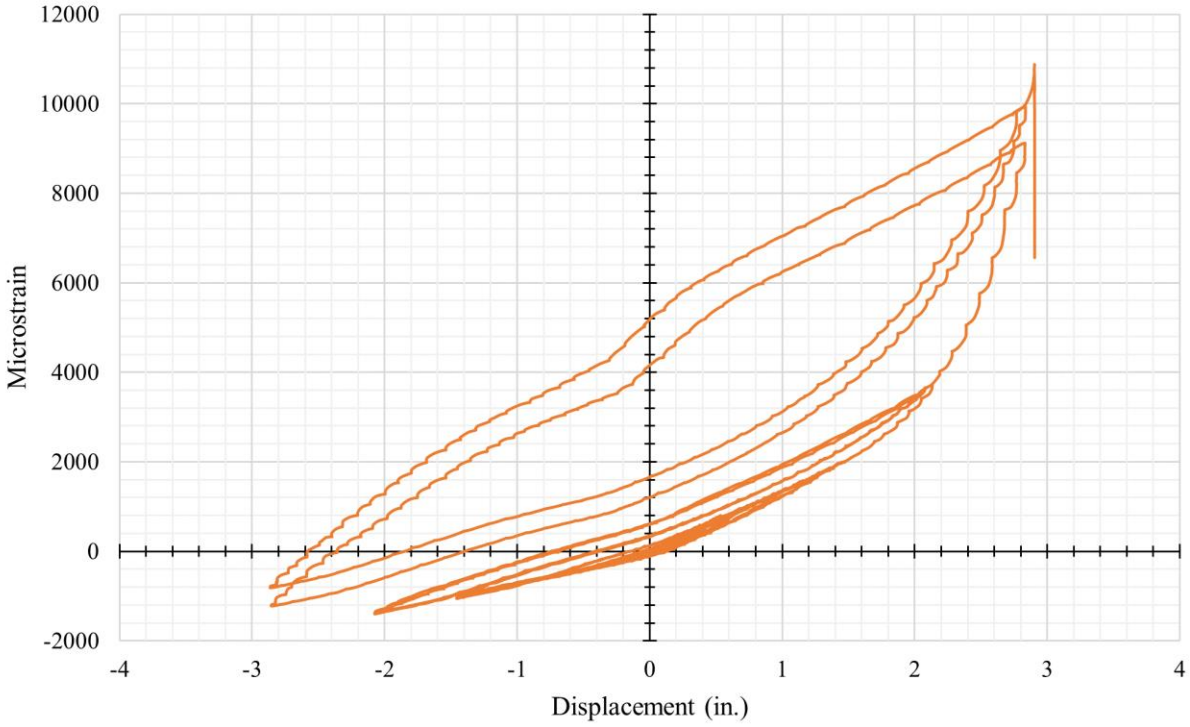

Figure 5-27: HS-SCC 2 SW1 Steel Strain Gauge vs. Displacement at Column Head

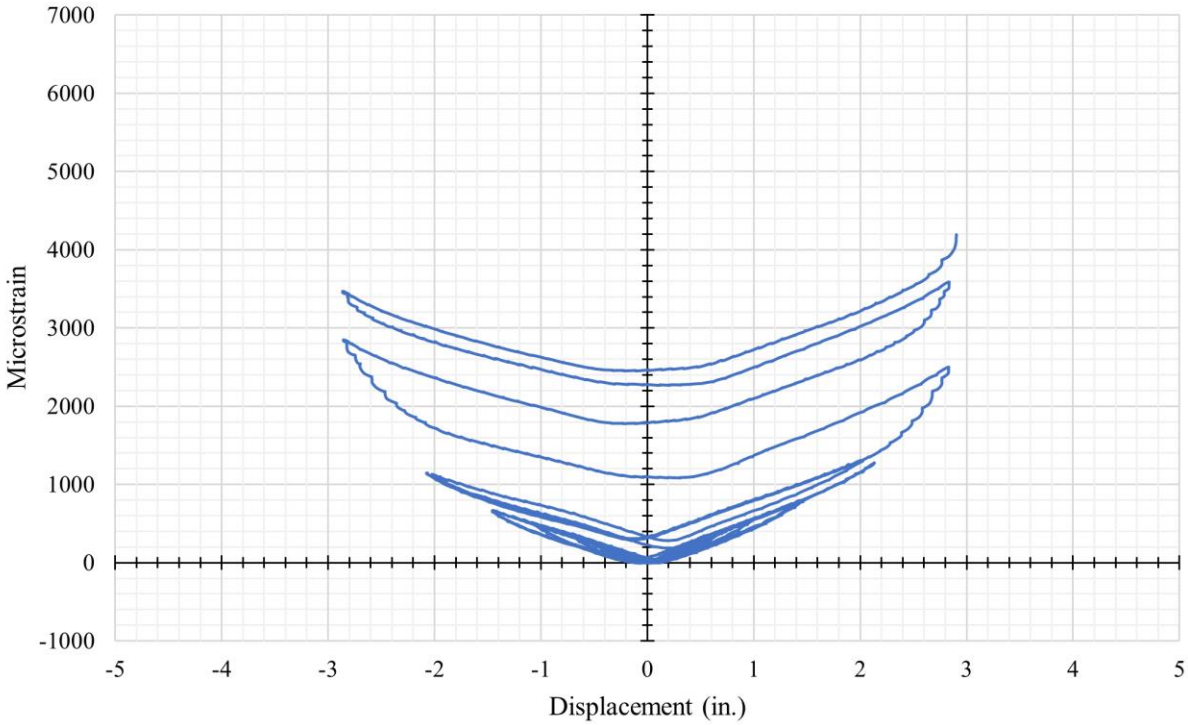

Figure 5-28: HS-SCC 2 SN1 Steel Strain Gauge vs. Displacement at Column Head

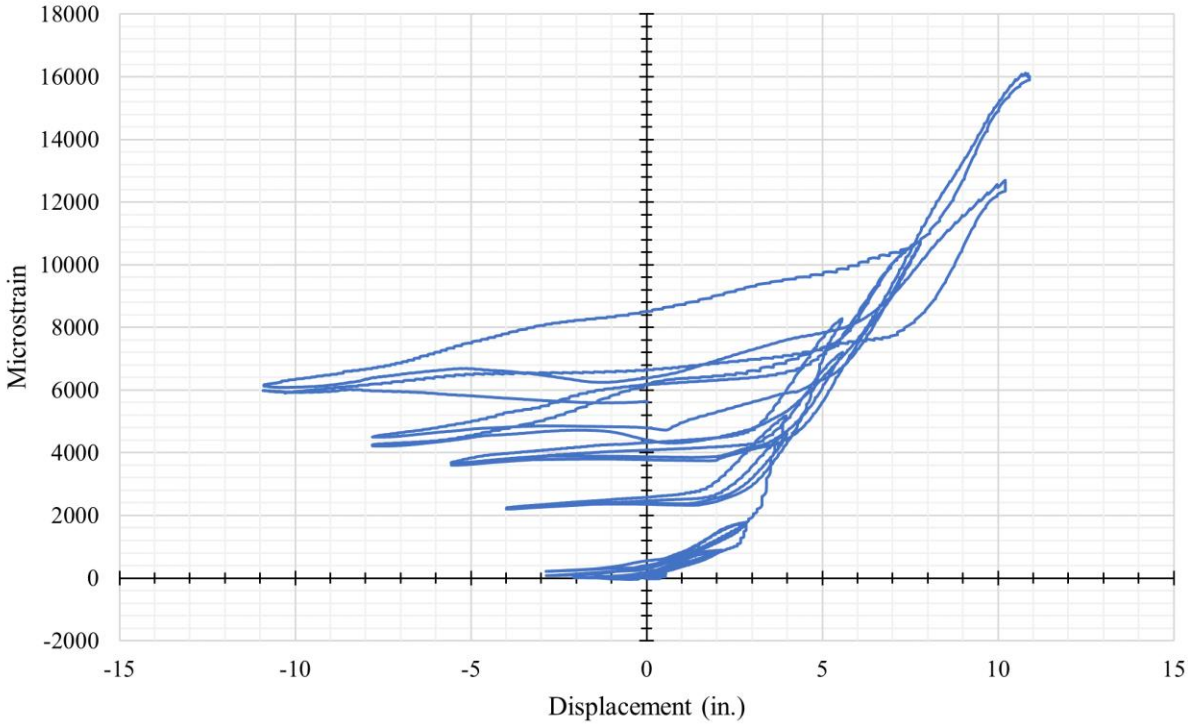

Figure 5-29: HS-SCC 2 GE1 GFRP Strain Gauge vs. Displacement at Column Head

5.2.5 UHPC 1 HC-FCS Column Specimen Testing Results & Discussion

UHPC 1 was the third HC-FCS column specimen tested and the first UHPC column specimen tested. The specimen ready for testing is shown in Figure 5-30. Due to the nature of HC-FCS columns, the outer GFRP layer prevented the observation of cracking in the concrete core during testing. However, a gap formed between the column and base during testing, and eventually the GFRP shell began to show minimal signs of distress at larger displacements. Figure 5-31 shows the specimen and the gap between the GFRP tube and the concrete base during testing. Figure 5-32 shows the GFRP tube's condition after testing was completed.

Figure 5-30: UHPC 1 Column Specimen Before Testing

After testing, the lower 15 inches of the GFRP tube was sectioned off, split in half, and removed from the column to reveal the concrete core underneath, as shown in Figure 5-33. The GFRP tube was cut along the top neutral axis to limit disturbance to the concrete core that might obscure accurate crack observation along the extreme fibers. Next, the concrete core was removed by cutting and jackhammering so that the damage to the steel tube could be observed. The UHPC had to be cut loose and jackhammered away from the steel tube due to the presence of steel fibers leading to increased durability. The steel tube was found to have buckled along the

extreme fibers of both sides of the column with minimal fractures on both sides. Figure 5-34 illustrates the steel tube damage after concrete removal.

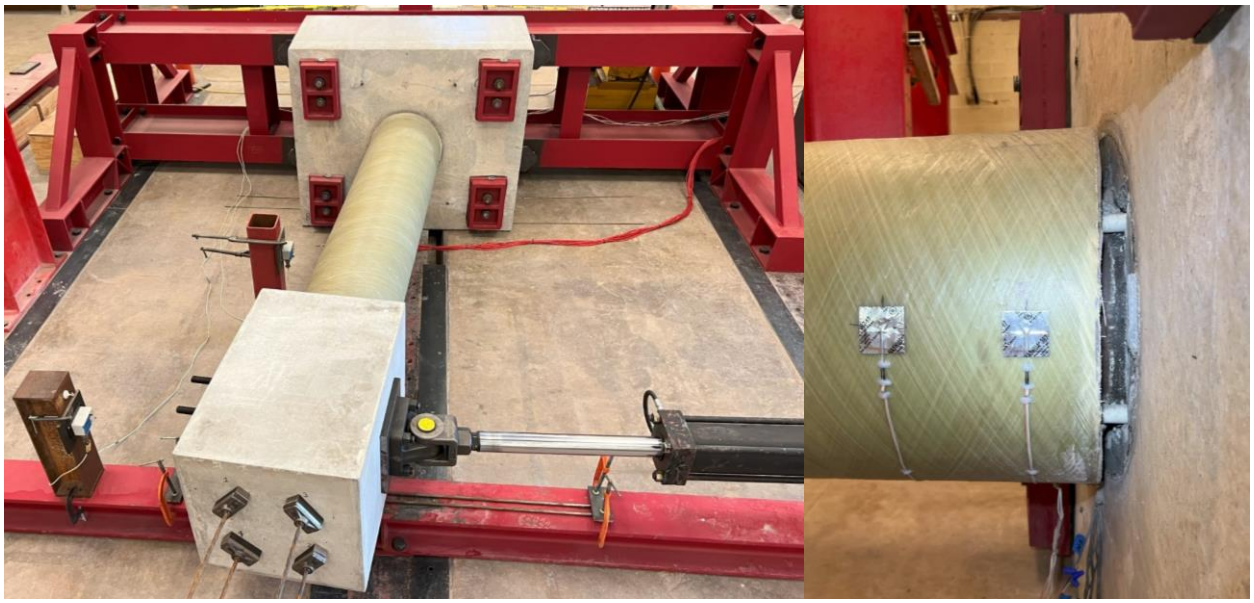

Figure 5-31: UHPC 1 Column Specimen (l) and GFRP Tube Separation During Testing (r)

Figure 5-32: UHPC 1 GFRP Tube West Side (l) and East Side (r) Damage After Testing

During testing, the instrumentation captured the load and displacement at the column head, which is plotted in Figure 5-35. The maximum load sustained by the column was 48.6 kips at a measured displacement of 7.77 inches in the eastward, or extension, direction. Additionally, strain gauges on the steel reinforcement captured the strain in the steel tube at each extreme fiber

and along the neutral axis of the column. A representative strain gauge plot from the steel tube at the extreme fiber is shown in Figure 5-36, while a gauge at the neutral axis is shown in Figure 5-37. Furthermore, external strain gauges on the GFRP tube captured the hoop strain at each extreme fiber, and a representative plot is shown in Figure 5-38.

Figure 5-33: UHPC 1 Concrete Core West Side (l) and East Side (r) Damage After Testing

Figure 5-34: UHPC 1 Steel Tube West (l), Top (m), and East Side (r) Damage After Testing

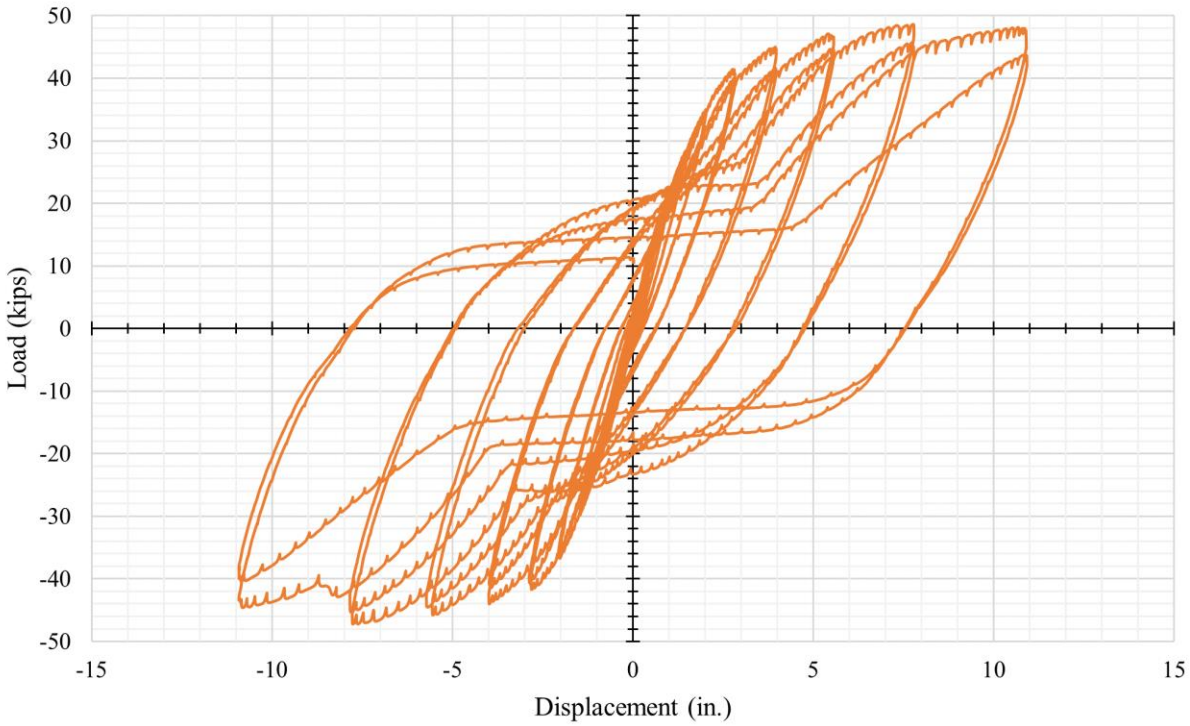

Figure 5-35: UHPC 1 Column Lateral Load vs. Displacement at Column Head

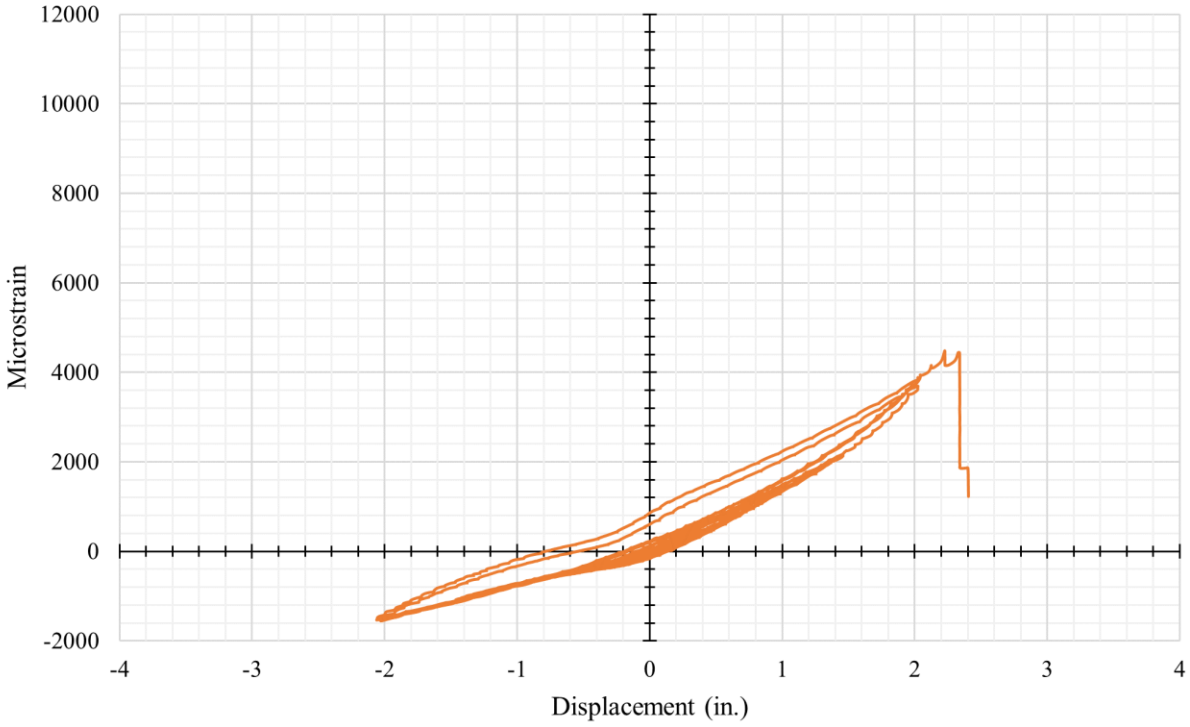

Figure 5-36: UHPC 1 SW1 Steel Strain Gauge vs. Displacement at Column Head

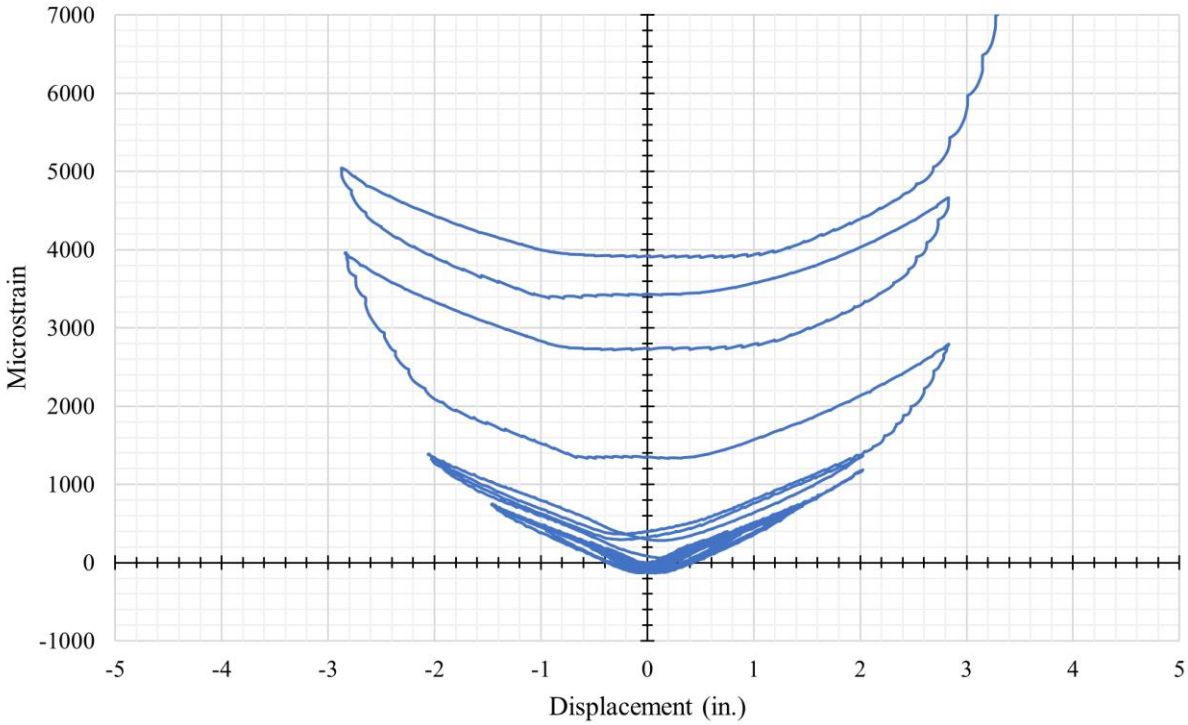

Figure 5-37: UHPC 1 SN1 Steel Strain Gauge vs. Displacement at Column Head

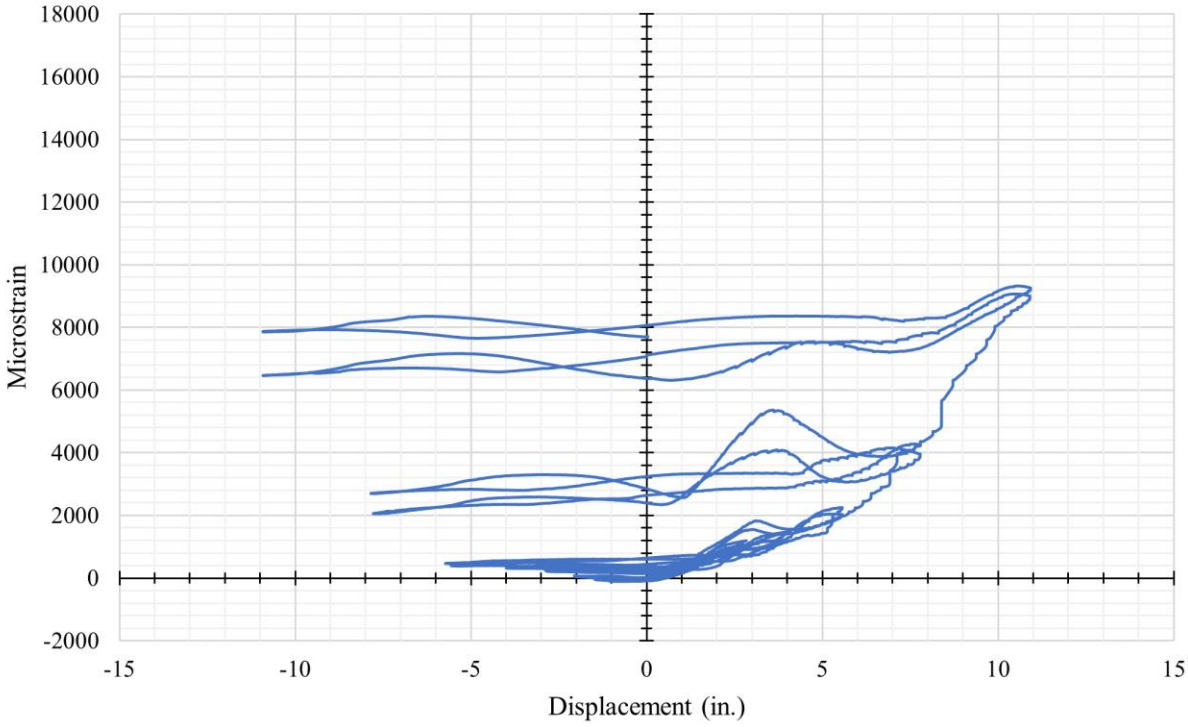

Figure 5-38: UHPC 1 GE1 GFRP Strain Gauge vs. Displacement at Column Head

5.2.6 UHPC 2 HC-FCS Column Specimen Testing Results & Discussion

UHPC 2 was the last HC-FCS column specimen tested. The specimen ready for testing is shown in Figure 5-39. UHPC 2 displayed similar behavior and damage characteristics to that of UHPC 1. Similar to the first UHPC HC-FCS specimen tested, a gap formed between the column and base during testing, and eventually the GFRP shell began to show minimal signs of distress at larger displacements. Figure 5-40 shows the specimen and the gap between the GFRP tube and the concrete base during testing. Figure 5-41 shows the GFRP tube's condition after testing was completed.

Figure 5-39: UHPC 2 Column Specimen Before Testing

After testing, the lower 18 inches of the GFRP tube, was sectioned off, split in half, and removed from the column to reveal the concrete core underneath as shown in Figure 5-42. The outer shell of the concrete core was removed by jackhammering to reveal the crushed concrete as shown in Figure 5-43. Next, the remaining concrete core was removed by cutting and jackhammering so that the damage to the steel tube could be observed. The steel tube was found to have buckled along the extreme fibers of both sides of the column with minimal fractures on both sides. Figure 5-44 illustrates the steel tube damage after concrete removal.

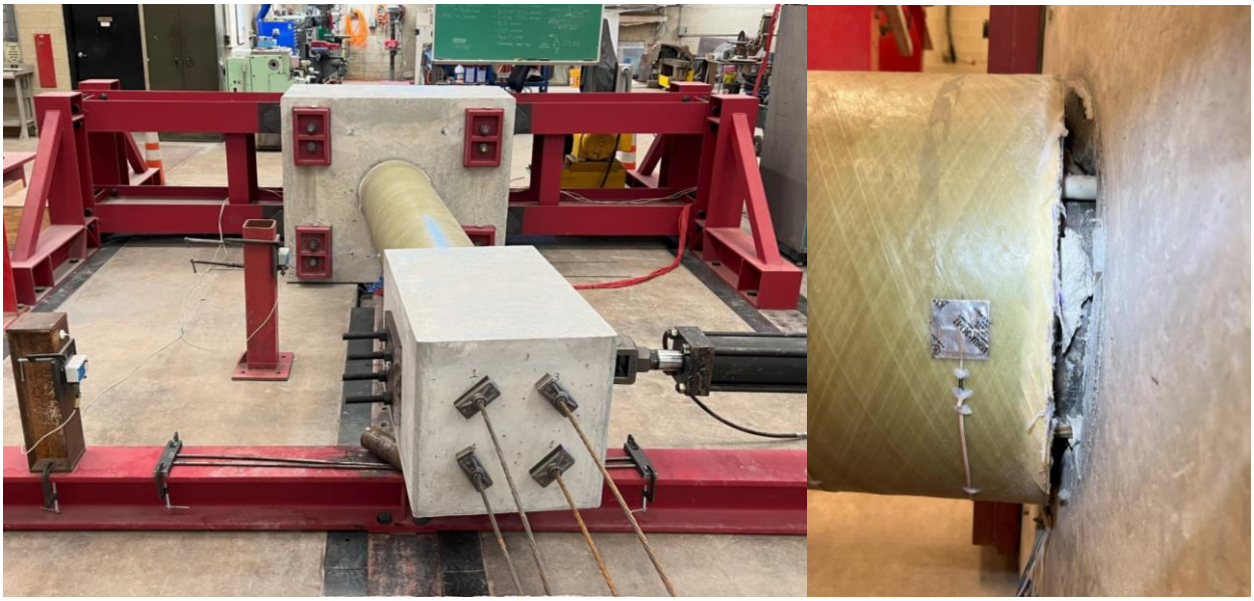

Figure 5-40: UHPC 2 Column Specimen (l) and GFRP Tube Separation During Testing (r)

Figure 5-41: UHPC 2 GFRP Tube West Side (l) and East Side (r) Damage After Testing

Figure 5-42: UHPC 2 Concrete Core West Side (l) and East Side (r) After Testing

Figure 5-43: UHPC 2 Concrete Core After Testing and Light Concrete Removal

Figure 5-44: UHPC 2 Steel Tube West (l), Top (m), and East Side (r) Damage After Testing

During testing, the instrumentation captured the load and displacement at the column head, which is plotted in Figure 5-45. The maximum load sustained by the column was 48.0 kips at a measured displacement of 7.64 inches in the eastward, or extension, direction. Additionally, strain gauges on the steel reinforcement captured the strain in the steel tube at each extreme fiber and along the neutral axis of the column. A representative strain gauge plot from the steel tube at the extreme fiber is shown in Figure 5-46, while a gauge at the neutral axis is shown in Figure 5-47. Furthermore, external strain gauges on the GFRP tube captured the hoop strain at each extreme fiber, and a representative plot is shown in Figure 5-48.

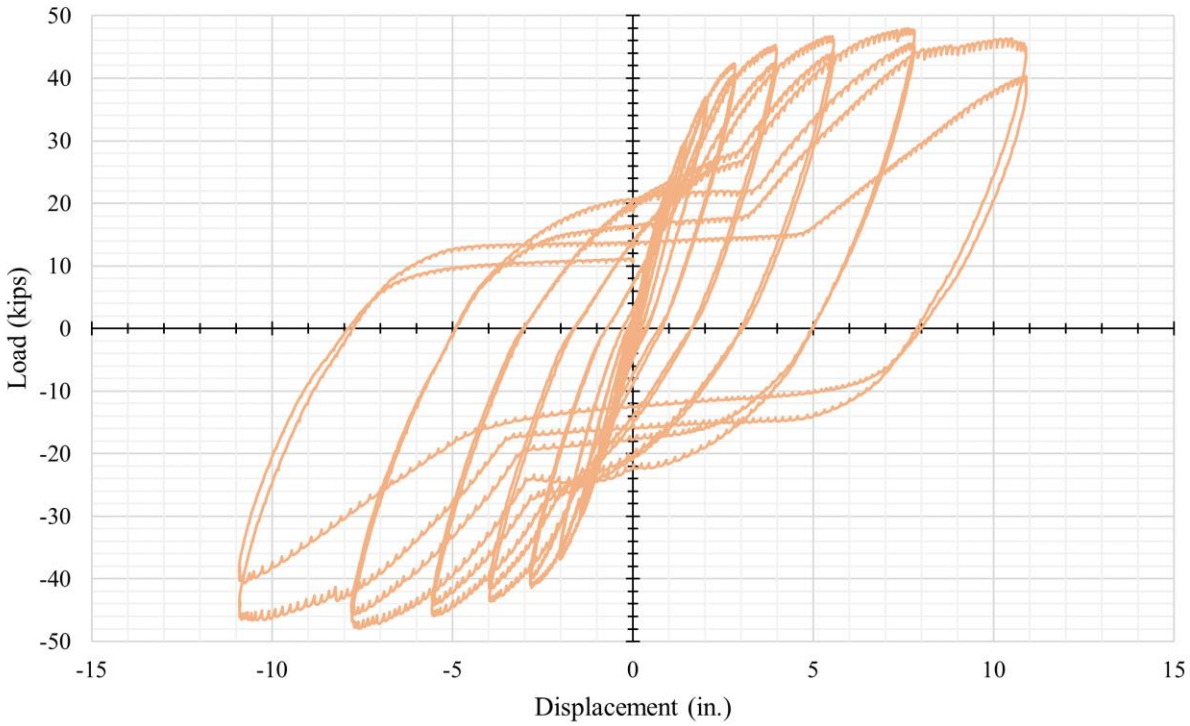

Figure 5-45: UHPC 2 Column Lateral Load vs. Displacement at Column Head

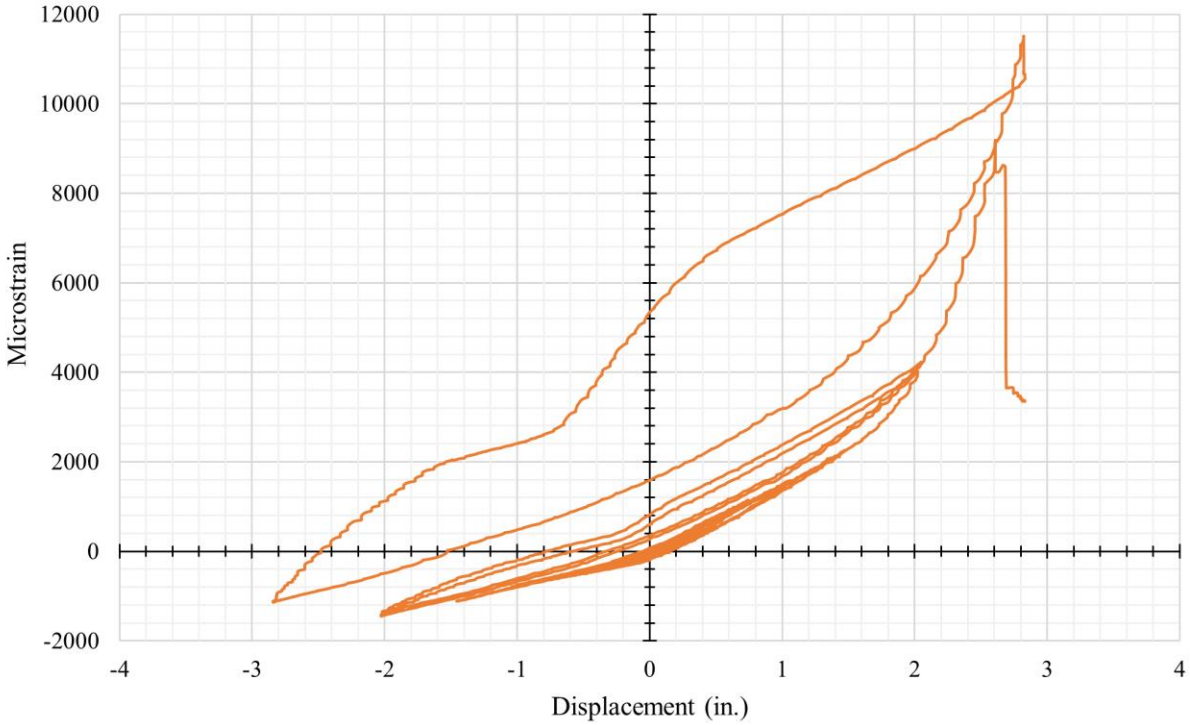

Figure 5-46: UHPC 2 SW1 Steel Strain Gauge vs. Displacement at Column Head

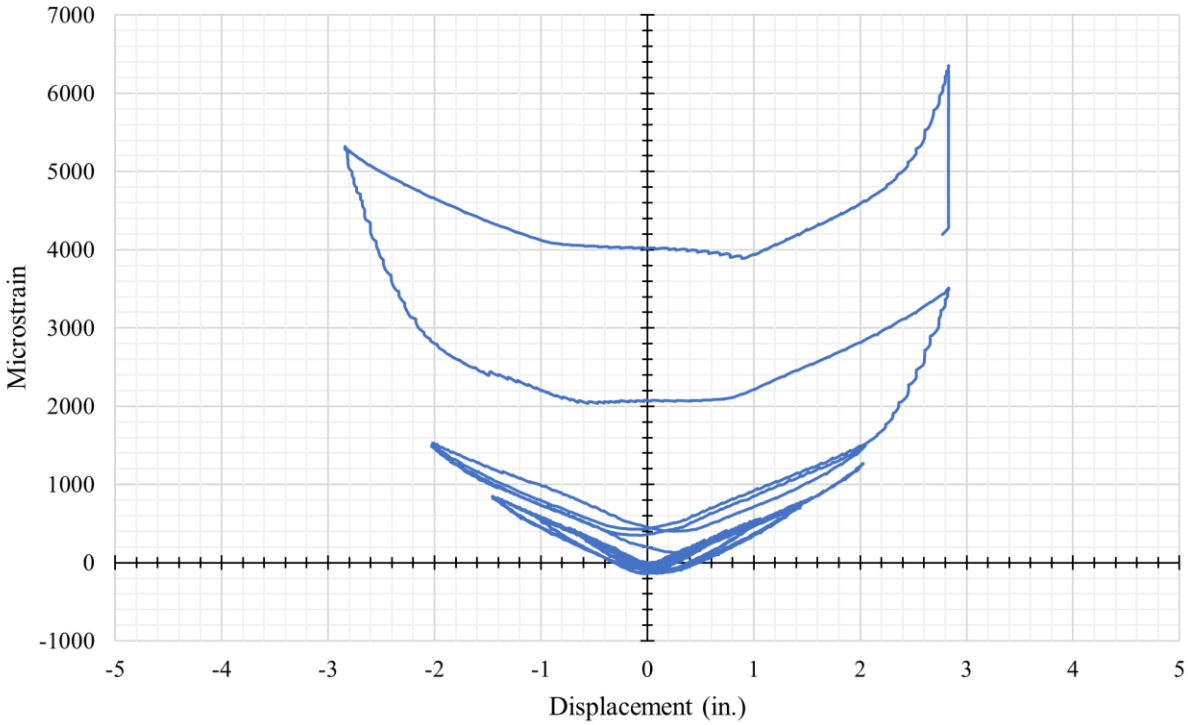

Figure 5-47: UHPC 2 SN1 Steel Strain Gauge vs. Displacement at Column Head

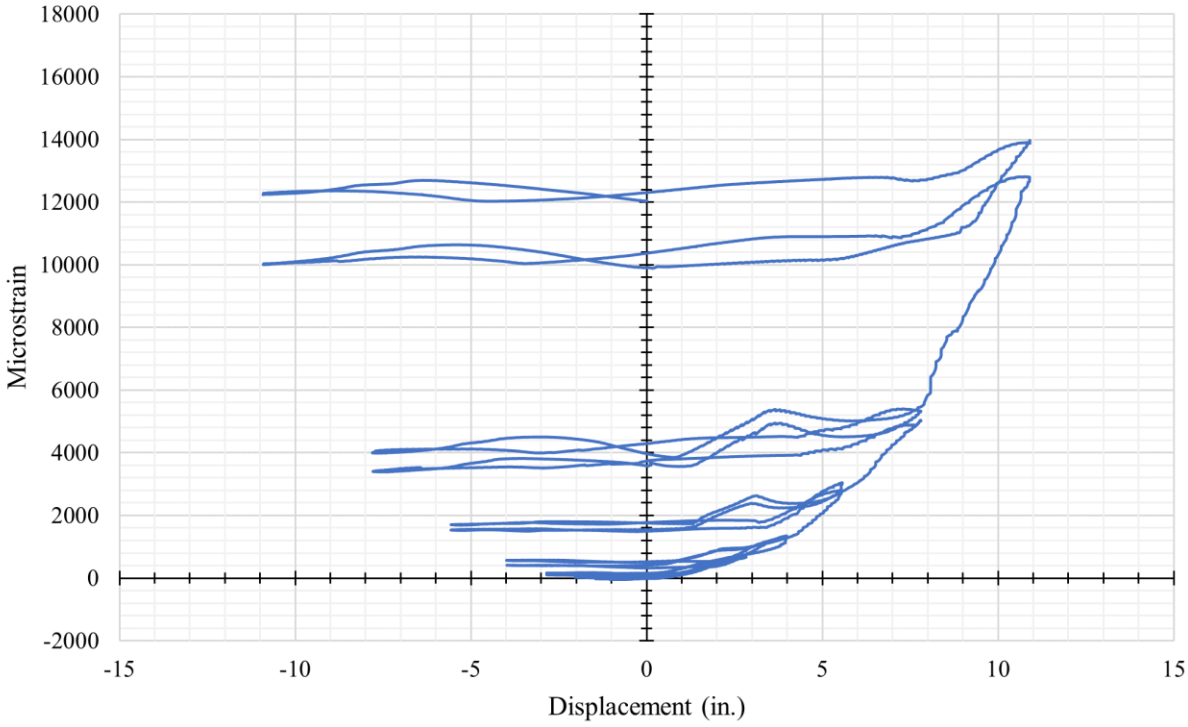

Figure 5-48: UHPC 2 GE1 GFRP Strain Gauge vs. Displacement at Column Head

Chapter 6: Analysis of RC and HS-SCC HC-FCS Column Testing Results

The RC column specimen and HS-SCC HC-FCS column specimens were tested according to the prescribed testing procedure. Both column types exhibited traditional linear elastic and inelastic column behavior. The results of each column test were analyzed including the load versus displacement, strain versus displacement at various locations, and forensic photographs of the damage sustained by the column after testing.

6.1 Analysis of RC Column Specimen Testing Results

The RC column specimen functioned as a control specimen to validate the column testing frame, setup, and procedure and served as a baseline comparison for column performance. The specimen exhibited the expected traditional, spiral-tied column behavior. It demonstrated linear elastic behavior before transitioning into inelastic behavior beyond a certain load and displacement. During testing, the outer shell spalled, the longitudinal bars buckled and eventually ruptured at the extreme fibers, the concrete core crushed, and the transverse spiral tie and longitudinal reinforcement provided adequate confinement of the concrete core.

6.1.1 Analysis of Load versus Displacement Plot

The peak moment capacity of the RC column was 249 kip-ft at a displacement of 7.8 inches. The specimen exhibited excellent symmetry between the extension and retraction cycles as shown by similar peak loads for opposite cycles shown in Figure 6-1. Linear elastic behavior was observed until a displacement of approximately 1.5 inches, after which the behavior began to transition to inelastic behavior. This was determined by analyzing the plot of the load versus displacement at the column head shown in Figure 6-2. Similarly, gradual stiffness degradation was observed approaching the same displacement followed by increasingly significant stiffness softening. The first cycle of each displacement interval closely followed the second cycle of the previous interval and, in general, the second cycle of any displacement interval did not reach the same maximum load as the first cycle of that interval due to the damage sustained from the previous cycle. As the longitudinal steel reinforcement began to yield and buckle, the load versus displacement plot began to plateau, with some stain hardening observed. The column specimen was considered failed after observing a significant reduction in capacity during and after the 7.78-inch displacement interval.

Three distinct drops, or discontinuities, were observed in the measured load during the cycles of the final, 10.89-inch displacement interval. Each discontinuity corresponds to a longitudinal bar rupturing at or near the extreme fiber. The first bar ruptured on the extension portion of the first cycle, while the second and third bars ruptured on the retraction portion of the first and second cycles, respectively. The fractured bars prevented the specimen from reaching the peak load of the previous displacement interval and ultimately led to the failure of the column. Before the longitudinal bars ruptured, the specimen exhibited a noticeable drop in capacity on the second cycle of the 7.78-inch displacement interval. This initial drop indicates buckling of the longitudinal bars in compression at the extreme fiber and significant crushing of the core concrete that led to the rupturing of the longitudinal bars in tension at the opposite extreme fiber.

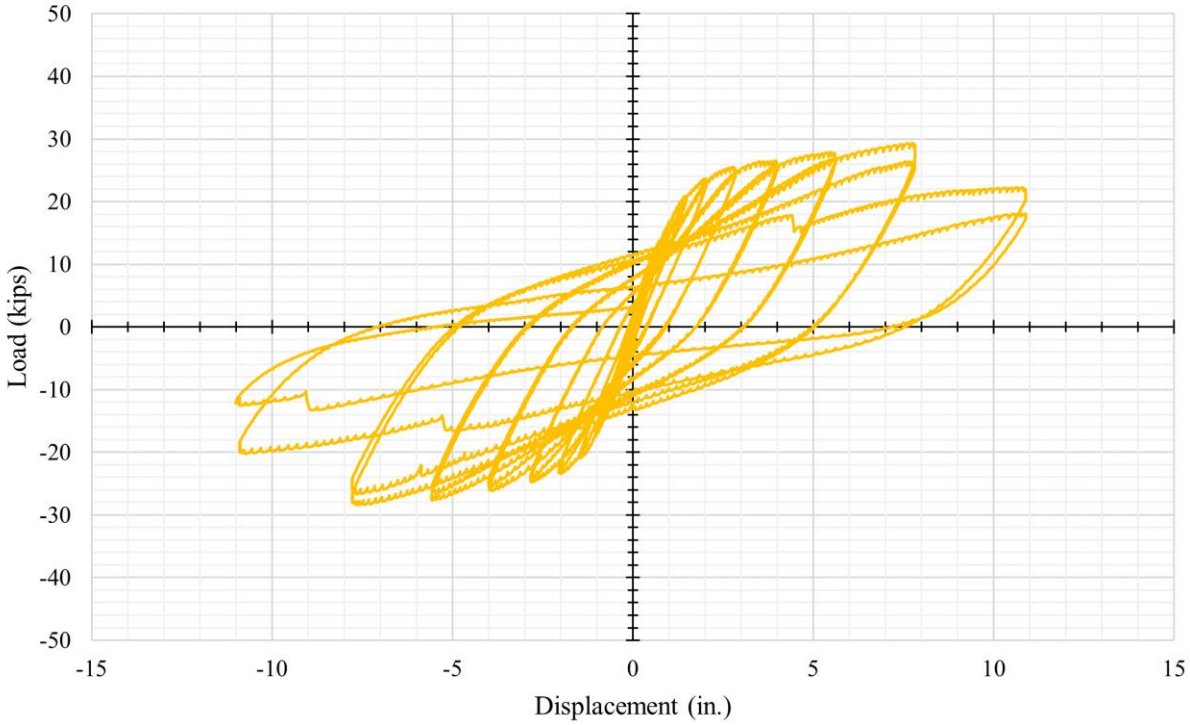

Figure 6-1: RC Column Lateral Load vs. Displacement at Column Head

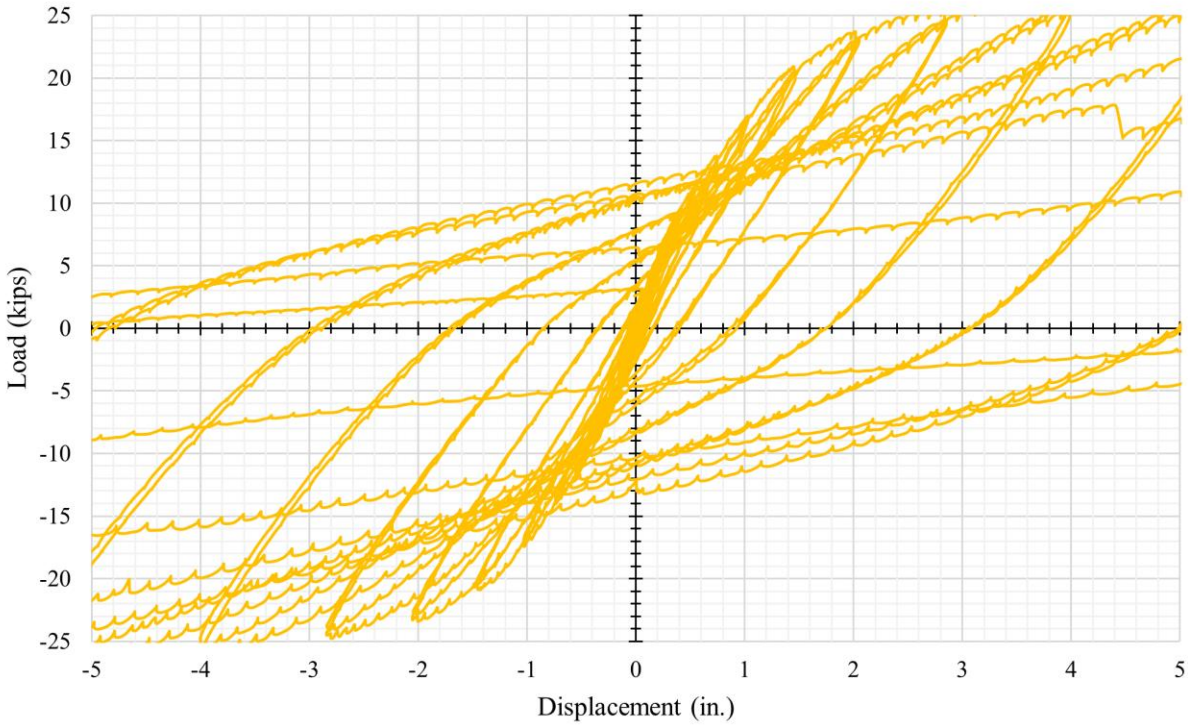

Figure 6-2: Determining Elastic Transition for the RC Column Using Lateral Load vs. Displacement at Column Head

6.1.2 Analysis of Steel Reinforcement Strain Gauge Plots

The strain gauges provided approximately consistent results at comparative locations on the steel reinforcement as shown in Figure 6-3. However, due to the nature of the column, the gauges were subject to damage during testing and failed early at varying displacements. There was no discernable trend between the gauges at lower and higher levels. Strain gauges at the extreme fibers were damaged sooner and failed earlier than gauges at the neutral axis. Figure 6-3 also illustrates the linear elastic behavior of the column before a displacement of approximately 1.5 inches. Beyond that displacement, the strain did not return to zero and began to show plastic deformation. Furthermore, the shape of the neutral axis strain gauge plots was indicative of the neutral axis migrating during testing. This was shown by the lack of negative, or compressive, strain values. As the neutral axis migrated away from the center, toward the direction of loading, the center of the column began to experience tension. This process was then mirrored as the loading was reversed, resulting in a strain gauge plot that resembles a “V” in shape.

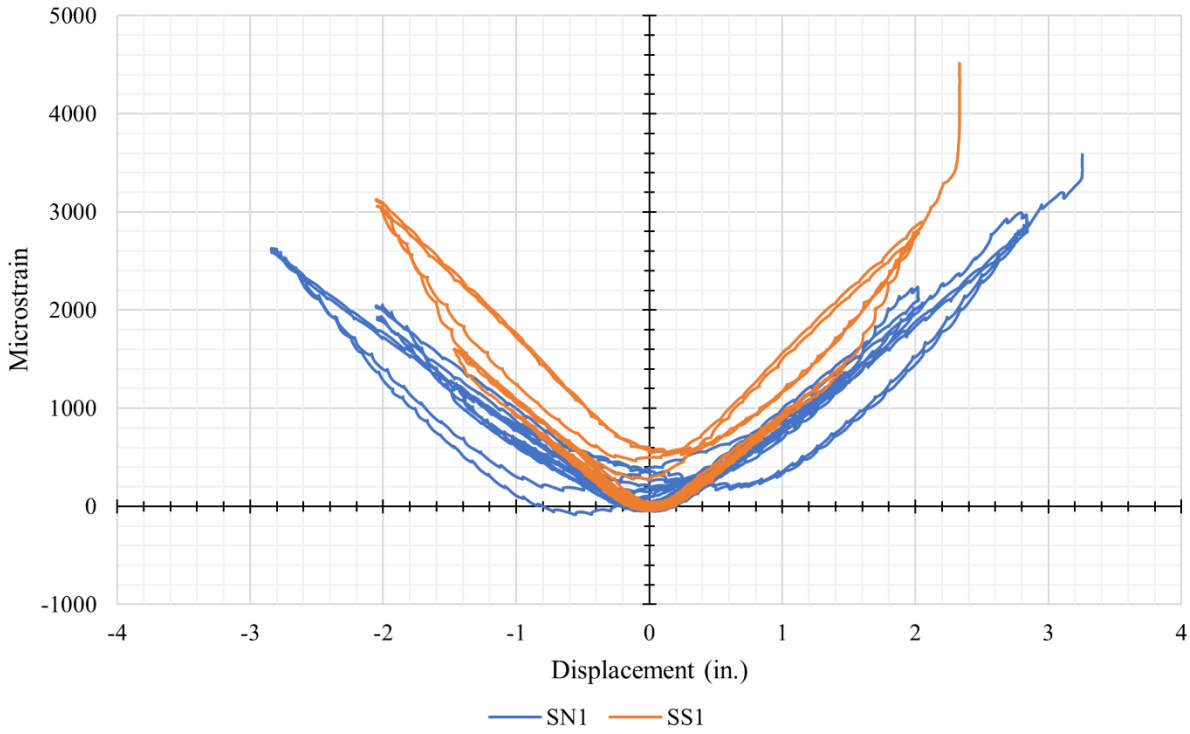

Figure 6-3: RC SN1 and SS1 Steel Strain Gauges vs. Displacement at Column Head

6.1.3 Analysis of Column Specimen Damage After Testing

The damage to the column specimen extended from the concrete base to beyond half of the column height, with the most severe damage extending approximately 9 inches from the top of the base. Additionally, concentric circumferential cracking along the height of the column was observed during testing before significant concrete spalling occurred. The longitudinal bars were observed to have buckled in two directions, both outward from the column and along the circumferential directions, as shown in Figure 6-4. The outward buckling was conducive to traditional buckling failure while the buckling in the circumferential direction indicated effective transverse spiral reinforcement confinement. Furthermore, the concrete core was adequately intact, and the column was still capable of sustaining the applied constant axial compressive load.

The concrete base was observed to provide adequate flexural and shear capacity with light spalling at the interface with the column testing frame. The column reinforcement was not observed to have been pulled out of the column base, therefore the embedment depth and hook lengths were effective. Furthermore, each corner of the column base rotated an average

maximum of approximately 0.07 inches or less than a tenth of an inch. The rotation caused a proportional effect on the measured displacement at the column head by reducing the measured displacement. The displacement data was not corrected for this effect. The column testing frame did not sustain any permanent deformation and functioned as essentially rigid. The RC column exhibited traditional, expected spiral-tied reinforced concrete column behavior, and validated the column testing frame, testing setup, and testing procedure.

Figure 6-4: RC Column Concentric Circumferential Cracking During Testing (l) and Buckled and Ruptured Longitudinal Bars After Testing (r)

6.2 Analysis of HS-SCC 1 HC-FCS Column Testing Results

The first HS-SCC HC-FCS column specimen served as the first column to be tested in the newly developed and constructed column testing frame. The specimen exhibited aspects of traditional column behavior such as linear elastic behavior before transitioning into inelastic behavior beyond a certain load and deflection. During testing, a gap formed between the GFRP tube and the top of the column base at larger deflections, the steel tube yielded and buckled, the concrete core crushed, and the GFRP tube ruptured.

6.2.1 Analysis of Load versus Displacement Plot

The peak moment capacity of the HS-SCC 1 HC-FCS column was 384 kip-ft at a displacement of 5.6 inches. The observed peak loads were reasonably symmetrical between the

extension and retraction cycles, as shown in Figure 6-5. Linear elastic behavior was observed until a displacement of approximately 1.5 inches, after which the behavior began to transition to inelastic behavior. This was determined by analyzing the plot of the load versus displacement at the column head shown in Figure 6-6. Similarly, gradual stiffness degradation was observed approaching a displacement of approximately 2 inches, followed by moderate stiffness softening at a displacement of approximately 3 inches and significant stiffness softening at a displacement of approximately 4 inches. Beyond an approximate displacement of 4 inches, the capacity of the specimen gradually declined. The first cycle of each displacement interval closely followed the second cycle of the previous interval and, in general, the second cycle of any displacement interval did not reach the same maximum load as the first cycle of that interval due to the damage sustained from the previous cycle. The initial loss of stiffness was attributed to the steel tube yielding and the concrete core cracking. The loss of capacity was attributed to the concrete core crushing and the steel tube buckling due to the loss of confinement from the concrete core. As the column experienced increased displacement and severe strains, the load versus displacement plot began to plateau, with some strain hardening observed.

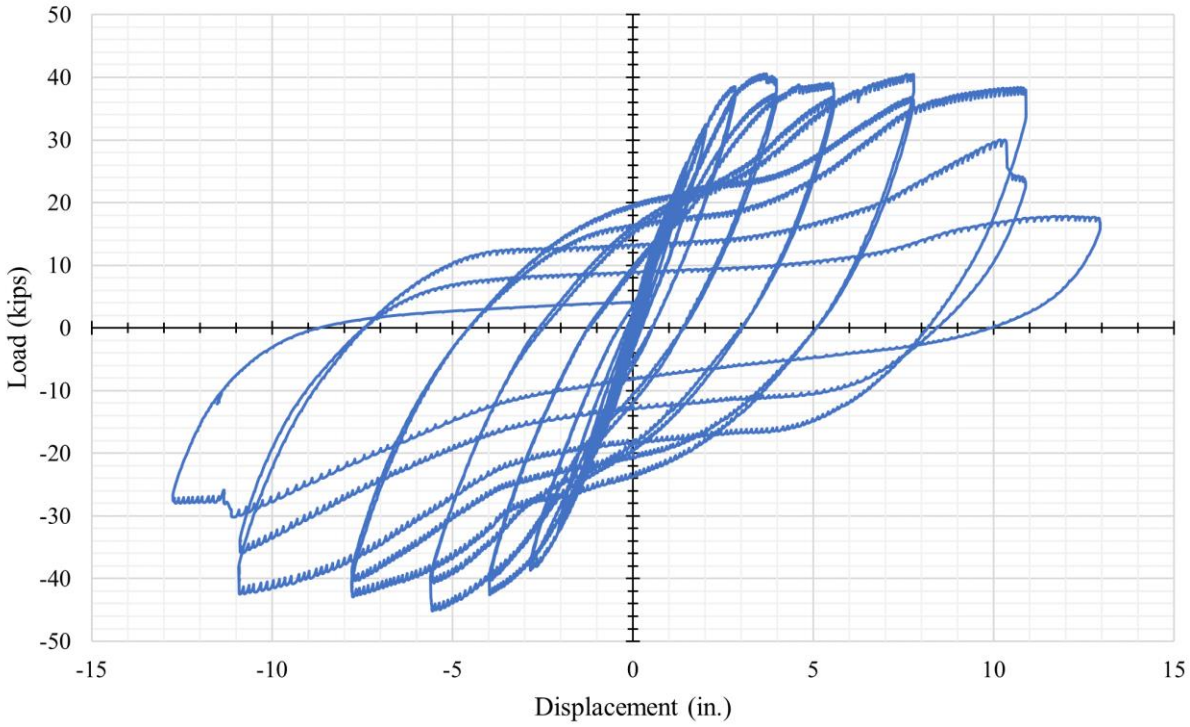

Figure 6-5: HS-SCC 1 Column Lateral Load vs. Displacement at Column Head

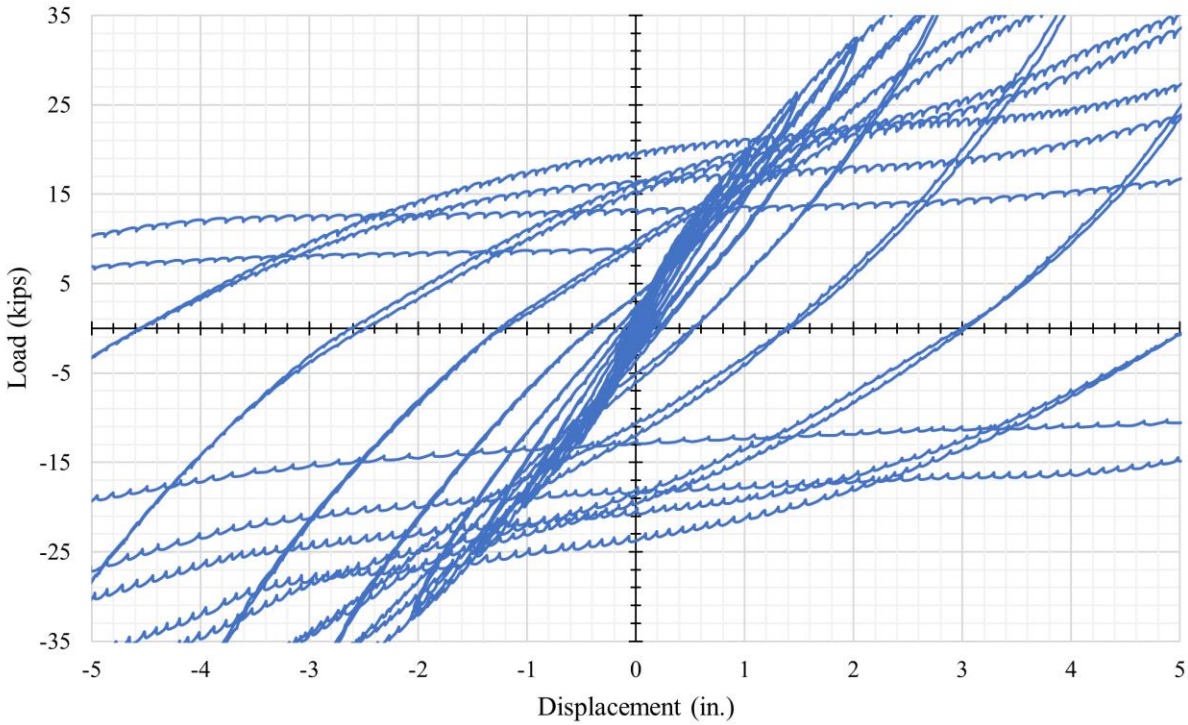

Figure 6-6: Determining Elastic Transition for HS-SCC 1 Using Lateral Load vs. Displacement at Column Head

At larger displacements and later cycles, an upturn was observed on the load versus displacement plot. During the beginning of each displacement cycle, the load gradually increased or held constant before an upturn in the sustained load was observed. The upturn was attributed to the yielding and buckling of the steel tube after the concrete core was crushed. As the load on the column was reversed, the side of the column in which the steel tube was previously buckled was gradually straightened from the tension caused by the load reversal. Concurrently, the side of the column in which the steel tube was previously in tension began to buckle. Eventually, the straightened region began to yield from the tension caused by the load reversal after the opposite side had completely buckled, resulting in a notable upturn in the sustained load on the load versus displacement plot. At larger displacements, the upturn became shallower as the steel tube fatigued. A discontinuity was observed on the second cycle of the 10.89-inch displacement interval when the column was displaced in the extension direction. This distinct drop in capacity was indicative of the steel tube fracturing in tension due to fatigue at the extreme fiber opposite from the direction of loading. The column specimen was considered failed after observing a significant reduction in capacity during and after the second 10.89-inch displacement interval.

The first column specimen was pushed an additional cycle beyond the final 10.89-inch displacement interval to approximately 13 inches in either direction. The maximum stroke length of the hydraulic actuator was utilized and only one cycle was completed due to safety considerations. There was no notable upturn on the extension side due to the steel tube fracturing on the previous extension cycle, whereas a similar upturn to the previous cycle was observed on the retraction side. The load capacity observed during the additional cycle greatly plateaued on the extension cycle while regaining residual strength on the retraction cycle before finally tearing the steel tube.

6.2.2 Analysis of Steel Tube Strain Gauge Plots

Figure 6-7 depicts the strain gauges on the steel tube at the extreme fibers of the column. Limited strain gauge data was obtained due to the testing procedure of the first column, however, the data that was obtained yielded consistent results at comparative locations on the steel tube and GFRP tube. The strain gauges on the steel tube were oriented perpendicular to the base, along the height of the column. Strain gauges at similar locations and levels exhibited symmetry at similar displacements, and in general, gauges higher up the column, or farther from the top of the column base, exhibited lower strains. The shape of the plot resembled loops, similar to the shape of the load versus displacement plot. The plots for gauges on opposite sides of the column were mirrored because one side of the column was in compression while the other was in tension. The higher captured tensile strains rather than compression strains were attributed to the steel reinforcement functioning as the sole tension element, whereas the concrete core and steel reinforcement both supported the compressive load on the opposite side, with the concrete core supporting a greater portion of the load before crushing.

Figure 6-8 depicts the lower level of strain gauges on the steel tube at the neutral axis of the column. Strain gauges at similar locations and levels exhibited symmetry at similar displacements, and in general, gauges higher up the column, or farther from the top of the column base, exhibited lower strains. The shape of the plot resembled a “V”, which was indicative of the neutral axis of the column migrating during testing. The migration of the neutral axis was shown by the lack of significant negative, or compressive, strain measurements. As the neutral axis migrated away from its initial position at the center of the column, toward the

direction of loading, the center of the column began to experience tension. This process was then mirrored as the loading was reversed, resulting in the observed plot and shape.

Due to the missing strain gauge data from the first part of the column testing, it was difficult to corroborate observations from the load versus displacement plot. The data that would have depicted the transition from elastic to inelastic behavior, as well as various stages of stiffness softening, was not obtained. However, prominent plastic deformation was shown by residual strain at zero displacement from the data that was obtained. Further plastic deformation was observed at and beyond the 2.97-inch displacement interval. Strain gauge data was not obtained beyond a displacement of approximately 4 inches, likely due to significant damage to the column specimen from the steel tube buckling and the concrete core crushing, with the lower gauges failing first.

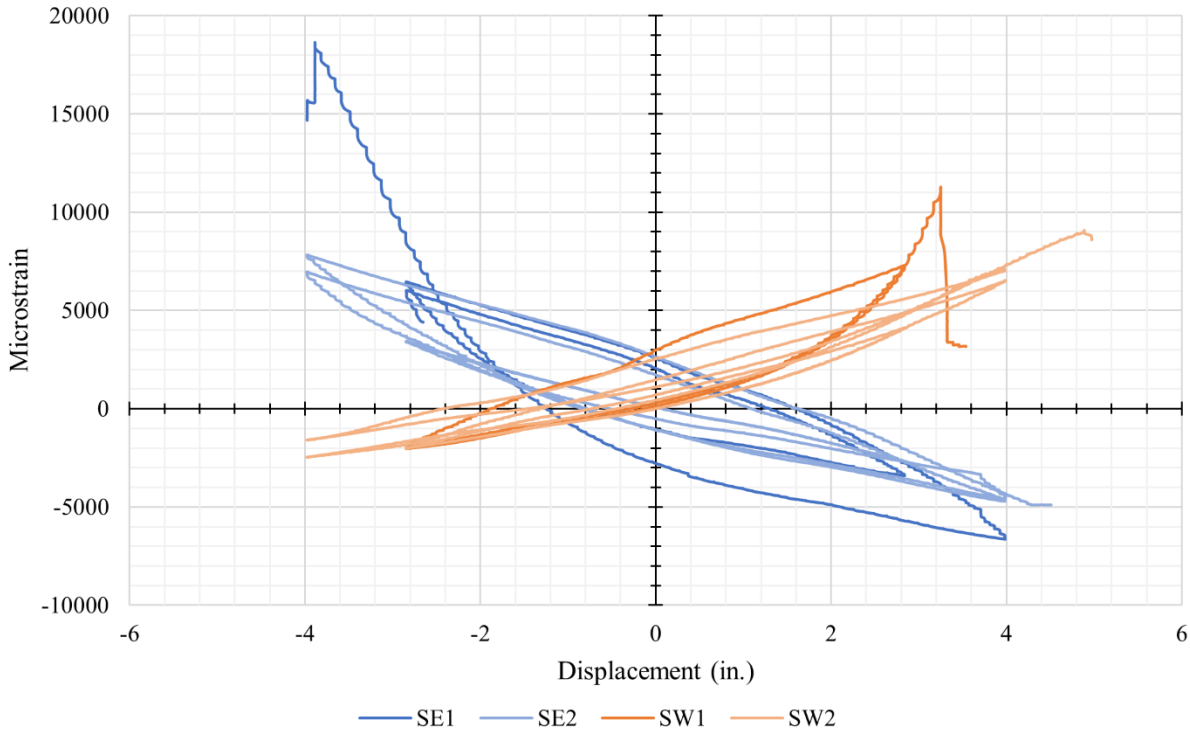

Figure 6-7: HS-SCC 1 Extreme Fiber Strain Gauges vs. Displacement at Column Head

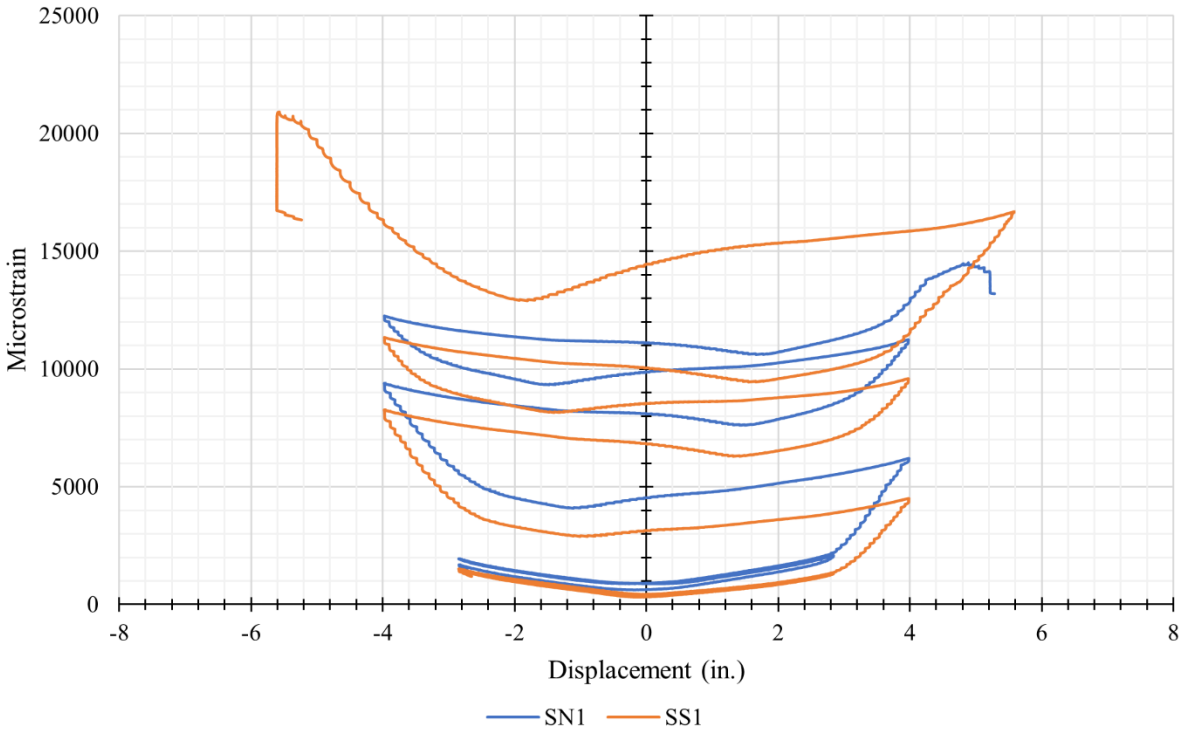

Figure 6-8: HS-SCC 1 SN1 and SN2 Steel Strain Gauges vs. Displacement at Column Head

6.2.3 Analysis of GFRP Tube Strain Gauge Plots

Figure 6-9 depicts the lower level of strain gauges on the GFRP tube at the extreme fibers of the column. The strain gauges on the GFRP tube were oriented parallel to the base, along the circumference of the column. Strain gauges at similar locations and levels on the GFRP tube exhibited moderate symmetry at similar displacements. In general, gauges higher up the column, or farther from the top of the column base, exhibited lower strains, as shown in Figure 6-10. The GFRP tube confined the concrete core and was compressed into the concrete base at larger deflections, therefore, only tensile hoop strains were measured due to the orientation and placement of the strain gauges. A notable transition in the plot was observed between a displacement of approximately 3 inches and 4 inches, as shown in Figure 6-11, and emphasized with the addition of two straight line segments. The strain gauge plot was approximately linear leading up to and after the transition in the graph. The transition correlates with the significant stiffness softening and loss of capacity of the column and was attributed to the concrete core crushing and applying increased pressure to the GFRP tube.

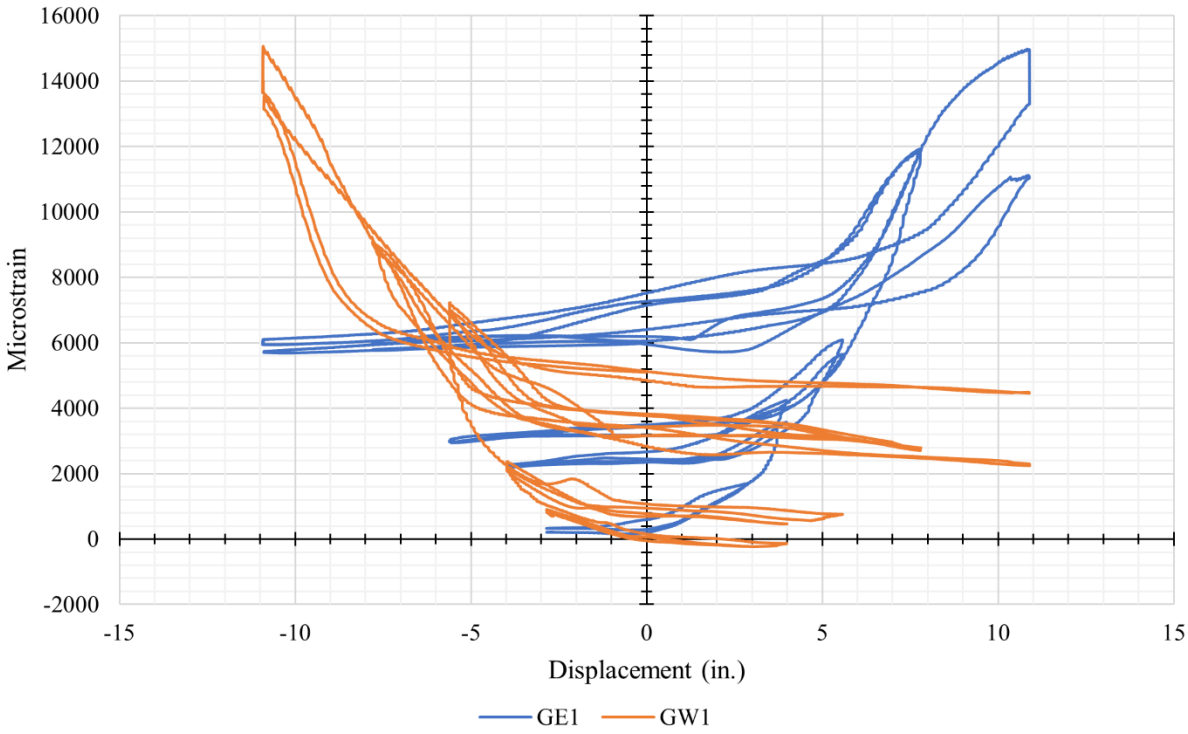

Figure 6-9: HS-SCC 1 Lower GFRP Strain Gauges vs. Displacement at Column Head

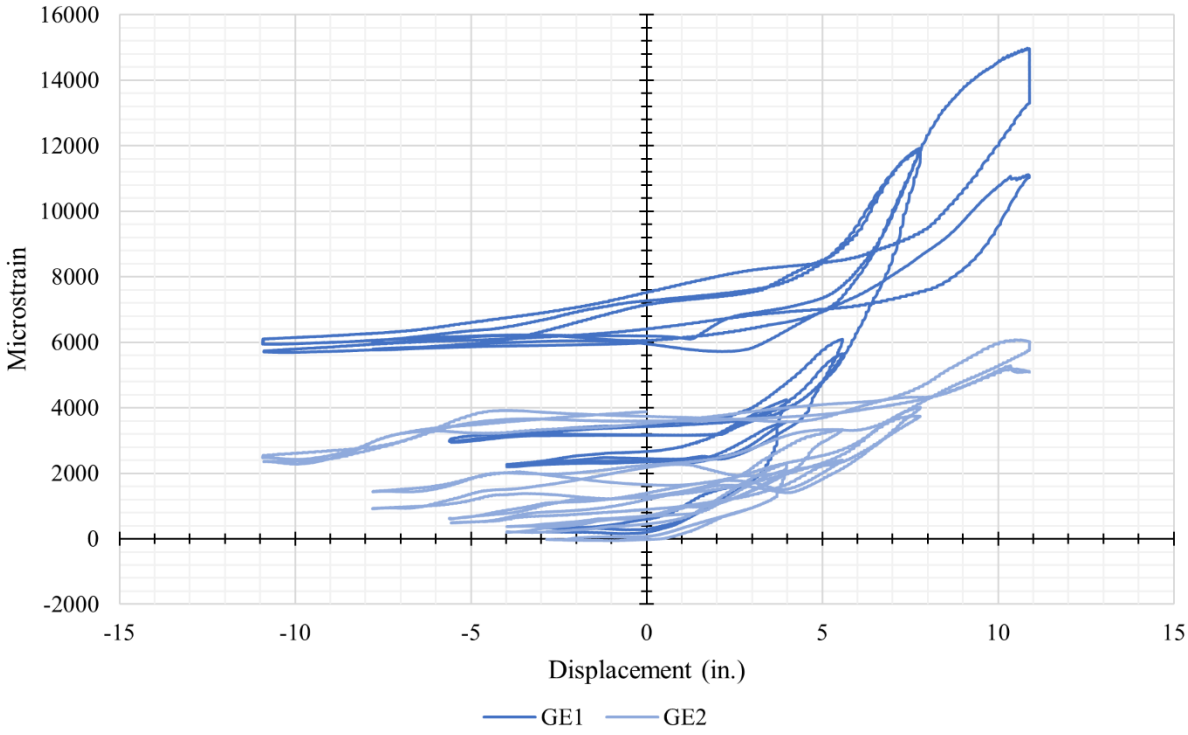

Figure 6-10: HS-SCC 1 East GFRP Strain Gauges vs. Displacement at Column Head

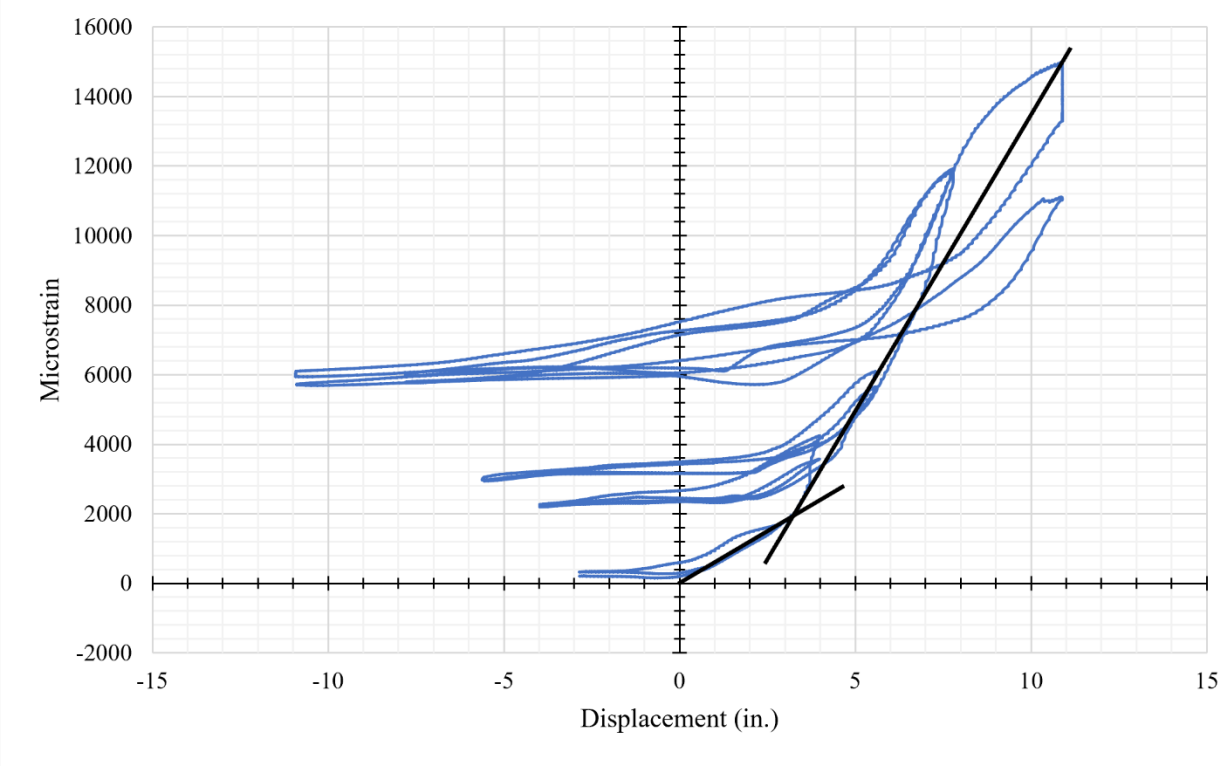

Figure 6-11: Determining HS-SCC 1 GFRP Strain Transition Using GE1 GFRP Strain Gauge vs. Displacement at Column Head

6.2.4 Analysis of Column Specimen Damage After Testing

The damage to the column specimen was assumed to extend from the concrete base to past half of the column height. The most severe damage to the column was observed to extend approximately 12 inches from the top of the base. Minimal damage to the GFRP tube was observed at smaller displacements during testing, however, the additional, maximum displacement cycle caused considerable damage to the GFRP tube as the tube was compressed into the concrete base, as shown in Figure 6-12. This aligned with observations made from the GFRP strain gauge plots. The GFRP tube was damaged approximately 3 to 4 inches from the top of the base and typically failed along the orientation of the fibers, as shown in Figure 6-13.

The concrete core was crushed in a conical shape with the lower approximately 3 inches nearest to the column base turned to powder, as shown in Figure 6-14. This indicated that the steel tube and GFRP tube sufficiently confined the concrete core, and the concrete reached its ultimate strain without rupturing the GFRP tube. Additionally, the area of crushed concrete was

roughly triangular with the most severe damage along the extreme fiber. The concrete core was no longer bonded to the steel tube after testing and was easily removed.

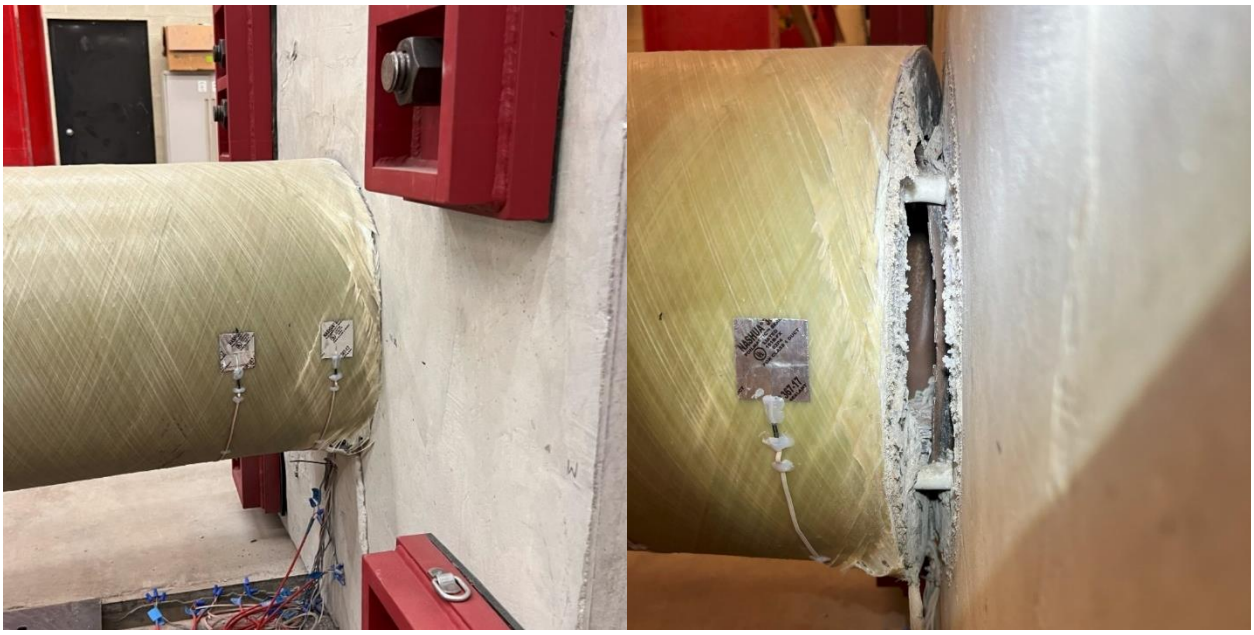

Figure 6-12: HS-SCC 1 GFRP Tube Compression (l) and Fractured Steel Tube (r) During Testing

Figure 6-13: HS-SCC 1 GFRP Tube West Side (l) and East Side (r) Damage After Testing

Figure 6-14: HS-SCC 1 Concrete Core After Testing and Light Removal of Concrete

The steel tube was observed to have buckled at the extreme axis with a vertical compressed fold, or crease, parallel to the column base and a depressed region on either side of the extreme axis, as shown in Figure 6-15. The crease on the west side of the column had fractured during testing and completely separated. The observed fracture resembled a fatigue failure due to limited necking and corroborated the discontinuity and drop in capacity shown on the load versus displacement plot. Despite the damage, the steel tube remained mostly intact, and the column was still capable of sustaining the applied constant axial compressive load.

The concrete base was observed to provide adequate flexural and shear capacity with light spalling at the interface with the column testing frame and lateral clamping mechanisms. During testing, a gap formed at the interface between the column and the base. This was indicative of the concrete core and GFRP tube sliding along the steel tube after the bond between the concrete core and the steel tube was broken. However, the steel tube was not observed to have been pulled out of the column base, therefore the embedment depth and supplemental anchorage were effective. Furthermore, each corner of the column base rotated an average maximum of approximately 0.17 inches. The rotation caused a proportional effect on the measured displacement at the column head by reducing the measured displacement. The displacement data was not corrected for this effect.

Figure 6-15: HS-SCC 1 Steel Tube Top (l) and West Side (r) Damage After Testing

6.3 Analysis of HS-SCC 2 HC-FCS Column Testing Results

Similar to the first HS-SCC HC-FCS column tested, the HS-SCC 2 specimen exhibited aspects of traditional column behavior such as linear elastic behavior before transitioning into inelastic behavior beyond a certain load and deflection. During testing, a gap formed between the GFRP tube and the top of the column base at larger deflections, the steel tube yielded and buckled, the concrete core crushed, and the GFRP tube ruptured.

6.3.1 Analysis of Load versus Displacement Plot

The peak moment capacity of the HS-SCC 2 HC-FCS column was 370 kip-ft at a displacement of 5.2 inches. The observed peak loads were reasonably symmetrical between the extension and retraction cycles, as shown in Figure 6-16. Linear elastic behavior was observed until a displacement of approximately 1.5 inches, after which the behavior began to transition to inelastic behavior. This was determined by analyzing the plot of the load versus displacement at the column head shown in Figure 6-17. Similarly, gradual stiffness degradation was observed approaching a displacement of approximately 2 inches, followed by moderate stiffness softening at a displacement of approximately 3 inches and significant stiffness softening at a displacement of approximately 4 inches. Beyond an approximate displacement of 4 inches, the capacity of the specimen gradually declined. The first cycle of each displacement interval closely followed the

second cycle of the previous interval and, in general, the second cycle of any displacement interval did not reach the same maximum load as the first cycle of that interval due to the damage sustained from the previous cycle. The initial loss of stiffness was attributed to the steel tube yielding and the concrete core cracking. The loss of capacity was attributed to the concrete core crushing and the steel tube buckling due to the loss of confinement from the concrete core. As the column experienced increased displacement and severe strains, the load versus displacement plot began to plateau, with some strain hardening observed.

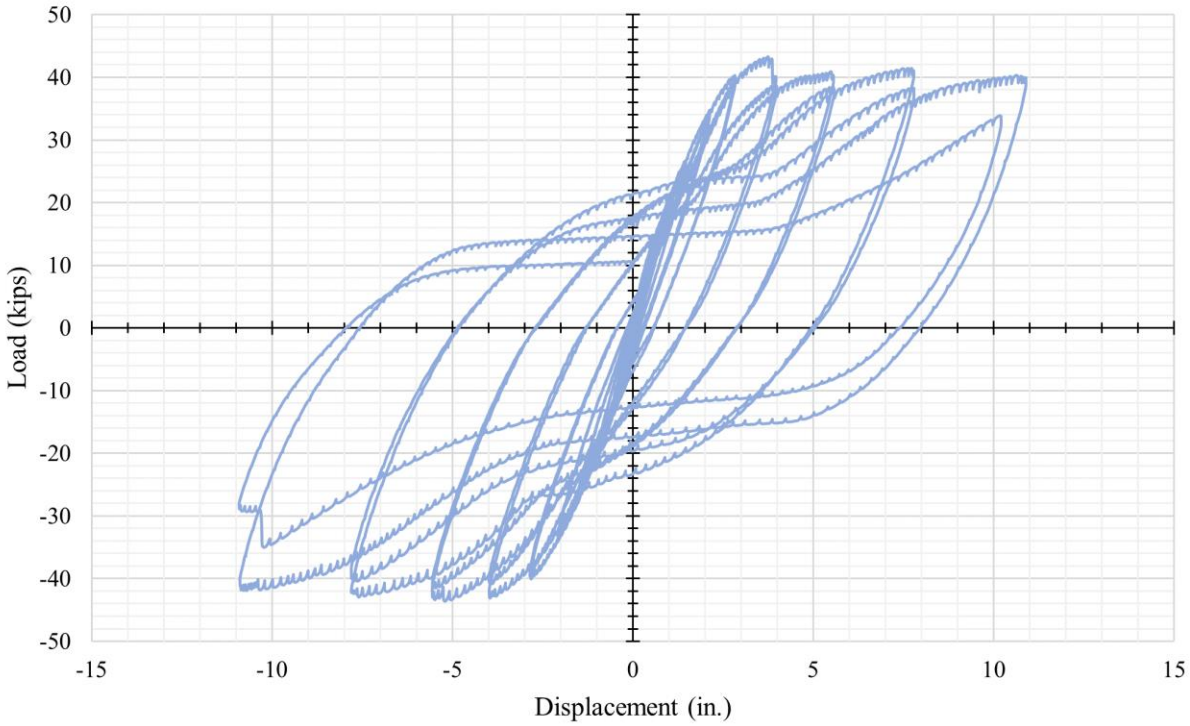

Figure 6-16: HS-SCC 2 Column Lateral Load vs. Displacement at Column Head

At larger displacements and later cycles, an upturn was observed on the load versus displacement plot. During the beginning of each displacement cycle, the load gradually increased or held constant before an upturn in the sustained load was observed. The upturn was attributed to the yielding and buckling of the steel tube after the concrete core was crushed. As the load on the column was reversed, the side of the column in which the steel tube was previously buckled was gradually straightened from the tension caused by the load reversal. Concurrently, the side of the column in which the steel tube was previously in tension began to buckle. Eventually, the straightened region began to yield from the tension caused by the load reversal after the opposite

side had completely buckled, resulting in a notable upturn in the sustained load on the load versus displacement plot. At larger displacements, the upturn became shallower as the steel tube fatigued. A discontinuity was observed on the second cycle of the 10.89-inch displacement interval when the column was displaced in the retraction direction. This distinct drop in capacity was indicative of the steel tube fracturing in tension due to fatigue at the extreme fiber opposite from the direction of loading. The column specimen was considered failed after observing a significant reduction in capacity during and after the second 10.89-inch displacement interval.

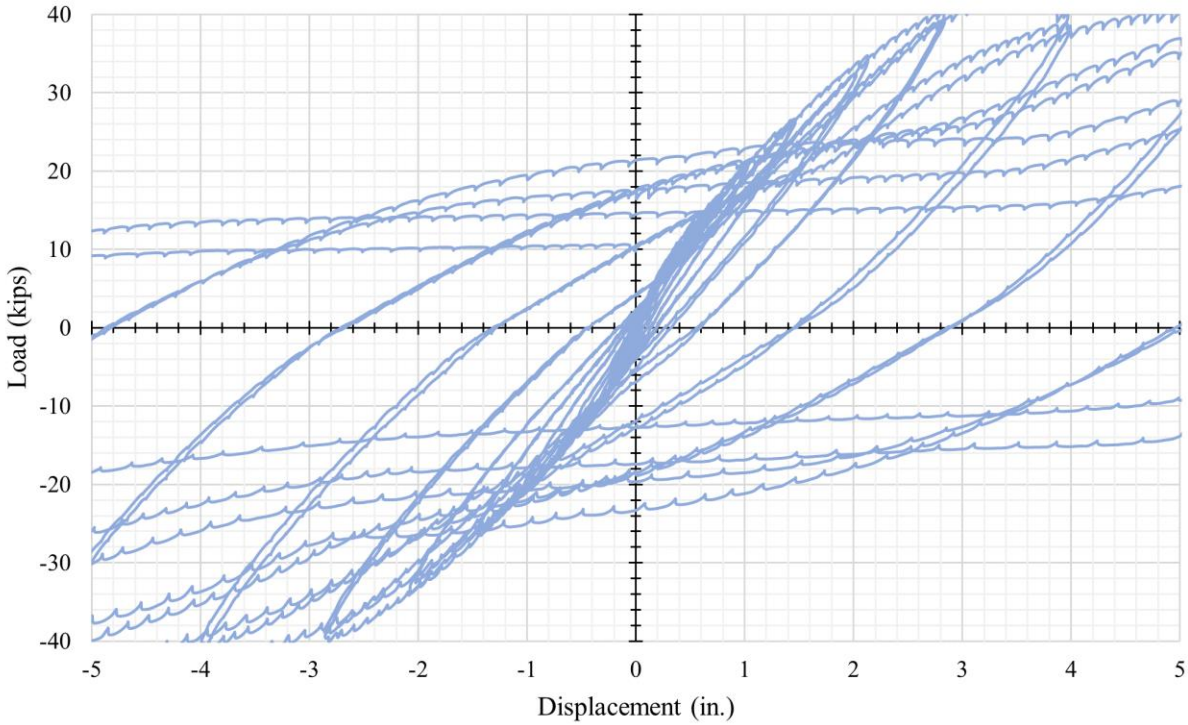

Figure 6-17: Determining Elastic Transition for HS-SCC 2 Using Lateral Load vs. Displacement at Column Head

6.3.2 Analysis of Steel Tube Strain Gauge Plots

Figure 6-18 depicts the strain gauges on the steel tube at the extreme fibers of the column. Strain gauge SE1 was omitted due to a significant offset in the data caused by intermittent issues with the data acquisition during testing. The strain gauges on the steel tube were oriented perpendicular to the base, along the height of the column. Strain gauges at similar locations and levels exhibited symmetry at similar displacements, and in general, gauges higher up the column, or farther from the top of the column base, exhibited lower strains. The shape of

the plot resembled loops, similar to the shape of the load versus displacement plot. The plots for gauges on opposite sides of the column were mirrored because one side of the column was in compression while the other was in tension. The higher captured tensile strains rather than compression strains were attributed to the steel reinforcement functioning as the sole tension element, whereas the concrete core and steel reinforcement both supported the compressive load on the opposite side, with the concrete core supporting a greater portion of the load before crushing.

Figure 6-19 depicts the lower level of strain gauges on the steel tube at the neutral axis of the column. Strain gauges at similar locations and levels exhibited symmetry at similar displacements, and in general, gauges higher up the column, or farther from the top of the column base, exhibited lower strains. The shape of the plot resembled a "V" which was indicative of the neutral axis of the column migrating during testing. The migration of the neutral axis was shown by the lack of significant negative, or compressive, strain measurements. As the neutral axis migrated away from its initial position at the center of the column, toward the direction of loading, the center of the column began to experience tension. This process was then mirrored as the loading was reversed, resulting in the observed plot and shape.

The steel tube strain gauge plots also corroborated observations from the load versus displacement plot. The transition from elastic to inelastic behavior was observed at a displacement of approximately 1.5 inches, after which, plastic deformations were observed, as shown in Figure 6-20 and Figure 6-21. A significant change in the measured strains due to stiffness softening was observed beyond a displacement of approximately 2 inches. Prominent plastic deformation was shown by residual strain at zero displacement. Further plastic deformation was observed at and beyond the 2.97-inch displacement interval. Strain gauge data was not obtained beyond a displacement of approximately 4 inches, likely due to significant damage to the column specimen from the steel tube buckling and the concrete core crushing, with the lower gauges failing first.

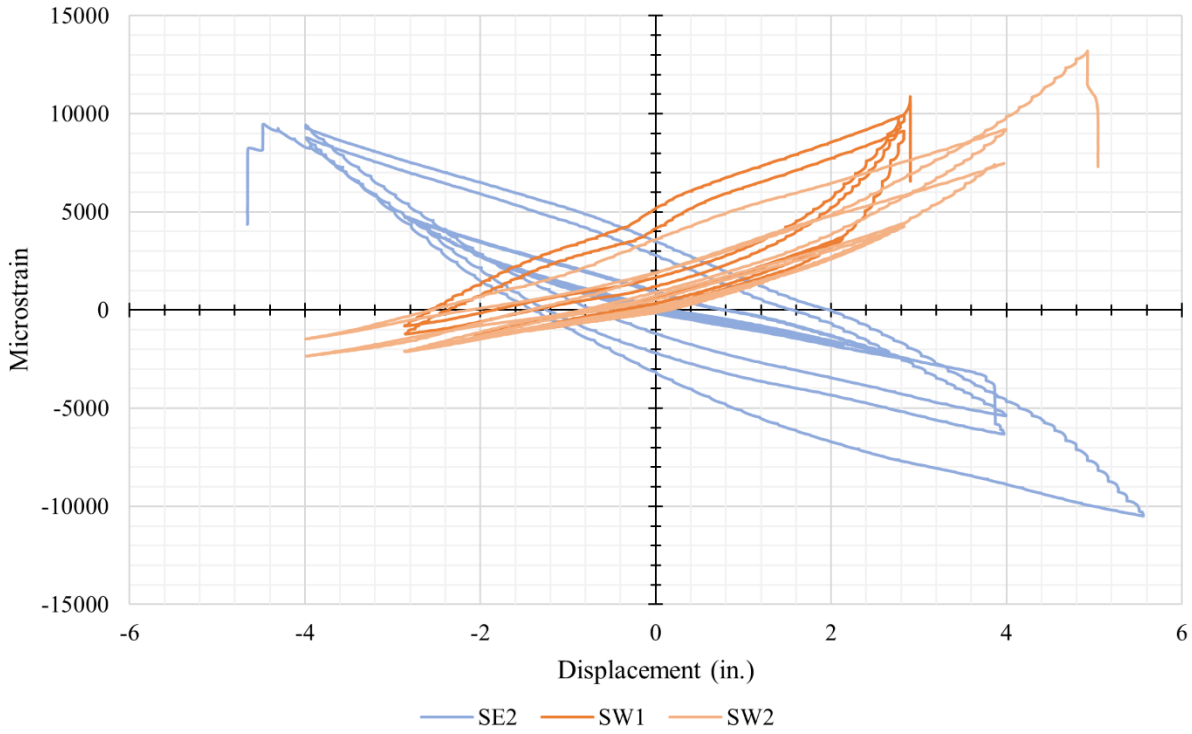

Figure 6-18: HS-SCC 2 Extreme Fiber Strain Gauges vs. Displacement at Column Head

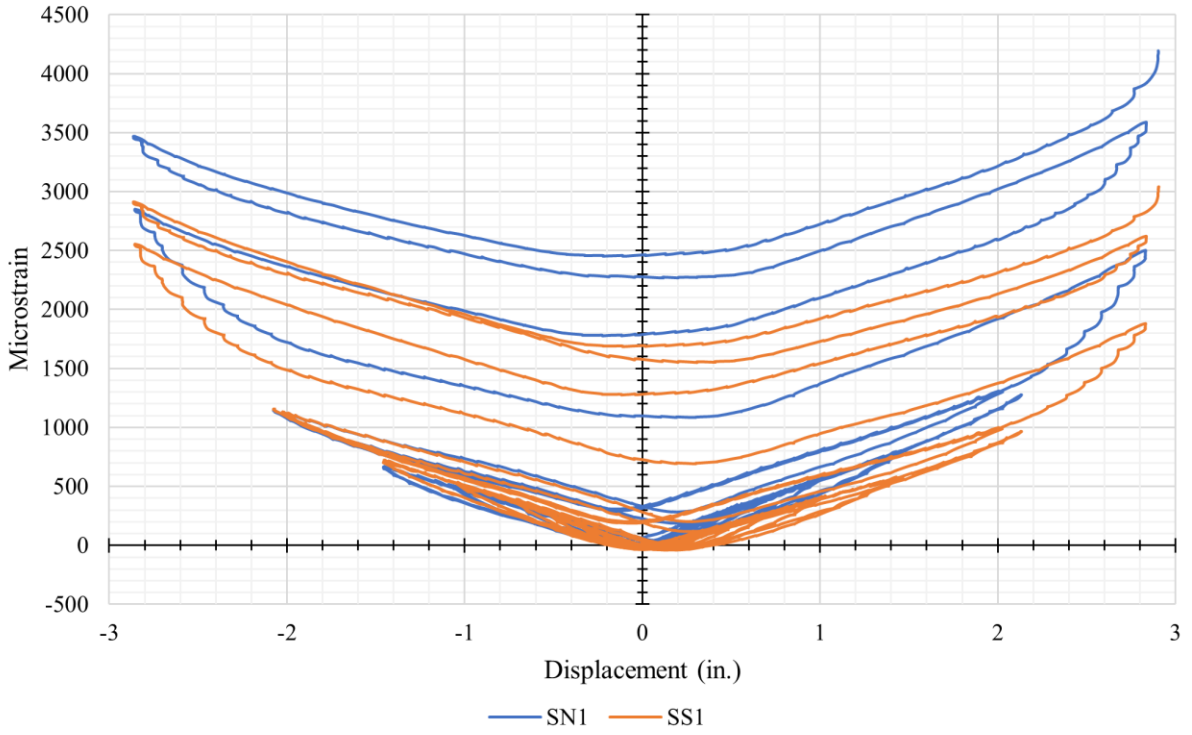

Figure 6-19: HS-SCC 2 Neutral Axis Steel Strain Gauges vs. Displacement at Column Head

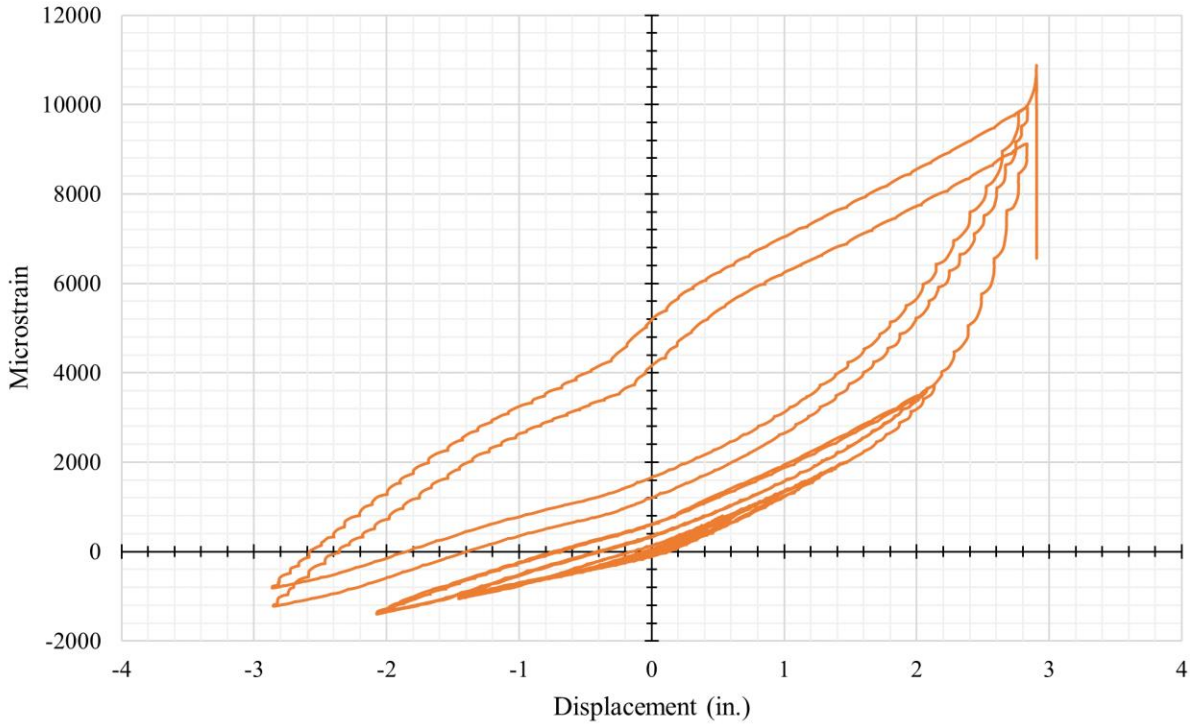

Figure 6-20: HS-SCC 2 SW1 Steel Strain Gauge vs. Displacement at Column Head

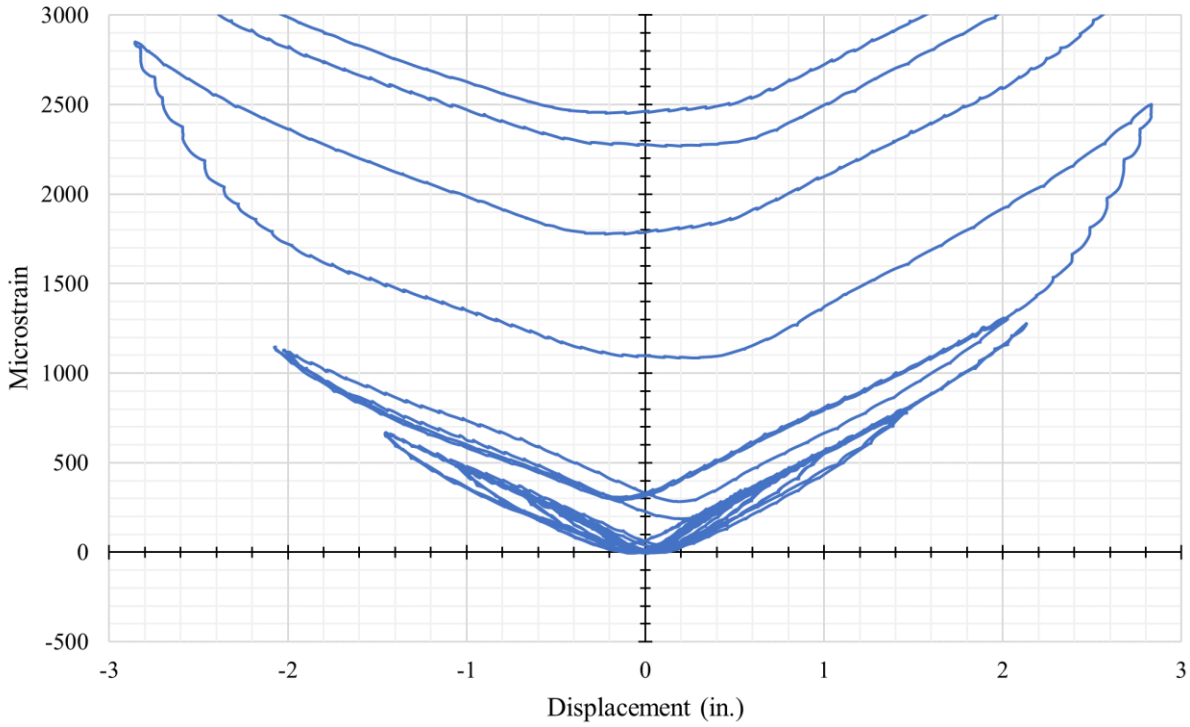

Figure 6-21: HS-SCC 2 SN1 Steel Strain Gauge vs. Displacement at Column Head

6.3.3 Analysis of GFRP Tube Strain Gauge Plots

Figure 6-22 depicts the lower level of strain gauges on the GFRP tube at the extreme fibers of the column. The strain gauges on the GFRP tube were oriented parallel to the base, along the circumference of the column. Strain gauges at similar locations and levels on the GFRP tube exhibited moderate symmetry at similar displacements. In general, gauges higher up the column, or farther from the top of the column base, exhibited lower strains, as shown in Figure 6-23. The GFRP tube confined the concrete core and was compressed into the concrete base at larger deflections, therefore, only tensile hoop strains were measured due to the orientation and placement of the strain gauges. A notable transition in the plot was observed between a displacement of approximately 3 inches and 4 inches, as shown in Figure 6-24, and emphasized with the addition of two straight line segments. The strain gauge plot was approximately linear leading up to and after the transition in the graph. The transition correlates with the significant stiffness softening and loss of capacity of the column and was attributed to the concrete core crushing and applying increased pressure to the GFRP tube.

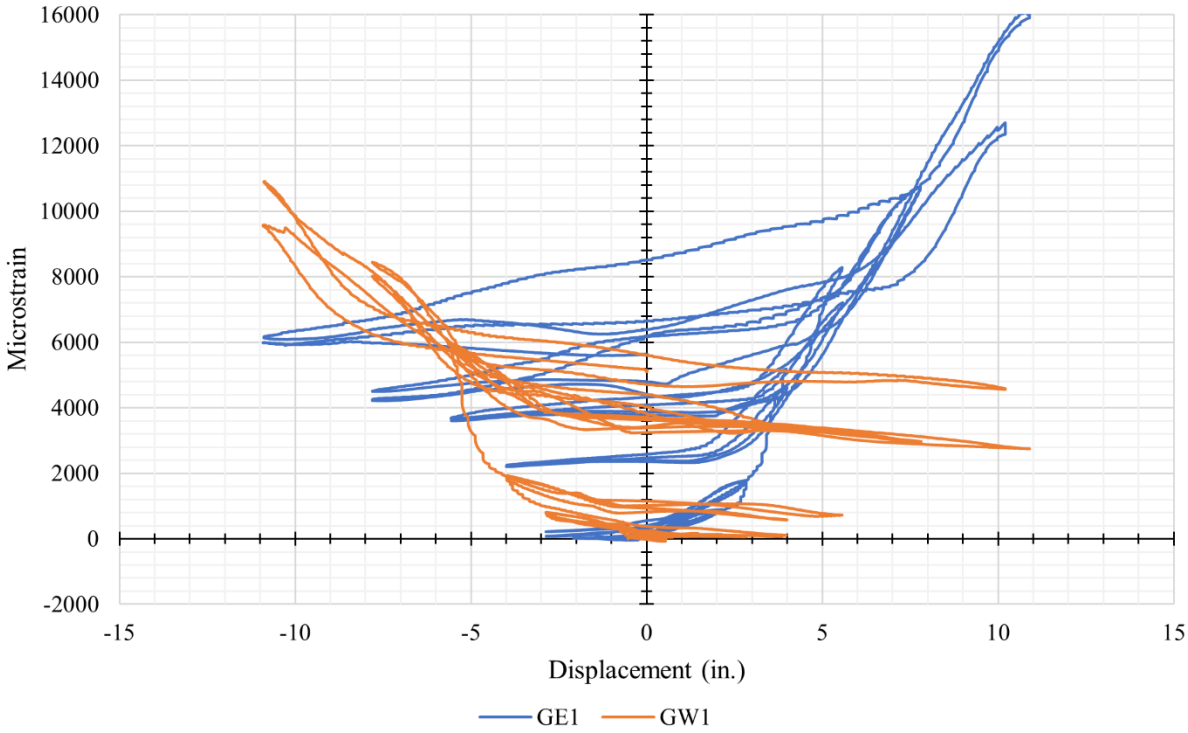

Figure 6-22: HS-SCC 2 Lower GFRP Strain Gauges vs. Displacement at Column Head

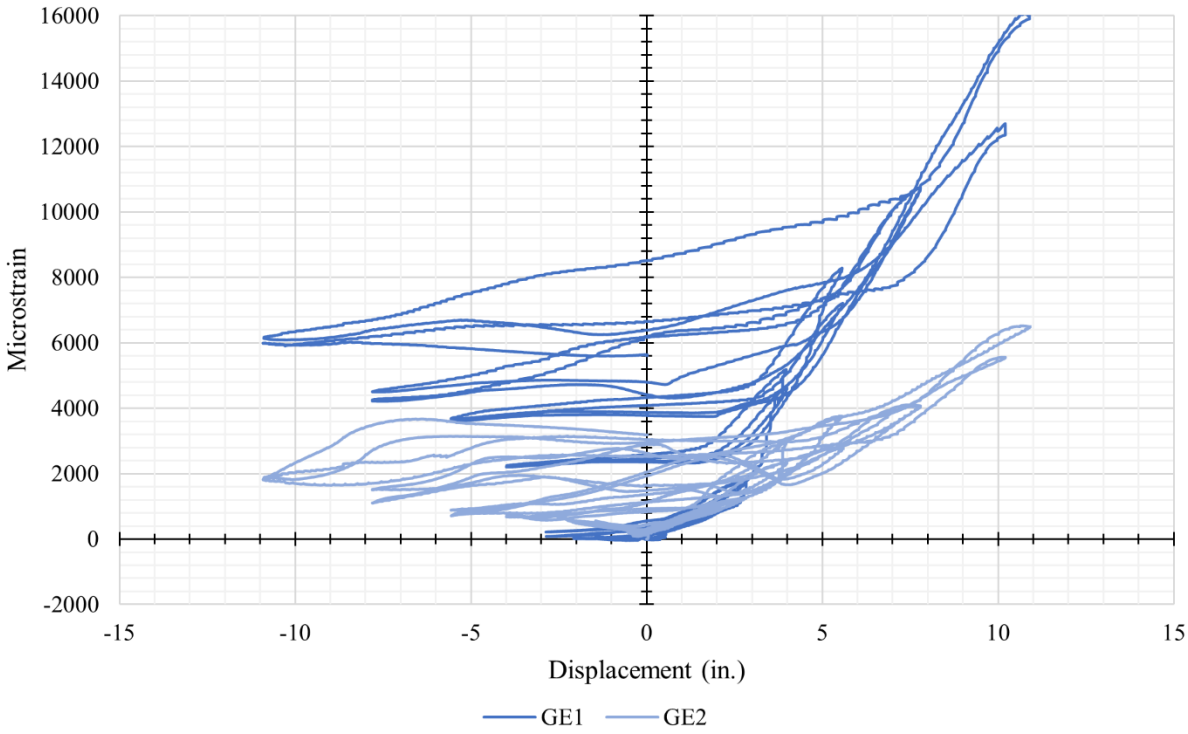

Figure 6-23: HS-SCC 2 East Side GFRP Strain Gauges vs. Displacement at Column Head

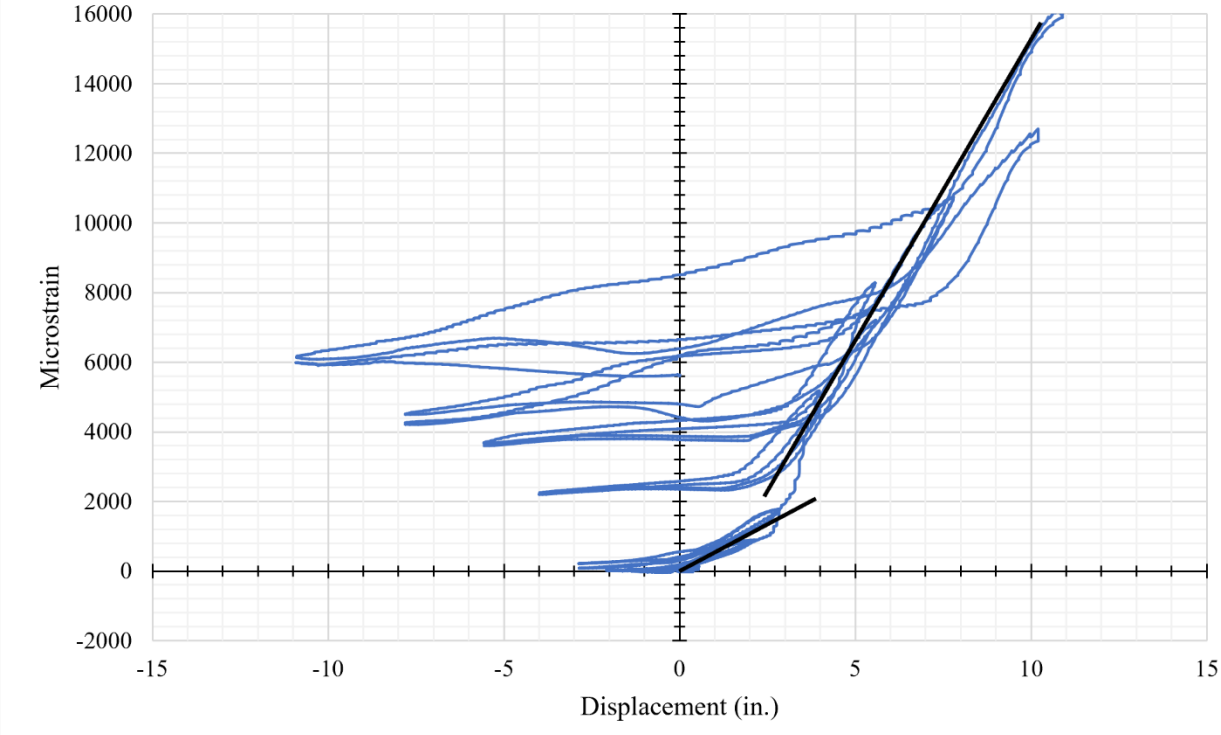

Figure 6-24: Determining HS-SCC 2 GFRP Strain Transition Using GE1 GFRP Strain Gauge vs. Displacement at Column Head

6.3.4 Analysis of Column Specimen Damage After Testing

The damage to the column specimen was assumed to extend from the concrete base to past half of the column height. The most severe damage to the column was observed to span approximately 12 inches from the top of the base. Minimal damage to the GFRP tube was observed at smaller displacements during testing while it was predominantly damaged at larger displacements as the tube was compressed into the concrete base. This aligned with observations made from the GFRP strain gauge plots. The GFRP tube was damaged approximately 2 to 3 inches from the top of the base and typically failed along the orientation of the fibers, as shown in Figure 6-25.

Figure 6-25: HS-SCC 2 GFRP Tube West Side (l) and East Side (r) Damage After Testing

The concrete core was crushed in a conical shape with the lower approximately 3 inches nearest to the column base turned to powder, as shown in Figure 6-26. This indicated that the steel tube and GFRP tube sufficiently confined the concrete core, and the concrete reached its ultimate strain without rupturing the GFRP tube. Additionally, the area of crushed concrete was roughly triangular with the most severe damage along the extreme fiber. The concrete core was no longer bonded to the steel tube after testing and was easily removed.

Figure 6-26: HS-SCC 2 Concrete Core After Testing and Light Removal of Concrete

The steel tube was observed to have buckled at the extreme axis with a vertical compressed fold, or crease, parallel to the column base and a depressed region on either side of the extreme axis, as shown in Figure 6-27. The crease exhibited tears in the steel where the steel tube had fractured during testing but did not completely separate. The observed tears resemble a fatigue failure and corroborate the discontinuity and drop in capacity shown on the load versus displacement plot. Despite the damage, the steel tube remained mostly intact, and the column was still capable of sustaining the applied constant axial compressive load.

The concrete base was observed to provide adequate flexural and shear capacity with light spalling at the interface with the column testing frame and lateral clamping mechanisms. During testing, a gap formed at the interface between the column and the base. This was indicative of the concrete core and GFRP tube sliding along the steel tube after the bond between the concrete core and the steel tube was broken. However, the steel tube was not observed to have been pulled out of the column base, therefore the embedment depth and supplemental anchorage were effective. Furthermore, each corner of the column base rotated an average maximum of approximately 0.15 inches. The rotation caused a proportional effect on the measured displacement at the column head by reducing the measured displacement. The displacement data was not corrected for this effect.

Figure 6-27: HS-SCC 2 Steel Tube West (l) and East Side (r) Damage After Testing

6.4 Comparison of HS-SCC HC-FCS Column Testing Results

The HS-SCC HC-FCS column specimens were identical in design and construction and performed likewise during testing. Both column specimens exhibited linear elastic behavior before transitioning into inelastic behavior beyond a certain load and deflection. Additionally, both columns performed similarly during testing including a gap observed at the column and base interface at larger deflections, the steel tube yielded and buckled, the concrete core crushed, and the GFRP tube ruptured.

6.4.1 Comparison of Load versus Displacement Plots

The peak moment capacity and corresponding displacement of HS-SCC 1 and HS-SCC 2 were 384 kip-ft at 5.6 inches and 370 kip-ft at 5.2 inches, respectively. The variation between the determined peak moments and displacements was approximately 4% and 8%, respectively. The peak moment capacity of HS-SCC 1 occurred during the retraction cycle while the peak moment capacity of HS-SCC 2 occurred during the extension cycle. The observed peak loads at each cycle of each specimen were reasonably similar between the extension and retraction cycles, as shown in Figure 6-28. Due to the complicated loading procedure and testing process of HS-SCC 1, the observed peak loads were reasonably symmetrical between the extension and retraction

cycles when compared to HS-SCC 2. The complicated testing procedure likely introduced variation in the column testing results.

Both columns demonstrated linear elastic behavior until a displacement of approximately 1.5 inches. Additionally, both columns exhibited similar stiffness degradation after a displacement of approximately 2 inches, followed by significant stiffness softening at a displacement of approximately 4 inches. Both columns experienced a loss of capacity after a displacement of approximately 4 inches and exhibited similar plateaus beyond the loss of capacity. Furthermore, both columns demonstrated comparable behavior during testing, including the path of each subsequent cycle, the presence, and occurrence of upturns in the measured load, and discontinuities caused by fracturing of the steel tube. Lastly, both HS-SCC 1 and 2 were determined to have failed after observing a significant reduction in capacity during and after the second 10.89-inch displacement interval.

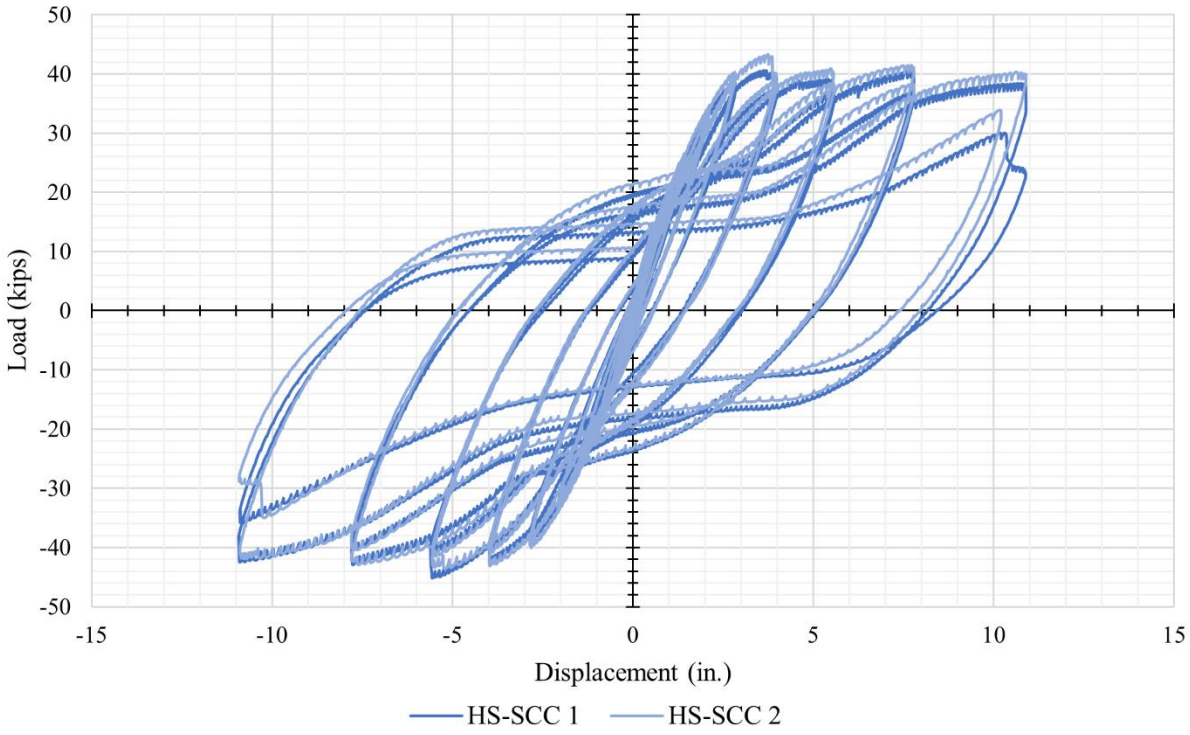

Figure 6-28: Comparing HS-SCC HC-FCS Lateral Load vs. Displacement at Column Head

6.4.2 Comparison of Steel Tube and GFRP Tube Strain Gauge Plots

Figure 6-29 compares strain gauges on the steel tube at the extreme fibers of the column for the HS-SCC 1 and HS-SCC 2 specimens. The shape of both plots was consistent with both

resembling loops. Figure 6-30 compares strain gauges on the steel tube at the neutral axis of the column for the HS-SCC 1 and 2 specimens and depicts similar behavior. Both plots resembled a "V" shape that indicated similar neutral axis migration during testing. The steel tube strain gauge data obtained from both specimens validated observations from the load versus displacement plots and supported the observed transition and stiffness softening displacements. Figure 6-31 compares strain gauges on the GFRP tube at the extreme fibers of the column for the HS-SCC 1 and HS-SCC 2 specimens. The shape of both plots was consistent with both exhibiting only tensile hoop strains and a similar transition between a displacement of approximately 3 inches and 4 inches. An offset was observed between similar strain gauge plots. This was likely due to the complicated testing procedure of HS-SCC 1, which also lacked the initial strain gauge data. However, gauges at the same positions on each column produced highly similar shapes and therefore validated the offset data. Due to the consistency of the plots, it was assumed that the missing initial strain gauge data for HS-SCC 1 would closely match that of HS-SCC 2. Therefore, HS-SCC 2 would serve as the representative HS-SCC HC-FCS column specimen for comparing the performance of different column types.

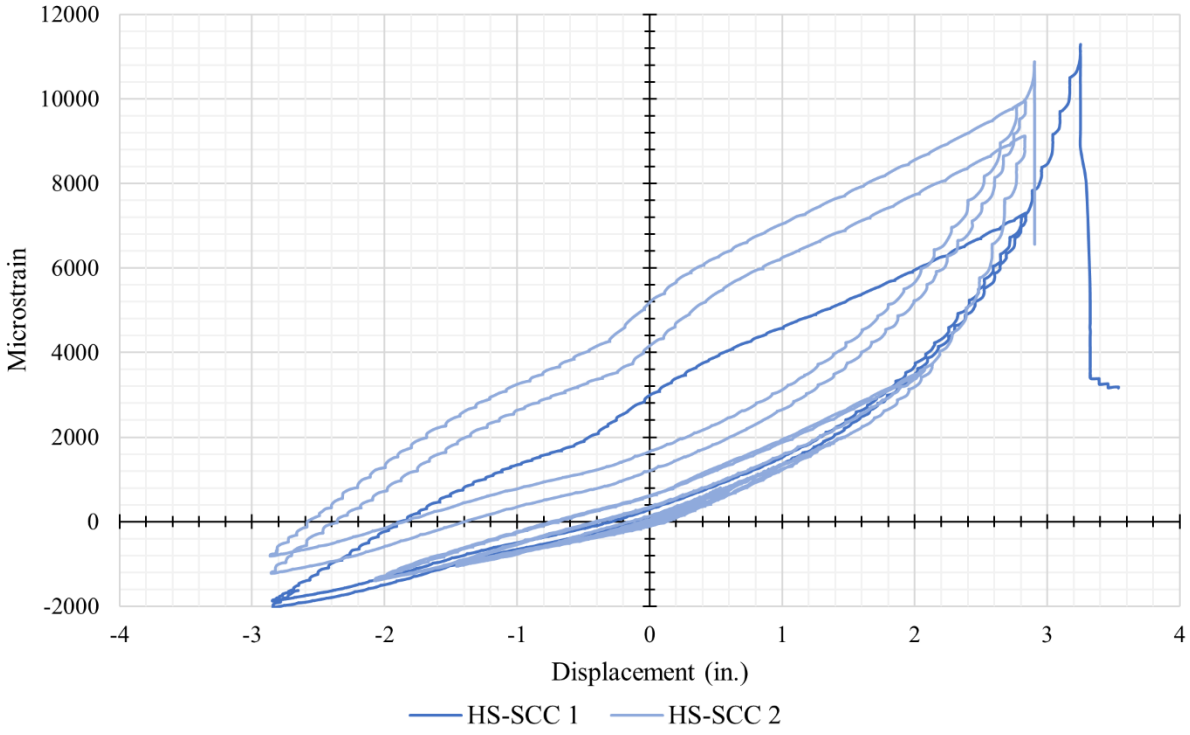

Figure 6-29: Comparing HS-SCC SW1 Strain Gauge vs. Displacement at Column Head

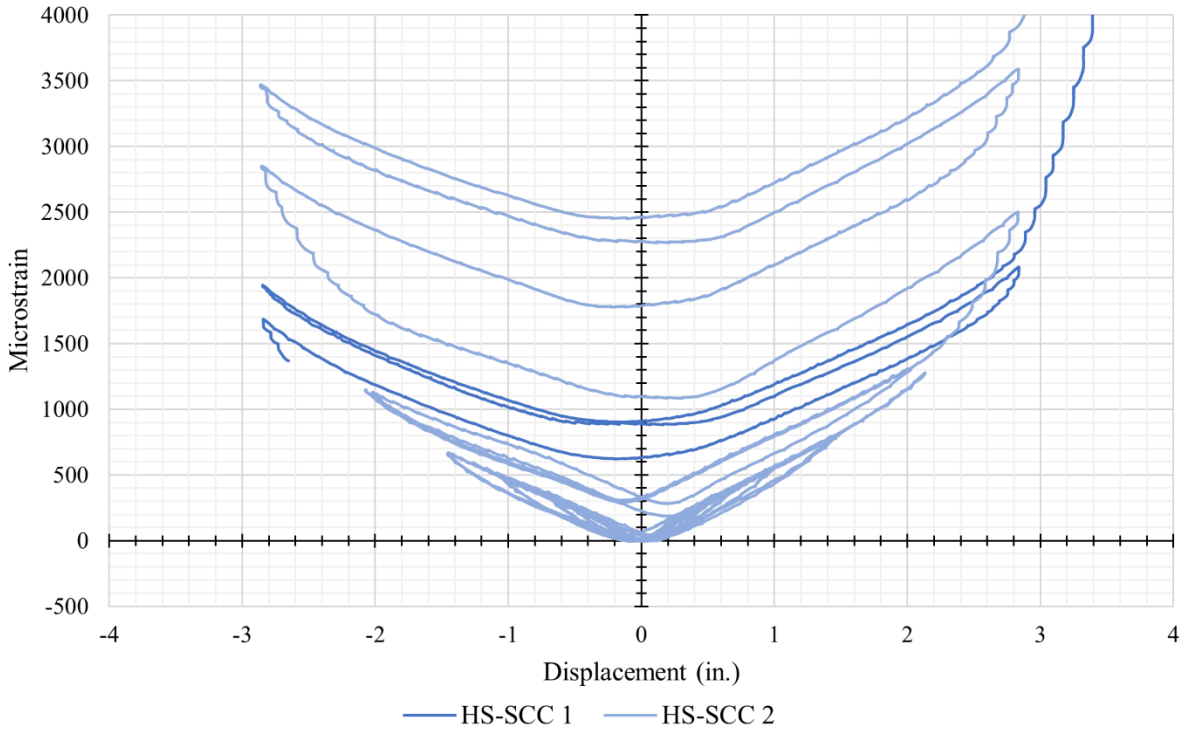

Figure 6-30: Comparing HS-SCC SN1 Strain Gauge vs. Displacement at Column Head

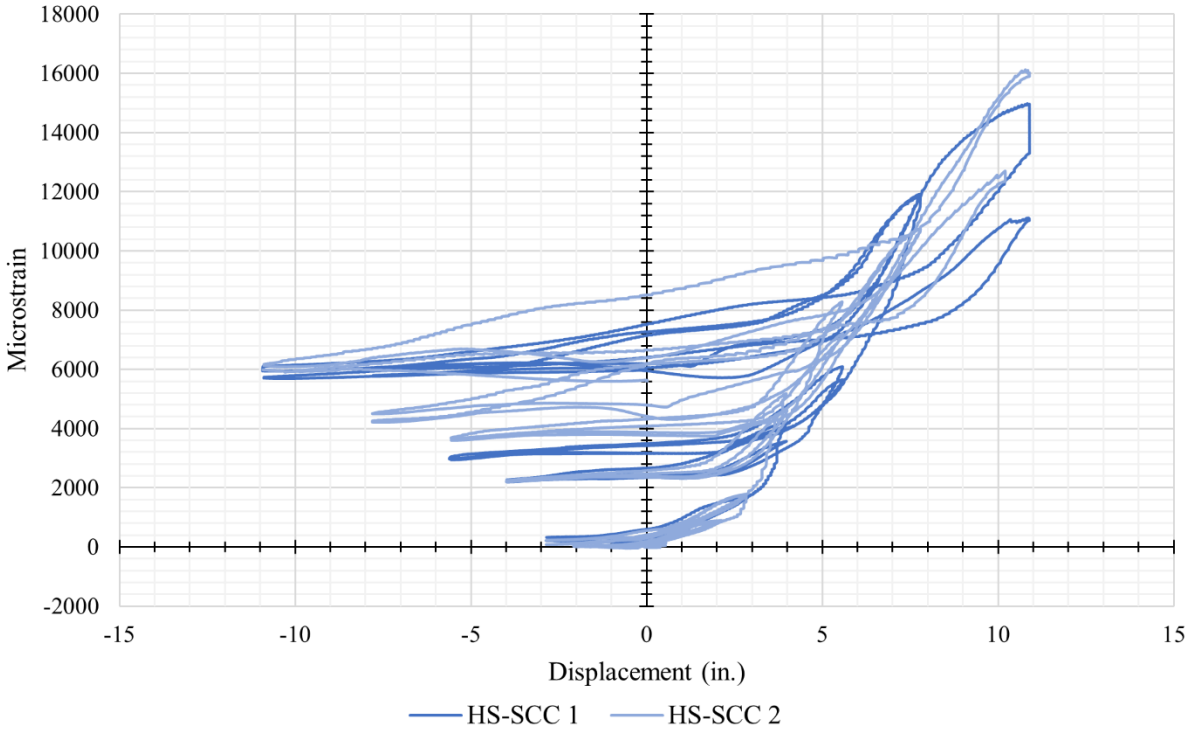

Figure 6-31: Comparing HS-SCC GE1 Strain Gauges vs. Displacement at Column Head

6.4.3 Comparison of Column Specimen Damage After Testing

The damage to each column specimen extended to approximately the same distance from the concrete base with the most severe damage for both observed approximately 12 inches from the top of the base. Both specimens suffered comparable damage to the GFRP tube, concrete core, and steel tube. In both cases, the GFRP sufficiently confined the concrete core and ruptured at larger displacements, the concrete core crushed and became powder nearest to the base with a conical failure, and the steel tube buckled in a consistent shape with fractures or tears in the steel tube along the vertical creases. Figure 6-32 compares the damage to the GFRP tube. Figure 6-33 compares the damage to the concrete core. Figure 6-34 compares the damage to the steel tube. Both columns were capable of sustaining the applied constant axial compressive load after testing. Additional damage was observed on the HS-SCC 1 specimen from the additional, maximum displacement cycle. However, the increased damage was consistent with exacerbated damage on the HS-SCC 2 specimen.

Figure 6-32: Comparing HS-SCC 1 (l) and HS-SCC 2 (r) GFRP Tube Damage After Testing

Both concrete bases performed consistently with minimal damage. Both specimens exhibited a gap at the interface between the column and the base during testing, but neither steel tube was observed to have pulled out of the column base. The corner of each column base rotated an average maximum of approximately 0.17 inches for HS-SCC 1 and 0.15 inches for HS-SCC 2. Despite the additional, maximum displacement cycle experienced by HS-SCC 1, the average

maximum base rotation of each column only differed by approximately 10%. The comparative maximum base rotation indicates that the maximum base rotation likely occurred at the point of maximum column stiffness that was similar for both column specimens.

Figure 6-33: Comparing HS-SCC 1 (l) and HS-SCC 2 (r) Concrete Core After Testing and Light Removal of Concrete

Figure 6-34: Comparing HS-SCC 1 (l) and HS-SCC 2 (r) Steel Tube Damage After Testing

Chapter 7: Analysis of UHPC HC-FCS Column Testing Results

The UHPC HC-FCS column specimens were tested according to the prescribed testing procedure. The specimens exhibited traditional linear elastic and inelastic column behavior. The results of each column test were analyzed including the load versus displacement, strain versus displacement at various locations, and forensic photographs of the damage sustained by the column after testing.

7.1 Analysis of UHPC 1 HC-FCS Column Testing Results

The first UHPC HC-FCS column specimen tested was UHPC 1. The specimen exhibited aspects of traditional column behavior such as linear elastic behavior before transitioning into inelastic behavior beyond a certain load and deflection. During testing, a gap formed between the GFRP tube and the top of the column base at larger deflections, the steel tube yielded and buckled, the concrete core crushed, and the GFRP tube ruptured.

7.1.1 Analysis of Load versus Displacement Plot

The peak moment capacity of the UHPC 1 HC-FCS column was 413 kip-ft at a displacement of 7.8 inches. The observed peak loads were reasonably symmetrical between the extension and retraction cycles, as shown in Figure 7-1. Linear elastic behavior was observed until a displacement of approximately 1 inch, after which the behavior began to transition to inelastic behavior. This was determined by analyzing the plot of the load versus displacement at the column head shown in Figure 7-2. Similarly, gradual stiffness degradation was observed approaching a displacement of approximately 2 inches, followed by moderate stiffness softening at a displacement of approximately 3 inches and significant stiffness softening at a displacement of approximately 4 inches. The initial loss of stiffness was attributed to the steel tube yielding and buckling, with minimal cracking in the concrete core. Increasingly significant stiffness softening occurred beyond a displacement of approximately 4 inches with the sustained load beginning to plateau approaching a displacement of approximately 8 inches. The sustained load beginning to plateau was attributed to the concrete core starting to crush. The capacity of the specimen gradually increased until a displacement of approximately 8 inches. The continued increase in capacity was attributed to the concrete core remaining intact and continuing to support the column, despite the yielded and buckled steel tube. The concrete core was able to

remain intact due to the presence of the steel fibers that increased the confinement and ductility of the concrete core, despite the loss of confinement from the buckled steel tube. The first cycle of each displacement interval closely followed the second cycle of the previous interval and, in general, the second cycle of any displacement interval did not reach the same maximum load as the first cycle of that interval due to the damage sustained from the previous cycle. As the column was displaced beyond approximately 8 inches, the load versus displacement plot began to plateau.

At larger displacements and later cycles, an upturn was observed on the load versus displacement plot. During the beginning of each displacement cycle, the load gradually increased or held constant before an upturn in the sustained load was observed. The upturn was attributed to the yielding and buckling of the steel tube and the support of the intact concrete core. As the load on the column was reversed, the side of the column in which the steel tube was previously buckled was gradually straightened from the tension caused by the load reversal. Concurrently, the side of the column in which the steel tube was previously in tension began to buckle and the concrete core was compressed against the concrete base. Eventually, the straightened region began to yield from the tension caused by the load reversal after the opposite side had completely buckled and began to bear on the concrete core, resulting in a notable upturn in the sustained load on the load versus displacement plot. At larger displacements, the upturn became shallower as the steel tube fatigued and the concrete core crushed.

A discontinuity was observed on the first cycle of the 10.89-inch displacement interval when the column was displaced in the retraction direction. This slight drop in capacity was attributed to the GFRP tube rupturing due to the concrete core crushing and applying increased pressure underneath. The column specimen was not considered failed due to the lack of a significant reduction in capacity during and after the second 10.89-inch displacement interval. The final cycle of the last displacement interval demonstrated a notable upturn in sustained load and therefore the concrete core and steel tube were concluded to be mostly intact. The specimen was not displaced further due to safety considerations and the potential risk of fracturing the post-tensioned prestressing strands.

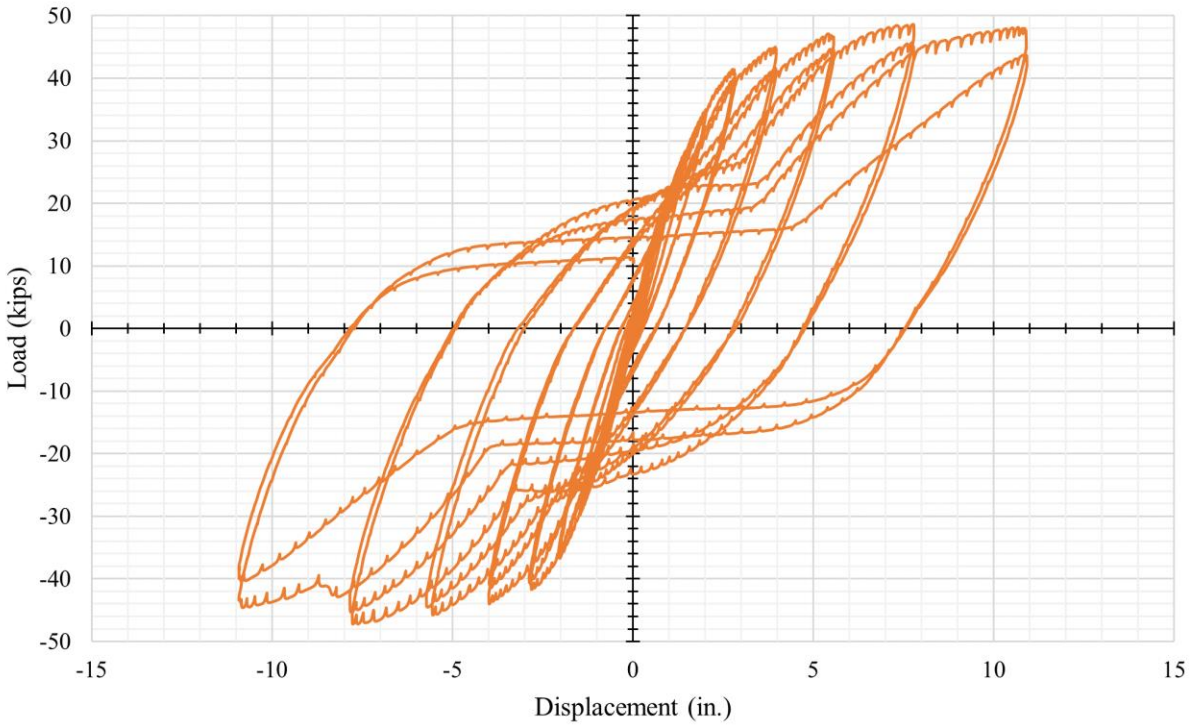

Figure 7-1: UHPC 1 Column Lateral Load vs. Displacement at Column Head

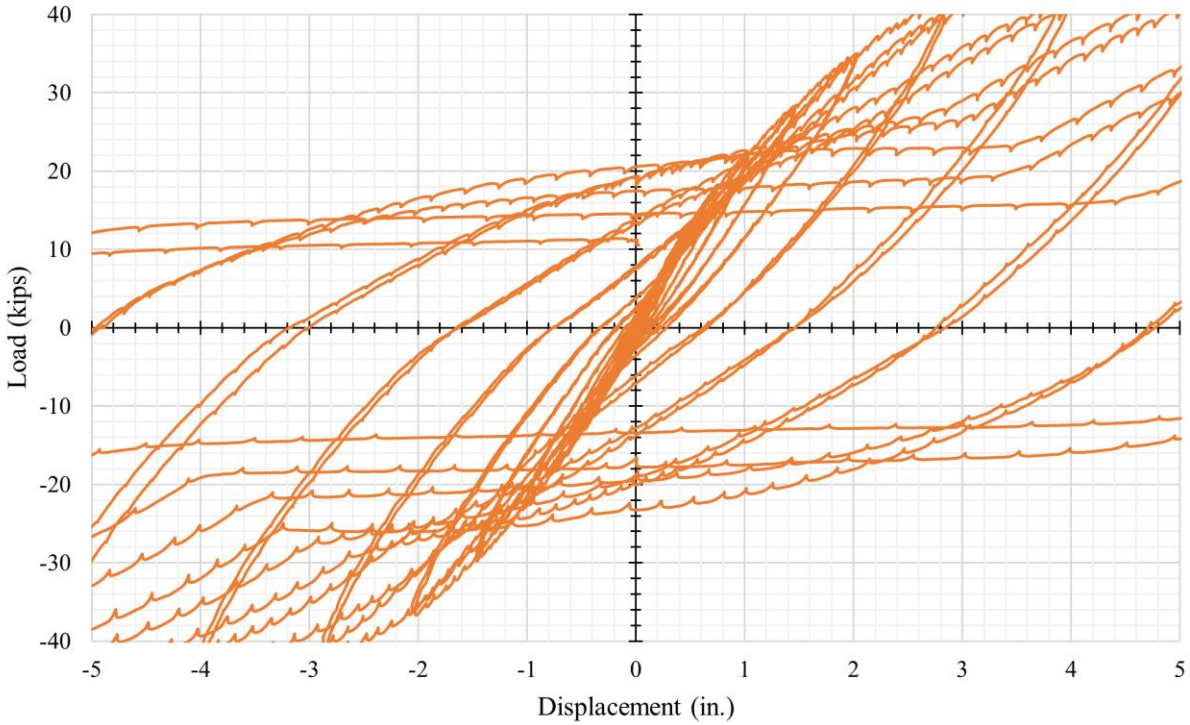

Figure 7-2: Determining Elastic Transition for UHPC 1 Using Lateral Load vs. Displacement at Column Head

7.1.2 Analysis of Steel Tube Strain Gauge Plots

Figure 7-3 depicts the strain gauges on the steel tube at the extreme fibers of the column. Strain gauge SE1 had a slight offset in the data with an erroneous spike, both of which were caused by intermittent issues with the data acquisition during testing. The strain gauges on the steel tube were oriented perpendicular to the base, along the height of the column. Strain gauges at similar locations and levels exhibited symmetry at similar displacements, and in general, gauges higher up the column, or farther from the top of the column base, exhibited lower strains. The shape of the plot resembled loops, similar to the shape of the load versus displacement plot. The plots for gauges on opposite sides of the column were mirrored because one side of the column is in compression while the other is in tension. The higher captured tensile strains rather than compression strains were attributed to the steel reinforcement functioning as the major tension element, whereas the concrete core and steel reinforcement both supported the compressive load on the opposite side, with the concrete core supporting a greater portion of the load before crushing.

Figure 7-4 depicts the lower level of strain gauges on the steel tube at the neutral axis of the column. Strain gauges at similar locations and levels exhibited symmetry at similar displacements, and in general, gauges higher up the column, or farther from the top of the column base, exhibited lower strains. The shape of the plot resembled a “V”, which was indicative of the neutral axis of the column migrating during testing. The migration of the neutral axis was shown by the lack of significant negative, or compressive, strain measurements. As the neutral axis migrated away from its initial position at the center of the column, toward the direction of loading, the center of the column began to experience tension. This process was then mirrored as the loading was reversed, resulting in the observed plot and shape.

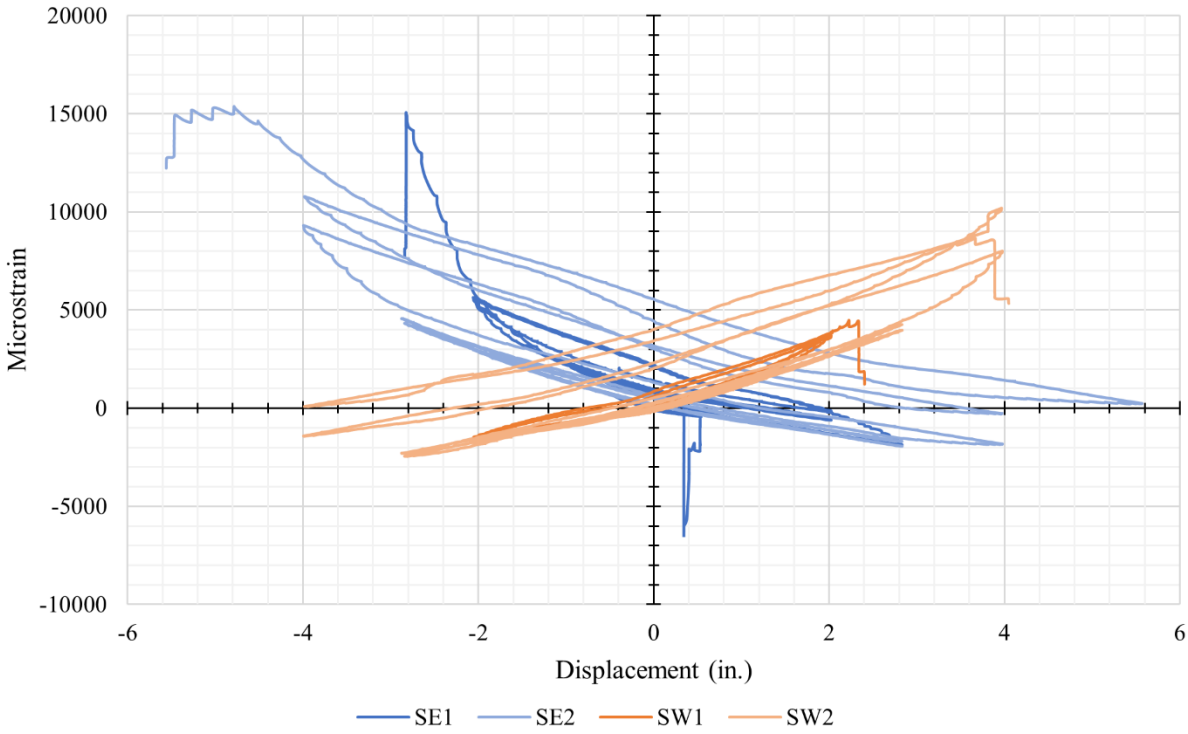

Figure 7-3: UHPC 1 Extreme Fiber Strain Gauges vs. Displacement at Column Head

The steel tube strain gauge plots also corroborated observations from the load versus displacement plot. The transition from elastic to inelastic behavior was observed at a displacement of approximately 1 inch, after which plastic deformations were observed, as shown in Figure 7-5 and Figure 7-6. A significant change in the measured strains due to stiffness softening was observed beyond a displacement of approximately 2 inches. Prominent plastic deformation was shown by residual strain at zero displacement. Further plastic deformation was observed at and beyond the 2.97-inch displacement interval. Strain gauge data was not obtained beyond a displacement of approximately 4 inches, likely due to significant damage to the column specimen from the steel tube yielding and buckling while the concrete core remained intact, with the lower gauges failing first.

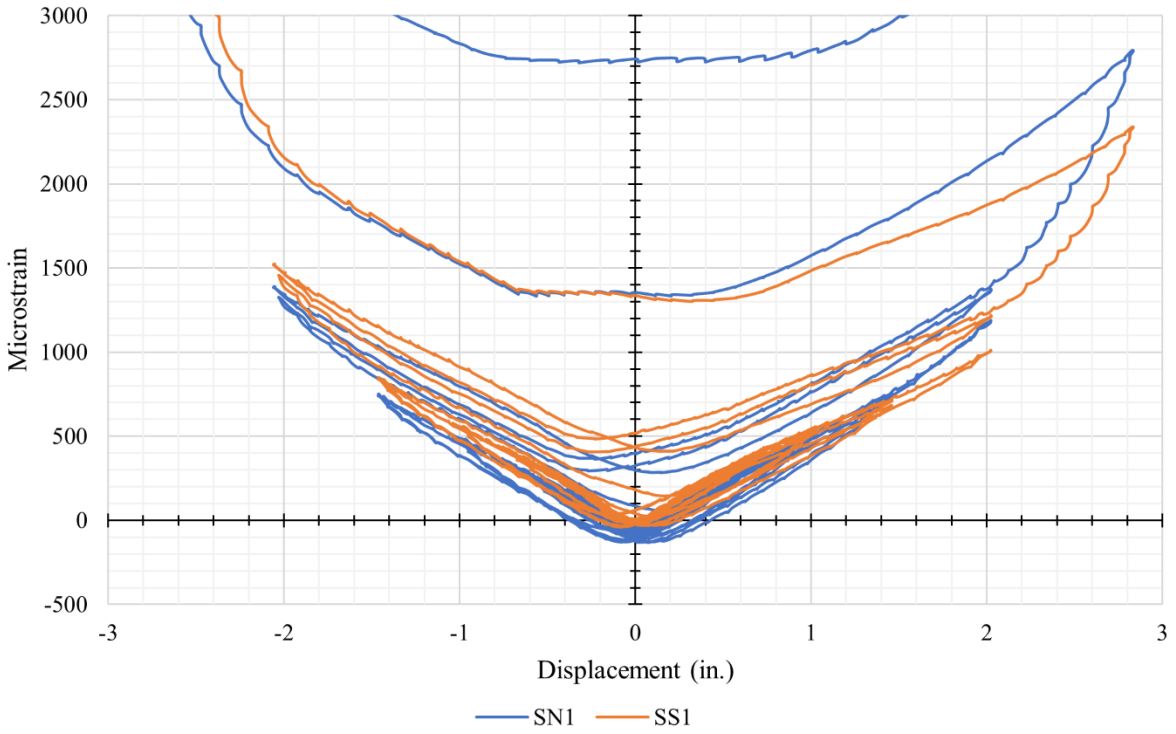

Figure 7-4: UHPC 1 Neutral Axis Steel Strain Gauges vs. Displacement at Column Head

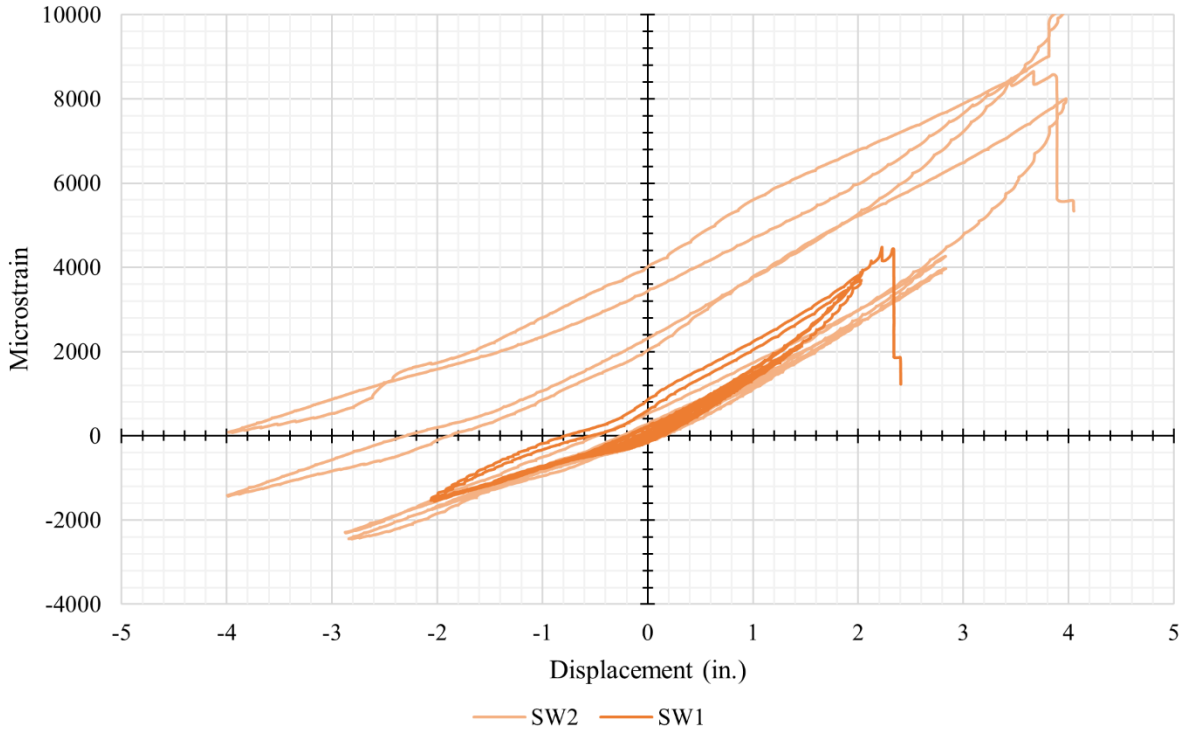

Figure 7-5: UHPC 1 SW1 and SW2 Steel Strain Gauge vs. Displacement at Column Head

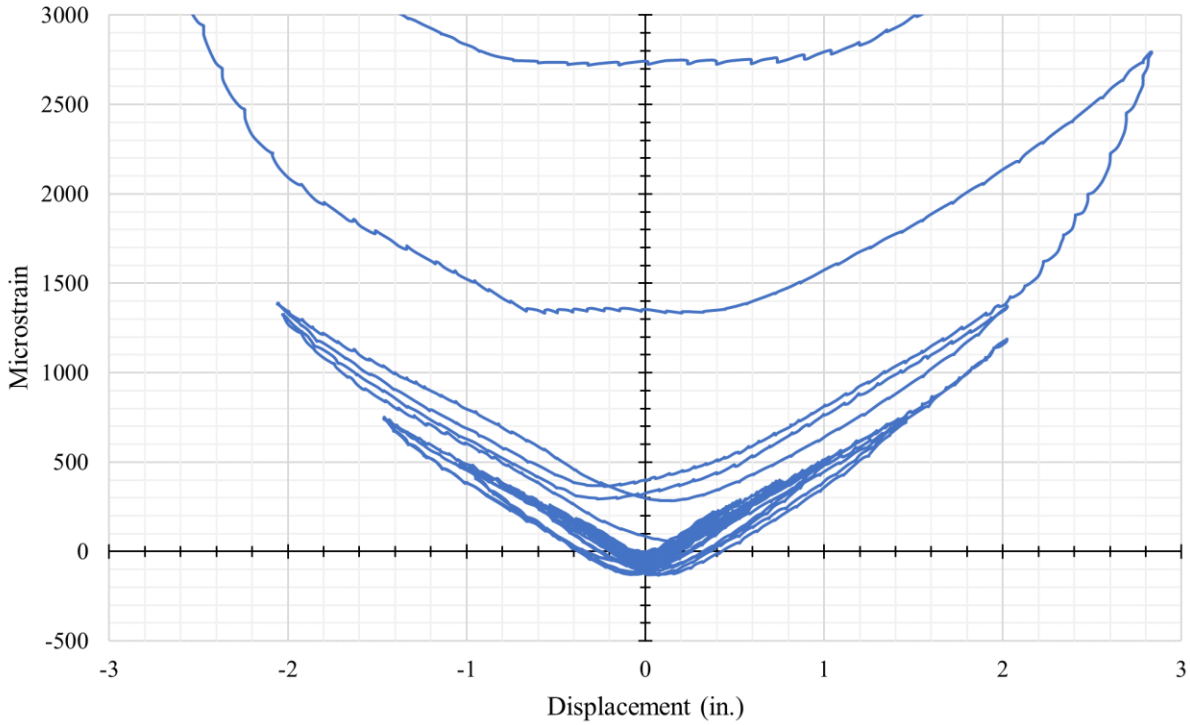

Figure 7-6: UHPC 1 SN1 Steel Strain Gauge vs. Displacement at Column Head

7.1.3 Analysis of GFRP Tube Strain Gauge Plots

Figure 7-7 depicts the lower level of strain gauges on the GFRP tube at the extreme fibers of the column. The strain gauges on the GFRP tube were oriented parallel to the base, along the circumference of the column. Strain gauges at similar locations and levels on the GFRP tube exhibited moderate symmetry at similar displacements. In general, gauges higher up the column, or farther from the top of the column base, exhibited lower strains, as shown in Figure 7-8. The GFRP tube confined the concrete core and was compressed into the concrete base at larger deflections, therefore, only tensile hoop strains were measured due to the orientation and placement of the strain gauges. A notable transition in the plot was observed at a displacement of approximately 6 inches, as shown in Figure 7-9, and emphasized with the addition of two straight line segments. The strain gauge plot was approximately linear leading up to and after the transition in the graph, with a steeper approximately linear slope after the transition. The transition occurred at approximately the same displacement as the sustained load began to plateau, therefore the transition was attributed to the concrete core crushing and applying increased pressure to the GFRP tube.

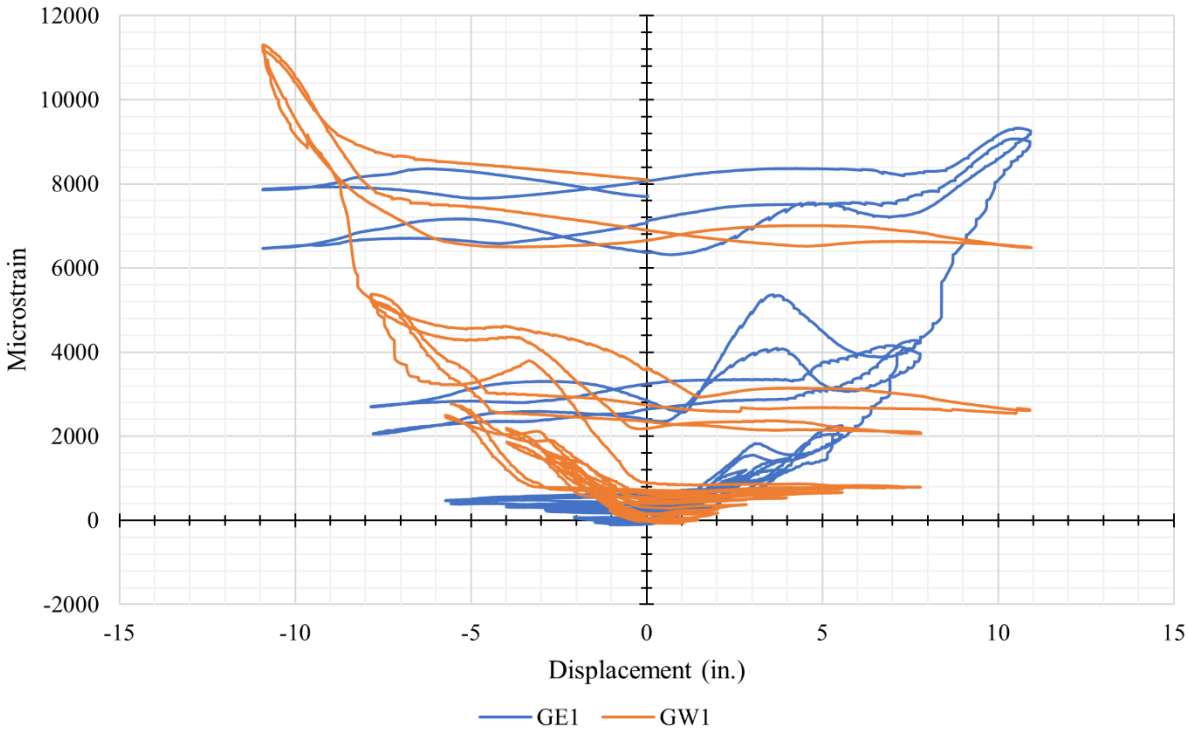

Figure 7-7: UHPC 1 Lower GFRP Strain Gauges vs. Displacement at Column Head

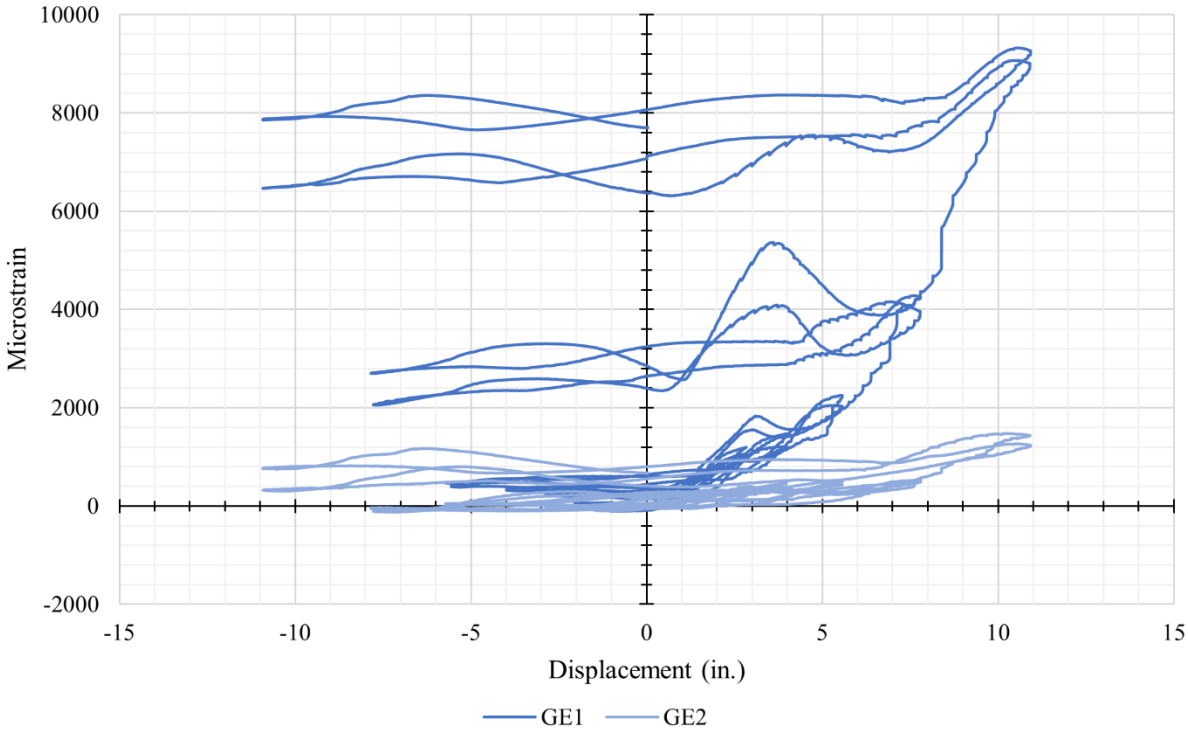

Figure 7-8: UHPC 1 East Side GFRP Strain Gauges vs. Displacement at Column Head

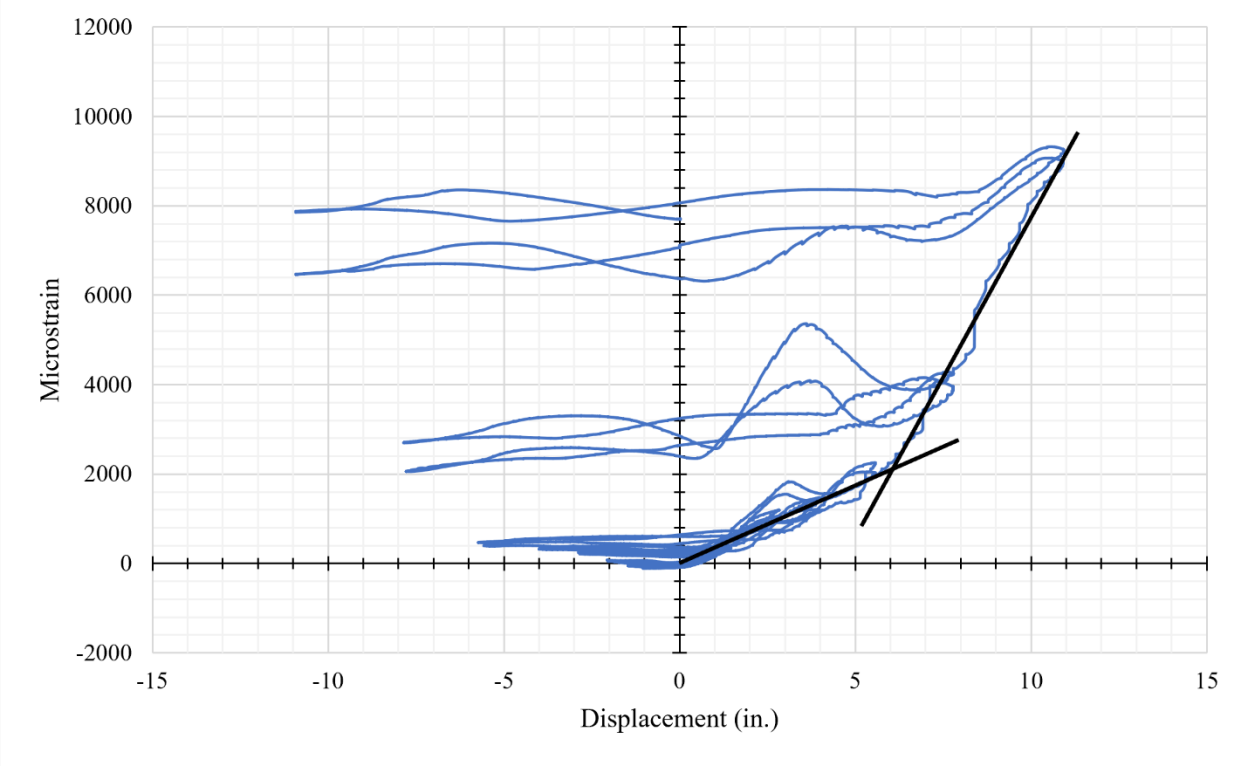

Figure 7-9: Determining UHPC 1 GFRP Strain Transition Using GE1 GFRP Strain Gauge vs. Displacement at Column Head

7.1.4 Analysis of Column Specimen Damage After Testing

The damage to the column specimen was assumed to extend from the concrete base to past half of the column height. The most severe damage to the column was observed to extend approximately 6 inches from the top of the base. Minimal damage to the GFRP tube was observed at smaller displacements during testing and was predominantly damaged at larger displacements as the tube was compressed into the concrete base, as shown in Figure 7-10. This aligned with observations made from the GFRP strain gauge plots. The GFRP tube was damaged approximately 1 to 1.5 inches from the top of the base and typically failed along the orientation of the fibers, as shown in Figure 7-11.

The area of the crushed concrete at the bottom of the concrete core was roughly triangular with the most severe damage along the extreme fiber, as shown in Figure 7-12. Longitudinal cracks were observed to extend along each extreme fiber. Due to the presence of steel fibers, the crushed concrete was removed by jackhammering to reveal the shape of the crushed region below. The concrete core was crushed in a conical shape, as shown in Figure

7-13. The lower approximately 3 inches nearest to the column base was reduced to rubble and held together by the steel fibers. This indicated that the concrete core was sufficiently confined by some combination of the steel tube, embedded steel fibers, and GFRP tube. Fiber settling was observed in the concrete core due to the high flow of 13 inches at casting. A void was discovered underneath the concrete core at the buckled region of the steel tube that was created by the steel tube buckling inward, away from the concrete core, as shown in Figure 7-13. The concrete core was no longer bonded to the steel tube after testing and, once the concrete was separated from itself, was easily removed.

The steel tube was observed to have buckled at the extreme axis with two diagonal compressed folds, or creases, parallel to the column base that converged below the extreme fiber and a depressed region along the extreme fiber, as shown in Figure 7-14. The crease exhibited tears in the steel where the steel tube had begun to fracture during testing. The observed tears indicated that the steel tube would have likely fractured from fatigue with additional cycles or increased displacement. Despite the damage, the steel tube remained intact, and the column was still capable of sustaining the applied constant axial compressive load.

Figure 7-10: UHPC 1 GFRP Tube Compression (l) and Separation (r) During Testing

Figure 7-11: UHPC 1 GFRP Tube West Side (l) and East Side (r) Damage After Testing

Figure 7-12: UHPC 1 Concrete Core West Side (l) and East Side (r) Damage After Testing

The concrete base was observed to provide adequate flexural and shear capacity with spalling and minor damage at the interface with the column testing frame and lateral clamping mechanisms. During testing, a gap formed at the interface between the column and the base. This was indicative of the concrete core and GFRP tube sliding along the steel tube after the bond between the concrete core and the steel tube was broken. However, the steel tube was not

observed to have been pulled out of the column base, therefore the embedment depth and supplemental anchorage were effective. Furthermore, each corner of the column base rotated an average maximum of approximately 0.15 inches. The rotation would cause a proportional effect on the measured displacement at the column head, reducing the measured displacement. The displacement data was not corrected for this effect.

Figure 7-13: UHPC 1 Concrete Core After Light (l) and Significant (r) Concrete Removal

Figure 7-14: UHPC 1 Steel Tube West (l) and East Side (r) Damage After Testing

7.2 Analysis of UHPC 2 HC-FCS Column Testing Results

Similar to the first UHPC HC-FCS column tested, the UHPC 2 specimen exhibited aspects of traditional column behavior such as linear elastic behavior before transitioning into inelastic behavior beyond a certain load and deflection. During testing, a gap formed between the GFRP tube and the top of the column base at larger deflections, the steel tube yielded and buckled, the concrete core crushed, and the GFRP tube ruptured.

7.2.1 Analysis of Load versus Displacement Plot

The peak moment capacity of the UHPC 1 HC-FCS column was 408 kip-ft at a displacement of 7.6 inches. The observed peak loads were reasonably symmetrical between the extension and retraction cycles, as shown in Figure 7-15. Linear elastic behavior was observed until a displacement of approximately 1 inch, after which the behavior began to transition to inelastic behavior. This was determined by analyzing the plot of the load versus displacement at the column head shown in Figure 7-16. Similarly, gradual stiffness degradation was observed approaching a displacement of approximately 2 inches, followed by moderate stiffness softening at a displacement of approximately 3 inches and significant stiffness softening at a displacement of approximately 4 inches. The initial loss of stiffness was attributed to the steel tube yielding and buckling, with minimal cracking in the concrete core. Increasingly significant stiffness softening occurred beyond a displacement of approximately 4 inches with the sustained load beginning to plateau approaching a displacement of approximately 8 inches. The sustained load beginning to plateau was attributed to the concrete core starting to crush. The capacity of the specimen gradually increased until a displacement of approximately 8 inches. The continued increase in capacity was attributed to the concrete core remaining intact and continuing to support the column, despite the yielded and buckled steel tube. The concrete core was able to remain intact due to the presence of the steel fibers that increased the confinement and ductility of the concrete core, despite the loss of confinement from the buckled steel tube. The first cycle of each displacement interval closely followed the second cycle of the previous interval and, in general, the second cycle of any displacement interval did not reach the same maximum load as the first cycle of that interval due to the damage sustained from the previous cycle. As the column was displacement beyond approximately 8 inches, the load versus displacement plot began to plateau.

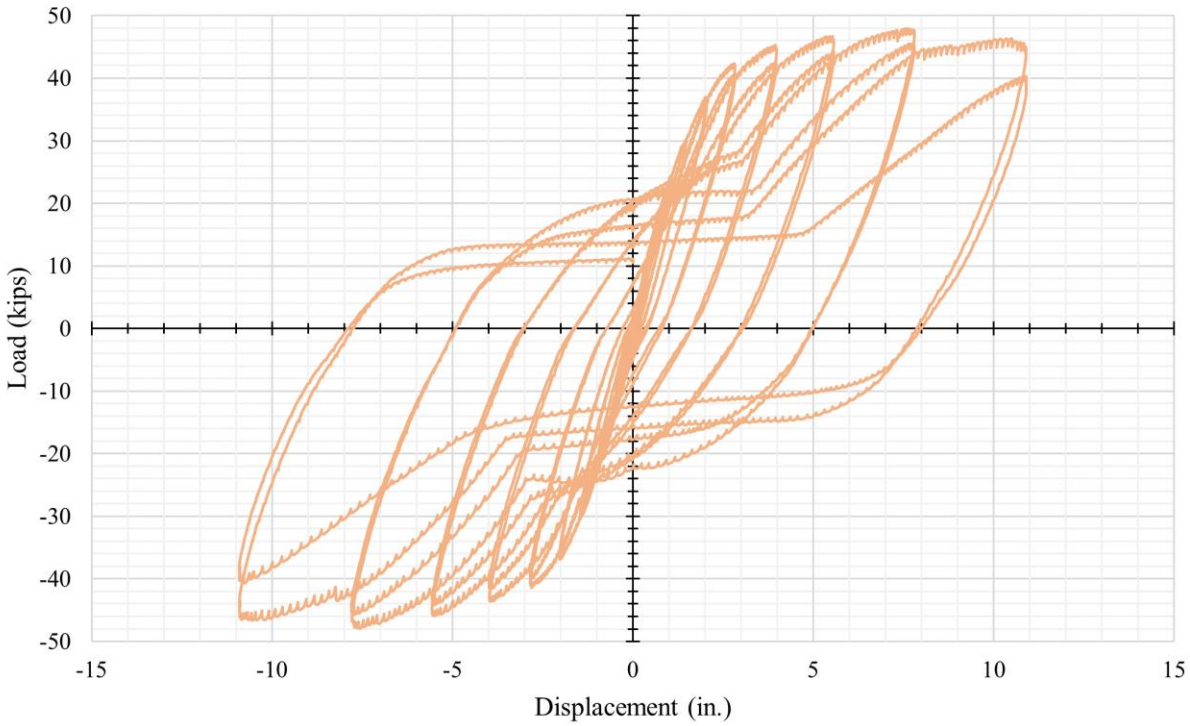

Figure 7-15: UHPC 2 Column Lateral Load vs. Displacement at Column Head

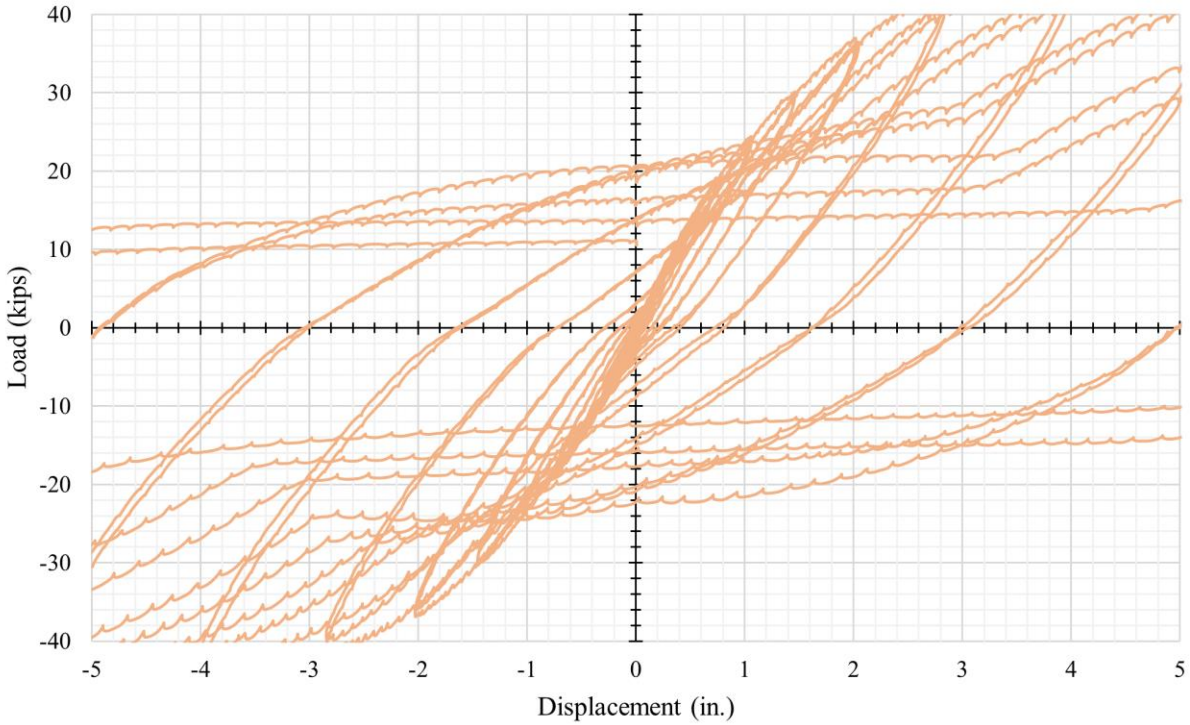

Figure 7-16: Determining Elastic Transition for UHPC 2 Using Lateral Load vs. Displacement at Column Head

At larger displacements and later cycles, an upturn was observed on the load versus displacement plot. During the beginning of each displacement cycle, the load gradually increased or held constant before an upturn in the sustained load was observed. The upturn was attributed to the yielding and buckling of the steel tube and the support of the intact concrete core. As the load on the column was reversed, the side of the column in which the steel tube was previously buckled was gradually straightened from the tension caused by the load reversal. Concurrently, the side of the column in which the steel tube was previously in tension began to buckle and the concrete core was compressed against the concrete base. Eventually, the straightened region began to yield from the tension caused by the load reversal after the opposite side had completely buckled and began to bear on the concrete core, resulting in a notable upturn in the sustained load on the load versus displacement plot. At larger displacements, the upturn became shallower as the steel tube fatigued and the concrete core crushed.

A small discontinuity was observed on the first cycle of the 10.89-inch displacement interval when the column was displaced in the retraction direction. This minimal drop in capacity was attributed to the GFRP tube rupturing due to the concrete core crushing and applying increased pressure underneath. The column specimen was not considered failed due to the lack of a significant reduction in capacity during and after the second 10.89-inch displacement interval. The final cycle of the last displacement interval demonstrated a notable upturn in sustained load and therefore the concrete core and steel tube were concluded to be mostly intact. The specimen was not displaced further due to safety considerations and the potential risk of fracturing the post-tensioned prestressing strands.

7.2.2 Analysis of Steel Tube Strain Gauge Plots

Figure 7-17 depicts the strain gauges on the steel tube at the extreme fibers of the column. The strain gauges on the steel tube were oriented perpendicular to the base, along the height of the column. Strain gauges at similar locations and levels exhibited symmetry at similar displacements, and in general, gauges higher up the column, or farther from the top of the column base, exhibited lower strains. The shape of the plot resembled loops, similar to the shape of the load versus displacement plot. The plots for gauges on opposite sides of the column were mirrored because one side of the column is in compression while the other is in tension. The higher captured tensile strains rather than compression strains were attributed to the steel

reinforcement functioning as the major tension element, whereas the concrete core and steel reinforcement both supported the compressive load on the opposite side, with the concrete core supporting a greater portion of the load before crushing.

Figure 7-18 depicts the lower level of strain gauges on the steel tube at the neutral axis of the column. Strain gauges at similar locations and levels exhibited symmetry at similar displacements, and in general, gauges higher up the column, or farther from the top of the column base, exhibited lower strains. The shape of the plot resembled a "V", which was indicative of the neutral axis of the column migrating during testing. The migration of the neutral axis was shown by the lack of significant negative, or compressive, strain measurements. As the neutral axis migrated away from its initial position at the center of the column, toward the direction of loading, the center of the column began to experience tension. This process was then mirrored as the loading was reversed, resulting in the observed plot and shape.

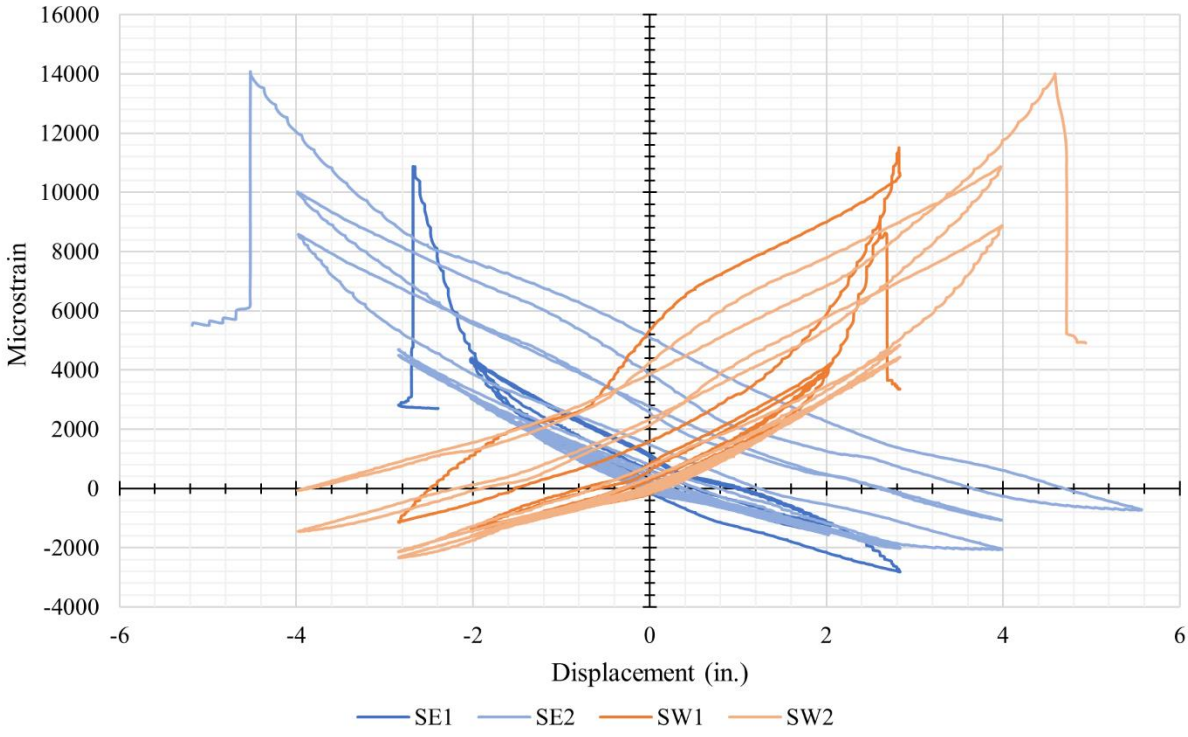

Figure 7-17: UHPC 2 Extreme Fiber Strain Gauges vs. Displacement at Column Head

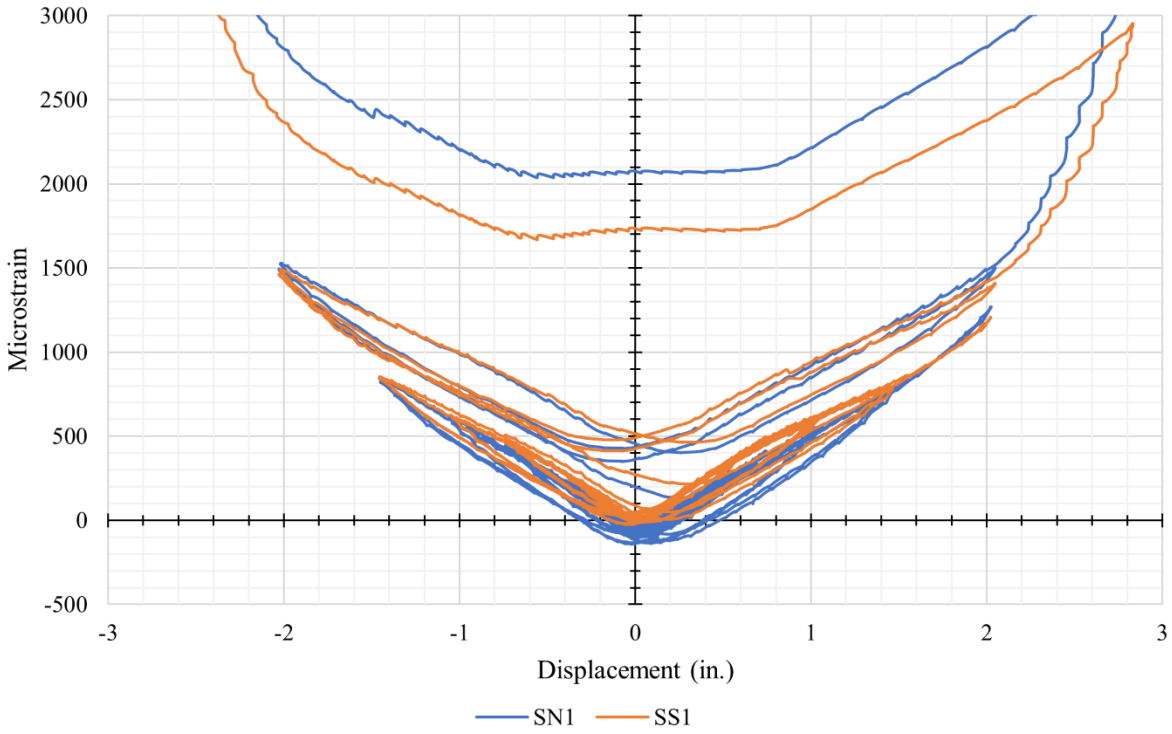

Figure 7-18: UHPC 2 Neutral Axis Steel Strain Gauges vs. Displacement at Column Head

The steel tube strain gauge plots also corroborated observations from the load versus displacement plot. The transition from elastic to inelastic behavior was observed at a displacement of approximately 1 inch, after which plastic deformations were observed, as shown in Figure 7-19 and Figure 7-20. A significant change in the measured strains due to stiffness softening was observed beyond a displacement of approximately 2 inches. Prominent plastic deformation was shown by residual strain at zero displacement. Further plastic deformation was observed at and beyond the 2.97-inch displacement interval. Strain gauge data was not obtained beyond a displacement of approximately 4 inches, likely due to significant damage to the column specimen from the steel tube yielding and buckling while the concrete core remained intact, with the lower gauges failing first.

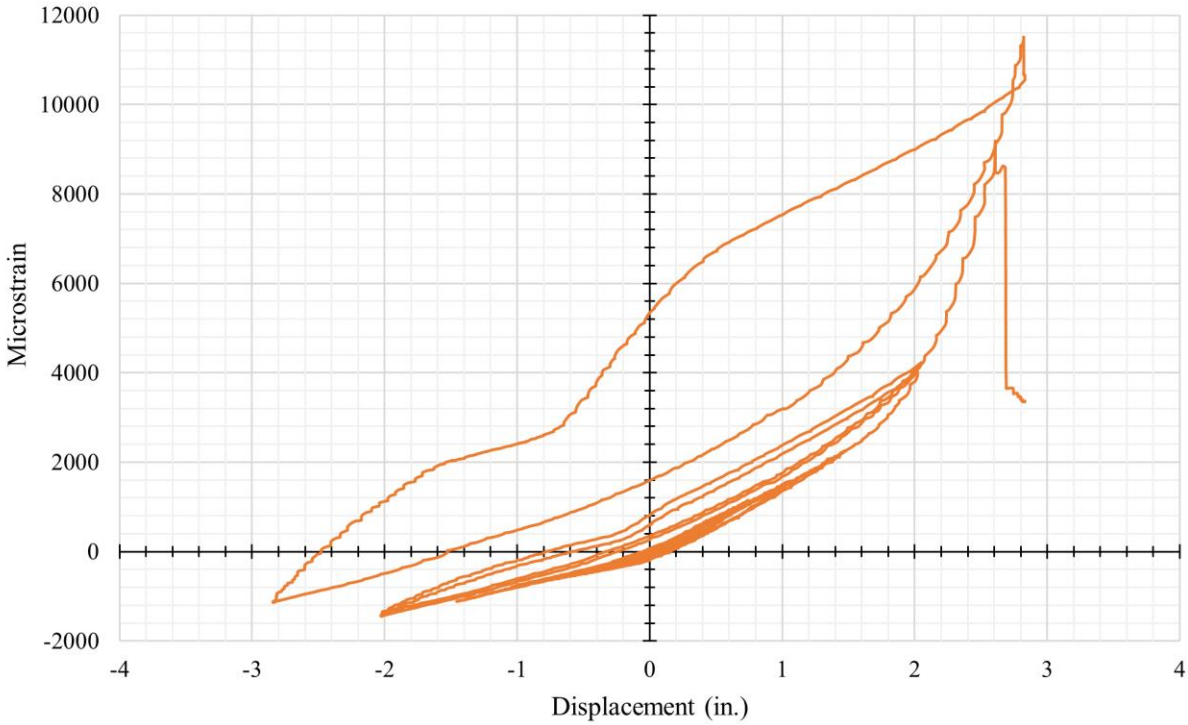

Figure 7-19: UHPC 2 SW1 Steel Strain Gauge vs. Displacement at Column Head

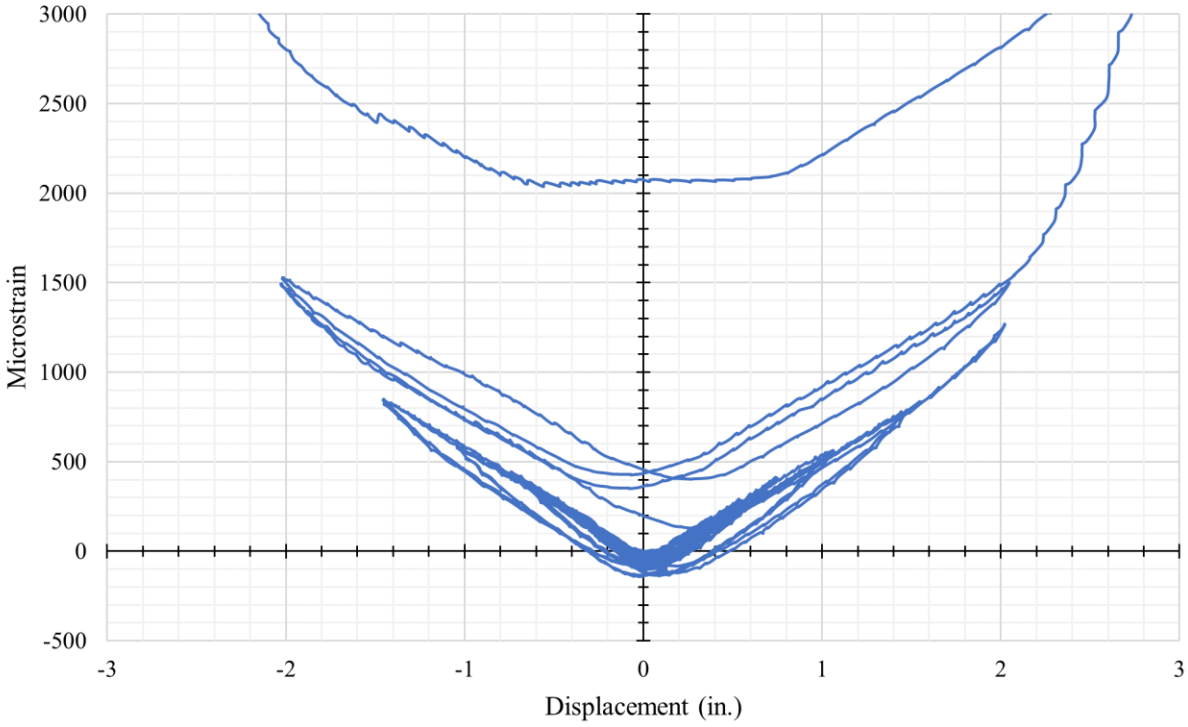

Figure 7-20: UHPC 2 SN1 Steel Strain Gauge vs. Displacement at Column Head

7.2.3 Analysis of GFRP Tube Strain Gauge Plots

Figure 7-21 depicts the lower level of strain gauges on the GFRP tube at the extreme fibers of the column. The strain gauges on the GFRP tube were oriented parallel to the base, along the circumference of the column. Strain gauges at similar locations and levels on the GFRP tube exhibited moderate symmetry at similar displacements. In general, gauges higher up the column, or farther from the top of the column base, exhibited lower strains, as shown in Figure 7-22. The GFRP tube confined the concrete core and was compressed into the concrete base at larger deflections, therefore, only tensile hoop strains were measured due to the orientation and placement of the strain gauges. A notable transition in the plot was observed at a displacement of approximately 6 inches, as shown in Figure 7-23, and emphasized with the addition of two straight line segments. The strain gauge plot was approximately linear leading up to and after the transition in the graph, with a steeper approximately linear slope after the transition. The transition occurred at approximately the same displacement as the sustained load began to plateau, therefore the transition was attributed to the concrete core crushing and applying increased pressure to the GFRP tube.

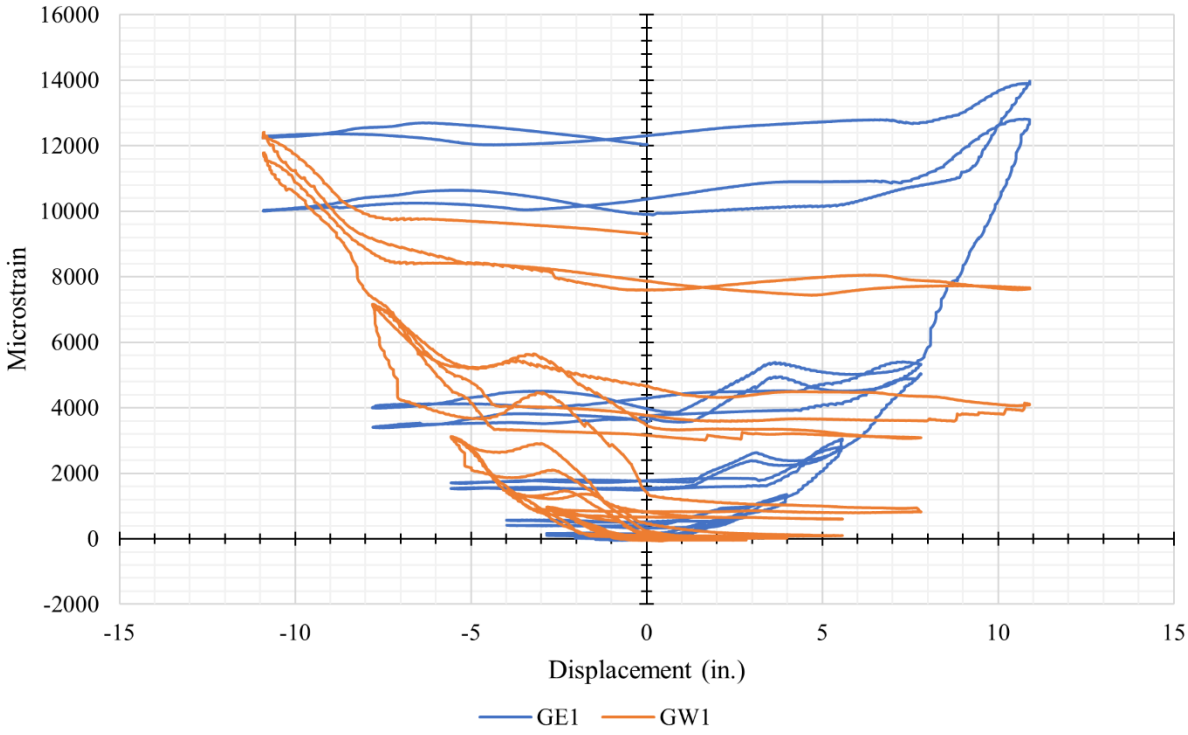

Figure 7-21: UHPC 2 Lower GFRP Strain Gauges vs. Displacement at Column Head

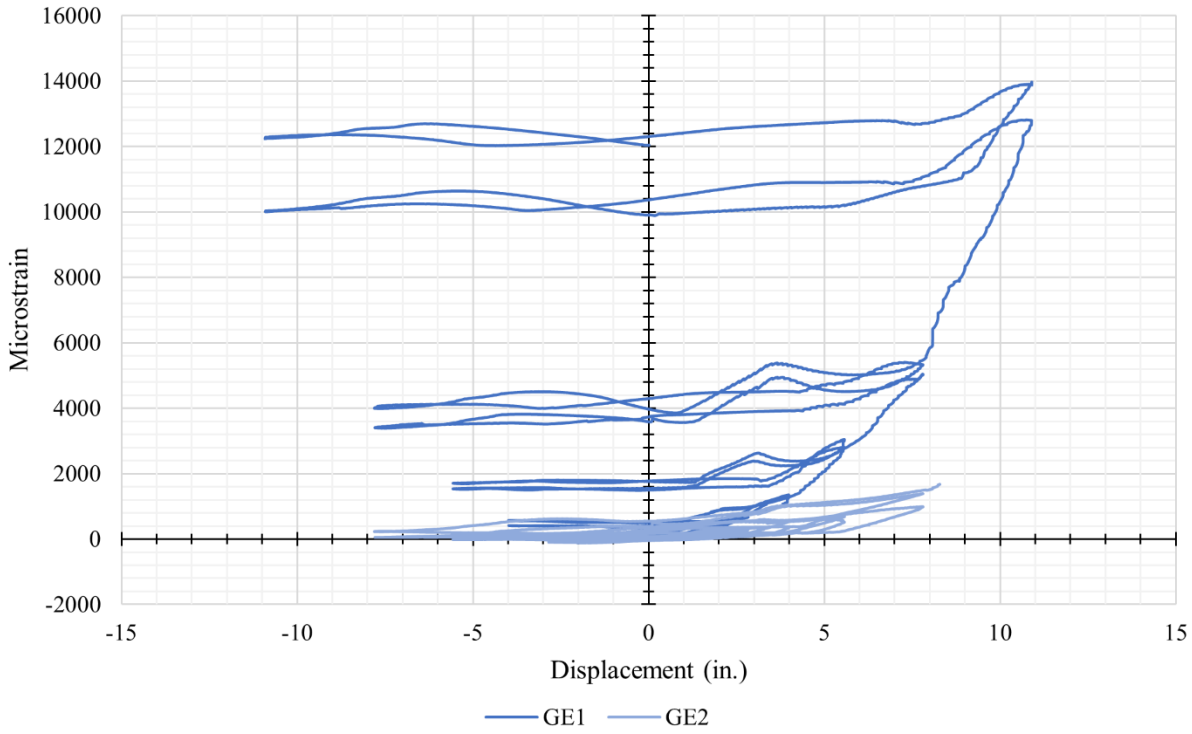

Figure 7-22: UHPC 2 East Side GFRP Strain Gauges vs. Displacement at Column Head

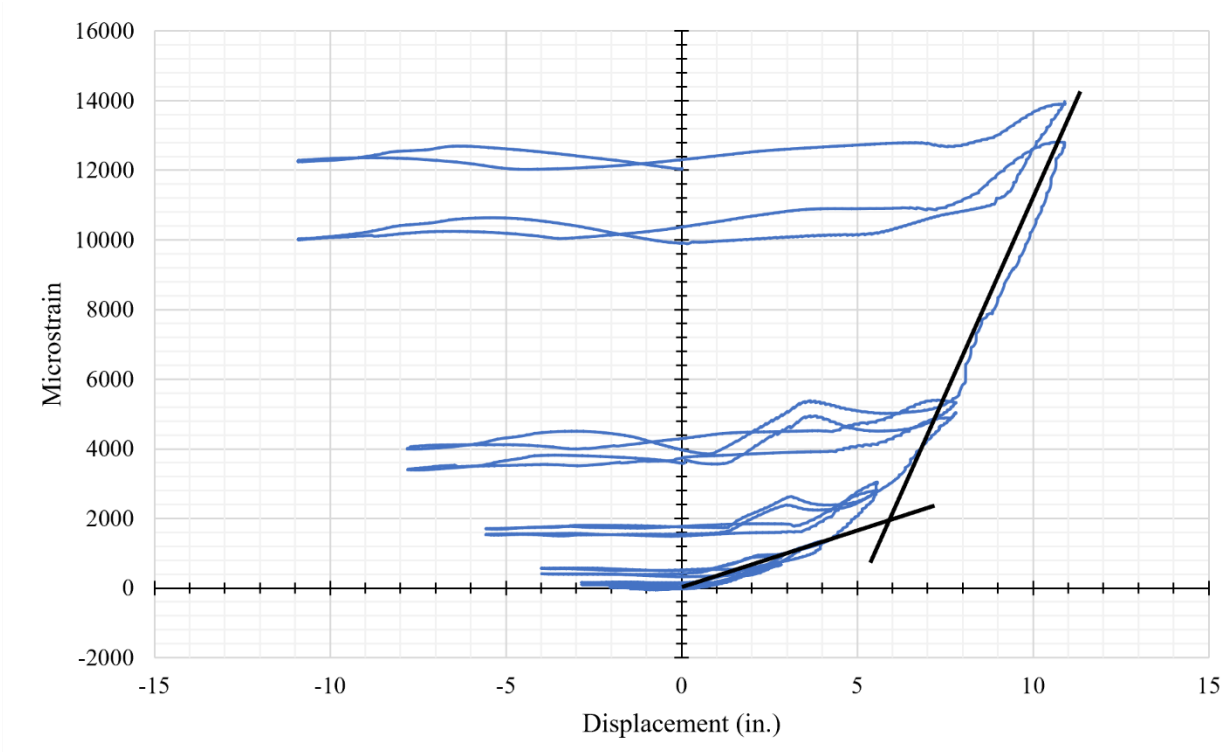

Figure 7-23: Determining UHPC 2 GFRP Strain Transition Using GE1 GFRP Strain Gauge vs. Displacement at Column Head

7.2.4 Analysis of Column Specimen Damage After Testing

The damage to the column specimen was assumed to extend from the concrete base to past half of the column height. The most severe damage to the column was observed to extend approximately 6 inches from the top of the base. Minimal damage to the GFRP tube was observed at smaller displacements during testing and was predominantly damaged at larger displacements as the tube was compressed into the concrete base. This aligned with observations made from the GFRP strain gauge plots. The GFRP tube was damaged approximately 1 to 1.5 inches from the top of the base and typically failed along the orientation of the fibers, as shown in Figure 7-24.

The area of the crushed concrete at the bottom of the concrete core was roughly triangular with the most severe damage along the extreme fiber, as shown in Figure 7-25. The cracking along the bottom of the concrete core converged at approximately 16 inches from the top of the concrete base, as shown in Figure 7-26. After the cracking converged, a longitudinal crack was observed to extend along each extreme fiber, past half the height of the column, as shown in Figure 7-27 and Figure 7-28. Due to the presence of steel fibers, the crushed concrete was removed by jackhammering to reveal the shape of the crushed region below. The concrete core was crushed in a conical shape, as shown by the lighter-colored powder in Figure 7-29. The lower approximately 3 inches nearest to the column base was reduced to rubble and held together by the steel fibers. This indicated that the concrete core was sufficiently confined by some combination of the steel tube, embedded steel fibers, and GFRP tube. Normal fiber distribution was observed while the concrete core was deconstructed. A void was discovered underneath the concrete core at the buckled region of the steel tube that was created by the steel tube buckling inward, away from the concrete core, as shown by the shadows in Figure 7-30. The concrete core was no longer bonded to the steel tube after testing and, once the concrete was separated from itself, was easily removed. During the concrete removal process, the cross-section of the concrete core was revealed and the longitudinal crack along the extreme fiber on either side of the column was observed to penetrate the full depth of the thickness of the concrete core, as shown in Figure 7-31.

The steel tube was observed to have buckled at the extreme axis with two diagonal compressed folds, or creases, parallel to the column base that converged below the extreme fiber

and a depressed region along the extreme fiber, as shown in Figure 7-32. The creases exhibited tears in the steel where the steel tube had begun to fracture during testing. Furthermore, a tear in the steel tube was also observed in the depressed region on the east side of the column. The observed tears indicated that the steel tube would have likely fractured from fatigue with additional cycles or increased displacement. Despite the damage, the steel tube remained intact, and the column was still capable of sustaining the applied constant axial compressive load.

Figure 7-24: UHPC 2 GFRP Tube West Side (l) and East Side (r) Damage After Testing

Figure 7-25: UHPC 2 Concrete Core West Side (l) and East Side (r) Damage After Testing

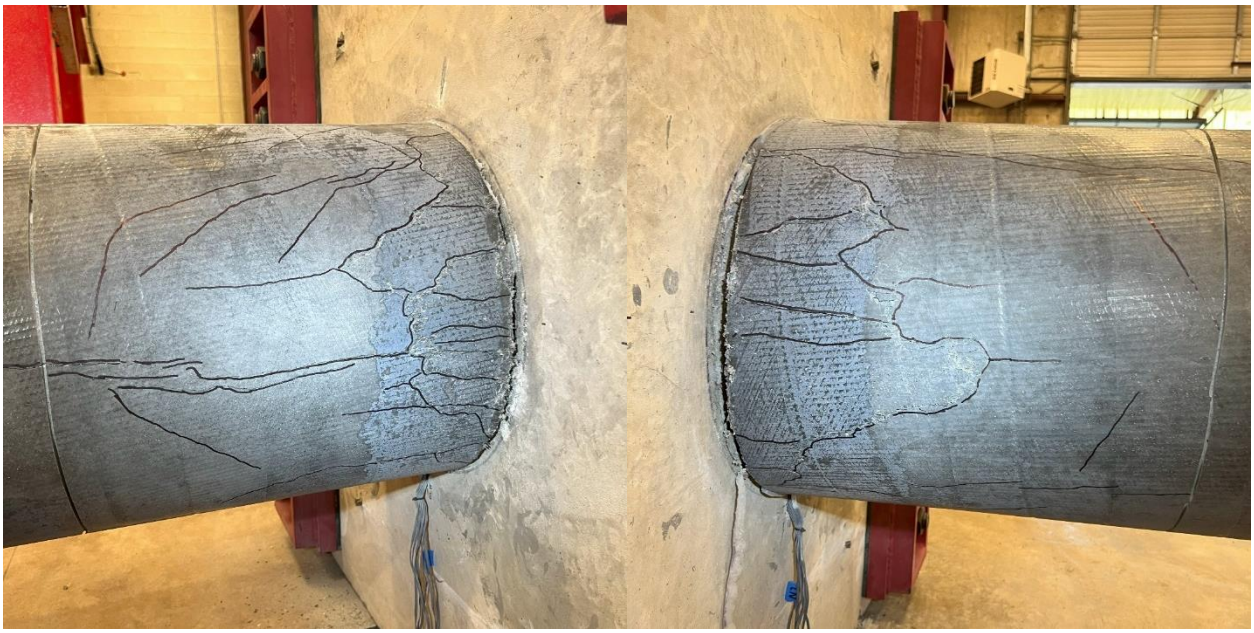

Figure 7-26: UHPC 2 Concrete Core West Side (l) and East Side (r) Crack Mapping

Figure 7-27: UHPC 2 Concrete Core West Side Cracking Along Column Height

Figure 7-28: UHPC 2 Concrete Core East Side Cracking Along Column Height

Figure 7-29: UHPC 2 Concrete Core After Testing and Light Concrete Removal

Figure 7-30: UHPC 2 Concrete Core After Testing and Significant Concrete Removal

Figure 7-31: UHPC 2 Concrete Core West (l) and East (r) Full-Depth Longitudinal Crack

The concrete base was observed to provide adequate flexural and shear capacity with spalling and minor damage at the interface with the column testing frame and lateral clamping mechanisms. During testing, a gap formed at the interface between the column and the base. This was indicative of the concrete core and GFRP tube sliding along the steel tube after the bond between the concrete core and the steel tube was broken. However, the steel tube was not

observed to have been pulled out of the column base, therefore the embedment depth and supplemental anchorage were effective. Furthermore, each corner of the column base rotated an average maximum of approximately 0.16 inches. The mounting location for measuring the displacement of the southwest corner of the concrete base was damaged during testing likely resulting in a slightly higher average maximum rotation. The rotation would cause a proportional effect on the measured displacement at the column head, reducing the measured displacement. The displacement data was not corrected for this effect.

Figure 7-32: UHPC 2 Steel Tube West (l) and East Side (r) Damage After Testing

7.3 Comparison of UHPC HC-FCS Column Testing Results

The UHPC HC-FCS column specimens were identical in design and construction and performed likewise during testing. Both column specimens exhibited linear elastic behavior before transitioning into inelastic behavior beyond a certain load and deflection. Additionally, both columns performed similarly during testing including a gap observed at the column and base interface at larger deflections, the steel tube yielded and buckled, the concrete core crushed, and the GFRP tube ruptured.

7.3.1 Comparison of Load versus Displacement Plots

The peak moment capacity and corresponding displacement of UHPC 1 and UHPC 2 were 413 kip-ft at 7.8 inches and 408 kip-ft at 7.6 inches, respectively. The variation between the

determined peak moments and displacements was approximately 1% and 3%, respectively. The peak moment capacity for both specimens occurred during the extension cycle. The observed peak loads at each cycle of each specimen were highly similar between the extension and retraction cycles, as shown in Figure 7-33.

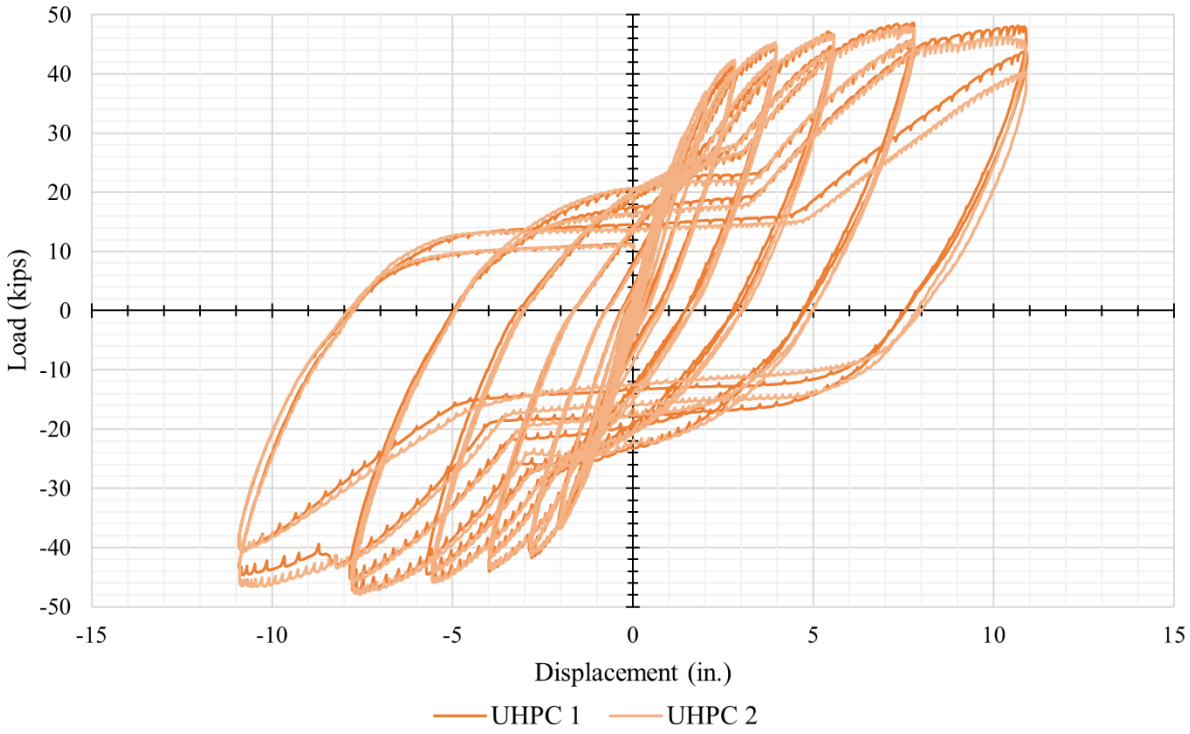

Figure 7-33: Comparing UHPC HC-FCS Lateral Load vs. Displacement at Column Head

Both columns demonstrated linear elastic behavior until a displacement of approximately 1 inch. Additionally, both columns exhibited similar stiffness degradation after a displacement of approximately 2 inches, followed by moderate stiffness softening at a displacement of approximately 3 inches, and significant stiffness softening was observed at a displacement of approximately 4 inches. Both columns experienced increasingly significant stiffness softening beyond a displacement of 4 inches and exhibited a similar gradual increase in capacity until beginning to plateau approaching a displacement of approximately 8 inches. Furthermore, both columns demonstrated comparable behavior during testing, including the path of each subsequent cycle, the presence, and occurrence of upturns in the measured load, and minimal discontinuities caused by crushing of the concrete core. Lastly, both UHPC 1 and 2 were not

considered to have failed due to the lack of a significant reduction in capacity during and after the second 10.89-inch displacement interval.

7.3.2 Comparison of Steel Tube and GFRP Tube Strain Gauge Plots

Figure 7-34 compares strain gauges on the steel tube at the extreme fibers of the column for the UHPC 1 and UHPC 2 specimens. The shape of both plots was consistent with both resembling loops. Figure 7-35 compares strain gauges on the steel tube at the neutral axis of the column for the UHPC 1 and 2 specimens and depicts similar behavior. Both plots resembled a "V" shape that indicated similar neutral axis migration during testing. The steel tube strain gauge data obtained from both specimens validated observations from the load versus displacement plots and supported the observed transition and stiffness softening displacements. Figure 7-36 compares strain gauges on the GFRP tube at the extreme fibers of the column for the UHPC 1 and UHPC 2 specimens. The shape of both plots was consistent with both exhibiting only tensile hoop strains and a similar transition at a displacement of approximately 6 inches.

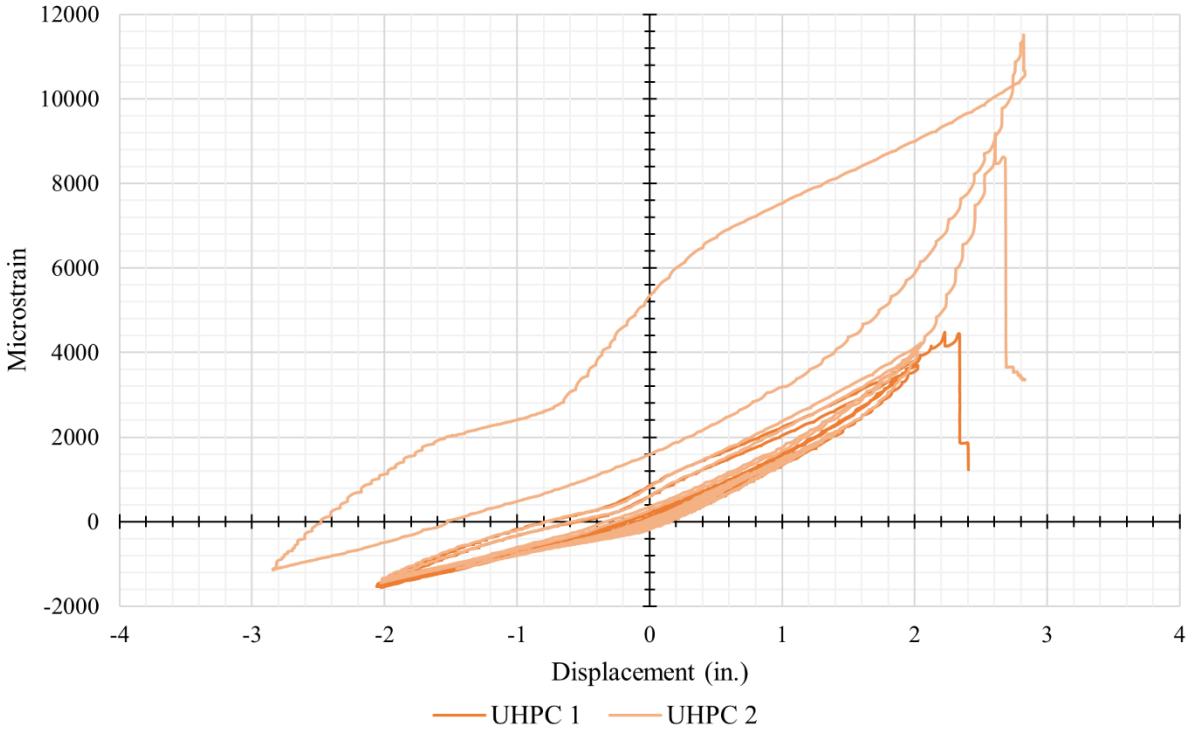

Figure 7-34: Comparing UHPC SW1 Strain Gauge vs. Displacement at Column Head

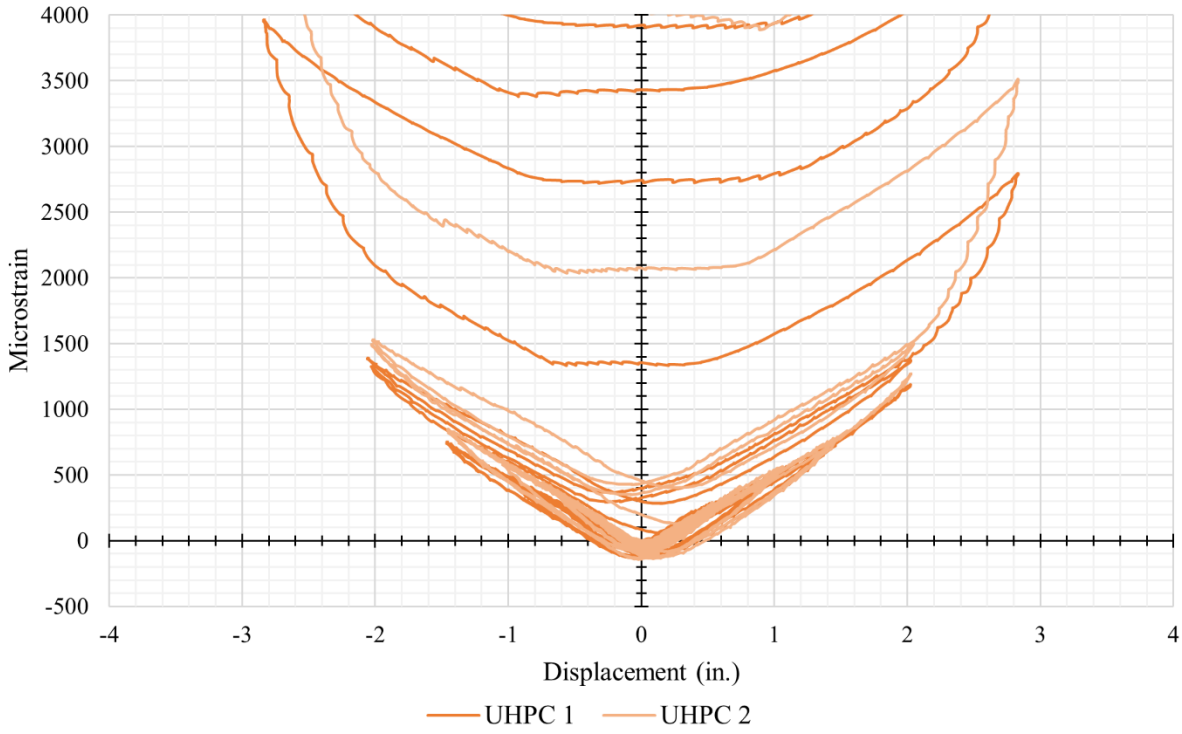

Figure 7-35: Comparing UHPC SN1 Strain Gauge vs. Displacement at Column Head

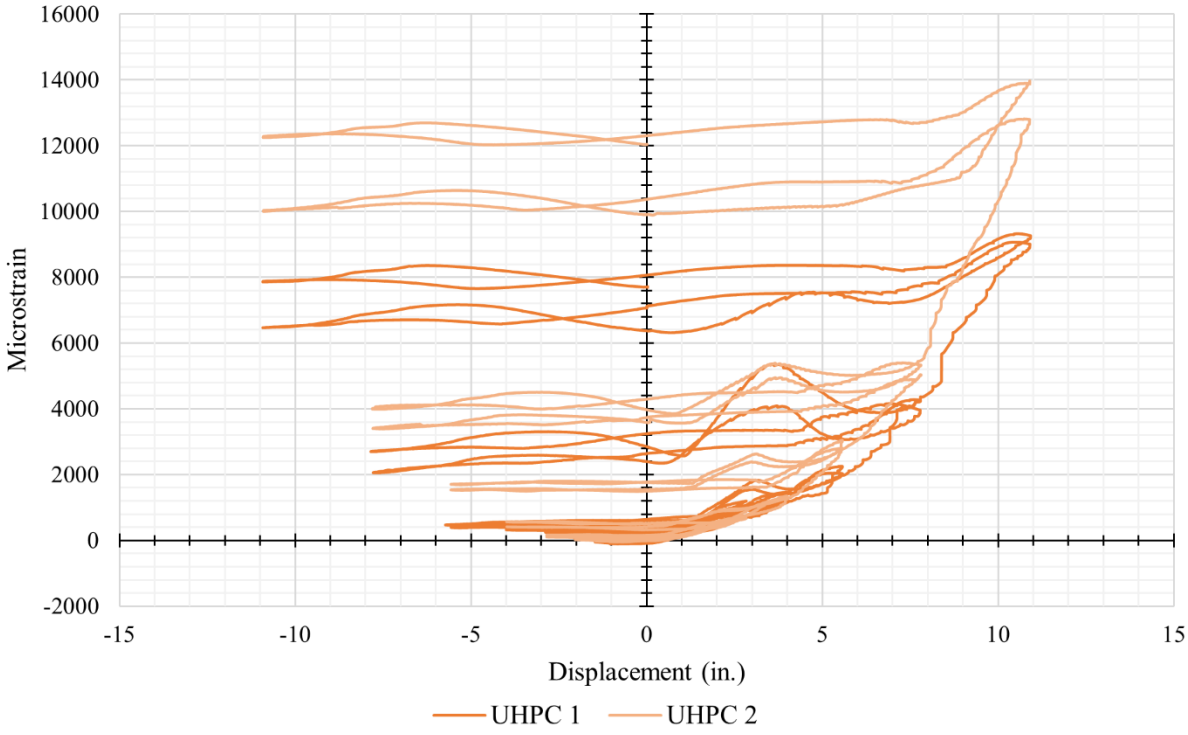

Figure 7-36: Comparing UHPC GE1 Strain Gauges vs. Displacement at Column Head

An offset was observed between similar strain gauge plots. This was likely due to inherent minor variations in material properties that were exacerbated as the column specimens were significantly damaged. However, gauges at the same positions on each column produced highly similar shapes and therefore validated the offset data. Due to the consistency of the plots and more intact strain gauge data, UHPC 2 was selected to serve as the representative UHPC HC-FCS column specimen for comparing the performance of different column types.

7.3.3 Comparison of Column Specimen Damage After Testing

The damage to each column specimen extended to approximately the same distance from the concrete base with the most severe damage for both observed approximately 6 inches from the top of the base. Both specimens suffered comparable damage to the GFRP tube, concrete core, and steel tube. In both cases, the GFRP sufficiently confined the concrete core and ruptured at larger displacements, the concrete core crushed and became powder nearest to the base with a conical failure, and the steel tube buckled in a consistent shape with fractures or tears in the steel tube along the diagonal creases. Figure 7-37 compares the damage to the GFRP tubes. Figure 7-38 and Figure 7-39 compare the damage to the concrete cores. Figure 7-40 compares the damage to the steel tubes. Different steel fiber distributions were observed at and near the bottom of the concrete core due to the different flows obtained at casting. However, both column specimens were observed to have comparable flexural capacities and overall performance, therefore the steel fiber distribution was concluded to not have a significant impact. Lastly, both columns were capable of sustaining the applied constant axial compressive load after testing.

Both concrete bases performed consistently with minimal damage. Both specimens exhibited a gap at the interface between the column and the base during testing, but neither steel tube was observed to have pulled out of the column base. The corner of each column base rotated an average maximum of approximately 0.15 inches for UHPC 1 and 0.16 inches for UHPC 2. Despite the damage sustained during testing by the mounting location for measuring the displacement of the southwest corner of the concrete base for UHPC 2, the average maximum base rotation of each column only differed by approximately 7%. The comparative maximum base rotation indicates that the maximum base rotation likely occurred at the point of maximum column stiffness that was similar for both column specimens.

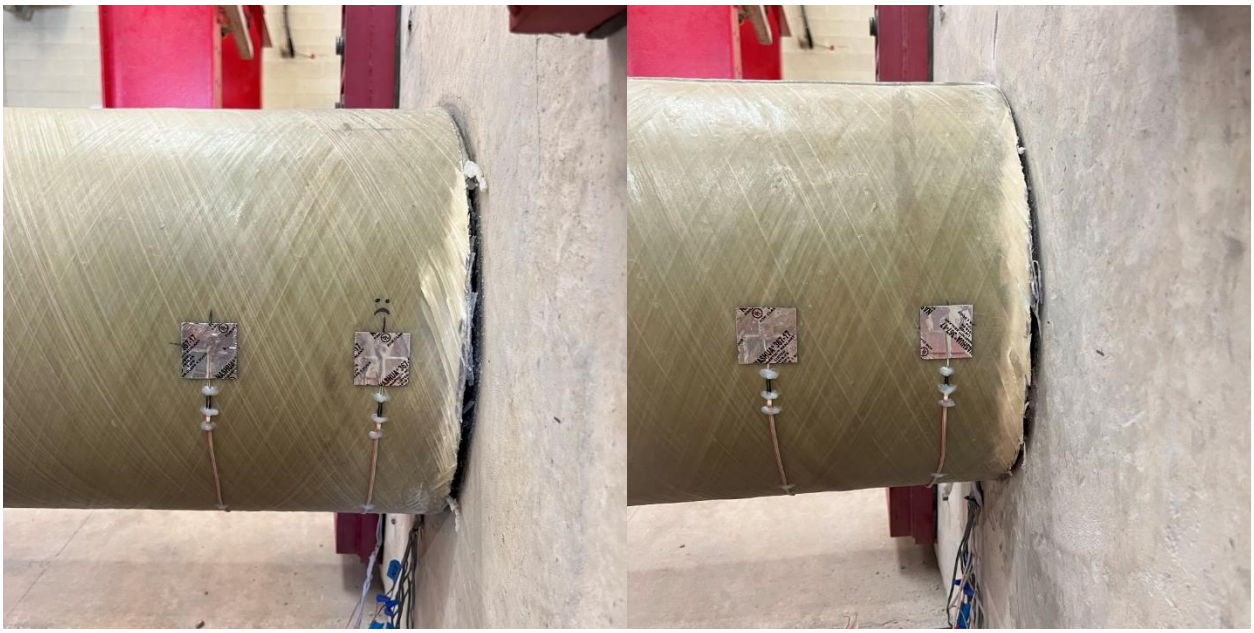

Figure 7-37: Comparing UHPC 1 (l) and UHPC 2 (r) GFRP Tube Damage After Testing

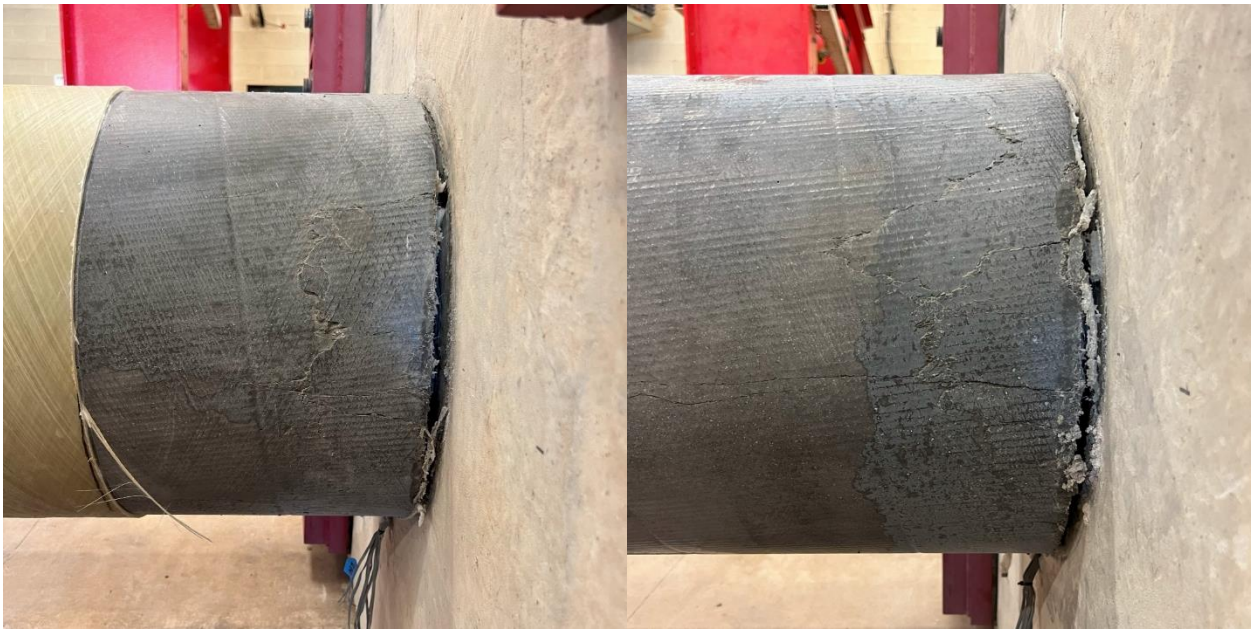

Figure 7-38: Comparing UHPC 1 (l) and UHPC 2 (r) Concrete Core After Testing

Figure 7-39: Comparing UHPC 1 (l) and UHPC 2 (r) Concrete Core After Testing and Light Removal of Concrete

Figure 7-40: Comparing UHPC 1 (l) and UHPC 2 (r) Steel Tube Damage After Testing

Chapter 8: Comparative Analysis of Column Specimen Types

The RC and HC-FCS column specimens were constructed similarly with the RC column requiring additional time due to additional complexity. The HC-FCS columns used a smaller quantity of materials and therefore weighed less per foot than the RC specimen. The RC column specimen served as a baseline comparison for column performance and was compared to the performance of an HS-SCC HC-FCS column. Next, an HS-SCC and a UHPC HC-FCS column were compared to analyze the performance of the different concrete core materials.

8.1 Comparative Analysis of Column Specimen Construction

The RC and HC-FCS column specimens were constructed following the same procedure and utilizing similar techniques. The RC column specimen required additional time and techniques to construct due to the additional complexity. The hollow nature of HC-FCS columns resulted in less complexity and less weight-per-foot than the RC column specimen. The HC-FCS column designs required less quantity of material but utilized higher quality materials than the RC column design.

8.1.1 Comparison of Column Specimen Construction Procedures

The column specimens were constructed by first assembling the column base and applicable column steel reinforcement. Each column base was assembled in the same manner with identical base reinforcement cages. The spiral-tied steel reinforcement cage for the RC column required significantly more time to assemble compared to the preparation of the steel tube for the HC-FCS columns. Additionally, placing and leveling the spiral-tied steel reinforcement cage within the column base cage and formwork required additional time and increased complications than the same procedure with the steel tubes. This was due to the hooks at the bottom of the column reinforcement cage and the flexibility of the cage. The steel tube configuration used consisted only of additional internal anchorages and no external anchorages. However, larger column diameters and loads could require external anchorages on the steel tube that might produce complicated procedures for placing the tube within the reinforcement cage of the foundation. Furthermore, additional external vibration was required during the casting of the HC-FCS columns to fill the embedded region of the steel tube with concrete and consolidate it, as opposed to the reinforcement cage of the RC column. Lastly, preparing the formwork and

casting the column was similar between column types, however, the RC column required additional consolidation compared to the self-consolidating concretes used for the HC-FCS columns. The HC-FCS columns also did not require the final step of stripping the formwork that was used for the RC column.

8.1.2 Comparison of Column Specimen Weight-per-Foot

By design, HC-FCS columns weigh less per foot of column than traditional RC columns. Table 8-1 provides the weight-per-foot of each column type and depicts how the HC-FCS columns tested weighed approximately two-thirds of the RC column tested. Additionally, the weight reduction scales with the diameter of the column, such that the larger the diameter of the column, the greater the reduction in weight of an HC-FCS column when compared to an RC column of similar diameter. The HC-FCS columns utilized higher quality materials that would lead to increased costs when compared to traditional columns. However, the increased cost for the higher quality materials could be offset by the reduced construction time due to the reduced complexity of HC-FCS columns when compared to traditional columns. Furthermore, the higher quality materials used for HC-FCS columns are more durable than traditional RC column materials and would likely reduce the maintenance cost of the column over the life of the structure.

Table 8-1: Column Weight-per-Foot for RC and HC-FCS Column Specimens

Column Type	RC		HC-FCS			
			HS-SCC		UHPC	
Element	Quantity (unit/ft)	Weight (lb/ft)	Quantity (unit/ft)	Weight (lb/ft)	Quantity (unit/ft)	Weight (lb/ft)
Concrete (ft^3/ft)	1.75	253.4	0.93	134.8	0.93	139.5
Long. Reinf.	8 No. 6	12.0	--		--	
Spiral Reinf.	4 No. 4	11.5	--		--	
Steel Tube	--		1	33.4	1	33.4
GFRP Tube	--		1	10.2	1	10.2
Total (lb/ft)	277		178		183	
Normalized	100%		64%		66%	

8.1.3 Comparison of Concrete Compressive Strengths

Table 8-2 presents the average concrete compressive strength of each component for each column specimen. The RC column concrete strength was higher than the original target of 5000 psi, which was attributed to a lower air content than targeted. The HS-SCC and UHPC strengths met the original targets, and the HS-SCC was approximately half the compressive strength of the UHPC. However, the presence of the steel fibers in the UHPC inhibits a direct comparison of performance based on the compressive strength of the concretes. Furthermore, UHPC 1 demonstrated a higher flow than recommended during casting. Some fiber settling and nonideal fiber distribution were observed at and near the bottom of the column specimen. However, there was no significant difference in concrete compressive strength between UHPC 1 and 2 due to the steel fibers having a minimal overall effect on the concrete compressive strength.

Each column specimen was tested well beyond 28 days after casting the concrete base and column components. Due to this, a decrease in concrete compressive strength was observed for the concrete bases and the RC and HS-SCC columns. The concrete bases experienced a decrease of approximately 13% from the 28-day and test-day compressive strength. The decrease in strength over time was attributed to the dry curing conditions that led to shrinkage of the concrete in the bases and associated cylinders. The large volume of concrete in the column bases likely caused the bases to be unaffected by the curing conditions and shrinkage, and therefore retain a higher compressive strength. Despite the decrease in compressive strength, the concrete bases performed adequately with minimal spalling to minor damage and sufficiently restrained the columns with no steel reinforcement pullout observed for all specimens.

The RC and HS-SCC columns experienced a decrease of approximately 3% and 5%, respectively, from the 28-day to test-day compressive strength. The decrease in strength was attributed to minimal concrete shrinkage and the normal variation between concrete cylinder compressive tests. The UHPC columns experienced an increase of approximately 4% from the 28-day to test-day compressive strength. The UHPC was likely unaffected by curing conditions and concrete shrinkage with the concrete retaining moisture due to its high particle packing density and the steel fibers reducing concrete shrinkage. The increase in compressive strength was expected but could also be attributed to the normal variation between concrete cylinder compressive tests.

Each specimen was tested within 3 to 7 days of casting the column cap, except for HS-SCC 1, for which testing was concluded approximately two months after casting the column cap. Therefore, the test-day strengths were lower than the 28-day compressive strengths as expected. The column caps performed adequately with no observable damage.

Table 8-2: Average Concrete Compressive Strengths for Column Types and Components

Specimen		Base		Column		Cap	
Type	Label	Avg. f_c' at 28 Days (psi)	Avg. f_c at Test Day (psi)	Avg. f_c' at 28 Days (psi)	Avg. f_c at Test Day (psi)	Avg. f_c' at 28 Days (psi)	Avg. f_c at Test Day (psi)
RC		4,650	4,060	7,630	7,410	10,140	9,060
HC-FCS	HS-SCC			10,010	9,490		
	UHPC			19,450	20,280		

8.2 Comparative Analysis of RC and HC-FCS Column Testing Results

The RC column specimen served as a control specimen that validated the column testing frame, setup, and testing procedure, as well as serving as a baseline comparison for traditional, spiral-tied reinforced concrete column performance. HS-SCC 2 was selected to be the representative HS-SCC HC-FCS column specimen and served as the HC-FCS column comparison to the RC column specimen. Both column types demonstrated linear elastic behavior before transitioning into inelastic behavior beyond a certain load and deflection. During testing, each column type yielded and buckled the steel reinforcement, crushed the concrete core, and demonstrated adequate confinement of the concrete core.

8.2.1 Comparison of Load versus Displacement Plots

The peak moment capacity and corresponding displacement of the RC column and the HS-SCC 2 HC-FCS column were 249 kip-ft at 7.8 inches and 370 kip-ft at 5.2 inches, respectively. The peak moment of HS-SCC 2 was approximately 33% greater than that of the RC column. Both peak moment capacities occurred during the extension cycle, with the peak moment capacity of the HS-SCC 2 specimen occurring at approximately 33% less displacement. Both specimens exhibited symmetry between the extension and retraction cycles, as shown in

Figure 8-1, with the RC column retaining a higher degree of symmetry. Linear elastic behavior was observed until a displacement of approximately 1.5 inches for both column types. Both column types exhibited gradual stiffness degradation initially, with the RC column experiencing significant stiffness softening at a displacement of approximately 2 inches while the HS-SCC 2 specimen experienced significant stiffness softening at a displacement of approximately 4 inches. The initial loss of stiffness of both column types was attributed to the steel reinforcement yielding and the concrete core cracking.

The capacity of the RC column continued to gradually increase beyond a displacement of approximately 2 inches while the capacity of the HS-SCC 2 column gradually declined beyond a displacement of approximately 4 inches. The lateral load versus displacement at the column head plots of both column types were approximately bilinear. As the steel reinforcement of both column types began to yield and buckle, the load versus displacement plots began to plateau, with some stain hardening observed. Both column types demonstrated comparable behavior during testing including the path of each subsequent cycle, the presence, and occurrence of upturns in the measured load, and discontinuities caused by the fracturing of the steel reinforcement at larger displacements. The RC and HS-SCC 2 specimens were considered failed after observing a significant reduction in capacity during and after the 7.78-inch and 10.89-inch displacement interval, respectively.

The HS-SCC 2 HC-FCS column specimen demonstrated superior performance to that of the RC column specimen. HS-SCC 2 demonstrated higher ductility due to exhibiting a similar elastic behavior transition point while achieving a higher capacity at a larger displacement than the RC specimen. The capacity of the RC column continued to gradually increase, but approximately plateaued in capacity after the concrete core was crushed, whereas the HS-SCC 2 column lost capacity and plateaued after the concrete core was crushed. However, it is worth noting that the GFRP tube containing the crushed concrete core of the HS-SCC 2 specimen would likely be much more impactful at much higher axial compressive loads such as in-service conditions. The HS-SCC 2 specimen also demonstrated a higher ductility index due to sustaining a larger displacement when the steel reinforcement fractured given that both specimens yielded the steel reinforcement at approximately the same displacement. Both column types lost

approximately 14% of the respective peak moment capacities after the steel reinforcement fractured.

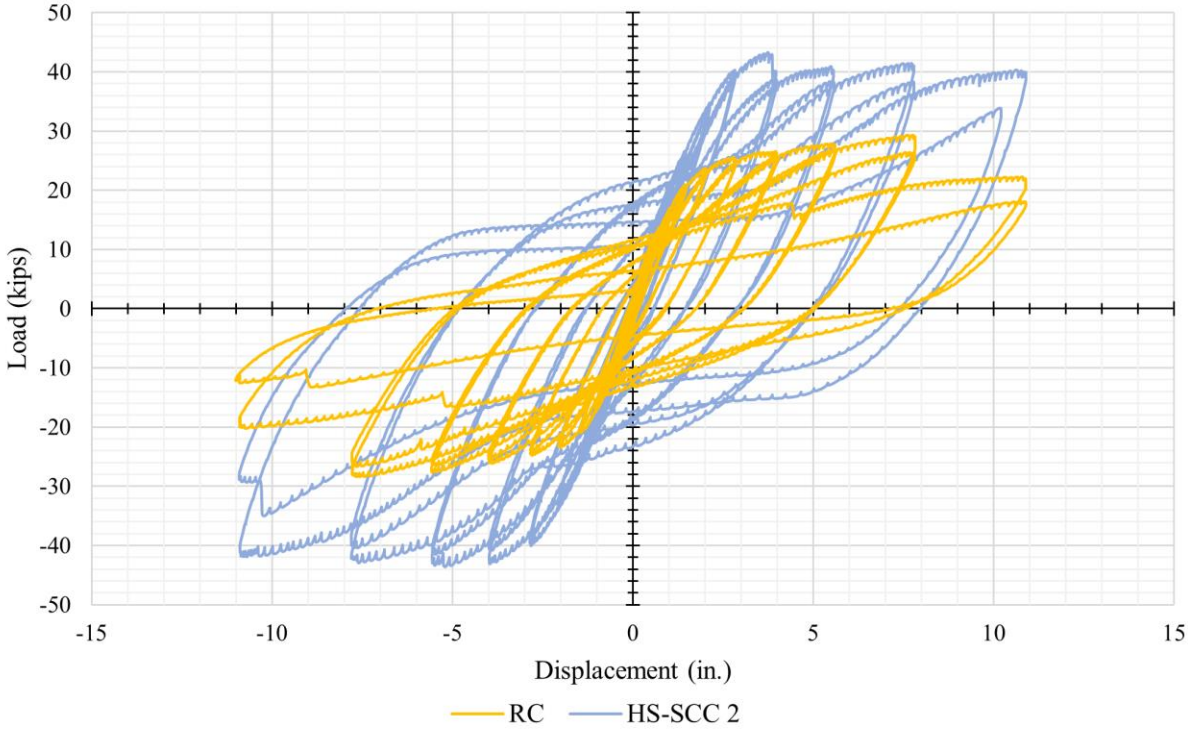

Figure 8-1: Comparing RC and HS-SCC 2 Lateral Load vs. Displacement at Column Head

8.2.2 Comparison of Steel Reinforcement Strain Gauge Plots

Figure 8-2 compares strain gauges on the steel reinforcement at the extreme fibers of the column for the RC and HS-SCC 2 specimens. The shape of both plots resembled loops with a steeper loop for the RC column plot. The steeper slope was due to the increased initial stiffness of the RC column. Due to the nature of the RC column, the strain gauges were subject to damage during testing and failed early at varying displacements, therefore limiting comparison beyond a displacement of approximately 1 inch.

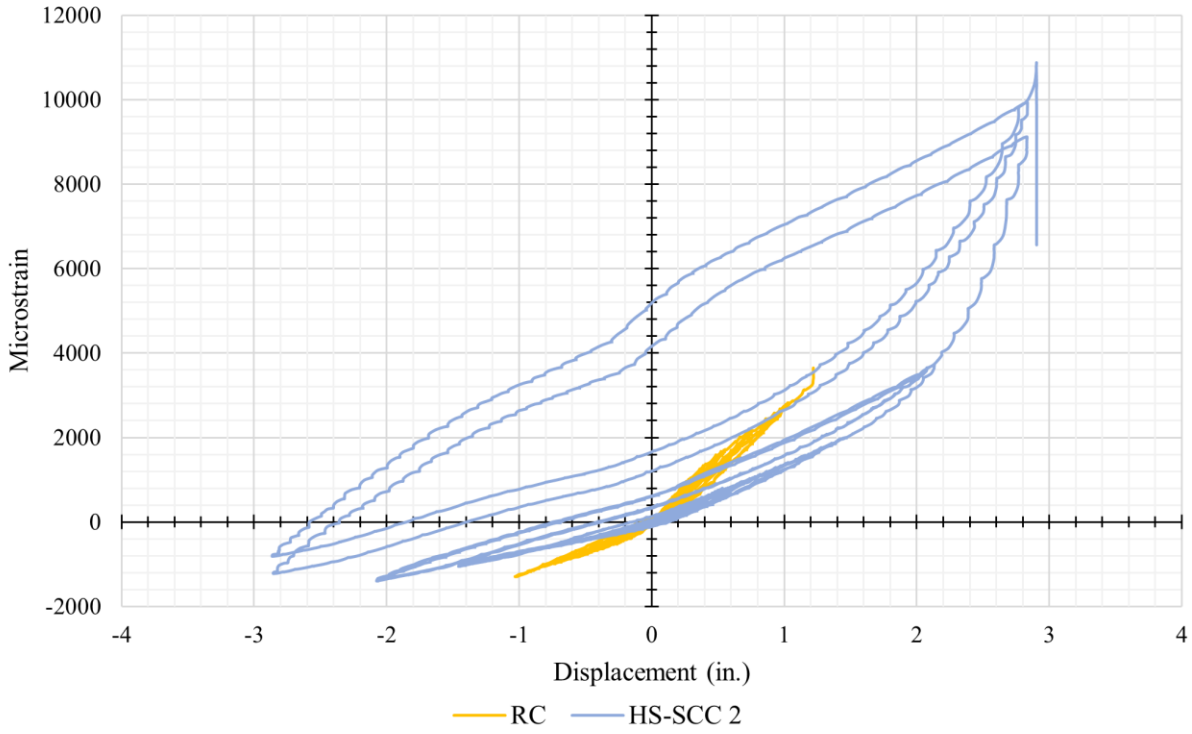

Figure 8-2: Comparing RC and HS-SCC 2 SW1 Steel Strain Gauge vs. Displacement at Column Head

Figure 8-3 compares strain gauges on the steel reinforcement at the neutral axis of the column for the RC and HS-SCC 2 specimens and depicts similar behavior. Both plots resembled a "V" shape that indicated similar neutral axis migration during testing. Similar to the extreme axis strain gauge plot, the plot of the RC column neutral axis strain gauges had a steeper slope due to the increased initial stiffness of the RC column. At a displacement of approximately 3 inches, the difference between the strain on the steel reinforcement decreased with the column types demonstrating comparable strains. This was due to the loss of stiffness of both columns as the respective steel reinforcements yielded and buckled. The steel reinforcement strain gauge data obtained from both specimens validated observations from the load versus displacement plots and supported the observed transition and stiffness softening displacements.

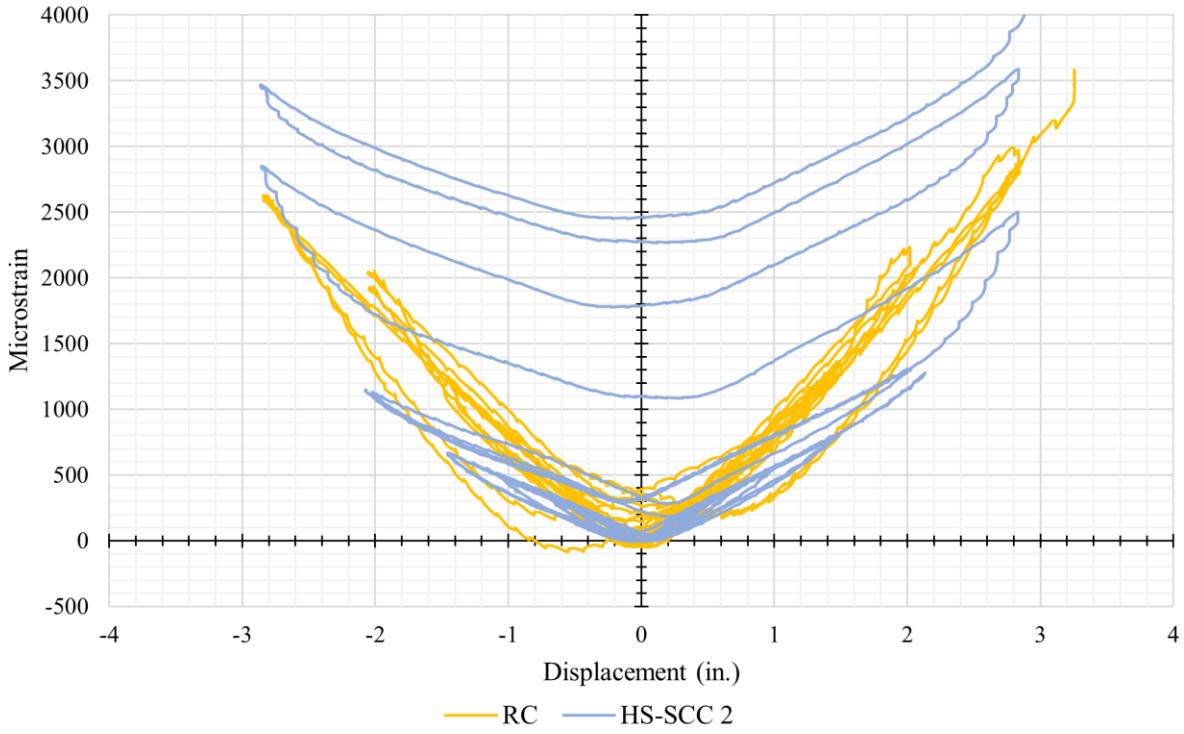

Figure 8-3: Comparing RC and HS-SCC 2 SN1 Steel Strain Gauge vs. Displacement at Column Head

8.2.3 Comparison of Column Specimen Damage After Testing

The damage to each column type extended to approximately the same distance from the concrete base along the column height, with the most severe damage observed approximately 9 inches from the top of the base for the RC column and approximately 12 inches from the top of the base for the HS-SCC 2 column. In both cases, the steel reinforcement yielded, the concrete core crushed and became powder nearest to the base with a conical failure, the steel reinforcement buckled and fractured along the extreme axis, and the concrete core was sufficiently confined by the respective confining element of that column type. Figure 8-4 compares the damage to the concrete core, and Figure 8-5 compares the damage to the steel reinforcement. Both column types similarly lost significant capacity as the concrete core crushed and subsequently buckled the steel reinforcement. After the significant loss of capacity, the RC column gradually increased in capacity before rupturing the steel reinforcement while the capacity of the HS-SCC 2 column plateaued, and the steel tube eventually fractured from fatigue.

The RC column specimen more clearly exhibited signs of distress before a significant loss of capacity and eventually column failure compared to the HC-FCS column specimen. The outer GFRP tube limited the ability to assess the HC-FCS column for damage and visible signs of distress. The GFRP tube itself was observed to show signs of distress, however, significant signs of distress did not occur until drastically large displacements, at which point the steel tube and concrete core were already severely damaged. However, both column types were observed to still be capable of sustaining the applied constant axial compressive load after the damage from testing.

Both concrete bases performed consistently with minimal damage. The steel reinforcement of either specimen was not observed to have pulled out of the column base. The corner of each column base rotated an average maximum of approximately 0.07 inches for the RC column and 0.15 inches for the HS-SCC 2 column. The average maximum base rotation of HS-SCC 2 was approximately twice that of the RC column. This was likely due to the maximum base rotation for both column types occurring at the point of maximum column stiffness, which was closely correlated with the peak moment capacity. The peak moment capacity of the HS-SCC 2 specimen was approximately 33% greater than that of the RC column.

Figure 8-4: Comparing RC (l) and HS-SCC 2 (r) Concrete Core After Testing and Light Removal of Concrete

Figure 8-5: Comparing RC (l) and HS-SCC 2 (r) Steel Reinforcement After Testing

8.3 Comparative Analysis of HS-SCC and UHPC HC-FCS Column Testing Results

The HS-SCC and UHPC HC-FCS column specimens were identical in design and construction while containing different concrete cores. The second specimen of each concrete type was selected to serve as the representative comparison column specimen for that concrete core type. Both column specimens exhibited linear elastic behavior before transitioning into inelastic behavior beyond a certain load and deflection. Additionally, both columns performed similarly during testing including a gap observed at the column and base interface at larger deflections, the steel tube yielded and buckled, the concrete core crushed, and the GFRP tube ruptured.

8.3.1 Comparison of Load versus Displacement Plots

The peak moment capacity and corresponding displacement of the HS-SCC 2 column and the UHPC 2 column were 370 kip-ft at 5.2 inches and 408 kip-ft at 7.6 inches, respectively. The peak moment of UHPC 2 was approximately 10% greater than that of HS-SCC 2. Both peak moment capacities occurred during the extension cycle, with the peak moment capacity of the UHPC 2 specimen occurring at approximately 46% more displacement. Both specimens exhibited symmetry between the extension and retraction cycles, as shown in Figure 8-6, with the UHPC 2 column retaining a higher degree of symmetry. Linear elastic behavior was observed

until a displacement of approximately 1.5 inches for HS-SCC 2 and 1 inch for UHPC 2. Both specimens exhibited gradual stiffness degradation initially and significant stiffness softening at a displacement of approximately 4 inches. The initial loss of stiffness of both column types was attributed to the steel reinforcement yielding and the concrete core cracking.

The capacity of the HS-SCC 2 column gradually declined while the capacity of the UHPC 2 column continued to gradually increase beyond a displacement of approximately 4 inches. The lateral load versus displacement at the column head plot of the HS-SCC 2 specimen was approximately bilinear while the plot of the UHPC 2 specimen was approximately trilinear. The loss of capacity of the HS-SCC 2 column was attributed to the concrete core crushing and the steel tube buckling due to the loss of confinement from the concrete core. The gradual increase in capacity of the UHPC 2 column after the same displacement was attributed to the concrete core remaining intact and continuing to support the column, despite the yielded and buckled steel tube. As the steel tube of both column specimens continued to yield and buckle, the load versus displacement plots began to plateau, with some stain hardening observed. Both column types demonstrated comparable behavior during testing including the path of each subsequent cycle, the presence, and occurrence of upturns in the measured load, and discontinuities caused by the fracturing of the steel tube or rupturing of the GFRP at larger displacements. The HS-SCC 2 specimen was considered to have failed after observing a significant reduction in capacity during and after the 10.89-inch displacement interval. The UHPC 2 specimen was not considered to have failed due to the lack of a significant reduction in capacity during and after the second 10.89-inch displacement interval.

The representative UHPC HC-FCS column specimen demonstrated superior performance to that of the representative HS-SCC HC-FCS column specimen. UHPC 2 demonstrated higher ductility due to exhibiting an approximately similar elastic behavior transition point while achieving a higher capacity at a larger displacement than the HS-SCC 2 specimen. The UHPC 2 column continued to gradually increase in strength after experiencing significant stiffness softening because the concrete core remained intact, whereas the HS-SCC 2 column lost capacity and plateaued after the concrete core was crushed. The presence of steel fibers in the UHPC core increased the confinement and ductility of the concrete core, despite the loss of confinement from the buckled steel tube at larger displacements, and therefore increased the peak flexural

capacity and ductility of the column specimen. Furthermore, the intact concrete core of the UHPC 2 specimen led to sharper upturns in the sustained load compared to that of the HS-SCC 2 specimen as observed on the load versus displacement plot. The sharper upturns were caused by the intact fiber-reinforced concrete core providing additional capacity and stiffness as the concrete core was put into bearing against the top of the column base.

Although the UHPC 2 specimen was not observed to have fractured the steel tube during testing due to the limitations of the testing setup, the UHPC 2 specimen would have likely demonstrated a higher ductility index due to sustaining a larger displacement when the steel tube would have fractured given that both specimens yielded the steel reinforcement at approximately the same displacement. The HS-SCC 2 specimen lost approximately 14% of its peak moment capacity after the steel reinforcement fractured whereas the UHPC 2 specimen lost approximately 17% of its peak moment capacity after the concrete core finally crushed.

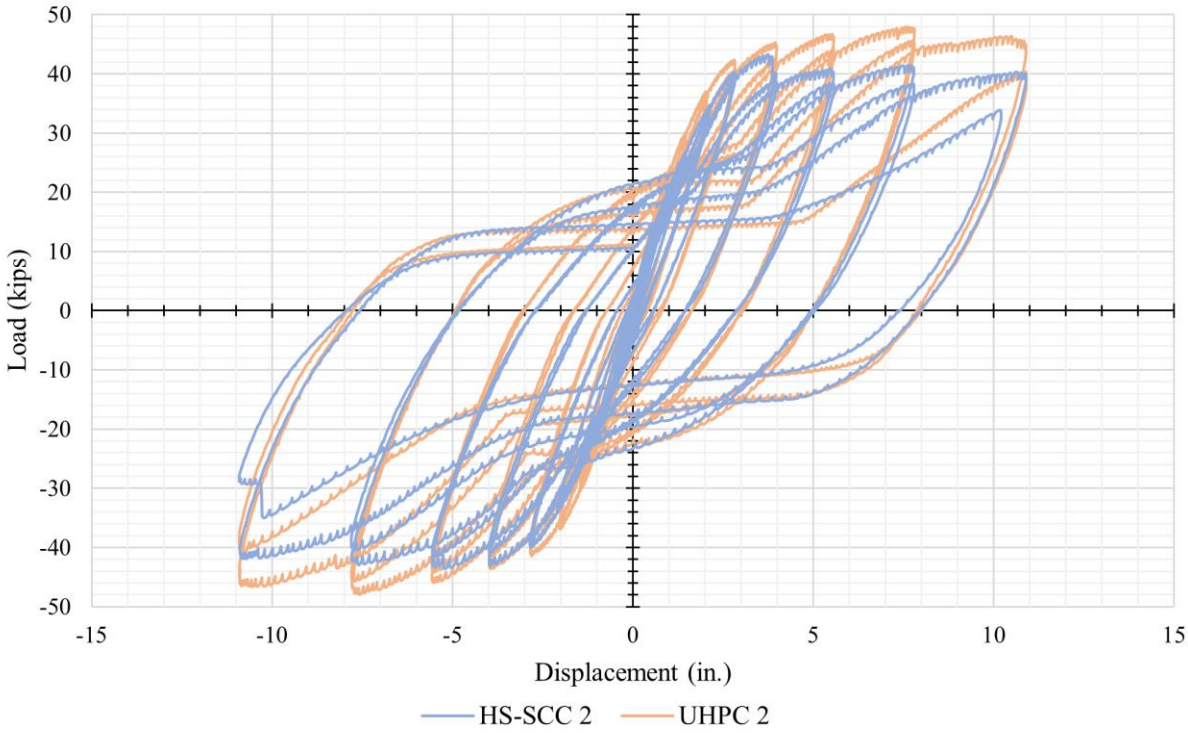

Figure 8-6: Comparing HS-SCC 2 and UHPC 2 Lateral Load vs. Displacement at Column Head

8.3.2 Comparison of Steel Tube Strain Gauge Plots

Figure 8-7 compares strain gauges on the steel tube at the extreme fibers of the column for the HS-SCC 2 and UHPC 2 specimens. The shape of both plots resembled loops with the plot of the UHPC 2 specimen exhibiting slightly higher strains at comparable displacements. The slightly higher strains were attributed to the increased initial stiffness of the UHPC 2 column provided by the UHPC core. Figure 8-8 compares strain gauges on the steel tube at the neutral axis of the column for the HS-SCC 2 and UHPC 2 specimens and depicts similar behavior. Both plots resembled a "V" shape that indicated similar neutral axis migration during testing. Similar to the extreme axis strain gauge plot, the plot of the UHPC 2 specimen neutral axis strain gauges exhibited higher strains than that of the HS-SCC 2 specimen at comparable displacements due to the increased initial stiffness of the UHPC 2 column.

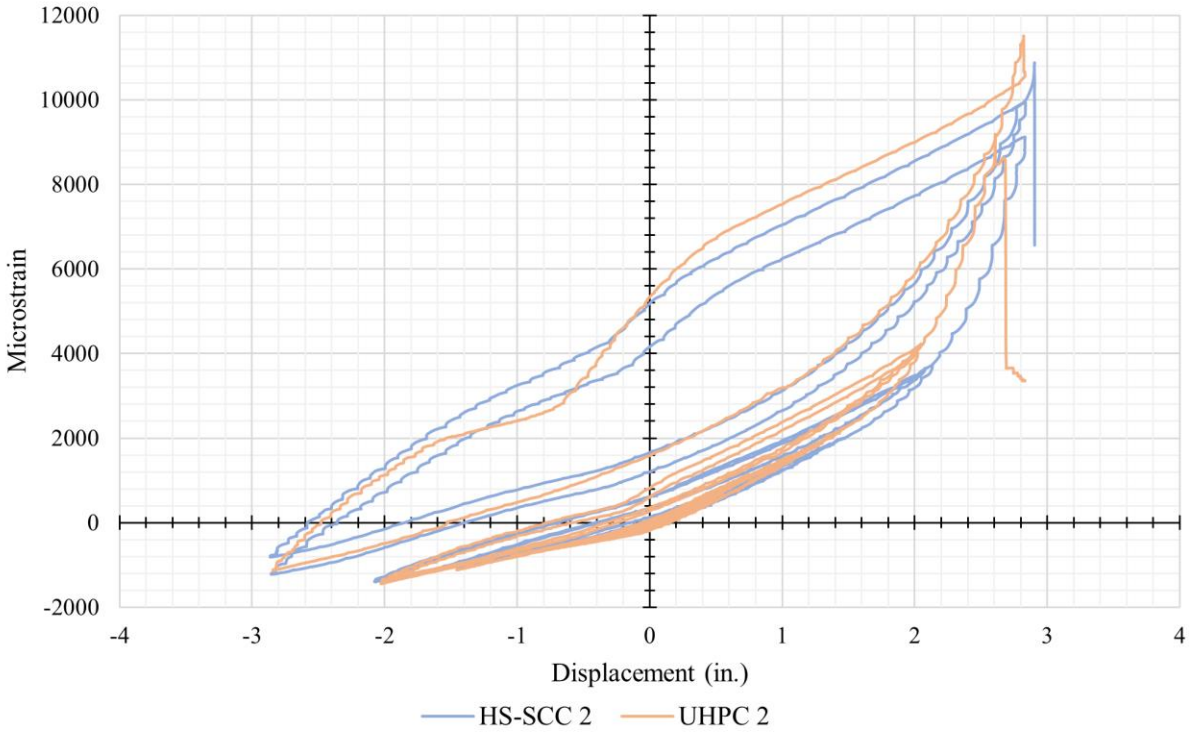

Figure 8-7: Comparing HS-SCC 2 and UHPC 2 SW1 Steel Strain Gauge vs. Displacement at Column Head

At a displacement of approximately 3 inches, the difference between the strain on the steel tube of each specimen greatly increased as the steel tube yielded and potentially began to buckle for the UHPC 2 specimen. This was likely due to the concrete core of the UHPC 2

specimen remaining intact and further yielding the steel tube, whereas the concrete core of the HS-SCC 2 specimen began to crush. The steel tube strain gauge data obtained from both specimens validated observations from the load versus displacement plots and supported the observed transition and stiffness softening displacements.

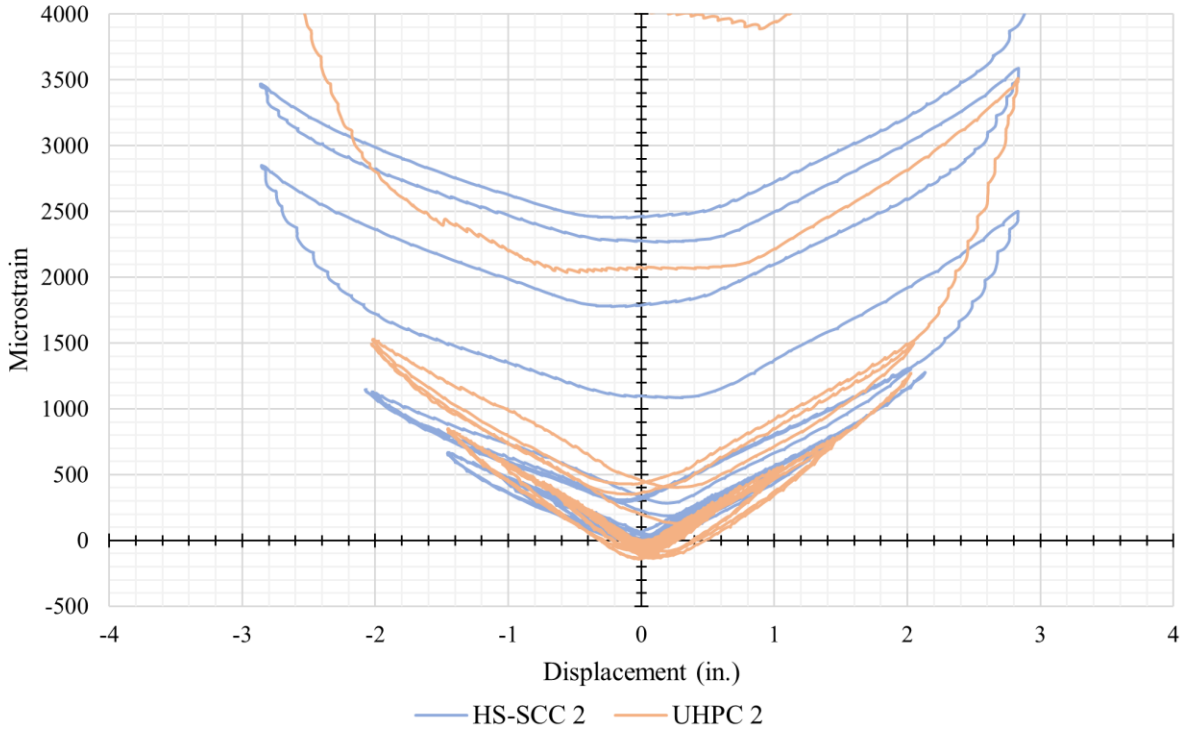

Figure 8-8: Comparing HS-SCC 2 and UHPC 2 SN1 Steel Strain Gauge vs. Displacement at Column Head

8.3.3 Comparison of GFRP Tube Strain Gauge Plots

Figure 8-9 compares strain gauges on the GFRP tube at the extreme fibers of the column for the HS-SCC 2 and UHPC 2 specimens. The shape of both plots was consistent with both exhibiting only tensile hoop strains and a transition point. The transition point for the HS-SCC 2 specimen was observed between a displacement of approximately 3 inches and 4 inches whereas the transition point for the UHPC 2 specimen was observed at a displacement of approximately 6 inches. The transitions occurred at approximately the same displacement as the sustained load began to plateau for each column specimen, and therefore were attributed to the displacement at which the concrete core crushed for each column specimen.

The GFRP tube sufficiently confined the concrete core of the HS-SCC 2 specimen such that the concrete reached its ultimate strain before crushing. The concrete core applied pressure to the GFRP tube leading up to and after crushing, as shown by the transition in the plot. The concrete core of the UHPC 2 specimen was confined more by the internal steel fibers of the UHPC than the GFRP tube, therefore the concrete core applied less pressure to the GFRP tube than the HS-SCC 2 specimen. The measured strains on the GFRP tube were notably lower for the UHPC 2 specimen until a displacement of approximately 8 inches, after which the crushed concrete core began applying additional pressure to the GFRP tube as the concrete core was further crushed and confined and restrained by the steel fibers.

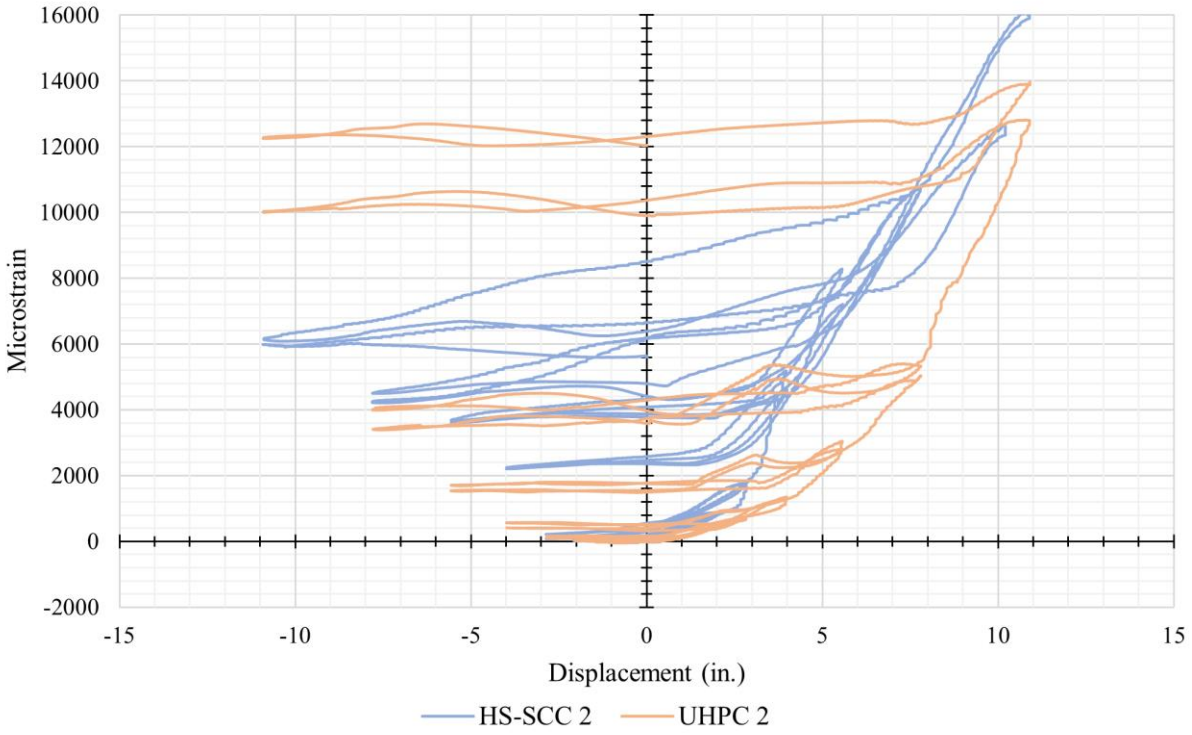

Figure 8-9: Comparing HS-SCC 2 and UHPC 2 GE1 GFRP Strain Gauge vs. Displacement at Column Head

8.3.4 Comparison of Column Specimen Damage After Testing

The damage to each specimen extended to approximately the same distance from the concrete base along the column height with the most severe damage observed approximately 12 inches from the top of the base for the HS-SCC 2 column and approximately 6 inches from the top of the base for the UHPC 2 column. Both specimens suffered comparable damage to the

GFRP tube, concrete core, and steel tube. In both cases, the GFRP sufficiently confined the concrete core and ruptured at larger displacements, the concrete core crushed and became powder nearest to the base with a conical failure, and the steel tube buckled with fractures or tears in the steel tube along the creases.

Figure 8-10 and Figure 8-11 compare the damage to the GFRP tube. The GFRP tube on the UHPC 2 specimen sustained less damage than that of the HS-SCC 2 specimen due to most of the damage being sustained at larger displacements once the concrete core was crushed. The difference in the observed damage also corroborates the assumed damage progression and obtained data from the GFRP strain gauges. The signs of distress of each column during testing and the resulting damage were obscured by the GFRP tube. The GFRP tube itself was observed to show signs of distress, however, significant signs of distress did not occur until drastically large displacements, at which the steel tube and concrete core were already severely damaged.

Figure 8-12 and Figure 8-13 compare the damage to the concrete core. Figure 8-14 and Figure 8-15 compare the damage to the steel tube. The increased ductility and confinement provided by the UHPC core localized the buckled region of the steel tube for the UHPC 2 specimen. This resulted in a different buckled shape of the steel tube between the concrete core types. The steel tube of the HS-SCC 2 column had a vertical crease and a depressed region on either side of the extreme axis whereas the steel tube of the UHPC 2 column had two diagonal creases that converged below the extreme fiber and a depressed region along the extreme fiber. Furthermore, the UHPC core reduced the damage from fatigue on the steel tube because the concrete core sustained much higher loads before crushing and continued to take load after crushing. This helped prevent the steel tube of the UHPC 2 specimen from enduring as much fatigue as the HS-SCC 2 specimen and limited the fracturing in the steel tube. Both column types were observed to still be capable of sustaining the applied constant axial compressive load after the damage from testing.

Both concrete bases performed consistently with minimal damage. Both specimens exhibited a gap at the interface between the column and the base during testing, but neither steel tube was observed to have pulled out of the column base. The corner of each column base rotated an average maximum of approximately 0.15 inches for the HS-SCC 2 column and 0.16 inches for the UHPC 2 column. The average maximum base rotation of each specimen was

approximately equal with the UHPC 2 specimen rotating approximately 7% more. This was likely due to the maximum base rotation for both column types occurring at the point of maximum column stiffness, which was closely correlated with the peak moment capacity. The peak moment capacity of the UHPC 2 specimen was approximately 10% greater than that of the HS-SCC 2 column.

Figure 8-10: Comparing HS-SCC 2 (l) and UHPC 2 (r) GFRP Tube West Side After Testing

Figure 8-11: Comparing HS-SCC 2 (l) and UHPC 2 (r) GFRP Tube East Side After Testing

Figure 8-12: Comparing HS-SCC 2 (l) and UHPC 2 (r) Concrete Core West Side After Testing and Light Removal of Concrete

Figure 8-13: Comparing HS-SCC 2 (l) and UHPC 2 (r) Concrete Core East Side After Testing and Light Removal of Concrete

Figure 8-14: Comparing HS-SCC 2 (l) and UHPC 2 (r) Steel Tube West Side After Testing

Figure 8-15: Comparing HS-SCC 2 (l) and UHPC 2 (r) Steel Tube East Side After Testing

Chapter 9: Findings, Conclusions, and Recommendations

The findings and conclusions of the research study that were discussed in previous chapters, and the recommendations for future research, are presented in this chapter. This includes the development of the column specimen testing frame and procedures, the design and construction of each column specimen and component, the testing and results of each column specimen, and the analysis and comparison of the testing results of each column specimen.

9.1 Overview of Research Study

The purpose of this study was to design, construct, and test half-scale hollow-core fiber-reinforced polymer tube-concrete core-steel tube (HC-FCS) column specimens with high-strength self-consolidating concrete (HS-SCC) and ultra-high-performance concrete (UHPC) used for the concrete cores of the specimens. A steel testing frame was developed and constructed that met the limitations of the facility and was capable of restraining and testing the column specimens to failure. The column specimens were constructed vertically and tested horizontally in the column testing frame. Additionally, a half-scale, traditional, spiral-tied reinforced concrete (RC) column was also constructed to validate the column specimen testing frame and serve as a baseline for column performance.

Each column specimen consisted of a reinforced concrete base, column section, and column cap. The concrete base provided a fixed-moment connection, restrained the column, and transferred the column loads to the testing frame. The column section was either the traditional RC control column or an HS-SCC or UHPC HC-FCS column specimen. The RC control column was designed following AASHTO and ACI guidelines and the ODOT Bridge Directives. The HC-FCS columns were designed based on recommendations from previous research studies. The column cap served as the mounting location for the lateral loading system and axial post-tensioning. The column base was constructed first, followed by the column section, and later the column cap. The base and column section were constructed vertically, while the column cap was constructed horizontally after the column was placed within the steel testing frame.

After the column specimen was secured to the testing frame, the column cap was added, and the lateral loading system was mounted. Each specimen was subject to a constant axial compressive load of approximately 5% of the axial capacity of the RC column that was applied

through post-tensioning along the height of the column. The lateral loading was displacement-controlled with each subsequent displacement increased by 40% after completing two cycles of the previous displacement per FEMA P-2082-1 (2020) guidelines. The column specimens were displaced to the extent of the testing frame and the lateral load and displacement at the column head were recorded. Additionally, the rotation of each corner of the base and the strain at various positions on the steel reinforcement and GFRP tube were recorded. Load versus displacement and strain versus displacement plots were developed and used to analyze and compare the behavior and performance of each column specimen and column type.

9.2 Findings

The findings associated with this research study were as follows.

9.2.1 Column Specimen Testing Frame and Procedure Findings

- The ¼-inch solid steel rollers allowed the column specimen to be drawn into the testing frame by the threaded steel anchoring rods.
- All eight anchoring rods typically passed through the concrete base and steel testing frame with one PVC pipe removed at most.
- All four prestressing strands typically passed through the cast-in-place PVC ducts with no issues and were able to be anchored at either end.
- All four threaded steel anchoring rods for mounting the loading assembly typically passed through the column cap with no issues.
- The weld restraining the bottom of the diagonal HSS support on the actuator mounting brace fractured at a lateral loading of approximately 38 kips in tension.
- The original single-through threaded steel rod design buckled nearing 41 kips.
- The load on the post-tensioning strands that applied the constant axial compressive load to the column exceeded approximately 80% of the specified ultimate tensile strength at the 10.89-inch displacement cycle.
- Although the loading system was designed to utilize the full stroke length of the actuator at 14 inches in both directions, a displacement of only 13 inches in the extension direction was achieved.

- The column testing frame adequately restrained and prevented lateral movement of the concrete base and transferred the applied column loads.
- The concrete base rotated during testing of the column specimens and the rotation was captured by the installed wire pots.
- The testing frame was capable of displacing the column specimens to the specified displacement intervals and to a displacement that resulted in a significant loss of capacity.
- The roller system that supported and prevented vertical deflection of the column head functioned less than ideal at larger displacements as the rollers dislodged or canted from the curvature of the larger displacements.
- The setup of the loading assembly was easily repeatable and streamlined the testing setup process.

9.2.2 RC Column Specimen Findings

- Due to the nature of the column, significant spalling was observed during testing that eventually revealed the transverse spiral tie and longitudinal reinforcement.
- The longitudinal bars were observed to buckle while in compression, and some eventually fractured while in tension. A total of three longitudinal bars were fractured during testing, including each bar at the extreme fiber on both sides of the column, and a bar next to one of the extreme fibers.
- The maximum load sustained by the column was 29.3 kips at a measured displacement of 7.77 inches in the eastward, or extension, direction.
- Due to the nature of the testing, the strain gauges were eventually damaged, leading to incoherent or constant readings. These errant readings were removed from the strain gauge plots by trimming the data back to the last comprehensible reading.
- The specimen exhibited excellent symmetry between the extension and retraction cycles as shown by similar peak loads for opposite cycles.
- Linear elastic behavior was observed until a displacement of approximately 1.5 inches, after which the behavior began to transition to inelastic behavior.
- Gradual stiffness degradation was observed approaching the same displacement followed by increasingly significant stiffness softening.

- The first cycle of each displacement interval closely followed the second cycle of the previous interval and, in general, the second cycle of any displacement interval did not reach the same maximum load as the first cycle of that interval due to the damage sustained from the previous cycle.
- As the longitudinal steel reinforcement began to yield and buckle, the load versus displacement plot began to plateau, with some stain hardening observed.

9.2.3 HS-SCC HC-FCS Column Specimen Findings

- HS-SCC 1 was the first column and the first HC-FCS column specimen tested. The testing consisted of three distinct segments with each corresponding to an issue encountered with the newly constructed and developed testing frame and procedure.
- Due to the nature of HC-FCS columns, the outer GFRP layer prevented the observation of cracking in the concrete core during testing.
- Minimal damage to the GFRP tube was observed at smaller displacements during testing while it was predominantly damaged at larger displacements as the tube was compressed into the concrete base.
- The concrete core was crushed in a conical shape with the lower approximately 3 inches nearest to the column base turned to powder.
- The steel tube was observed to have buckled at the extreme axis with a vertical compressed fold, or crease, parallel to the column base and a depressed region on either side of the extreme axis.
- Despite the damage, the column was still capable of sustaining the applied constant axial compressive load.
- The maximum load sustained by the HS-SCC 1 column was 45.2 kips at a measured displacement of 5.56 inches in the westward, or retraction, direction.
- The maximum load sustained by the HS-SCC 2 column was 43.6 kips at a measured displacement of 5.23 inches in the westward, or retraction, direction.
- Linear elastic behavior was observed until a displacement of approximately 1.5 inches, after which the behavior began to transition to inelastic behavior.
- Gradual stiffness degradation was observed approaching a displacement of approximately 2 inches, followed by moderate stiffness softening at a displacement of

approximately 3 inches and significant stiffness softening at a displacement of approximately 4 inches. Beyond an approximate displacement of 4 inches, the capacity of the specimen gradually declined.

- During the beginning of each displacement cycle at larger displacements and later cycles, the load gradually increased or held constant before an upturn in the sustained load was observed. The upturn was attributed to the yielding and buckling of the steel tube after the concrete core was crushed. As the load on the column was reversed, the side of the column in which the steel tube was previously buckled was gradually straightened from the tension caused by the load reversal. Concurrently, the side of the column in which the steel tube was previously in tension began to buckle.
- As the column experienced increased displacement and severe strains, the load versus displacement plot began to plateau, with some strain hardening observed.
- Strain gauges at similar locations and levels exhibited symmetry at similar displacements, and in general, gauges higher up the column, or farther from the top of the column base, exhibited lower strains.

9.2.4 UHPC HC-FCS Column Specimen Findings

- Due to the nature of HC-FCS columns, the outer GFRP layer prevented the observation of cracking in the concrete core during testing.
- Minimal damage to the GFRP tube was observed at smaller displacements during testing and was predominantly damaged at larger displacements as the tube was compressed into the concrete base.
- The concrete core was crushed in a conical shape and due to the presence of steel fibers, the crushed concrete was removed by jackhammering to reveal the shape of the crushed region below.
- The steel tube was observed to have buckled at the extreme axis with two diagonal compressed folds, or creases, parallel to the column base that converged below the extreme fiber and a depressed region along the extreme fiber.
- Despite the damage, the column was still capable of sustaining the applied constant axial compressive load.

- The maximum load sustained by the UHPC 1 column was 48.6 kips at a measured displacement of 7.77 inches in the eastward, or extension, direction.
- The maximum load sustained by the UHPC 2 column was 48.0 kips at a measured displacement of 7.64 inches in the eastward, or extension, direction.
- Linear elastic behavior was observed until a displacement of approximately 1 inch, after which the behavior began to transition to inelastic behavior.
- Gradual stiffness degradation was observed approaching a displacement of approximately 2 inches, followed by moderate stiffness softening at a displacement of approximately 3 inches and significant stiffness softening at a displacement of approximately 4 inches.
- Increasingly significant stiffness softening occurred beyond a displacement of approximately 4 inches with the sustained load beginning to plateau approaching a displacement of approximately 8 inches.
- During the beginning of each displacement cycle at larger displacements and later cycles, the load gradually increased or held constant before an upturn in the sustained load was observed. The upturn was attributed to the yielding and buckling of the steel tube and the support of the intact concrete core. As the load on the column was reversed, the side of the column in which the steel tube was previously buckled was gradually straightened from the tension caused by the load reversal. Concurrently, the side of the column in which the steel tube was previously in tension began to buckle and the concrete core was compressed against the concrete base.
- As the column was displaced beyond approximately 8 inches, the load versus displacement plot began to plateau.
- Strain gauges at similar locations and levels exhibited symmetry at similar displacements, and in general, gauges higher up the column, or farther from the top of the column base, exhibited lower strains.

9.3 Conclusions

The findings of this research study led to the following conclusions.

9.3.1 Column Specimen Testing Frame and Procedure Conclusions

- The original lateral loading assembly was required to be rebuilt to function properly and to test the column specimens until failure.
- The lateral displacement of the column specimens was limited by the available stroke length of the hydraulic actuator and by the geometric constraints on the post-tensioning strands.
- The rotation of the column bases effectively proportionally reduced the measured displacement of the column head.
- The roller system adequately supported and prevented vertical deflection of the column head despite the additional effort and maintenance required.
- The column testing frame required minimal adjustments and functioned as intended with minimal observable damage. Each column specimen was successfully anchored to the frame and loading apparatus and was displaced until a significant drop in capacity was observed.

9.3.2 RC Column Specimen Conclusions

- The peak moment capacity of the RC column was 249 kip-ft at a displacement of 7.8 inches.
- The shape of the steel strain gauge plot at the neutral axis of the column resembled a “V”, which was indicative of the neutral axis of the column migrating during testing toward the compressive side of the specimen.
- A noticeable drop in capacity on the second cycle of the 7.78-inch displacement interval was observed and indicated the buckling of the longitudinal bars in compression at the extreme fiber and significant crushing of the core concrete that led to the rupturing of the longitudinal bars in tension at the opposite extreme fiber.
- The outward buckling was conducive to traditional buckling failure while the buckling in the circumferential direction indicated effective transverse spiral reinforcement confinement.

- Each discontinuity in the measured load corresponds to a longitudinal bar rupturing at or near the extreme fiber that ultimately led to the failure of the column.
- The column specimen was considered failed after observing a significant reduction in capacity during and after the 7.78-inch displacement interval.
- The concrete core was adequately intact after testing, and the column was still capable of sustaining the applied constant axial compressive load.
- The concrete base was observed to provide adequate flexural and shear capacity with light spalling at the interface with the column testing frame. The column reinforcement was not observed to have been pulled out of the column base, therefore the embedment depth and hook lengths were effective.
- The RC column exhibited traditional, expected spiral-tied reinforced concrete column behavior, and validated the column testing frame, testing setup, and testing procedure.

9.3.3 HS-SCC HC-FCS Column Specimen Conclusions

- The peak moment capacity of the HS-SCC 1 HC-FCS column was 384 kip-ft at a displacement of 5.6 inches.
- The peak moment capacity of the HS-SCC 2 HC-FCS column was 370 kip-ft at a displacement of 5.2 inches.
- The variation between the determined peak moments and displacements was approximately 4% and 8%, respectively.
- The initial loss of stiffness was attributed to the steel tube yielding and the concrete core cracking. The loss of capacity was attributed to the concrete core crushing and the steel tube buckling due to the loss of confinement from the concrete core.
- The distinct drop in capacity observed on the second cycle of the 10.89-inch displacement interval was indicative of the steel tube fracturing in tension due to fatigue at the extreme fiber opposite from the direction of loading. The column specimen was considered failed after observing a significant reduction in capacity during and after the second 10.89-inch displacement interval.
- The steel tube strain gauge plots also corroborated observations from the load versus displacement plot such as the transition from elastic to inelastic behavior.

- The transition in the GFRP strain gauge plots correlates with the significant stiffness softening and loss of capacity of the column and was attributed to the concrete core crushing and applying increased pressure to the GFRP tube.
- The crushed concrete core indicated that the steel tube and GFRP tube sufficiently confined the concrete core, and the concrete reached its ultimate strain without rupturing the GFRP tube.
- The upturn in the sustained load observed from load versus displacement response combined with the observed failure of the steel tube corroborated the assumed behavior that the steel tube buckled while under compression and then straightened while under tension at larger displacements and later cycles.
- The observed fractures in the steel tube resembled a fatigue failure due to limited necking and corroborated the discontinuity and drop in capacity shown on the load versus displacement plot.
- The concrete base was observed to provide adequate flexural and shear capacity with light spalling at the interface with the column testing frame and lateral clamping mechanisms.
- The steel tube was not observed to have been pulled out of the column base, therefore the embedment depth and supplemental anchorage were effective.

9.3.4 UHPC HC-FCS Column Specimen Conclusions

- The peak moment capacity of the UHPC 1 HC-FCS column was 413 kip-ft at a displacement of 7.8 inches.
- The peak moment capacity of the UHPC 1 HC-FCS column was 408 kip-ft at a displacement of 7.6 inches.
- The variation between the determined peak moments and displacements was approximately 1% and 3%, respectively.
- The initial loss of stiffness was attributed to the steel tube yielding and buckling, with minimal cracking in the concrete core. The sustained load beginning to plateau was attributed to the concrete core starting to crush.
- The continued increase in capacity was attributed to the concrete core remaining intact and continuing to support the column, despite the yielded and buckled steel

tube. The concrete core was able to remain intact due to the presence of the steel fibers that increased the confinement and ductility of the concrete core, despite the loss of confinement from the buckled steel tube.

- The column specimen was not considered failed due to the lack of a significant reduction in capacity during and after the second 10.89-inch displacement interval.
- The steel tube strain gauge plots also corroborated observations from the load versus displacement plot such as the transition from elastic to inelastic behavior.
- The transition in the GFRP strain gauge plots correlates with the significant stiffness softening and loss of capacity of the column and was attributed to the concrete core crushing and applying increased pressure to the GFRP tube.
- The crushed concrete core indicated that the steel tube and GFRP tube sufficiently confined the concrete core, and the concrete reached its ultimate strain without rupturing the GFRP tube.
- Both column specimens were observed to have comparable flexural capacities and overall performance, therefore the steel fiber distribution was concluded to not have a significant impact.
- The lower approximately 3 inches of the concrete core nearest to the column base was reduced to rubble and held together by the steel fibers. This indicated that the concrete core was sufficiently confined by some combination of the steel tube, embedded steel fibers, and GFRP tube.
- The upturn in the sustained load observed from load versus displacement response combined with the observed failure of the steel tube and the final condition of the concrete core corroborated the assumed behavior that the steel tube buckled while under compression and then straightened while under tension at larger displacements and later cycles.
- The observed tears in the steel tube indicated that the steel tube would have likely fractured from fatigue with additional cycles or increased displacement.
- The concrete base was observed to provide adequate flexural and shear capacity with light spalling at the interface with the column testing frame and lateral clamping mechanisms.

- The steel tube was not observed to have been pulled out of the column base, therefore the embedment depth and supplemental anchorage were effective.

9.3.5 Comparative Analysis of Column Specimen Types Conclusions

- Constructing, placing, and leveling the spiral-tied steel reinforcement cage for the RC column required significantly more time compared to the preparation of the steel tube for the HC-FCS columns.
- The RC column required additional consolidation when casting the column section compared to the self-consolidating concretes used for the HC-FCS columns.
- The HC-FCS columns tested weighed approximately two-thirds of the RC column tested.
- The HC-FCS columns utilized higher quality materials that would lead to increased costs when compared to traditional columns, which could be offset by the reduced construction time due to the reduced complexity of HC-FCS columns.
- The higher quality materials used for HC-FCS columns are more durable than traditional RC column materials and would likely reduce the maintenance cost of the column over the life of the structure.
- The peak moment of HS-SCC 2 was approximately 33% greater than that of the RC column. Both peak moment capacities occurred during the extension cycle, with the peak moment capacity of the HS-SCC 2 specimen occurring at approximately 33% less displacement.
- HS-SCC 2 demonstrated higher ductility due to exhibiting a similar elastic behavior transition point while achieving a higher capacity at a larger displacement than the RC specimen.
- The HS-SCC 2 specimen also demonstrated a higher ductility index due to sustaining a larger displacement when the steel reinforcement fractured given that both specimens yielded the steel reinforcement at approximately the same displacement.
- The RC column specimen more clearly exhibited signs of distress before a significant loss of capacity and eventually column failure compared to the HC-FCS column specimen.

- The peak moment of UHPC 2 was approximately 10% greater than that of HS-SCC 2. Both peak moment capacities occurred during the extension cycle, with the peak moment capacity of the UHPC 2 specimen occurring at approximately 46% more displacement.
- UHPC 2 continued to gradually increase in strength after experiencing significant stiffness softening because the concrete core remained intact, whereas HS-SCC 2 lost capacity and plateaued after the concrete core was crushed.
- UHPC 2 demonstrated higher ductility due to exhibiting an approximately similar elastic behavior transition point while achieving a higher capacity at a larger displacement than the HS-SCC 2 specimen.
- The intact concrete core of the UHPC 2 specimen led to sharper upturns in the sustained load compared to that of the HS-SCC 2 specimen as observed on the load versus displacement plot.
- The UHPC 2 specimen would have likely demonstrated a higher ductility index due to sustaining a larger displacement when the steel tube would have fractured given that both specimens yielded the steel reinforcement at approximately the same displacement.
- The concrete core of the UHPC 2 specimen was confined more by the internal steel fibers of the UHPC than the GFRP tube, therefore the concrete core applied less pressure to the GFRP tube than the HS-SCC 2 specimen.
- The UHPC core of UHPC 2 reduced the damage from fatigue on the steel tube because the concrete core sustained much higher loads before crushing and continued to take load after crushing.
- The UHPC core of UHPC 2 enhanced the confinement of the steel tube as shown by the localized, more three-dimensional buckling shape of the steel tube and corresponding increase in overall column capacity and ductility compared to the HS-SCC 2 column.

9.4 Recommendations

The following recommendations are provided for future work on HC-FCS columns.

9.4.1 Column Specimen Testing Frame and Procedure Recommendations

- Redesign the roller system such that it is capable of supporting the column head at larger displacements as the curvature increases.
- Replace the current hydraulic actuator with one with additional stroke length to displace the column specimens further. An actuator with additional capacity would also facilitate testing larger diameter specimens.
- Redesign and implement a post-tensioning system that is capable of equalizing the load as the column is displaced such that a truly concentric axial load on the column is achieved and the post-tensioning strands do not near fracture level loads.
- Post-tension the threaded steel anchoring rods that anchor the concrete column base to the steel testing frame to reduce the damage sustained by the concrete bases.
- Adjust the measured lateral load at the column head for the measured rotation of the column base during or after testing to produce more accurate hysteresis loops.

9.4.2 HC-FCS Column Specimen Recommendations

- Move the steel tube strain gauges to the inside of the steel tube to prevent the early failure of the gauges from the damage caused by the concrete core sliding along the steel tube.
- Reduce the GFRP tube thickness for the given configurations to refine the design recommendations and reduce material usage.
- Remove the GFRP tube and use Sonotube formwork for the UHPC HC-FCS configuration to reduce material usage and take full advantage of the confining properties of the internal steel fibers in the UHPC. Removing the GFRP tube also enables viewing signs of distress on the concrete core of the column.
- Reduce the concrete core thickness for the given configurations to better determine the governing failure mechanism and the confinement provided by the concrete core.

- Experiment with different steel fiber percentages for the UHPC HC-FCS configuration to better determine the contribution of the steel fibers to the confinement of the steel tube and the flexural capacity of the column.
- Increase the steel tube thickness for the given configurations to increase the buckling capacity and fatigue resistance of the steel tube to better determine the governing failure mechanism.
- Use steel tubes with different exterior finishes to determine the impact of the bond between the concrete core and the steel tube.
- Test column specimens of different column diameters while still utilizing the current design recommendations and HS-SCC and the UHPC for the concrete core material to determine the scalability of the configurations.
- Test column specimens of different column lengths while still utilizing the current design recommendations and HS-SCC and the UHPC for the concrete core material to determine the scalability of the configurations.

References

AASHTO. (2020). *LRFD Bridge Design Specifications*, 9th Edition, American Association of State Highway and Transportation Officials, Washington, D.C.

Abdelkarim, O. and ElGawady, M. (2014). "Behavior of Hybrid FRP-Concrete-Steel Double-Skin Tubes Subjected to Cyclic Axial Compression," Proceedings, ASCE Structures Congress, pp. 1002-1013.

Albitar, M., Ozbakkaloglu, T., and Fanggi, B.A.L. (2015). "Behavior of FRP-HSC-Steel Double-Skin Tubular Columns Under Cyclic Axial Compression," Journal of Composites for Construction, V. 19, No. 2, 1943-5614.0000510.

American Concrete Institute. (2019). *Building Code Requirements for Structural Concrete* (ACI 318-19), Farmington Hills, MI: American Concrete Institute.

American Concrete Institute. (2018). *Details and Detailing of Concrete Reinforcement* (ACI 315-18), Farmington Hills, MI: American Concrete Institute.

ASTM C39. (2021). *Standard Test Method for Compressive Strength of Cylindrical Concrete Specimens*, West Conshohocken, PA.

Campos, R. (2020). "Effect of Fiber Content on Tensile Strength of Non-Proprietary Ultra-High Performance Concrete," MS Thesis, University of Oklahoma, Norman, OK.

Chhetri, S., Chicchi, R. A., and Seguirant, S., "Industry survey results on the use of prestressing strand lifting loops," PCI Journal (ISSN 0887-9672) V. 65, No. 4, July-August 2020.

Dyachkova, Y. (2020). "Effect of Steel Fiber Content on Mechanical Properties of Non-proprietary Ultra-High Performance Concrete," MS Thesis, University of Oklahoma, Norman, OK.

FEMA. (2020). *NEHRP Recommended Seismic Provisions for New Buildings and Other Structures, National Earthquake Hazards Reduction Program*, FEMA P-2082-1, Federal Emergency Management Agency, Washington, D.C.

Haber, Z.B., De la Vargas, I., Graybeal, B.A., Nakashoji, B., and El-Helou, R. (2018). Properties and Behavior of UHPC-Class Materials, FHWA-HRT-18-036, Federal Highway Administration, McLean, VA, 153 pp.

Han, L.H., Tao, Z., Liao, F.Y., and Xu, Y. (2010). "Tests on Cyclic Performance of FRP-Concrete–Steel Double-Skin Tubular Columns," Thin-Walled Structures, V. 4, pp. 430-439.

He, L., Lin, S., and Jiang, H. (2019). “Confinement Effect of Concrete-Filled Steel Tube Columns with Infill Concrete of Different Strength Grades,” Frontiers in Materials, V. 6, No. 71, 2019.00071.

Hoshikuma, J.I. and Priestley, M. (2000). Flexural Behavior of Circular Hollow Columns with a Single Layer of Reinforcement Under Seismic Loading, Structural Systems Research Project, University of California, San Diego, Department of Structural Engineering.

Li, W., Han, L.H., Chan, T. (2014). “Tensile Behavior of Concrete-Filled Double-Skin Steel Tubular Members,” Journal of Constructional Steel Research, V. 99, pp. 35-46.

Lu, H., Zhao, X., and Han, L. H. (2010). “Testing of Concrete-Filled Double Skin Tubular Stub Columns Exposed to Fire,” Journal of Constructional Steel Research, V. 66, Nos. 8-9, pp. 1069-1080.

Mander, J.B., Priestley, M.J.N., and Park, P. (1983). “Behavior of Ductile Hollow Reinforced Concrete Columns,” Bulletin of the New Zealand Society for Earthquake Engineering, V. 16, No. 4, pp. 273-290.

McDaniel, A. (2017). “Development of Non-Proprietary Ultra-High Performance Concrete Mix Designs,” MS Thesis, University of Oklahoma, Norman, OK.

Ozbakkaloglu, T. (2013). “Compressive Behavior of Concrete-Filled FRP Tube Columns: Assessment of Critical Column Parameters,” Engineering Structures, V. 51, pp. 188-199.

Ozbakkaloglu, T. and Idris, Y. (2014). “Seismic Behavior of FRP-High-Strength Concrete–Steel Double-Skin Tubular Columns,” Journal of Structural Engineering, V. 140, No. 6, 04014019.

Ozbakkaloglu, T. and Vincent, T. (2014). “Axial Compressive Behavior of Circular High-Strength Concrete-Filled FRP Tubes,” Journal of Composites for Construction, V. 18, No. 2, 1943-5614.0000410.

Perea, T., Leon, R. T., Hajjar, J. F., and Denavit, M. D. (2014). “Full-Scale Tests of Slender Concrete-Filled Steel Tubes: Interaction Behavior,” Journal of Structural Engineering, V. 140, No. 9, 1943-541X.0000949.

Prakash, S., Belarbi, A., and You, Y. (2010). “Seismic Performance of Circular RC Columns Subjected to Axial Force, Bending, and Torsion with Low and Moderate Shear,” Engineering Structures, V. 32, pp. 46-59.

Ranzo, G. and Priestley, M. (2001). Seismic Performance of Circular Hollow Columns Subjected to High Shear, Structural Systems Research Project, University of California, San Diego, Department of Structural Engineering.

Shakir-Khalil, H., and Illouli, S. (1987). “Composite columns of concentric steel tubes,” Proceedings, Conference on the Design and Construction of Non-Conventional Structures, V. 1, London, United Kingdom, pp. 73–82.

Teng, J.G., Yu, T., and Wong, Y.L. (2004). “Behavior of Hybrid FRP-Concrete-Steel Double-Skin Tubular Columns,” Proceedings, Second International Conference on FRP Composites in Civil Engineering, Adelaide, Australia, pp. 811-818.

Teng, J. G., Yu, T., Wong, Y. L., and Dong, S. L. (2007). “Hybrid FRP Concrete-Steel Tubular Columns: Concept and Behavior,” Construction and Building Materials, V. 21, No. 4, pp. 846–854.

Tiry, Z. (2023). “Design of Continuity Connections for Precast, Pretrensioned Girders Using Ultra-High Performance Concrete,” MS Thesis, University of Oklahoma, Norman, OK.

Yagishita F, Kitoh H, Sugimoto M, Tanihira T, Sonoda K. (2000). “Double-Skin Composite Tubular Columns Subjected to Cyclic Horizontal Force and Constant Axial Force,” Proceedings, Sixth ASCCS Conference, Los Angeles, California, March 22–24, pp. 497–503.

Yu, T., Wong, Y., Teng, J., Dong, S., and Lam, E. (2006). “Flexural Behavior of Hybrid FRP-Concrete-Steel Double-Skin Tubular Members,” Journal of Composite Construction, V. 10, No. 5, pp. 443–452.

Zahn, F., Park, R., and Priestley, M. (1990). “Flexural Strength and Ductility of Circular Hollow Reinforced Concrete Columns without Confinement on Inside Face,” ACI Structural Journal, V. 87, No. 2, pp. 156-166.

Zhang, B., Teng, J. G. and Yu, T. (2012). “Behavior of Hybrid Double-Skin Tubular Columns Subjected to Combined Axial Compression and Cyclic Lateral Loading,” Proceedings, Sixth International Conference on FRP Composites in Civil Engineering, Rome, Italy, pp. 1-7.

Zhu, Z., Ahmad, I., and Mirmiran, A. (2006). “Seismic Performance of Concrete-Filled FRP Tube Columns for Bridge Substructure,” Journal of Bridge Engineering, V. 11, No. 3, pp. 359–370.

Zohrevand, P. and Mirmiran, A. (2013). “Effect of Column Parameters on Cyclic Behavior of Ultra-High-Performance Concrete-Filled Fiber-Reinforced Polymer Tubes,” ACI Structural Journal, V. 110, No. 5, pp. 823-832.

Appendix

A.1 RC Column Supplemental Strain Gauge Plots

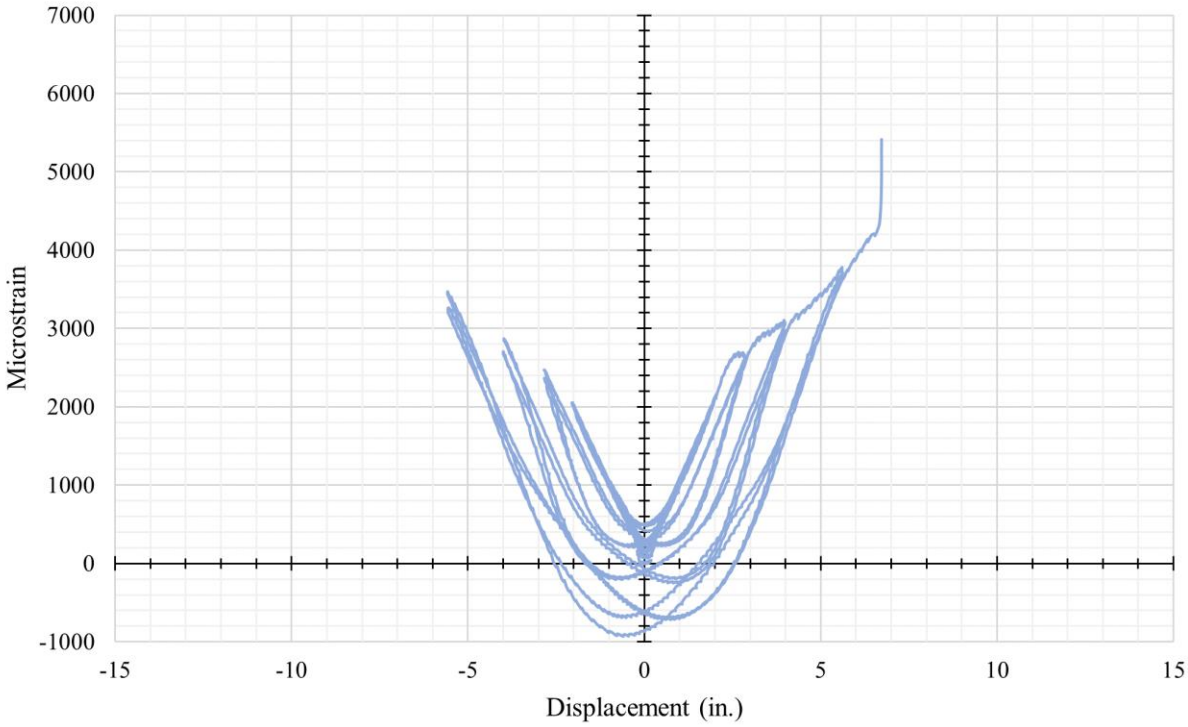

Figure A-1: RC SN2 Steel Strain Gauge vs. Displacement at Column Head

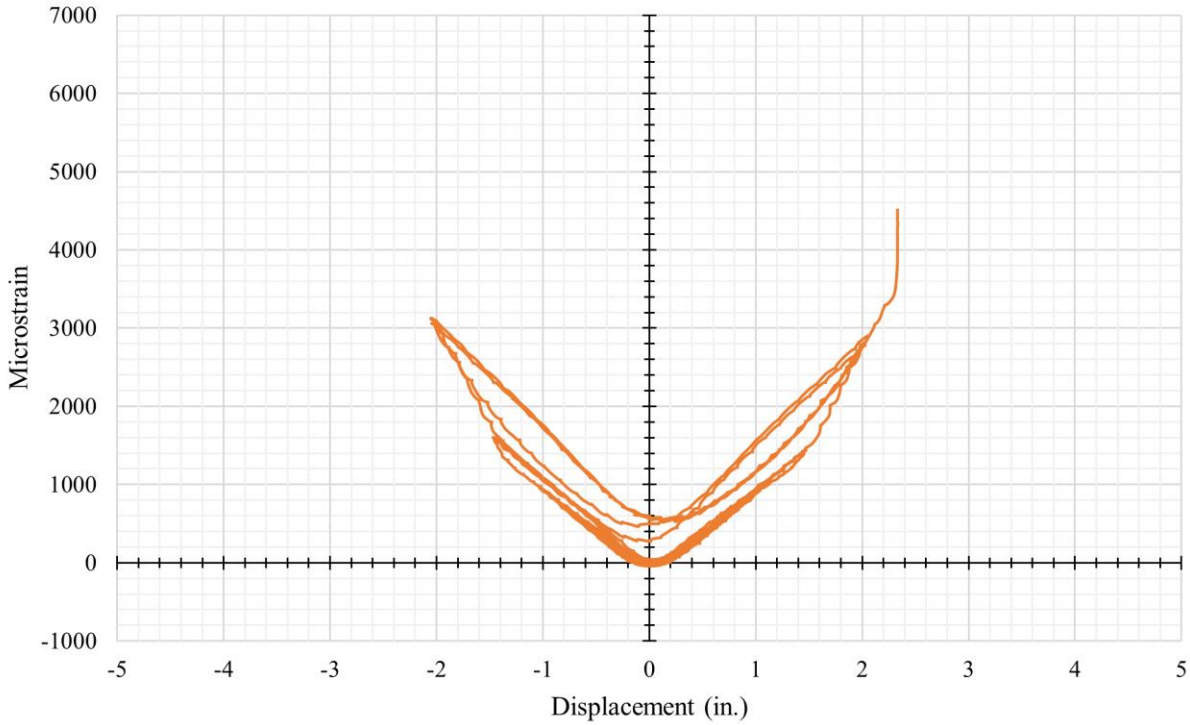

Figure A-2: RC SS1 Steel Strain Gauge vs. Displacement at Column Head

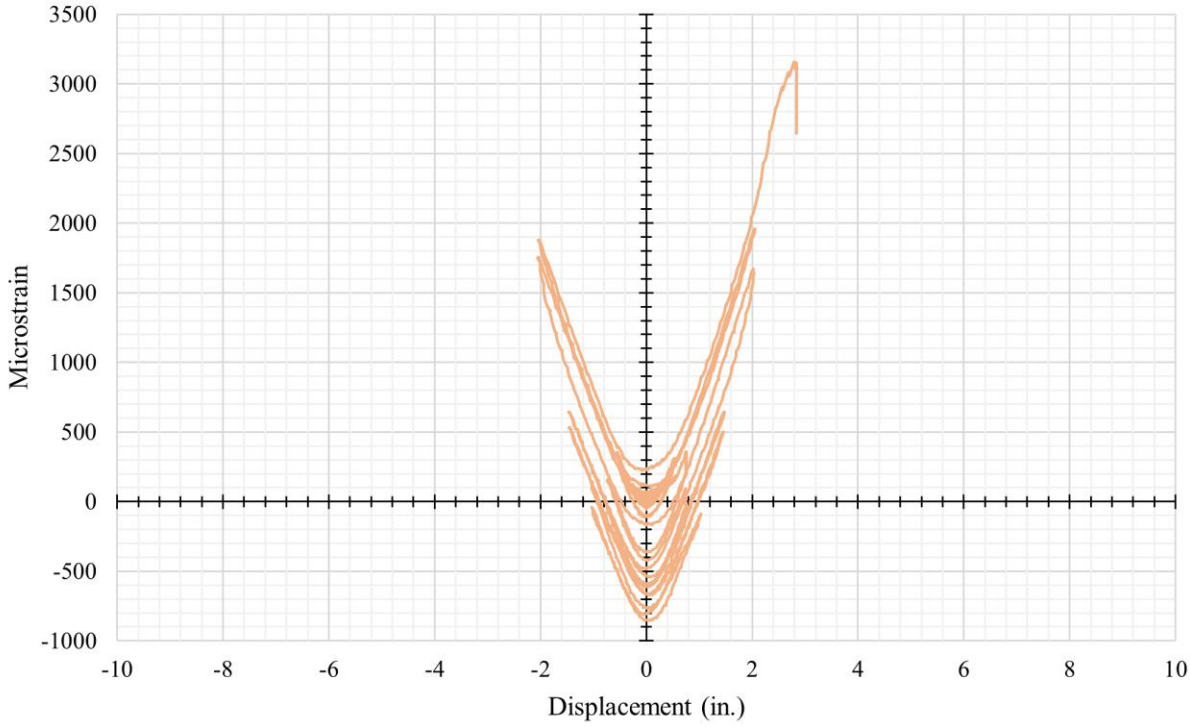

Figure A-3: RC SS2 Steel Strain Gauge vs. Displacement at Column Head

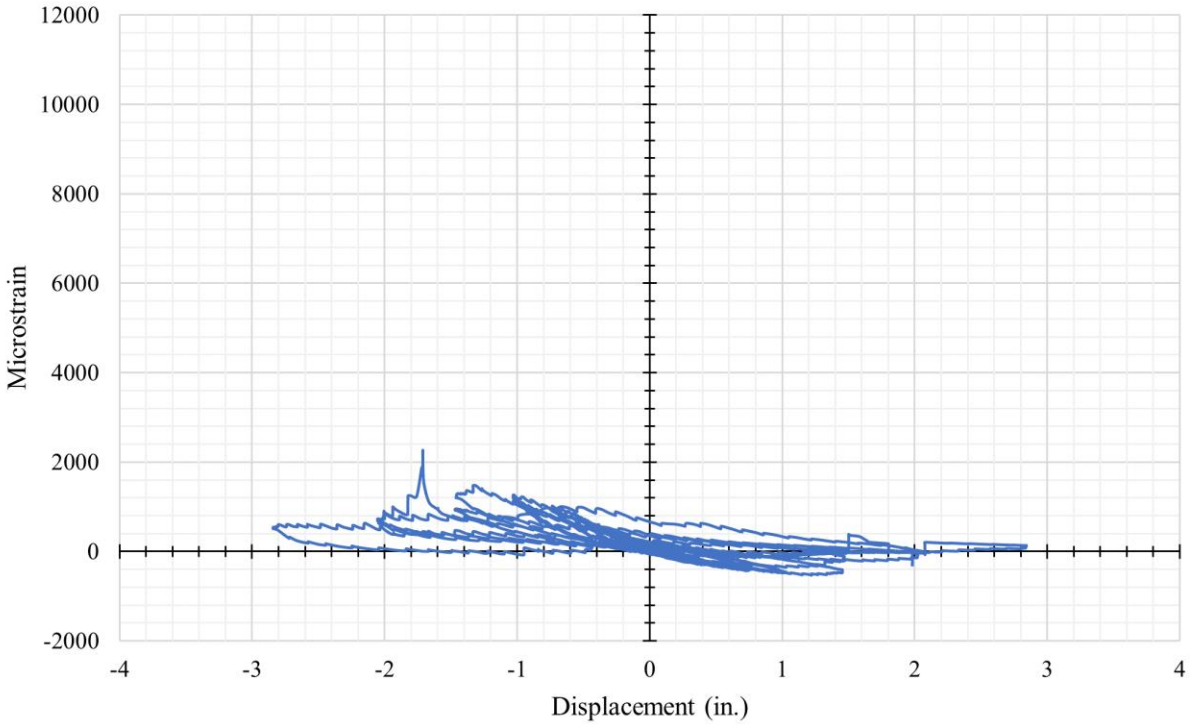

Figure A-4: RC SE1 Steel Strain Gauge vs. Displacement at Column Head

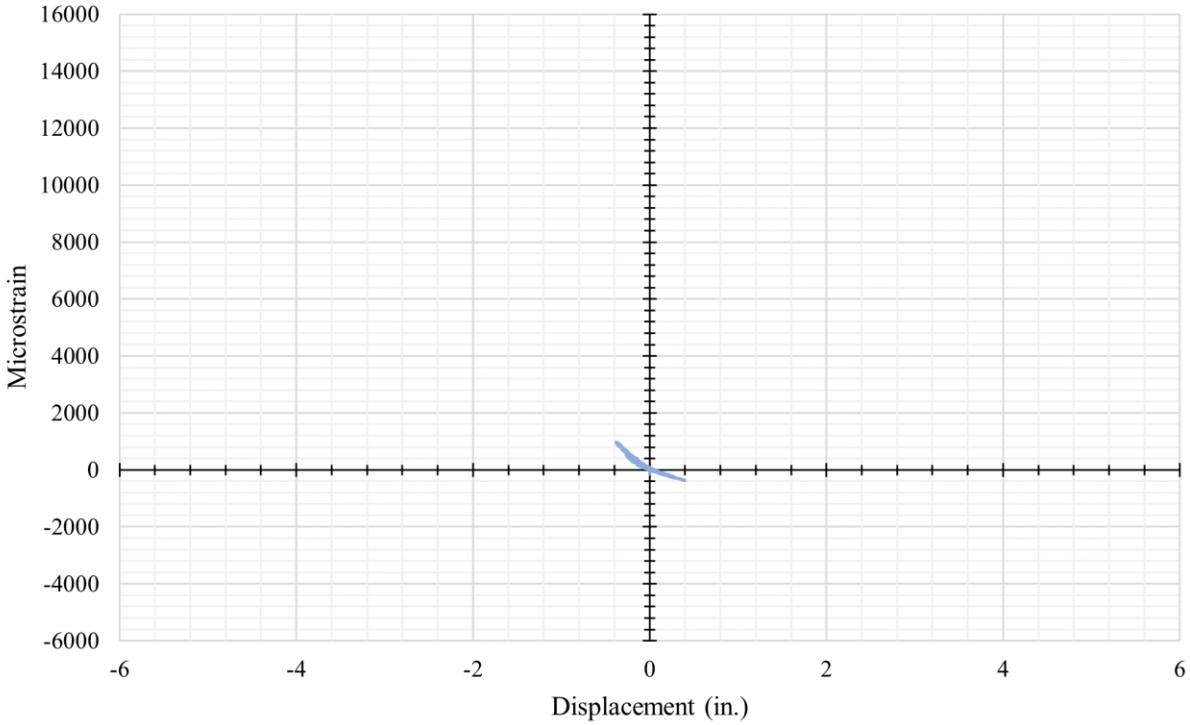

Figure A-5: RC SE2 Steel Strain Gauge vs. Displacement at Column Head

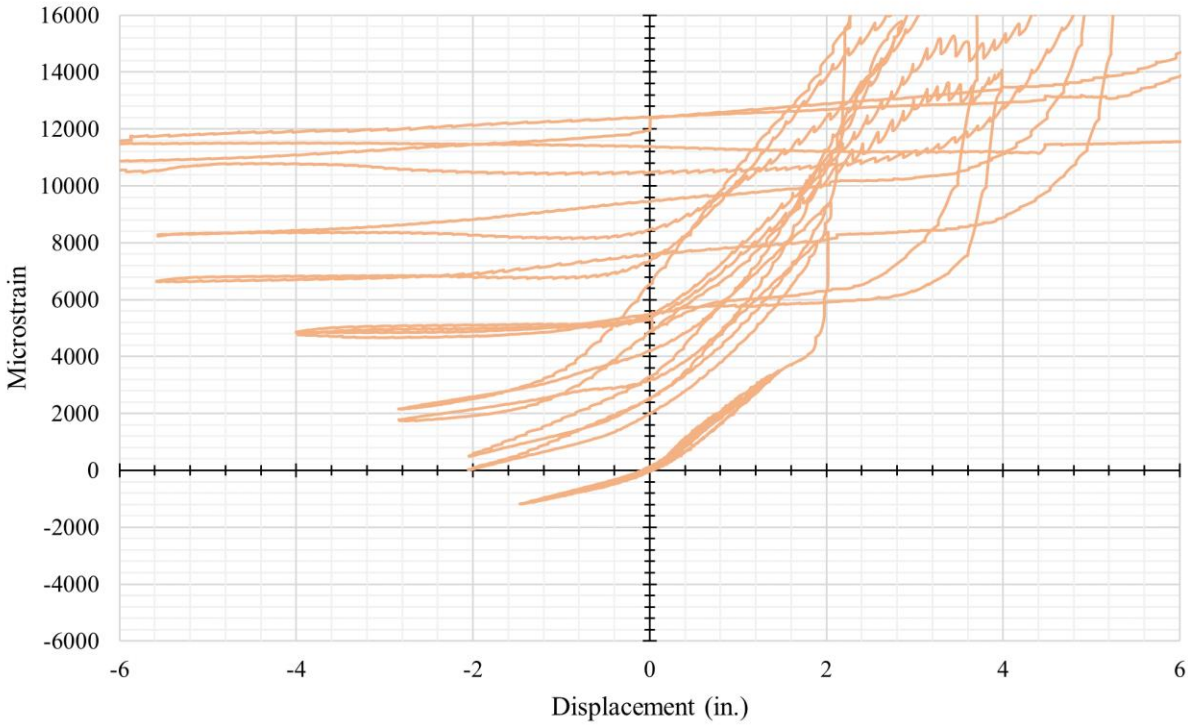

Figure A-6: RC SW2 Steel Strain Gauge vs. Displacement at Column Head

A.2 HS-SCC 1 Column Supplemental Strain Gauge Plots

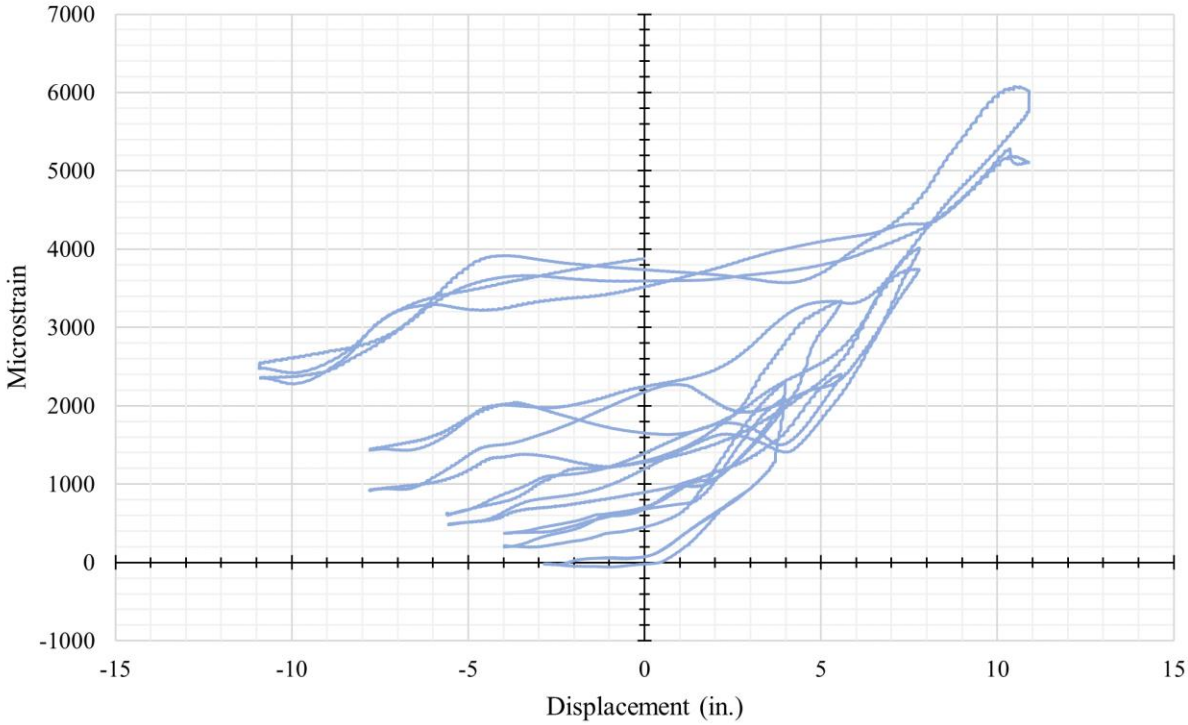

Figure A-7: HS-SCC 1 GE2 GFRP Strain Gauge vs. Displacement at Column Head

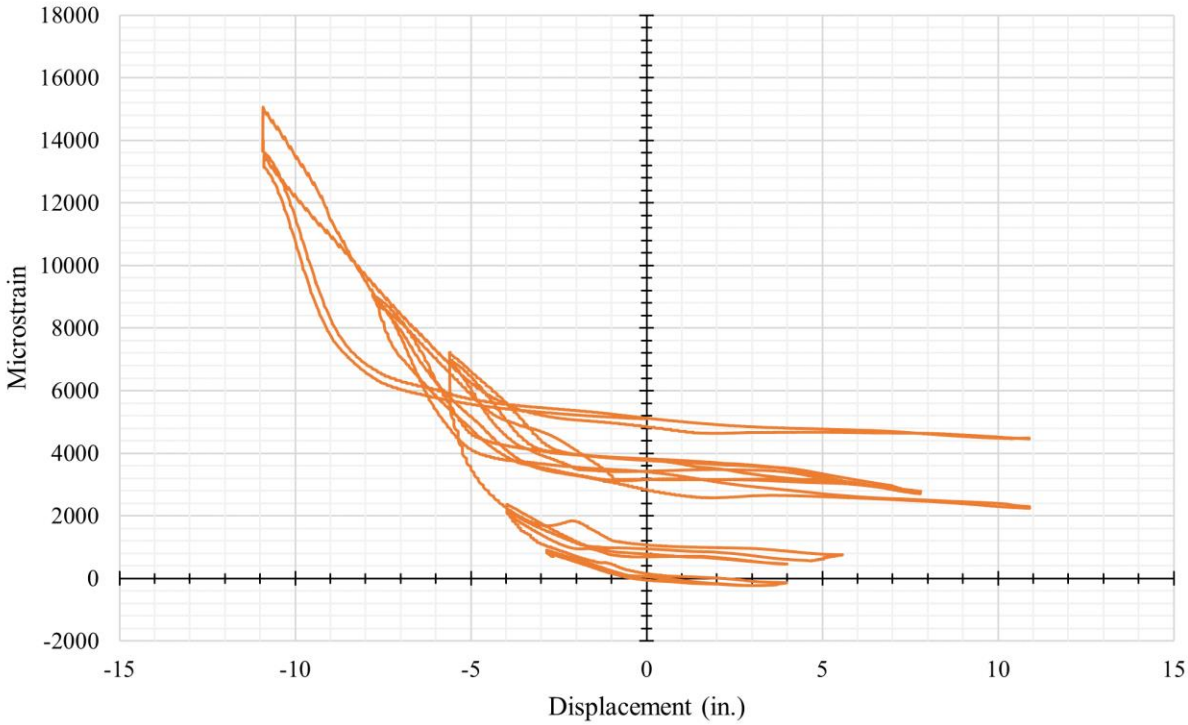

Figure A-8: HS-SCC 1 GW1 GFRP Strain Gauge vs. Displacement at Column Head

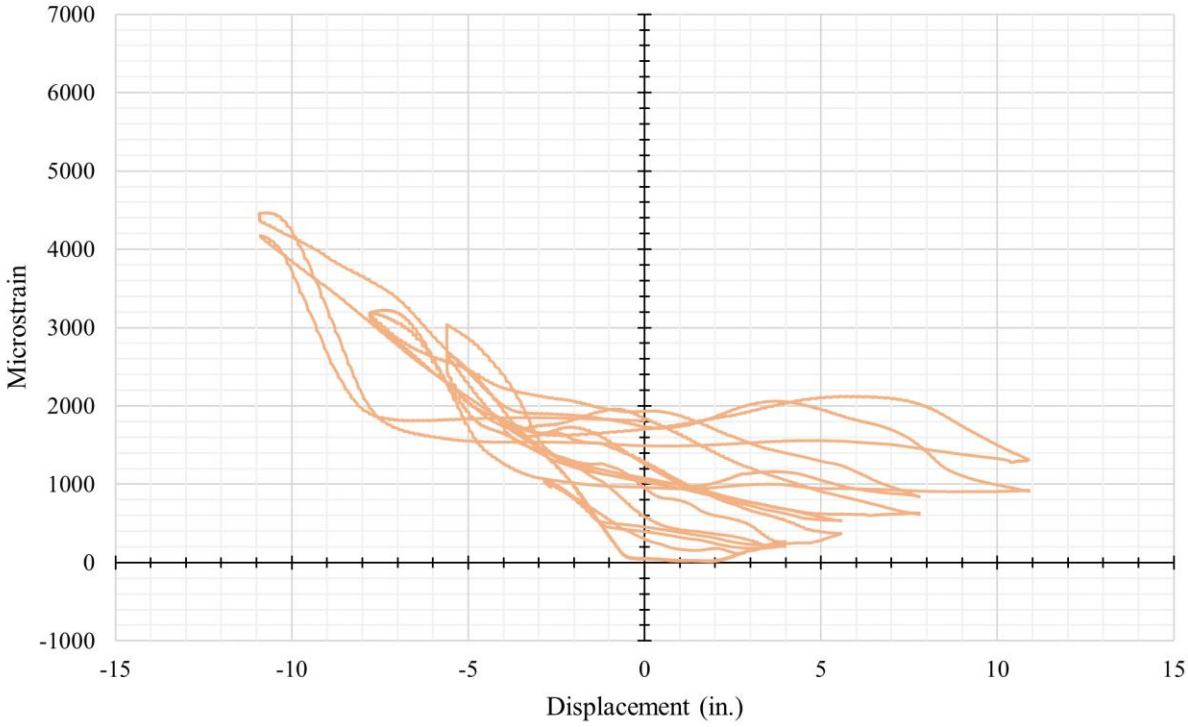

Figure A-9: HS-SCC 1 GW2 GFRP Strain Gauge vs. Displacement at Column Head

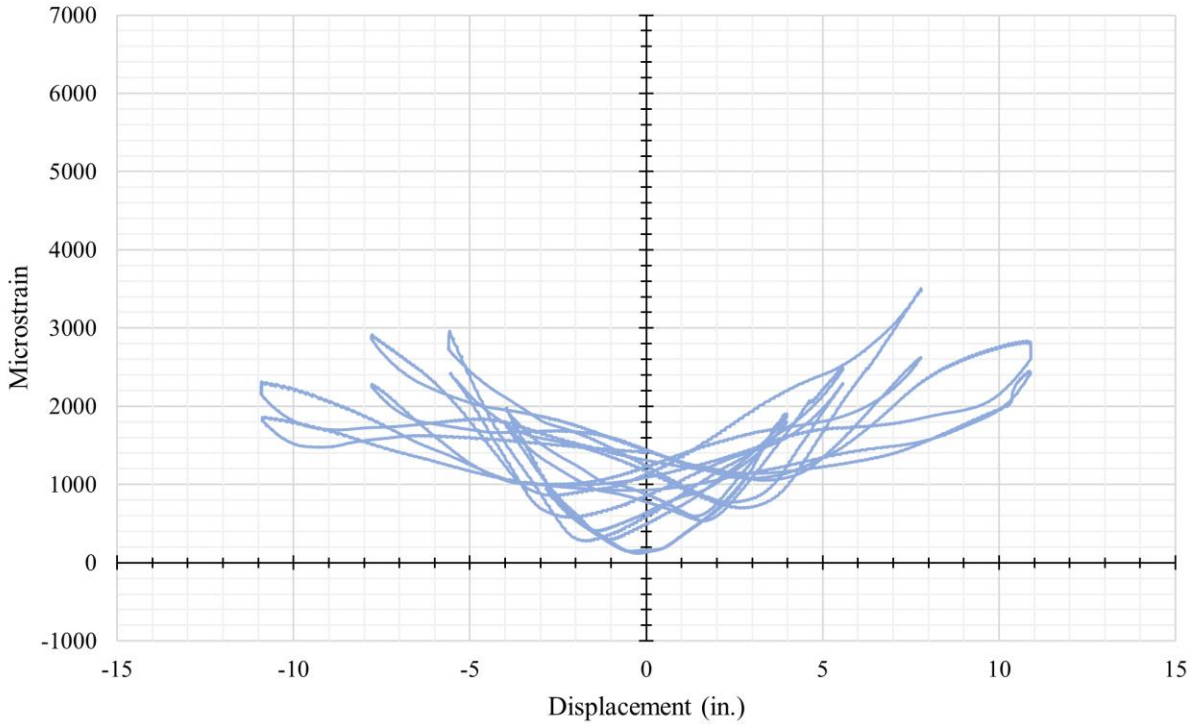

Figure A-10: HS-SCC 1 SN2 Steel Strain Gauge vs. Displacement at Column Head

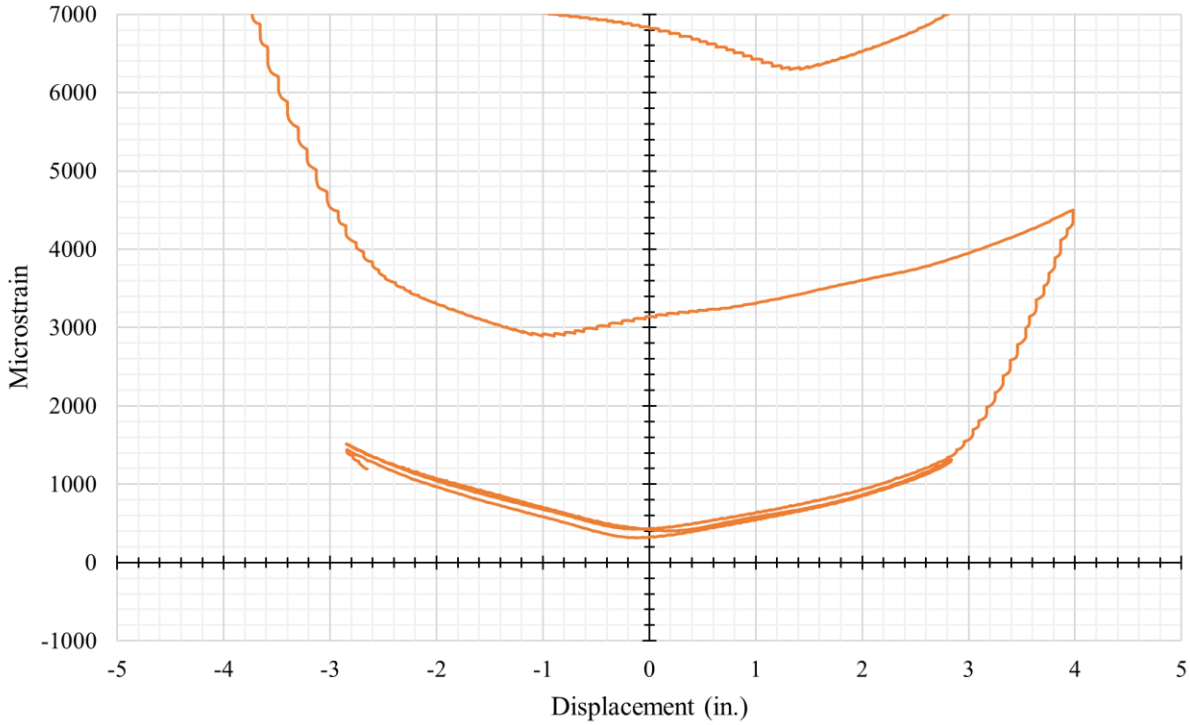

Figure A-11: HS-SCC 1 SS1 Steel Strain Gauge vs. Displacement at Column Head

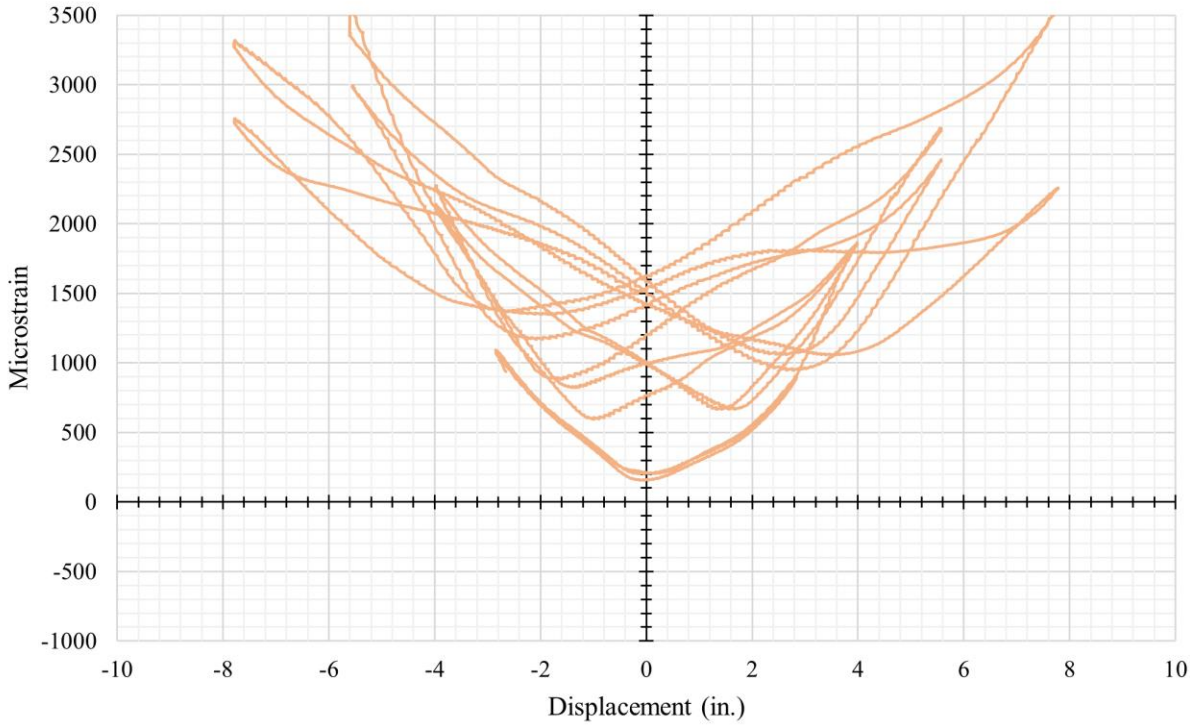

Figure A-12: HS-SCC 1 SS2 Steel Strain Gauge vs. Displacement at Column Head

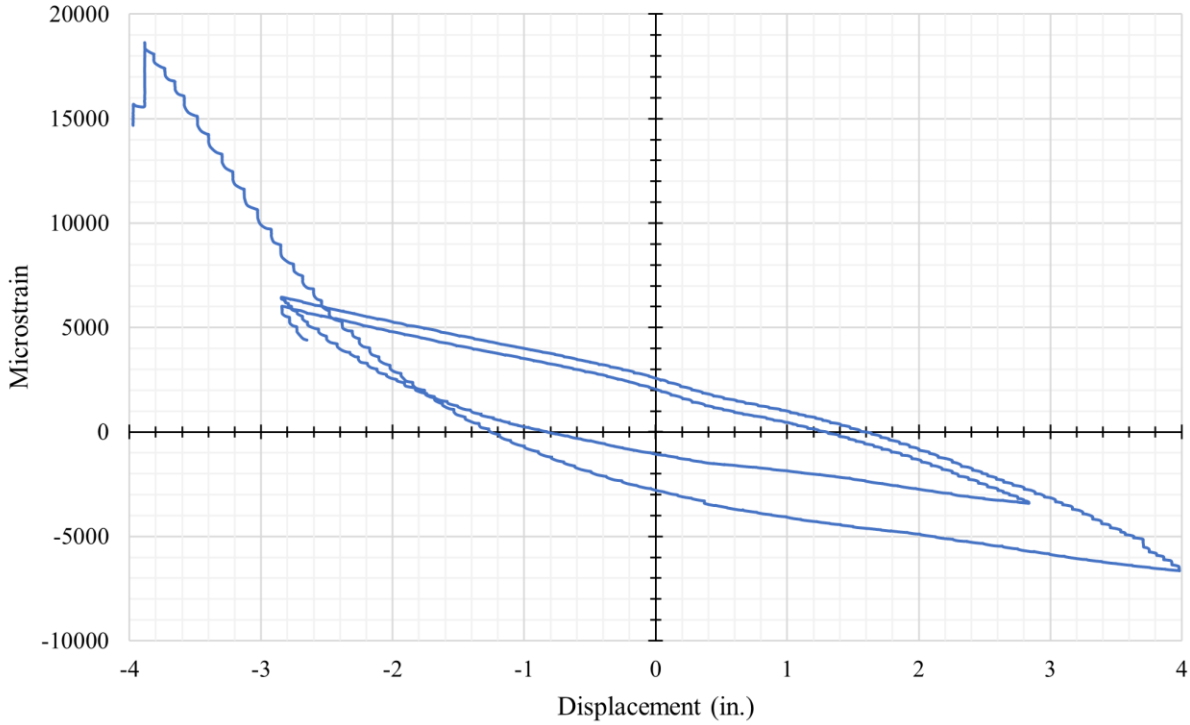

Figure A-13: HS-SCC 1 SE1 Steel Strain Gauge vs. Displacement at Column Head

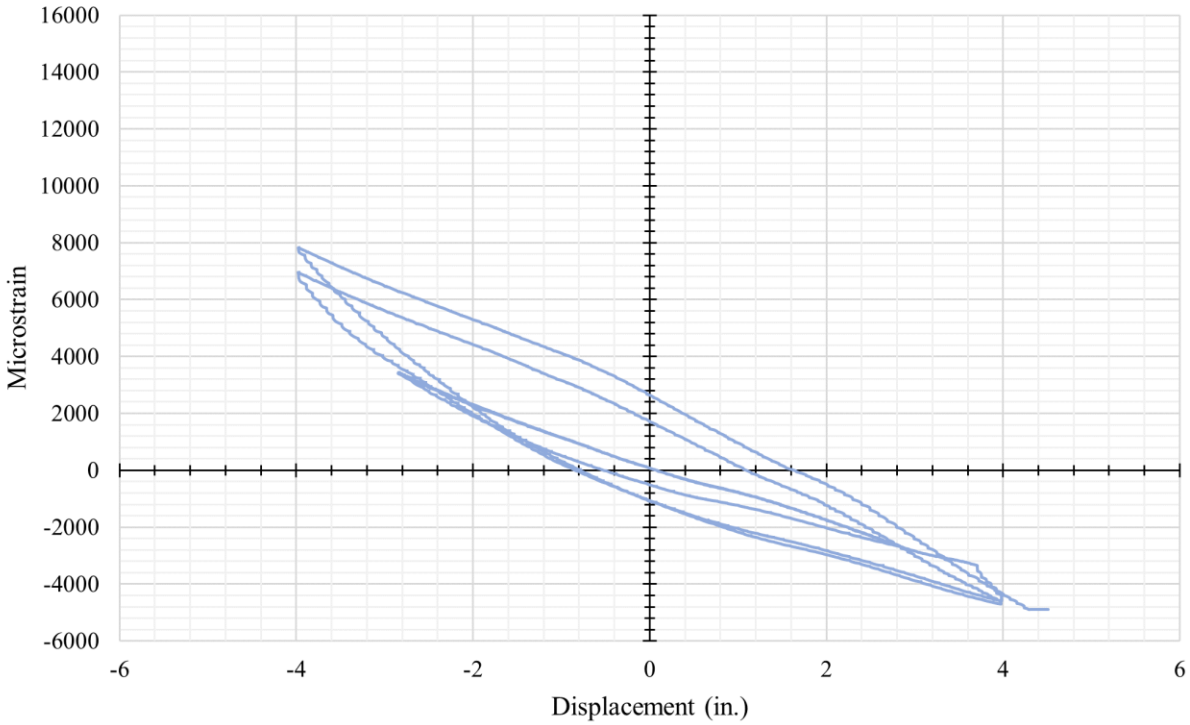

Figure A-14: HS-SCC 1 SE2 Steel Strain Gauge vs. Displacement at Column Head

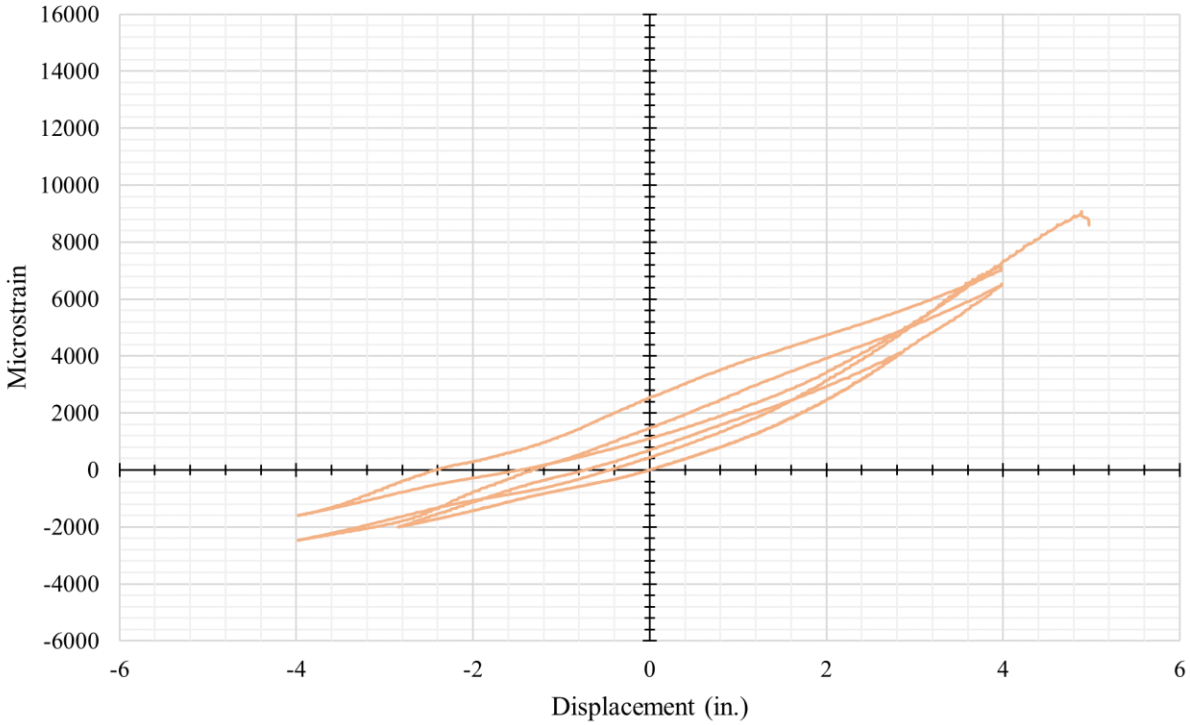

Figure A-15: HS-SCC 1 SW2 Steel Strain Gauge vs. Displacement at Column Head

A.3 HS-SCC 2 Column Supplemental Strain Gauge Plots

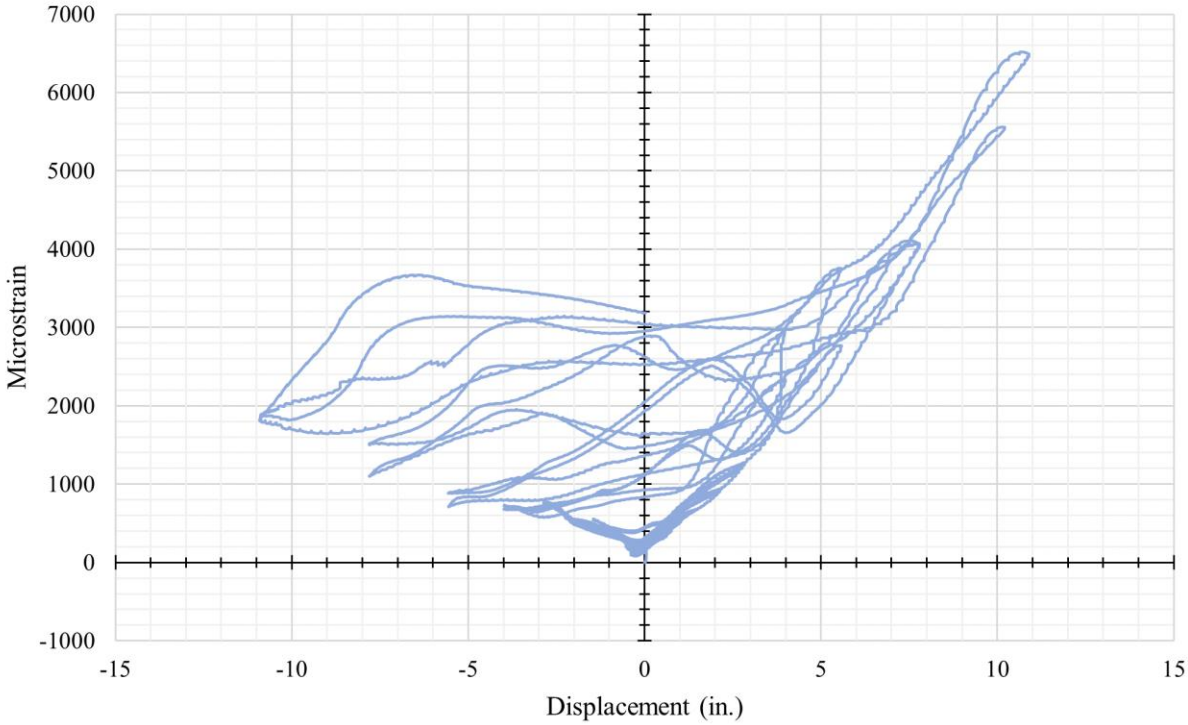

Figure A-16: HS-SCC 2 GE2 GFRP Strain Gauge vs. Displacement at Column Head

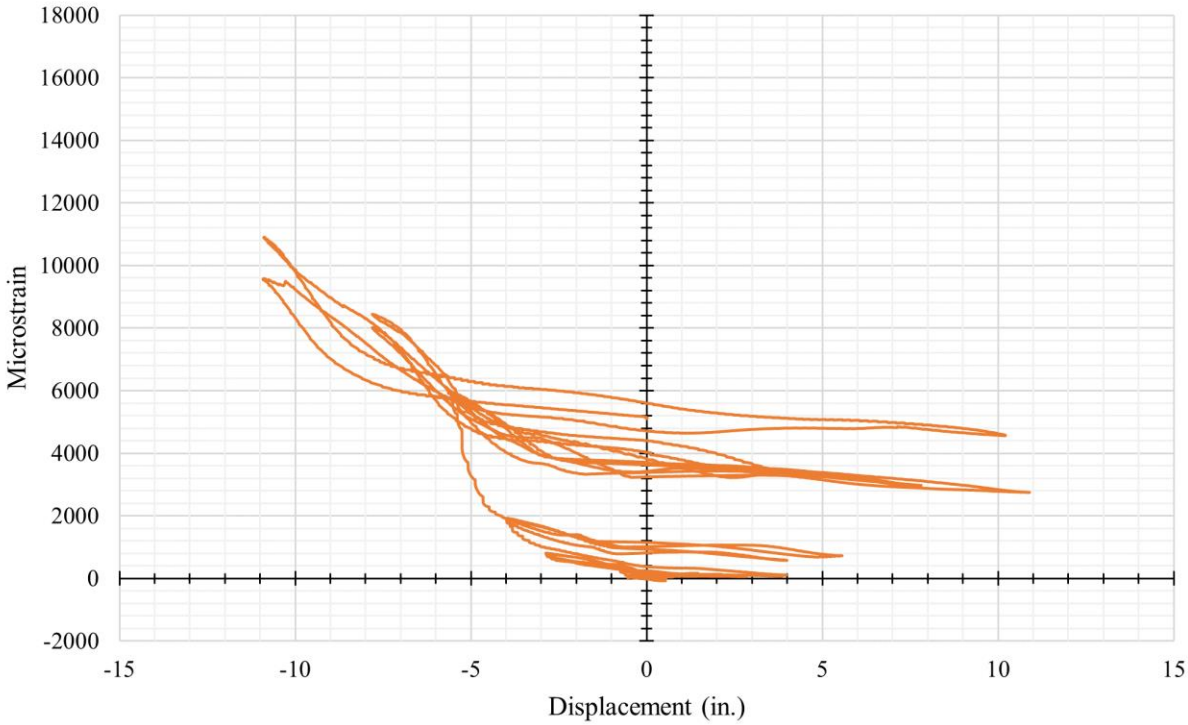

Figure A-17: HS-SCC 2 GW1 GFRP Strain Gauge vs. Displacement at Column Head

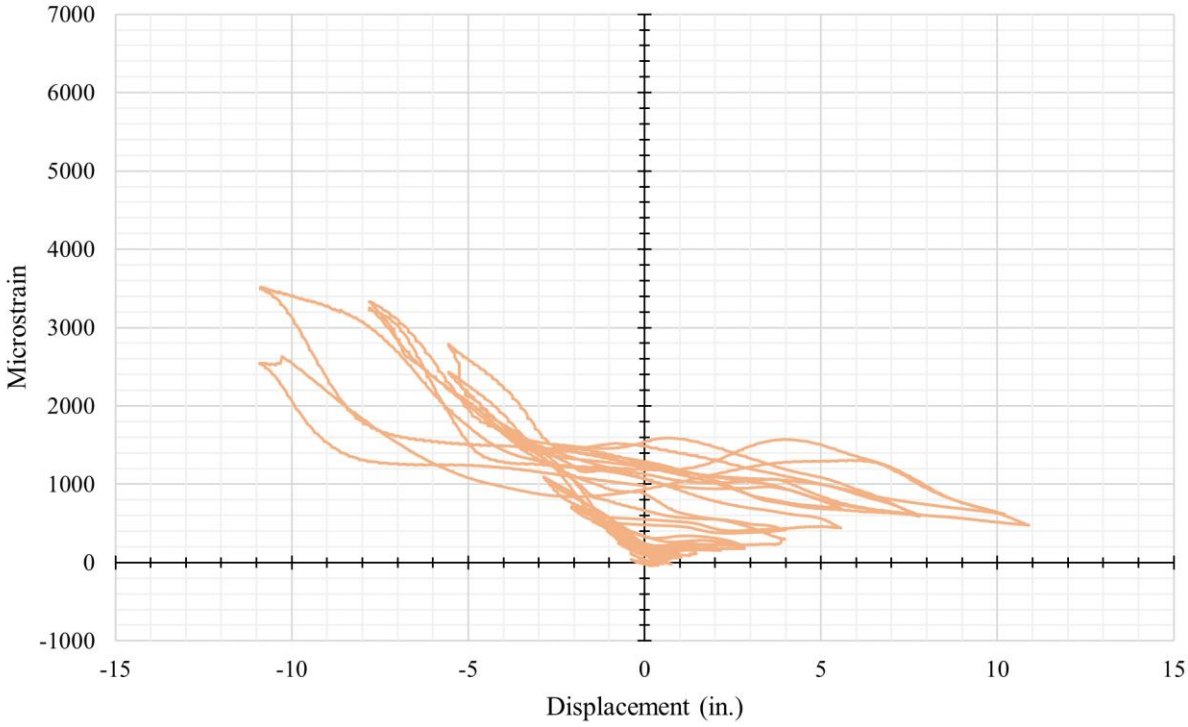

Figure A-18: HS-SCC 2 GW2 GFRP Strain Gauge vs. Displacement at Column Head

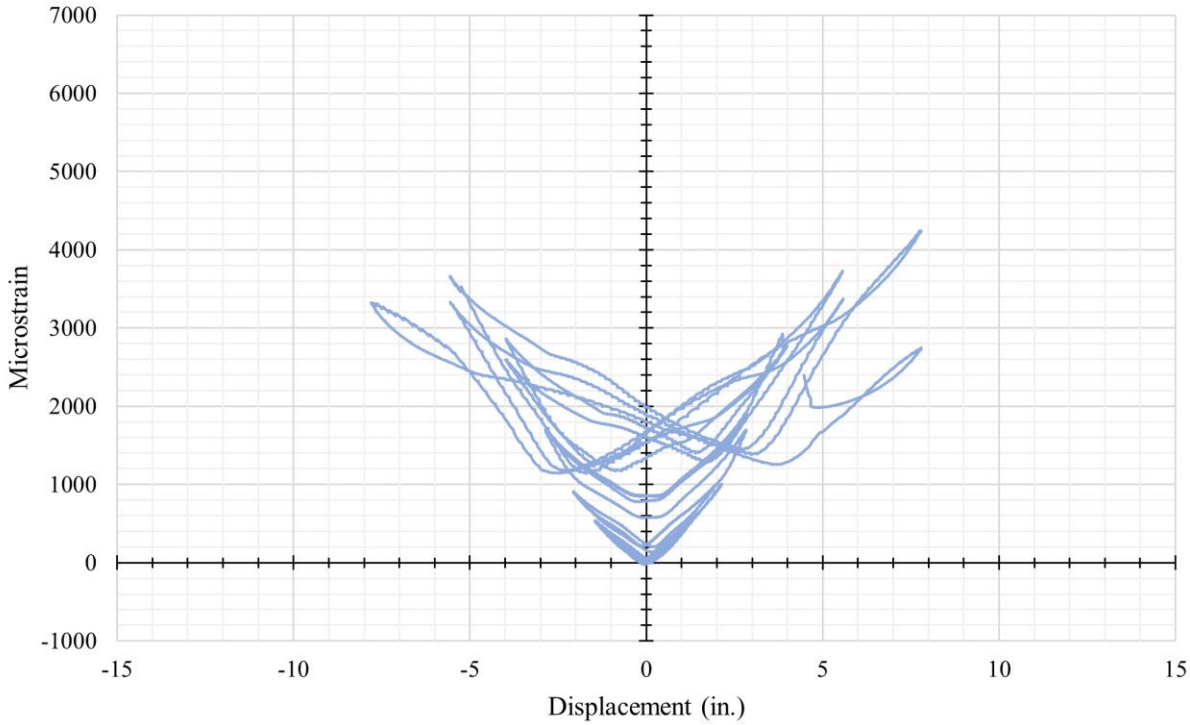

Figure A-19: HS-SCC 2 SN2 Steel Strain Gauge vs. Displacement at Column Head

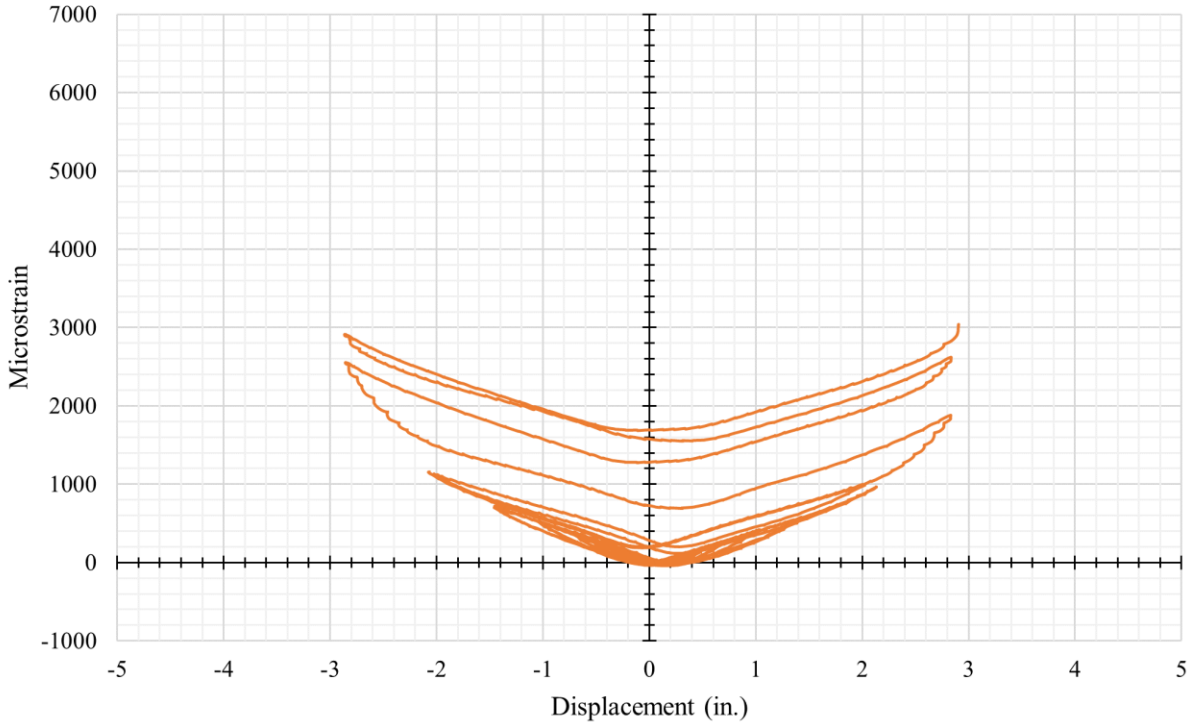

Figure A-20: HS-SCC 2 SS1 Steel Strain Gauge vs. Displacement at Column Head

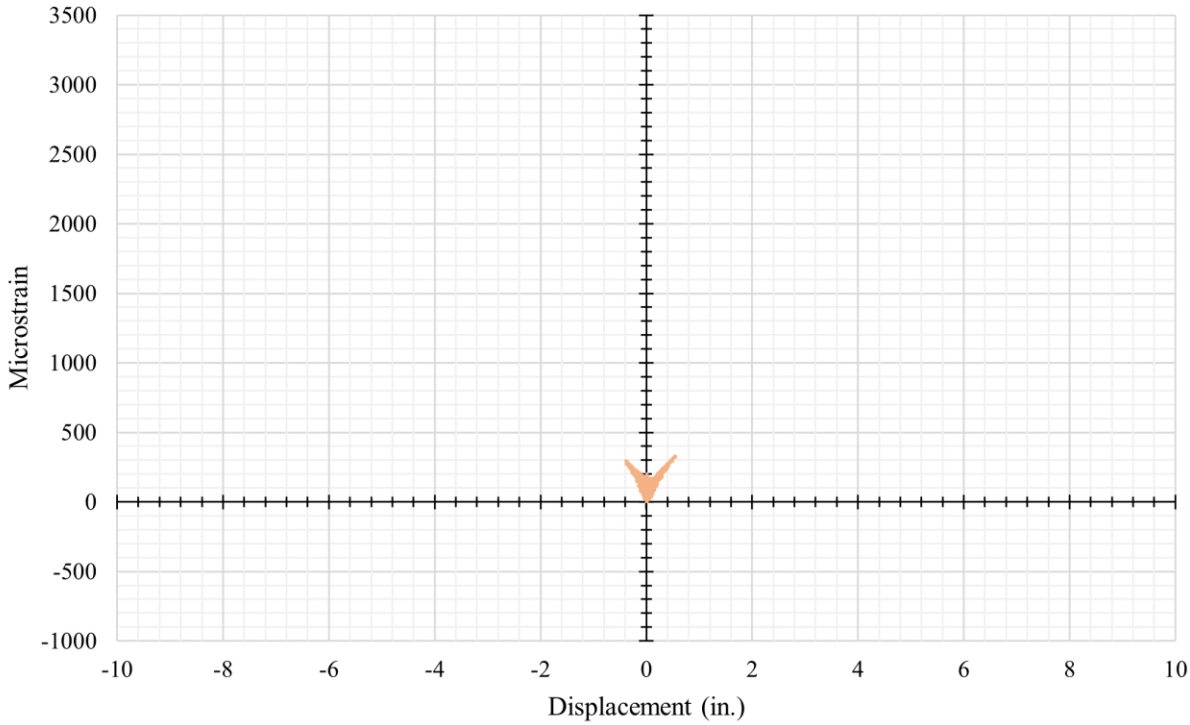

Figure A-21: HS-SCC 2 SS2 Steel Strain Gauge vs. Displacement at Column Head

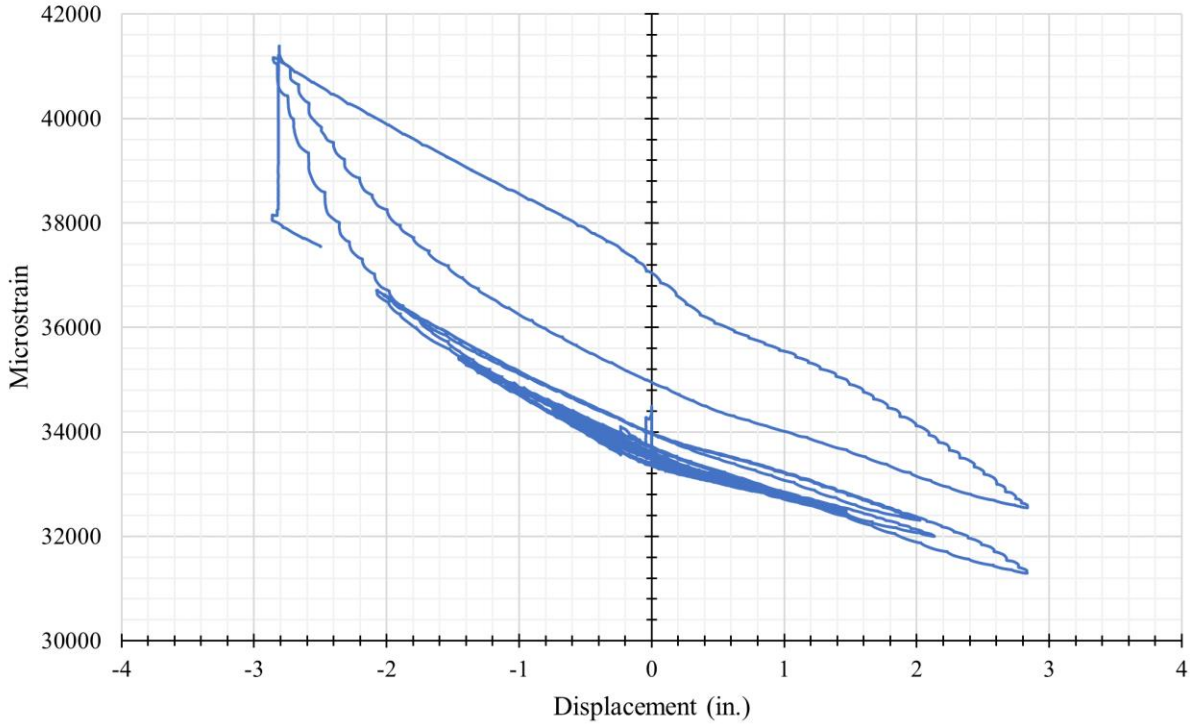

Figure A-22: HS-SCC 2 SE1 Steel Strain Gauge vs. Displacement at Column Head

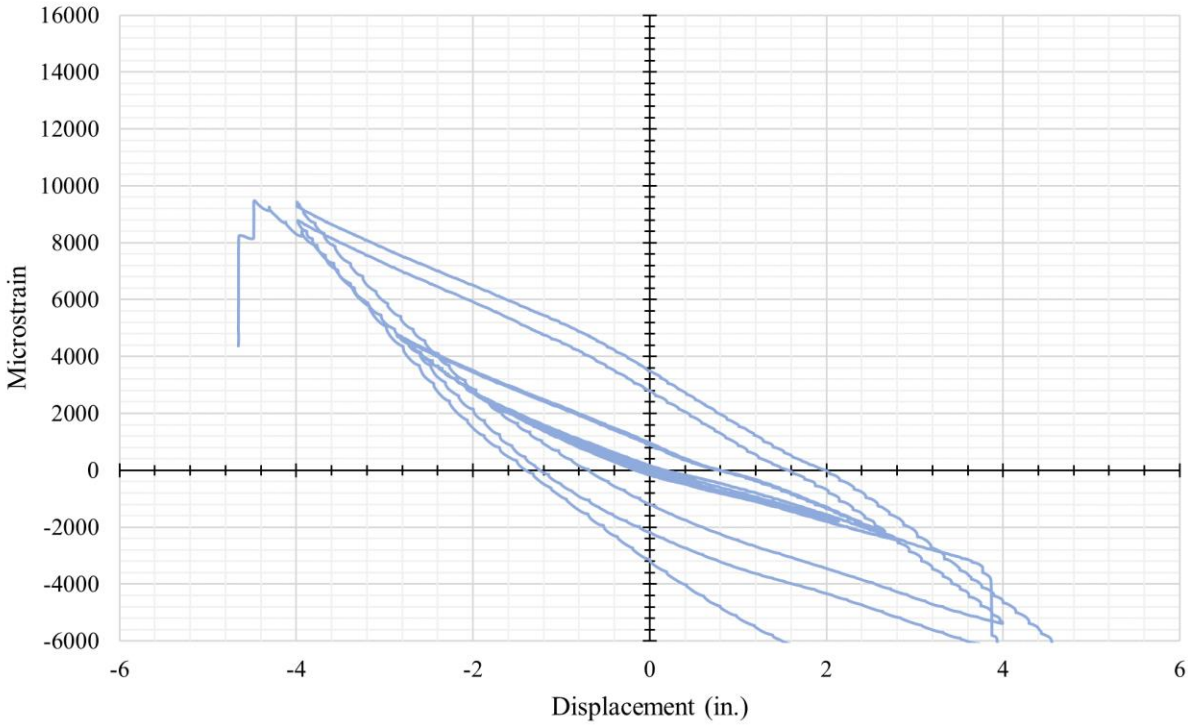

Figure A-23: HS-SCC 2 SE2 Steel Strain Gauge vs. Displacement at Column Head

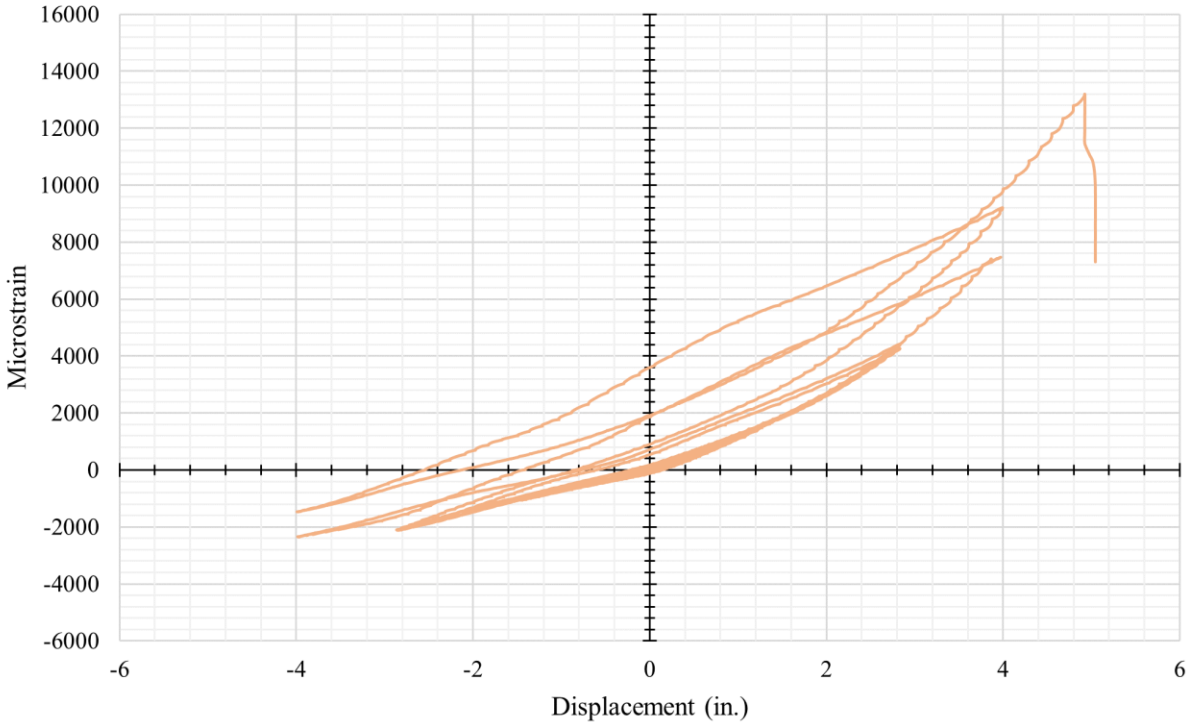

Figure A-24: HS-SCC 2 SW2 Steel Strain Gauge vs. Displacement at Column Head

A.4 UHPC 1 Column Supplemental Strain Gauge Plots

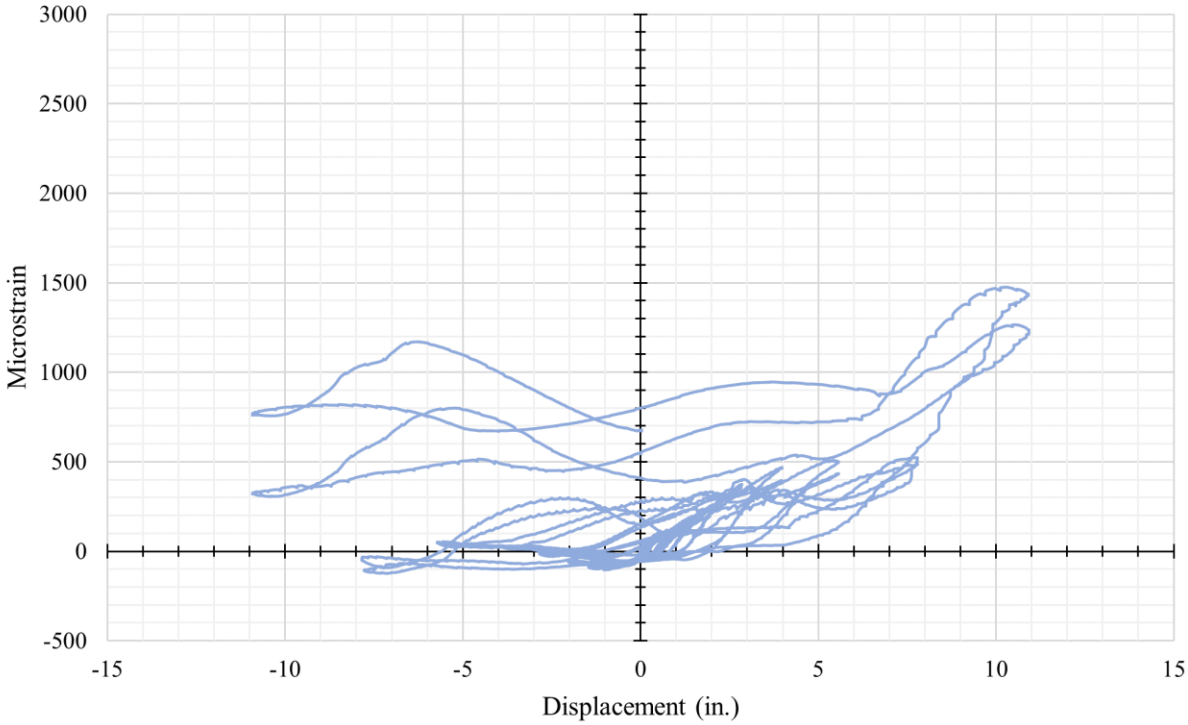

Figure A-25: UHPC 1 GE2 GFRP Strain Gauge vs. Displacement at Column Head

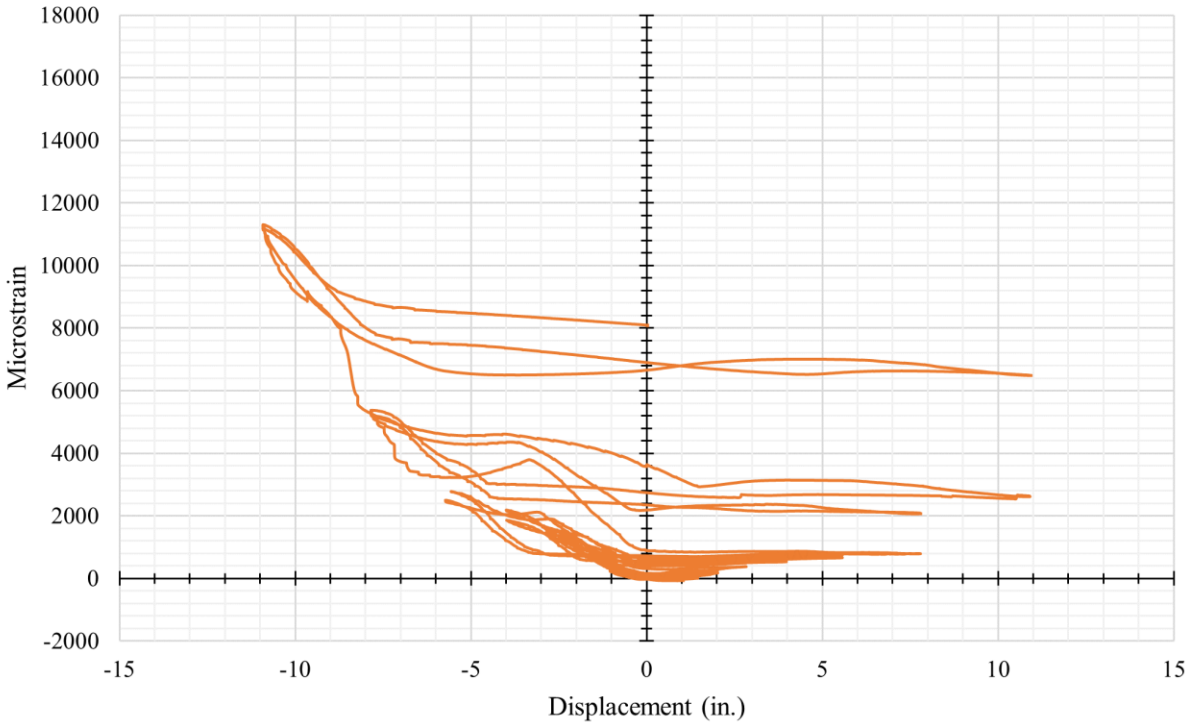

Figure A-26: UHPC 1 GW1 GFRP Strain Gauge vs. Displacement at Column Head

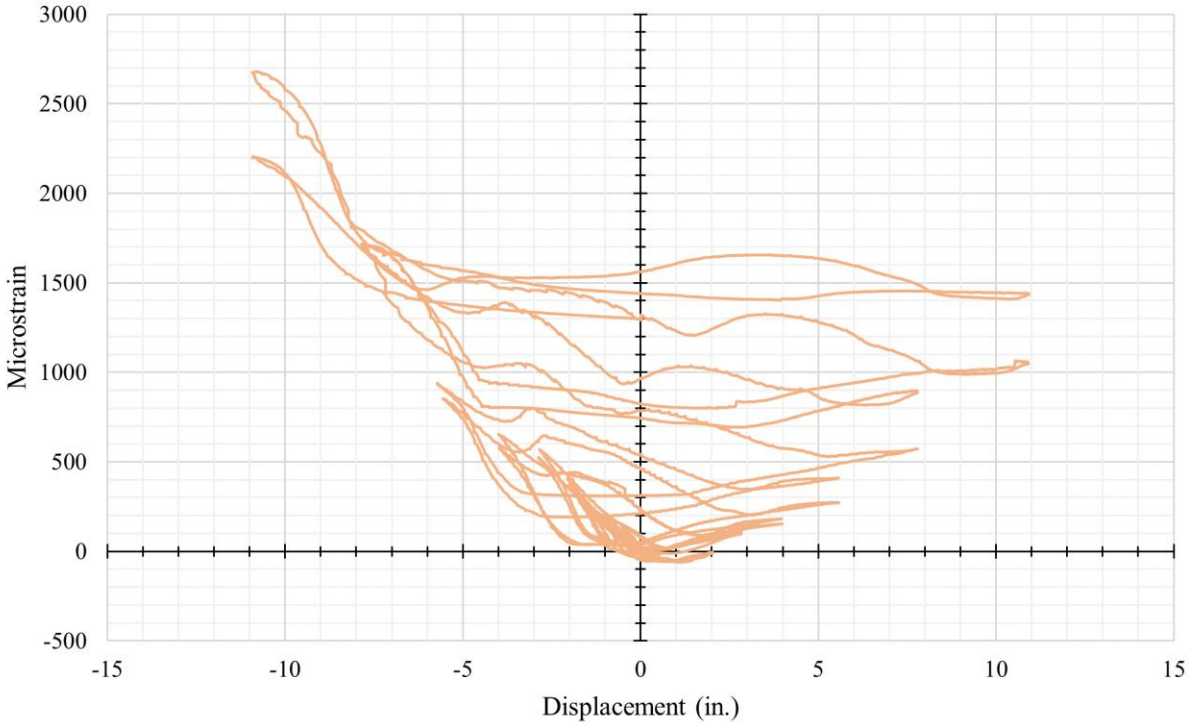

Figure A-27: UHPC 1 GW2 GFRP Strain Gauge vs. Displacement at Column Head

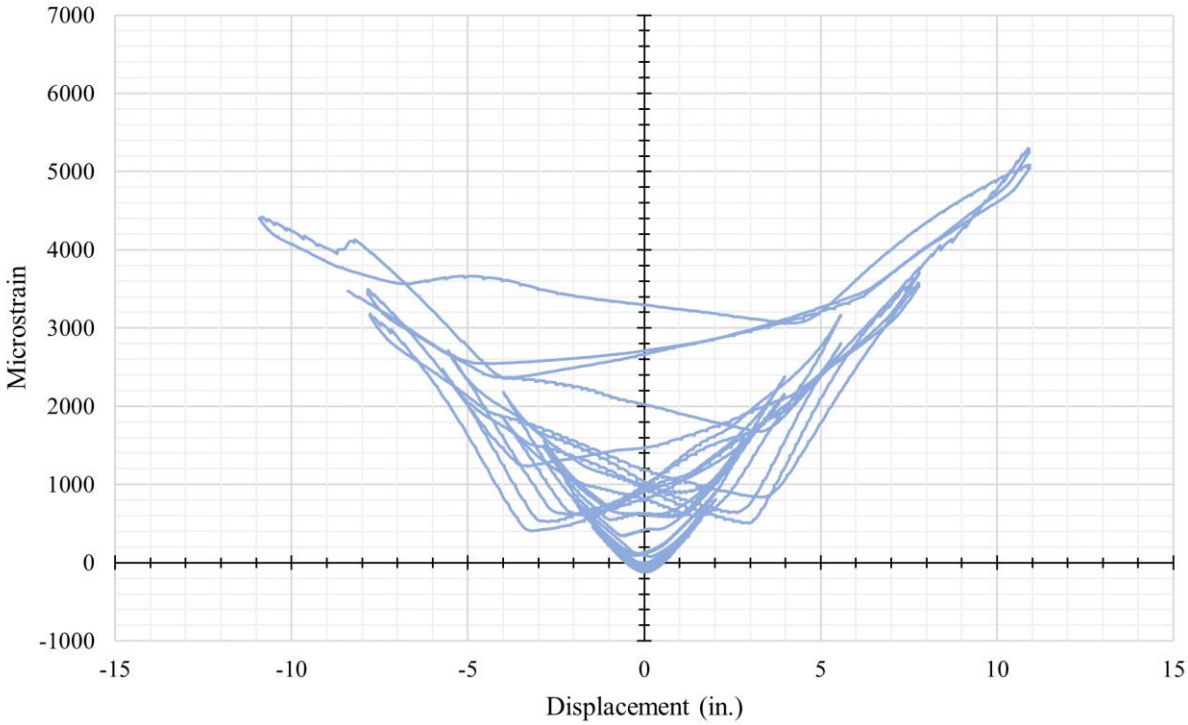

Figure A-28: UHPC 1 SN2 Steel Strain Gauge vs. Displacement at Column Head

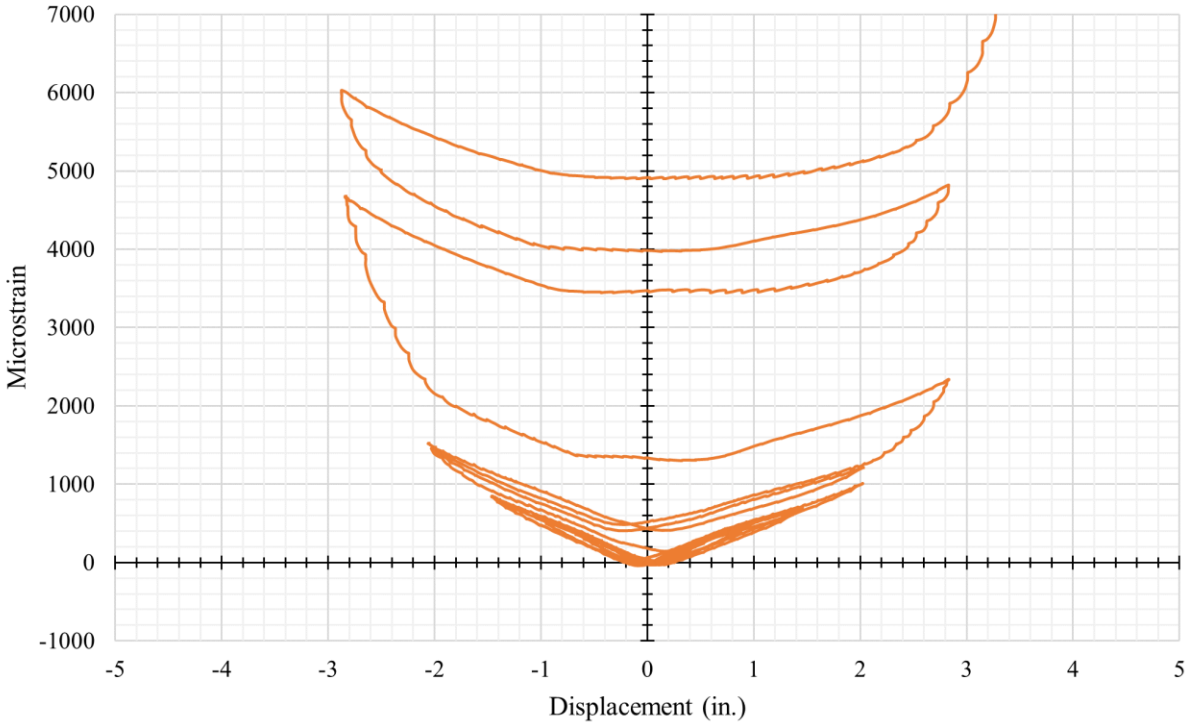

Figure A-29: UHPC 1 SS1 Steel Strain Gauge vs. Displacement at Column Head

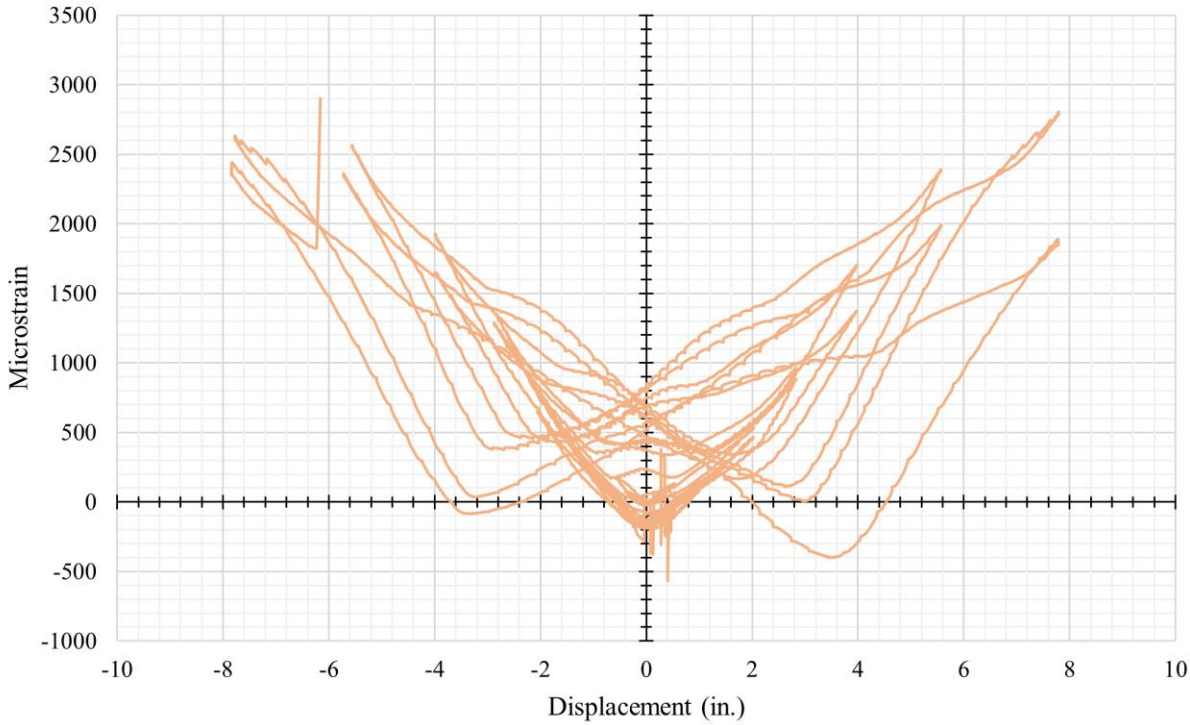

Figure A-30: UHPC 1 SS2 Steel Strain Gauge vs. Displacement at Column Head

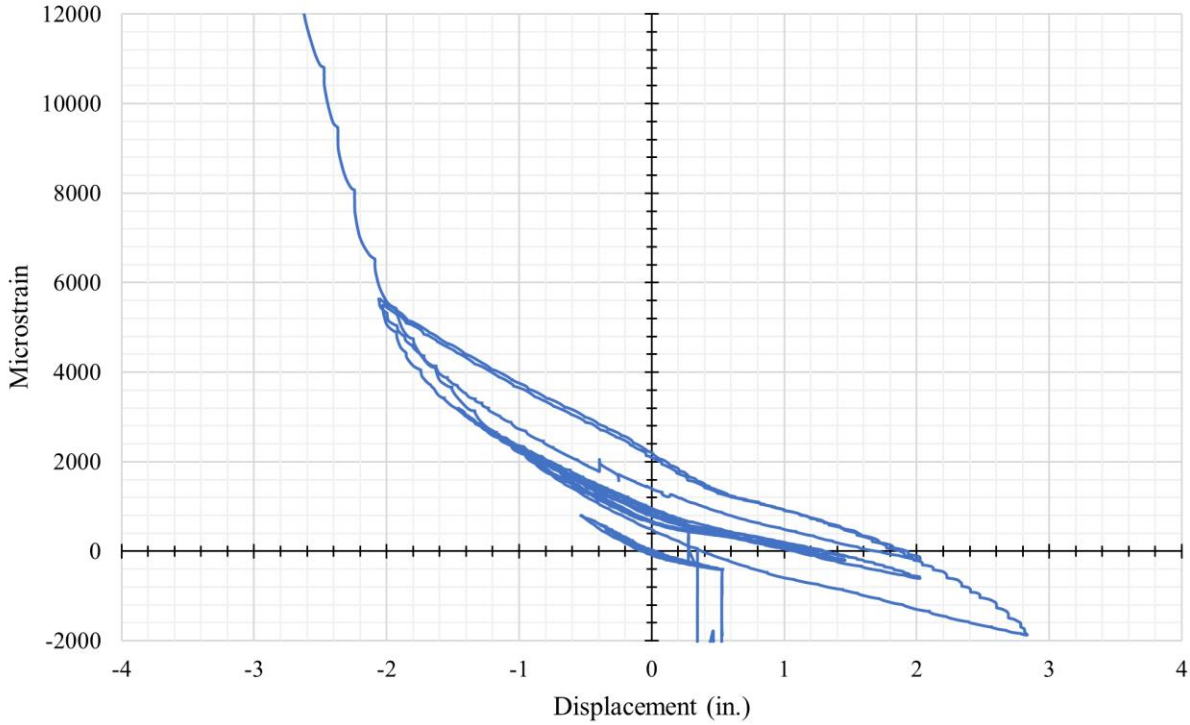

Figure A-31: UHPC 1 SE1 Steel Strain Gauge vs. Displacement at Column Head

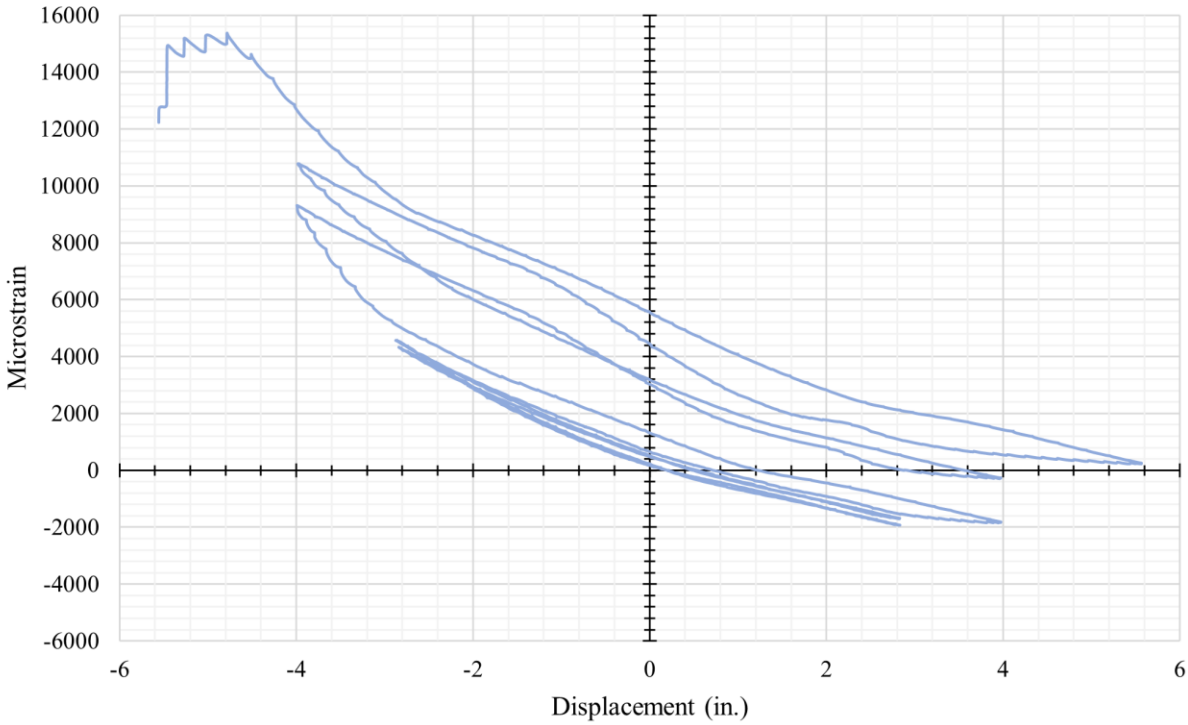

Figure A-32: UHPC 1 SE2 Steel Strain Gauge vs. Displacement at Column Head

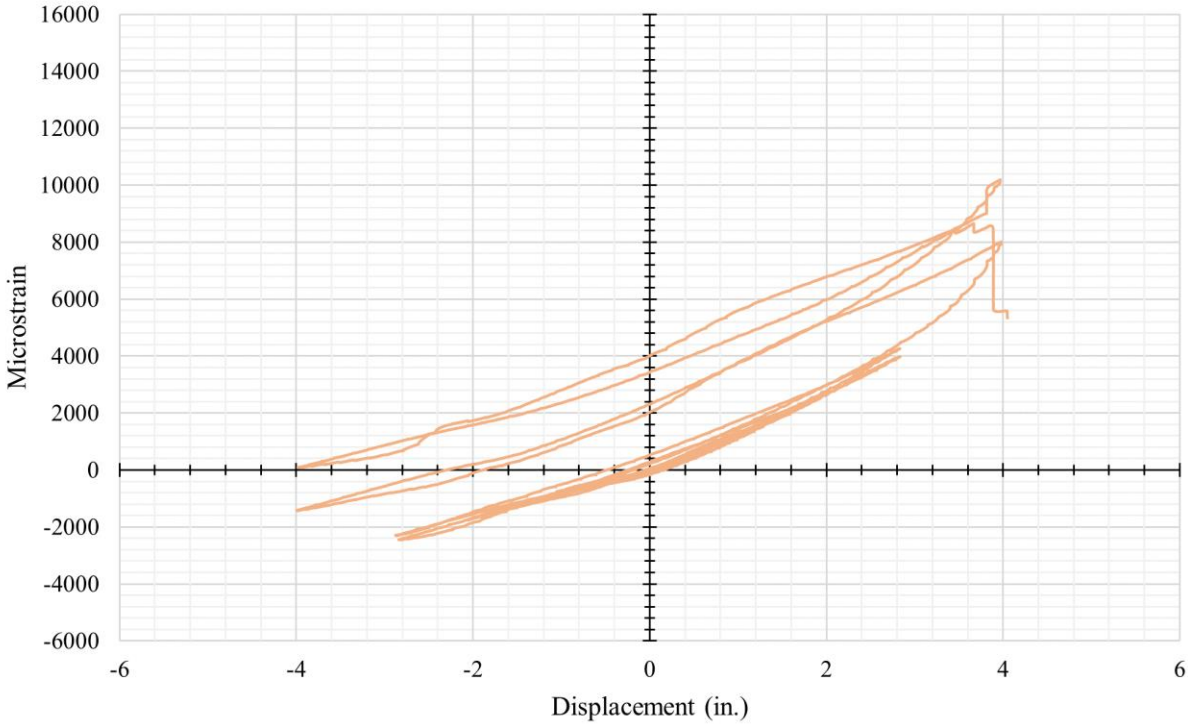

Figure A-33: UHPC 1 SW2 Steel Strain Gauge vs. Displacement at Column Head

A.5 UHPC 2 Column Supplemental Strain Gauge Plots

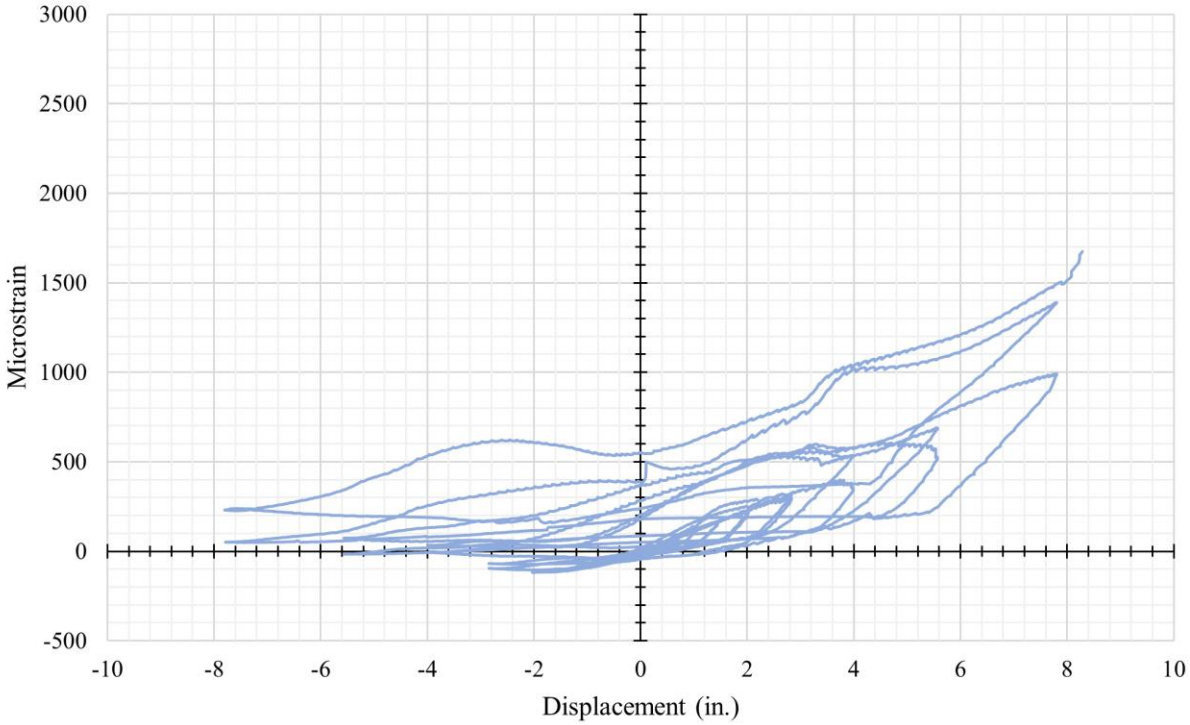

Figure A-34: UHPC 2 GE2 GFRP Strain Gauge vs. Displacement at Column Head

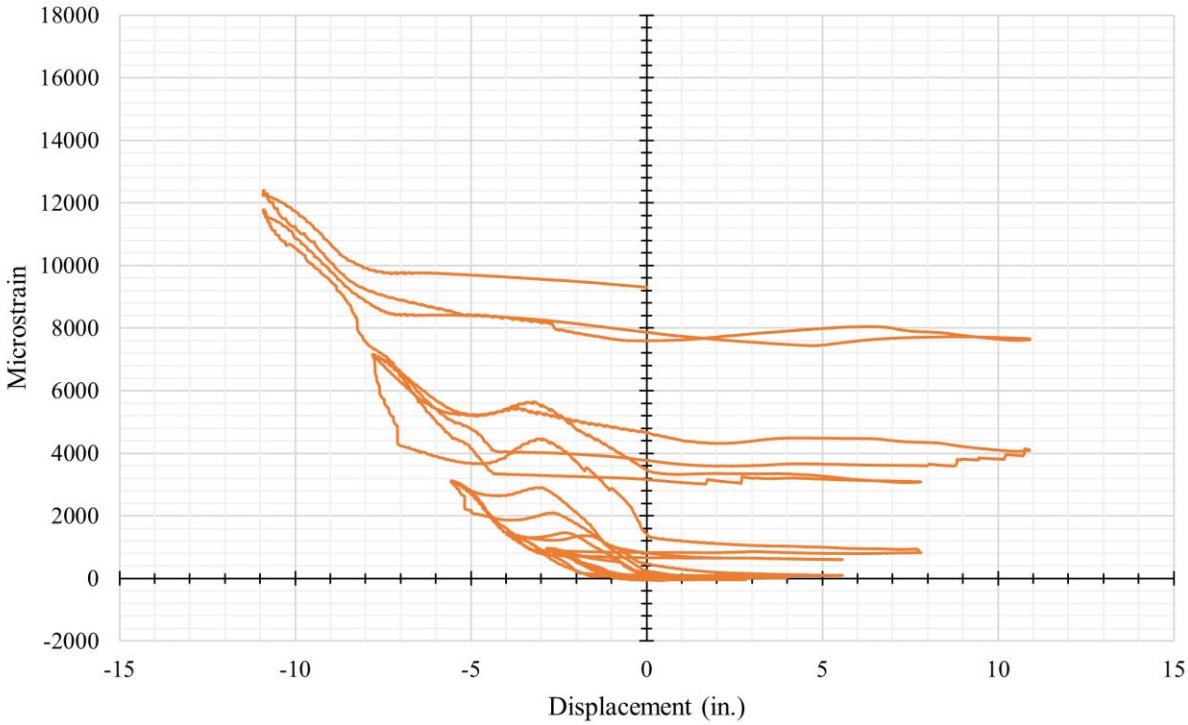

Figure A-35: UHPC 2 GW1 GFRP Strain Gauge vs. Displacement at Column Head

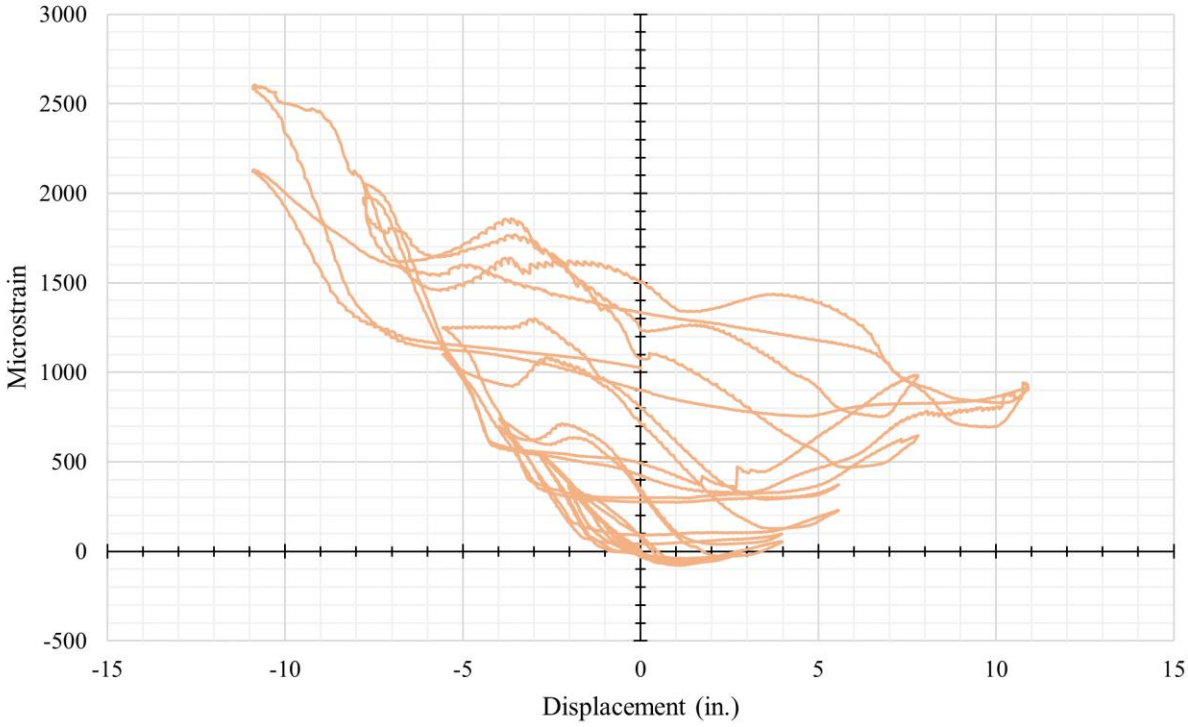

Figure A-36: UHPC 2 GW2 GFRP Strain Gauge vs. Displacement at Column Head

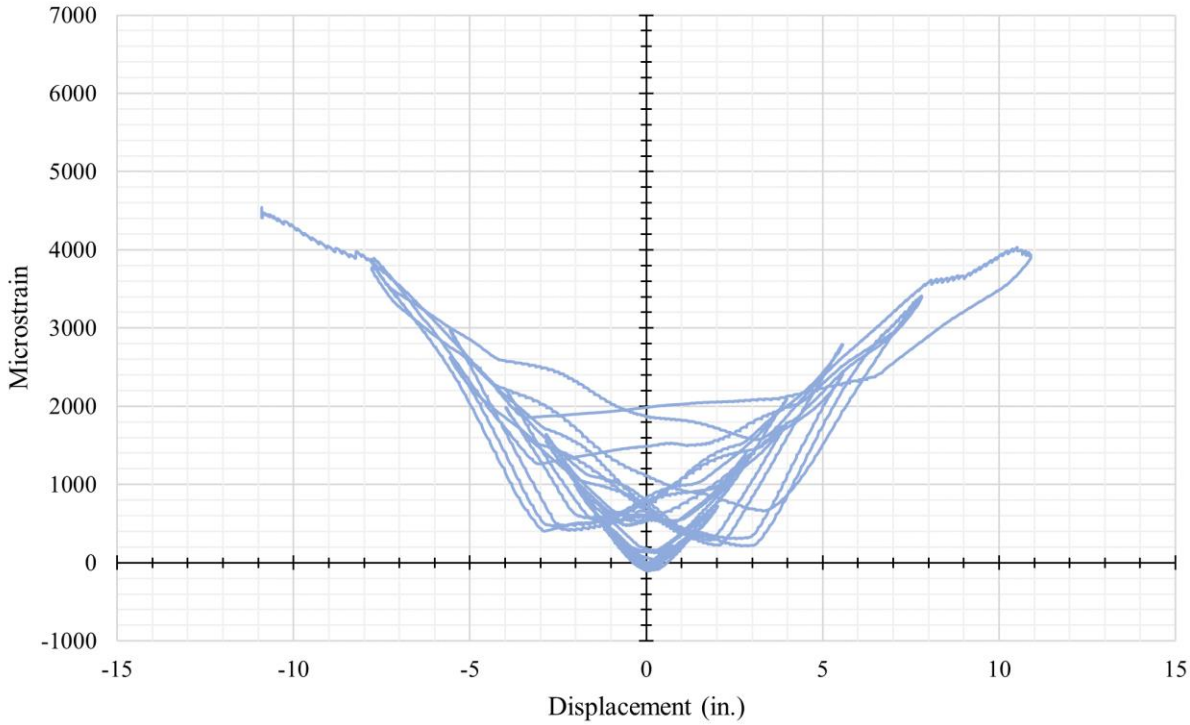

Figure A-37: UHPC 2 SN2 Steel Strain Gauge vs. Displacement at Column Head

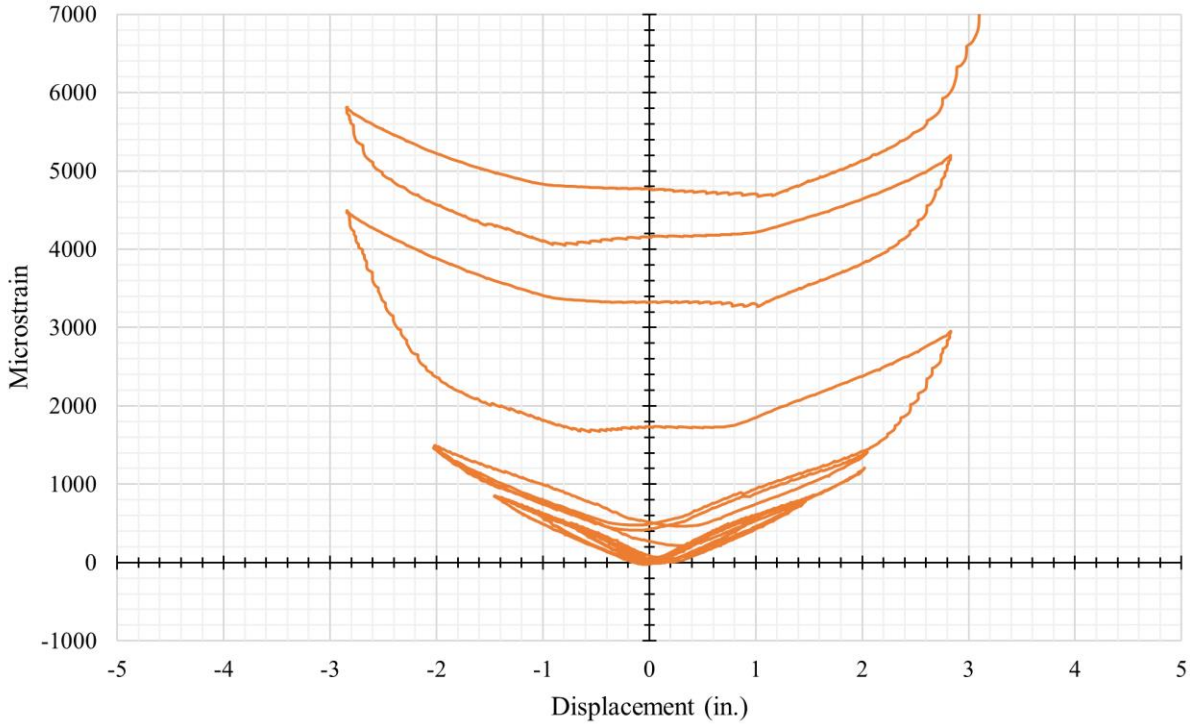

Figure A-38: UHPC 2 SS1 Steel Strain Gauge vs. Displacement at Column Head

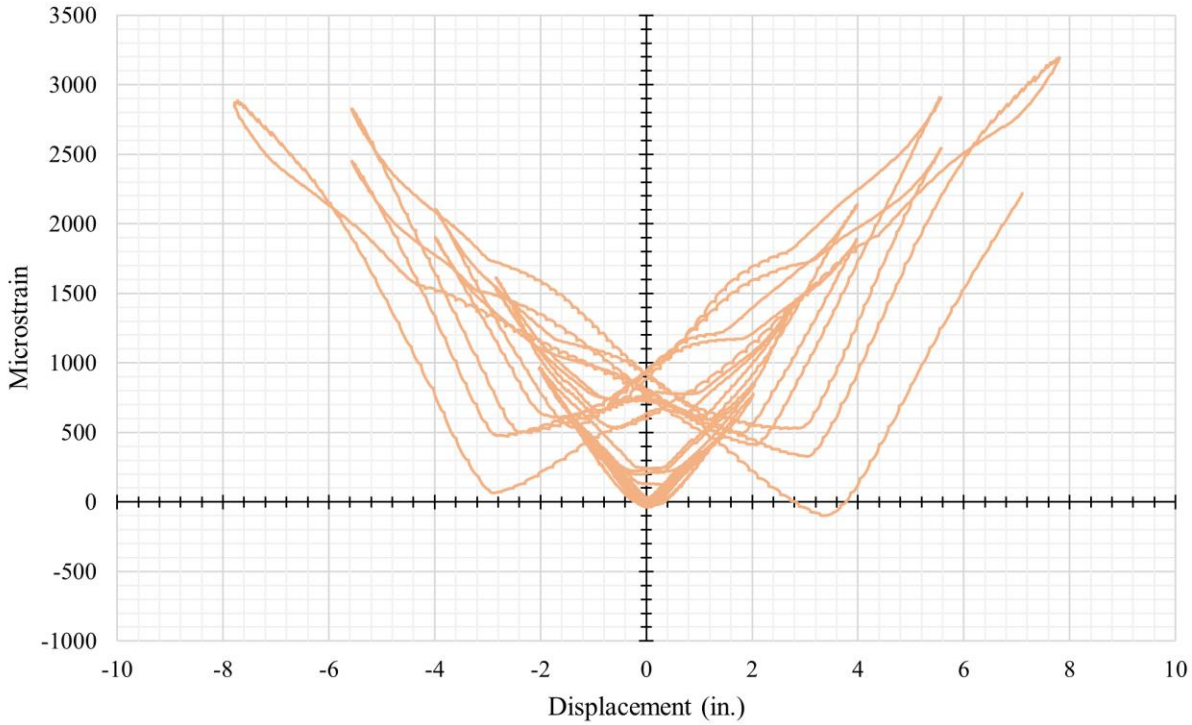

Figure A-39: UHPC 2 SS2 Steel Strain Gauge vs. Displacement at Column Head

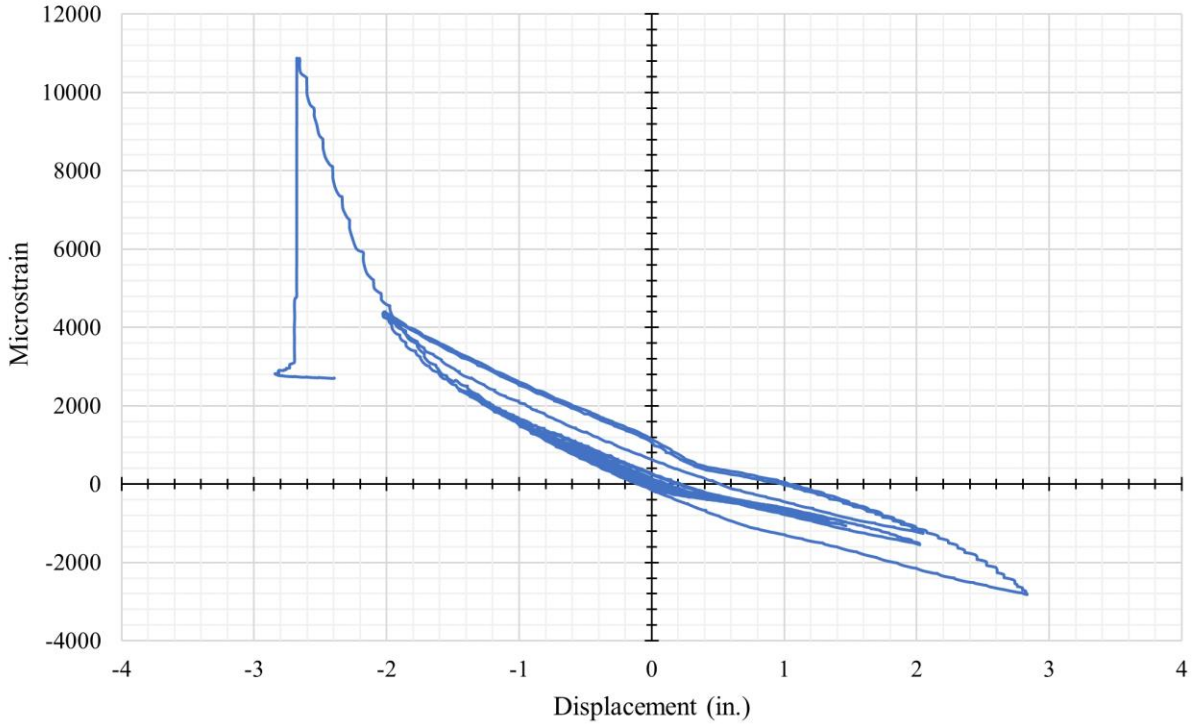

Figure A-40: UHPC 2 SE1 Steel Strain Gauge vs. Displacement at Column Head

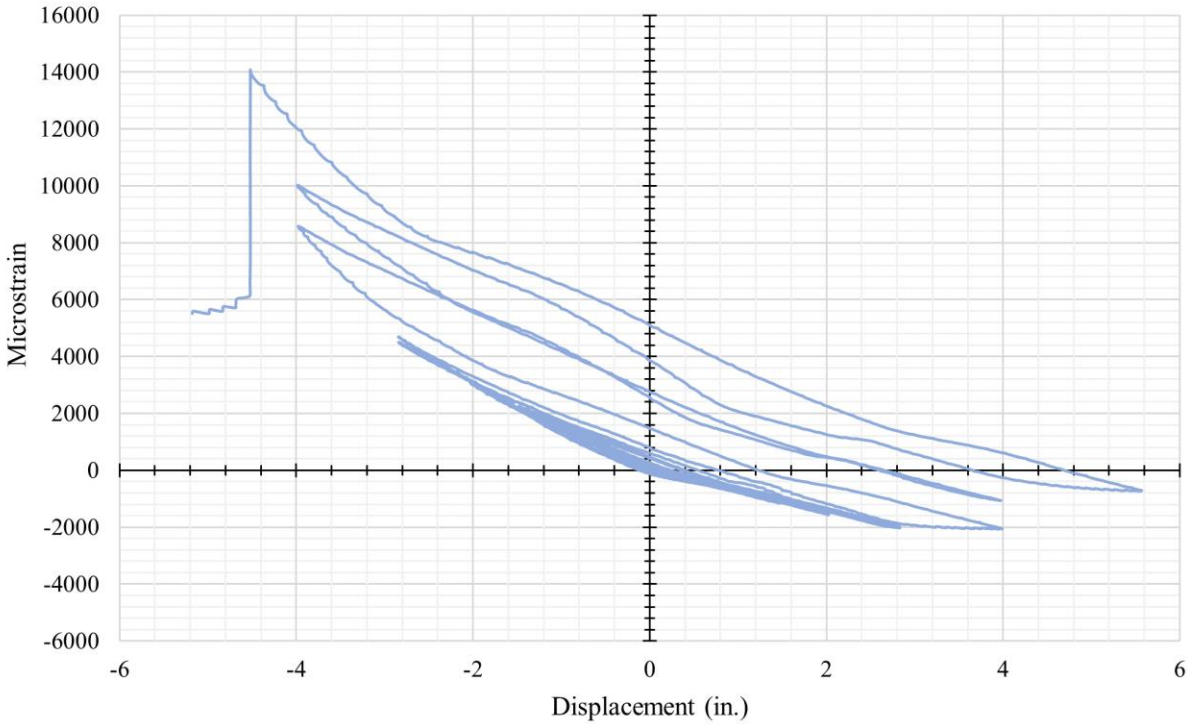

Figure A-41: UHPC 2 SE2 Steel Strain Gauge vs. Displacement at Column Head

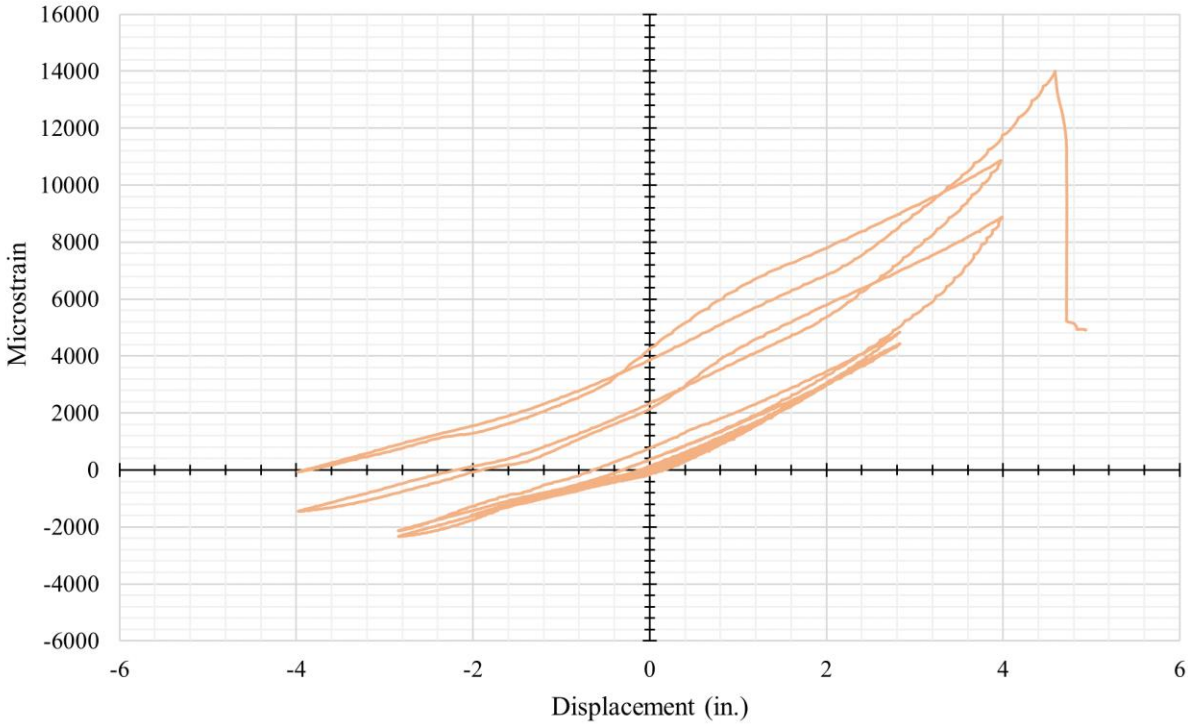

Figure A-42: UHPC 2 SW2 Steel Strain Gauge vs. Displacement at Column Head